PhD

3.º CICLO

FCUP
UA
Nova FCT
2024

Agro-industrial by-products as an unlimited source of phenolic compounds for different technological applications

Ana Rita Martins Pereira

FC

U.PORTO
FACULDADE DE CIÊNCIAS
UNIVERSIDADE DO PORTO

universidade de aveiro

NOVA
NOVA SCHOOL OF
SCIENCE & TECHNOLOGY

Agro-industrial by-products as an unlimited source of phenolic compounds for different technological applications

Ana Rita Martins Pereira
Doctoral Program in Sustainable Chemistry
Department of Chemistry and Biochemistry
Faculty of Sciences - University of Porto
2024

U.PORTO
FACULDADE DE CIÊNCIAS
UNIVERSIDADE DO PORTO

universidade de aveiro

NOVA
NOVA SCHOOL OF
SCIENCE & TECHNOLOGY

Agro-industrial by-products as an unlimited source of phenolic compounds for different technological applications

Ana Rita Martins Pereira

Thesis carried out within the scope of the Doctoral Program in Sustainable Chemistry
Department of Chemistry and Biochemistry
2024

Supervisor
Nuno Filipe da Cruz Batista Mateus
Full Professor, Faculty of Sciences - University of Porto

Co-supervisor
Joana Alexandra da Silva Oliveira Pinto da Silva,
Research associate, Associated Laboratory for Green Chemistry

AGRADECIMENTOS

A realização deste trabalho foi conseguida com a colaboração e o apoio de várias pessoas e instituições. Desta forma, gostaria de expressar o meu sincero agradecimento:

Ao Professor Doutor Nuno Mateus, orientador deste trabalho, agradeço-lhe toda a disponibilidade, orientação e os conhecimentos científicos que me foi transmitindo ao longo destes últimos anos, as suas críticas construtivas, sugestões e conselhos, todo o apoio e confiança que depositou em mim.

À Doutora Joana Oliveira, coorientadora deste trabalho, quero agradecer por todo o apoio diário, disponibilidade, motivação e confiança. Foram quatro anos de partilha de conhecimento que me ajudaram muito nesta jornada, agradeço-lhe todas as oportunidades e desafios que me foi propondo, por confiar em mim para realizar diferentes tarefas em áreas distintas da investigação científica, que contribuíram sem dúvida para um crescimento profissional e pessoal.

Ao Professor Doutor Victor de Freitas, agradeço-lhe pela oportunidade de ter trabalhado no seu grupo de investigação, bem como todas as oportunidades que me foi dando ao longo destes últimos anos. Agradeço a partilha de conhecimento científico e críticas construtivas que contribuíram para o meu crescimento profissional.

À doutora Zélia Azevedo, agradeço a ajuda incansável na realização das análises de LC-MS e GC-MS, bem como a sua inteira disponibilidade mostrando-se sempre pronta para ajudar e com total interesse.

Ao Professor Catedrático Jubilado Fernando Pina da Universidade Nova de Lisboa, agradeço pelos ensinamentos e disponibilidade na realização do trabalho em colaboração.

Ao Professor Emérito Alírio Rodrigues da Faculdade de Engenharia da Universidade do Porto, agradeço-lhe pelos trabalhos em colaboração, por toda a disponibilidade, partilha de críticas construtivas e conhecimento científico.

À Doutora Carina Costa da Faculdade de Engenharia da Universidade do Porto, agradeço toda a amabilidade, disponibilidade e passagem de conhecimento acerca da lenhina, pela preocupação e interesse em ajudar e colaborar para um trabalho melhor.

A todos os elementos do Departamento de Química e Bioquímica da Faculdade de Ciências que de alguma forma contribuíram para o sucesso deste trabalho.

A todos os colegas de trabalho do Food Polyphenol Lab, por todo o apoio, motivação, e ajuda no laboratório. Agradeço-lhes todos os bons momentos que partilhamos.

Um agradecimento especial à Paulinha e à Patrícia, pela amizade e companheirismo nesta jornada. Pelas longas horas de conversa e partilha de bons momentos e conhecimentos. Por estarem sempre disponíveis e com uma palavra de incentivo e conforto.

À Ana Luísa e à Iva por todo o carinho, amizade e motivação que me foram dando ao longo destes anos. Agradeço-lhes por todos os conselhos e especialmente pelos bons momentos que passamos.

À Sofia, à Mónica e à Alexandra por todo o apoio incondicional. Pela ajuda no laboratório, partilha de conhecimentos e diversão. Foram sempre um ombro amigo.

Ao Ricardo e ao Carlo, com quem tive a oportunidade de partilhar trabalhos científicos. Agradeço-lhes toda a disponibilidade, paciência, dedicação, companheirismo e passagem de conhecimentos.

À Natércia, ao Hélder, ao Carlos, ao Luís, à Susana, à Joana Azevedo e à Elsinha um agradecimento especial pelas boas palavras de incentivo, e sobretudo pelos bons momentos que proporcionaram.

Aos meus amigos, que estiveram presentes em todos os momentos, por todas as gargalhadas, amizade e amor. Foram um suporte fundamental nesta jornada.

Ao David, por todo o apoio incansável, pela paciência, compreensão e por todo o amor que partilhamos.

A toda a minha família, em especial aos meus pais, que foram o pilar em todas as ocasiões. Agradeço-lhes por todo o amor, apoio e motivação.

De entre as várias instituições que contribuíram para a realização deste trabalho, agradeço:

À Fundação para a Ciência e Tecnologia, pelo apoio financeiro concebido através da bolsa de Doutoramento (SFRH/ BD/146549/2019).

À Faculdade de Ciências de Universidade do Porto por fazer parte do meu percurso académico e mais uma vez me receber como estudante, contribuindo para o meu conhecimento científico.

Ao Laboratório Associado para a Química Verde (LAQV-REQUIMTE), por ter aceitado ser a entidade de acolhimento deste meu doutoramento em Química Sustentável.

PUBLICATIONS LIST

This work was developed within the scope of the doctoral program in sustainable chemistry at LAQV-REQUIMTE, in the Department of Chemistry and Biochemistry of the Faculty of Sciences at the University of Porto, with the financial support of a PhD fellowship (SFRH/BD/146549/2019) attributed by the Foundation for Science and Technology (FCT).

The results included in this thesis were published in international scientific journals and international and national scientific conferences through oral and panel communications.

PUBLICATION IN INTERNATIONAL SCIENTIFIC JOURNALS

BOOK CHAPTER

1. Pereira, A.R.; de Freitas, V.; Oliveira, J.; Chapter 7 - Development of lignin-based nanoparticles: Fabrication methods and functionalization approaches. In Lignin-Based Materials for Biomedical Applications; Santos, H., Figueiredo, P., Eds.; Elsevier: Amsterdam, The Netherlands, 2021; pp. 227–270. http://dx.doi.org/10.1016/b978-0-12-820303-3.00005-9

SCIENTIFIC ARTICLES

1. Pereira, A.R.; Bravo, C.; Ramos, R.M.; Costa, C.; Rodrigues, A.; de Freitas, V.; Mateus, N.; Dias, R.; Soares, S.; Oliveira, J.; New insights into pH-dependent complex formation between lignosulfonates and anthocyanins: Impact on color and oxidative stability. (Submitted)

2. Pereira, A.R.; Brandão, E.; Pinto, J.; de Pinho, P.G.; Costa, C.; Rodrigues, A.; Michelin, M.; Soares, S.; de Freitas, V.; Mateus, N.; Oliveira, J.; First insight into lignin valorization as a promising biopolymer for the modulation of the physicochemical properties of wine. https://doi.org/10.1021/acs.jafc.4c05442

3. Pereira, A.R.; Fernandes, V. C.; Delerue-Matos, C.; de Freitas, V.; Mateus, N.; Oliveira, J.; Exploring Acylated Anthocyanin-Based Extracts as a Natural Alternative to Synthetic Food Dyes: Stability and Application Insights. Food Chemistry. 2024. https://doi.org/10.1016/j.foodchem.2024.140945

4. Seco, A.; Pereira, A.R.; Pina, F.; Camuenho, A.; Oliveira, J.; Dias, R.; Brás, N.; Basílio, N.; Parola, A. J.; Lima, J.; De Freitas, V. Comparing the Chemistry of Malvidin 3-*O*-Glucoside and Malvidin 3,5-*O*-Diglucoside Networks: A Holistic Approach to the Acidic and Basic Paradigms with Implications in Biological Studies. Journal of Agricultural and Food Chemistry. 2024. https://doi.org/10.1021/acs.jafc.4c00552

5. Pereira, A.R., Costa, C., Mateus, N., de Freitas, V., Rodrigues, A., Oliveira, J.; Exploring the Potential of Vine Shoots as a Source of Valuable Extracts and Stable Lignin Nanoparticles for Multiple Applications. International Journal of Molecular Sciences. 2023; 24(6):5165. https://doi.org/10.3390/ijms24065165

ORAL COMMUNICATIONS

1. Pereira, A.R.; de Freitas, V.; Oliveira, J., “Acylated and polyacylated anthocyanins as a pallet of natural colors”, XXVIIth Portuguese-Galician International Conference on Chemistry, Porto, Portugal, 22-24 November 2023.

2. Pereira, A.R., Costa, C., de Freitas, V., Mateus, N., Rodrigues, A., Oliveira, J., “Red color stabilization of anthocyanins with lignosulfonates from the pulp industry”, International conference of polyphenols (ICP), Nantes, France, 3-6 July 2023.

3. Pereira A.R., Costa, C., de Freitas, V., Mateus, N., Rodrigues, A., Oliveira, J., “Valorization of vine shots to extract lignin – chemical and structural characterization”, XXVI Galician-Portuguese International Conference on Chemistry, Santiago de Compostela, Spain, 16-18 November 2022.

4. Pereira, A.R., Borges, A., de Freitas, V., Mateus, N., Pina, F., Oliveira, J., “Acylated and Polyacylated anthocyanins as a pallet of natural colors”, XVI Encontro de Química dos Alimentos, Castelo Branco, 23 - 26 outubro 2022.

PANEL COMMUNICATIONS

1. Pereira, A.R., de Freitas, V., Mateus, N., Oliveira, J., “Acylated and polyacylated anthocyanins as a pallet of natural colors.", 2nd Dare to Change, Porto, 2023.

2. Pereira, A.R., Costa, C., de Freitas, V., Mateus, N., Rodrigues, A., Oliveira, J., “Chemical and structural characterization of dioxane lignin extract from vine pruning material – a powerful biopolymer”, 8th EuChemS Chemistry Congress - in Lisbon, from 28 August to 1 September 2022.

RESUMO

Anualmente, a agroindústria gera grandes quantidades de subprodutos. Devido à excessiva produção e à falta de uma gestão sustentável, estes subprodutos são convencionalmente descartados e rejeitados em aterro. No entanto, esta prática enfrenta fortes críticas devido às suas implicações ambientais, sociais e económicas. Dependendo da matéria-prima e do processamento aplicado, os subprodutos provenientes do setor agroalimentar são uma fonte rica em proteínas, lípidos e hidratos de carbono, podendo conter compostos funcionais como os polifenóis, com aplicação nas indústrias alimentar, farmacêutica e cosmética. A biomassa lignocelulósica, obtida como subproduto de diversas culturas agrícolas, como o milho, o trigo e a cana-de-açúcar, é uma fonte de celulose, hemicelulose e lignina, que são componentes que fornecem integridade estrutural, flexibilidade e durabilidade, tornando esta biomassa um recurso importante para a produção de materiais sustentáveis de valor acrescentado.

Neste trabalho de doutoramento foram explorados métodos para valorizar as varas da videira, um importante subproduto da indústria vinícola, com foco na extração e aplicação da lignina. As condições de extração foram otimizadas para uma metodologia mais sustentável, utilizando-se água-etanol no pré-tratamento da biomassa em substituição do tolueno descrito na literatura. Processos de diálise foram também aplicados para avaliar a eficácia na pureza da lenhina isolada, em que análises químicas demonstraram um baixo teor em compostos inorgânicos, proteínas e proantocianidinas. Características estruturais como o peso molecular, o grau de condensação e a quantidade de monómeros e grupos funcionais presentes na estrutura da lenhina foram também determinados. A caracterização das nanopartículas de lenhina também revelou forte potencial de aplicação inclusive uma elevada atividade antioxidante.

Considerando as propriedades da lenhina como o elevado peso molecular, capacidade de adsorção e a presença de vários grupos funcionais, os lignosulfonatos (LS), e as lenhinas kraft (KL) e organosolv (OL) foram aplicadas como potenciais agentes moduladores das propriedades físico-químicas do vinho do Porto. Nesta prova de conceito, as amostras de vinho do Porto foram colocadas em contacto com os diferentes tipos de lenhina utilizando duas concentrações diferentes (25 e 100 g/hL) por 7 e 30 dias. Os LS e a KL demonstraram uma boa eficácia na redução de proteínas e proantocianidinas, associadas respetivamente com a turbidez e a adstringência do

vinho. Os LS também proporcionaram uma diminuição na interação dos polifenóis com as proteínas salivares ácidas ricas em prolina, envolvidas na perceção da adstringência. Um ligeiro aumento na quantidade de antocianinas foi também detetado na presença dos LS e da KL sugerindo uma dissociação dos agregados antociânicos. Relativamente ao aroma, os LS demonstraram uma forte influência nos teores finais de alguns voláteis permitindo uma redução de aromas indesejados como é o caso dos aromas de queijo e resina, e potenciando o aroma frutado. Estudos colorimétricos revelaram que visualmente não seria percetível uma alteração significativa da cor do vinho após o tratamento com a lenhina.

Com base em resultados anteriores, os lignosulfonatos (LS) foram também avaliados como possíveis agentes de estabilização das antocianinas. Por recurso a uma abordagem multitécnica demonstrou-se a formação do complexo entre os LS e a cianidina-3-*O*-glucósida (C3G) e o efeito nas propriedades cromáticas e oxidativas da antocianina. Os resultados demonstraram uma forte dependência com o valor de pH. Parâmetros termodinâmicos sugerem a ocorrência de interações espontâneas, sendo a pH 1 o complexo formado por meio de interações electroestáticas, enquanto a pH 3, os fenómenos hidrofóbicos tiveram uma forte contribuição. Uma maior constante de afinidade entre LS e C3G foi determinada para pH 3. Estudos de espectroscopia de UV-visível revelaram um desvio batocrómico para o comprimento de onda máximo de absorção para todos os valores de pH testados (pH 1, 3 e 4) e um efeito hipercrómico para pH 3 e 4, como resultado da intensificação da cor vermelha característica destes compostos nesta gama de pH. Estudos eletroquímicos demonstraram uma proteção oxidativa da antocianina na presença dos LS, aumentando a aplicabilidade destes compostos como antioxidantes naturais. As antocianinas constituem um dos grupos mais relevantes dos polifenóis, com uma vasta aplicação tecnológica devido à paleta de cores naturais que apresentam e aos múltiplos benefícios que acarretam para a saúde humana, nomeadamente as propriedades antioxidante e anti-inflamatória. Podem ser facilmente extraídas de subprodutos, tendo a vantagem de existir em grande abundância na natureza e de a sua valorização ser facilitada relativamente às restrições legislativas impostas pela EFSA (Autoridade Europeia para a Segurança Alimentar), tendo por base as alegações nutricionais e de saúde sobre os alimentos.

A acilação é também uma das estratégias utilizadas para aumentar a estabilidade das antocianinas, face a problemas associados com a perda de cor. Neste trabalho de doutoramento, extratos de antocianinas com diferentes graus de acilação foram

avaliados como potenciais corantes naturais para a indústria alimentar. A flor de hibiscos (antocianinas não aciladas, HC), a couve roxa (maioritariamente antocianinas diaciladas, RC) e a flor de chá de ervilha borboleta (antocianinas poliaciladas, BPF) foram selecionadas como fontes naturais para obtenção dos extratos. O extrato BPF demonstrou uma total preservação da cor à temperatura ambiente durante 7 dias aos diferentes valores de pH, e também uma maior estabilidade térmica e resistência à descoloração pelo bissulfito comparativamente aos extratos de HC e RC. Os resultados apresentaram uma correlação entre a estabilidade e a estrutura, pelo que antocianinas com estruturas mais complexas demonstraram uma maior estabilidade química e consequentemente, cromática. A aplicação em matrizes alimentares gelificantes resultou em diferentes cores apelativas e desafiantes para a indústria alimentar, dependentes do valor de pH e da composição química da matriz.

O efeito da glicosilação na estabilidade das antocianinas foi também avaliado neste trabalho de doutoramento, utilizando-se a malvidina monoglucósida (M3G) e diglucósida (M3,5diG). O comportamento destas moléculas foi estudado numa gama de pH, chamada de pH de transição, entre pH 7 e 9, onde a degradação ocorre de forma irreversível e mais rapidamente do que os diferentes estados de equilíbrio. Os resultados obtidos apontam para uma cinética de degradação maior no caso da antocianina monoglucósida. Análises de massa demonstraram que a via maioritária de degradação da M3G consiste na formação de estruturas mais complexas, nomeadamente dímeros e trímeros colorimétricos que mitigam a perda de cor da antocianina, fenómeno observado por espetroscopia de UV-visível. Estudos de Ressonância Magnética Nuclear (RMN) comprovaram ainda uma segunda via de degradação com a perda da unidade de glucose originando a forma aglicona (antocianidina), que posteriormente se degrada nos seus compostos de formação, o ácido siríngico e o 2,4,6-trihidroxibenzaldeído. A M3,5diG, entra em equilíbrio com uma nova espécie ($B4^{2-}$) identificada por espetroscopia de UV-visível e RMN, que retarda o estabelecimento do equilíbrio. O perfil cromatográfico não evidenciou a formação de estruturas oligoméricas que pudessem contribuir para a cor final em solução.

Palavras-chave: subprodutos, valorização, antocianinas, acilação, estabilidade cromática, copigmentação intramolecular, glicosilação, lenhina, adstringência, constante de associação, interações não covalentes, RMN, UV-vis, ITC, fluorescência, redox.

ABSTRACT

Annually, the agro-industry generates large quantities of byproducts. Due to excessive production and a lack of sustainable management, these byproducts are conventionally discarded and landfilled. However, this practice faces strong disapproval due to its environmental, social, and economic implications. Depending on the raw material and processing applied, byproducts from the agri-food sector are rich in proteins, lipids, and carbohydrates such as sugars and fibers. They can also contain functional compounds such as polyphenols with applications in the food, pharmaceutical, and cosmetic industries. Lignocellulosic biomass, obtained as by-products from various crops such as corn, wheat, and sugarcane, is a source of cellulose, hemicellulose, and lignin. These components provide structural integrity, flexibility, and durability, making this biomass a valuable resource for value-added sustainable products.

This doctoral research explores methods to transform vine shoots, a major by-product of the wine industry, into significant materials focusing on the extraction and application of lignin. Extraction conditions were optimized for greener methodology, using water-ethanol in biomass pretreatment instead of toluene described in the literature. Dialysis processes were also applied to assess the effectiveness of isolated lignin purity, with chemical analyses showing low levels of inorganic compounds, proteins, and proanthocyanidins. Structural characteristics such as molecular weight, condensation degree, and the amount of monomers and functional groups present in the lignin structure were determined using various analytical techniques. The characterization of lignin nanoparticles also revealed a strong potential for application, including a higher antioxidant activity.

Considering lignin's properties, such as high molecular weight, adsorption capacity, and the presence of various functional groups, lignosulfonates (LS), kraft lignin (KL), and organosolv lignin (OL) were applied as potential modulators of the physicochemical properties of Port wine. In this proof-of-concept study, Port wine samples were treated with different types of lignin at two concentrations (25 and 100 g/hL) for 7 and 30 days. LS and KL demonstrated good efficacy in reducing proteins and proanthocyanidins, associated with wine turbidity and astringency, respectively. LS also reduced the interaction between polyphenols and acidic proline-rich salivary proteins, involved in astringency perception. A slight increase in anthocyanin content was also detected in

the presence of LS and KL, suggesting a dissociation of anthocyanin aggregates. Concerning the wine aroma, LS significantly influenced the final volatile contents, reducing undesirable cheese and resin odors while enhancing fruity aromas. Colorimetric studies revealed no visually perceptible change in wine color after lignin treatment.

Regarding the results obtained in previous work, lignosulfonates (LS) were also evaluated as potential stabilizing agents for anthocyanins, employing a multi-technique approach to demonstrate the formation of the LS-C3G (C3G, cyanidin-3-*O*-glucoside) complex and its effects on the chromatic and oxidative properties of anthocyanins. The results showed a strong pH dependency. Thermodynamic parameters suggested spontaneous interactions, with electrostatic interactions forming the complex at pH 1, and hydrophobic interactions contributing significantly at pH 3. A higher affinity constant between LS and C3G was determined at pH 3. UV-visible spectroscopy studies revealed a bathochromic shift for the maximum absorption wavelength across all tested pH values (pH 1, 3, and 4) and a hyperchromic effect at pH 3 and 4, resulting in an intensified red color characteristic of these compounds within this pH range. Electrochemical studies indicated oxidative protection of anthocyanins in the presence of lignosulfonates, enhancing the applicability of these compounds as natural antioxidants. Anthocyanins are among the most significant groups of polyphenols, offering extensive technological applications due to their natural color palette and numerous health benefits, including antioxidant and anti-inflammatory properties. They can be easily extracted from byproducts since they are abundantly available in nature. Additionally, the valorization is facilitated by fewer legislative constraints imposed by the EFSA (European Food Safety Authority) based on nutritional and health claims concerning foods.

Acylation is another strategy used to enhance the stability of anthocyanins, addressing issues related to color loss. In this doctoral research, extracts of anthocyanins with varying degrees of acylation were evaluated as potential natural colorants for the food industry. Hibiscus flowers (non-acylated anthocyanins, HC), red cabbage (diacylated anthocyanins, RC), and butterfly pea flower tea (polyacylated anthocyanins, BPF) were selected as natural sources of the extracts. The BPF extract maintained complete color preservation at room temperature for 7 days across a range of pH values, exhibiting higher thermal stability and greater resistance to bisulfite discoloration than the HC and RC extracts. The results demonstrated a correlation between stability and structure, suggesting that anthocyanins with more complex

structures have greater chemical and chromatic stability. When applied to gelatine food matrices, the extracts produced a variety of appealing and distinctive colors, influenced by the pH and the chemical composition of the matrix, offering potential benefits for the food industry.

The effect of glycosylation on anthocyanin stability was also evaluated in this doctoral research, using malvidin-3-*O*-glucoside (M3G) and malvidin-3,5-*O*-diglucoside (M3,5diG). The behavior of these molecules was studied within a pH transition range of 7 to 9, where degradation occurs irreversibly and more rapidly than at other equilibrium states. The results indicated that the monoglucoside anthocyanin (M3G) had a higher degradation rate. Mass spectrometry analyses demonstrated that the primary degradation pathway of M3G involves the formation of more complex structures, such as colorimetric dimers and trimers, which mitigate anthocyanin color loss, as observed by UV-visible spectroscopy. Nuclear Magnetic Resonance (NMR) studies confirmed a secondary degradation pathway involving the loss of the glucose unit, leading to the aglycone form (anthocyanidin), which further degrades into its constituent compounds, syringic acid and 2,4,6-trihydroxybenzaldehyde. M3,5diG enters equilibrium with a new species ($B4^{2-}$), identified by UV-visible spectroscopy and NMR, which delays the establishment of equilibrium. The chromatographic profile did not show the formation of oligomeric structures that could contribute to anthocyanin color.

Keywords: byproducts, valorization, anthocyanins, acylation, color stability, intramolecular copigmentation, glycosylation, lignin, protein haze, astringency, association constant, non-covalent interactions, NMR, UV-vis, ITC, Fluorescence, Redox.

TABLE OF CONTENTS

LIST OF TABLES

LIST OF FIGURES

LIST OF ABBREVIATIONS

A	Anthocyanin quinoidal base
AH^+	Anthocyanin flavylium cation
Abs	Absorbance
ANOVA	Analysis of variance
B	Anthocyanin hemiketal
BPF	Butterfly pea flower
BCA	Bicinchoninic acid assay
BSA	Bovine serum albumin
C*c*	Anthocyanin *cis*-chalcone
C*t*	Anthocyanin *trans*-chalcone
^{13}C NMR	Carbon-13 nuclear magnetic resonance
DPPH	2,2-diphenyl-1-picrylhydrazyl
FTIR	Fourier-transform infrared spectroscopy
GC-MS	Gas chromatography-mass spectrometry
HC	Hibiscus calyxes
HPLC-DAD	High-performance liquid chromatography with diode-array detection
ITC	Isothermal titration calorimetry
LC-MS	Liquid chromatography-mass spectrometry
LNPs	Lignin Nanoparticles
LS	Lignosulfonates
KL	Kraft lignin
M3G	Malvidin-3-*O*-glucoside
M3,5diG	Malvidin-3,5-diglucoside
NMR	Nuclear Magnetic Resonance
NPs	Nanoparticles
OL	Organosolv lignin
PACs	Proanthocyanidins
^{31}P NMR	Phosphorus-31 nuclear magnetic resonance
RC	Red cabbage
SP	Salivary proteins
UV	Ultraviolet
UV-vis	Ultraviolet-visible

THESIS LAYOUT

This thesis is structured into four chapters. Chapter I introduces polyphenols based on anthocyanins and lignin, highlighting their abundance as by-products. Discussions on the chemistry and reactivity of anthocyanins are presented, emphasizing stabilization processes. Additionally, a detailed review of lignin extraction methods is included, along with an in-depth explanation of its characterization methods, chemical properties, and applications including the preparation of nanoparticles.

Chapters II and III discuss the results of the PhD work. The formal organization of these chapters does not necessarily follow the chronological order of the experimental activities but aims to deliver the results clearly and concisely. Each chapter´s content was adapted from papers published or submitted in a peer-reviewed journal. Chapter II focuses on studies involving lignin and its technological applications, organized into three parts. Part A is dedicated to the vine shoots reuse, a byproduct of winemaking, to extract lignin through greener and environmentally friendly methodologies. It was preparing nanoparticles as a viable strategy for diverse applications, with an emphasis on antioxidant activity. Part B explores the use of lignosulfonates, kraft lignin, and organosolv lignin as modulating agents for the physicochemical properties of wine. This section assesses various parameters of wine samples to determine the effects of lignin on wine quality. In a sequence of results observed in Part B, Part C explores the lignosulfonates as potential agents for stabilizing the color and oxidative properties of anthocyanins to increase their application as natural dyes and antioxidants.

Chapter III delves into the chemistry and stability of different anthocyanins under various conditions. It is divided into two parts. Part A provides a comparative study of anthocyanin-based extracts with different acylation patterns, evaluating the colorimetric and thermal stability focus on the food industry. Part B presents the degradation mechanisms of anthocyanins with different glycosylation patterns, identifying the degradation rates and the primary degradation products using a multi-approach technique.

Chapter IV provides a general conclusion of the main results obtained, offering a comparative analysis of the results. Final remarks and future perspectives related to the research activities are also discussed in this chapter.

SCOPES AND OBJECTIVES

Over the years, the global population has grown rapidly, with projections estimating it will reach 9 billion by 2050 (1). This population growth causes substantial changes on the planet to satisfy human demands. Although the food industry is under excessive pressure due to a constant demand for food, feeds, and fiber-rich crops, other sectors such as textiles, cosmetics, and pharmaceutical industries are struggling to keep up with population expansion. The most pressing problem, however, is the environmental impact. In addition to deforestation, soil degradation, and greenhouse gas emissions generated by intensive agricultural methods, all industries rely substantially on resource-intensive operations such as water consumption, chemical use, and waste production – about one-third of all food produced is lost or wasted yearly (2).

In response, industries are trying to reduce their ecological footprint by adopting more sustainable and environmentally friendly practices. Government organizations support this transition through regulatory frameworks, incentives for sustainability, consumer education campaigns, and investments in research and innovation (3). Agricultural research has shifted towards regenerative techniques, organic practices, and precision agriculture, promoting soil health, biodiversity conservation, and water efficiency. Consumers are also increasingly favoring plant-based diets, alternative protein sources, and natural extracts as colorants to meet nutritional needs while minimizing the environmental impact of food production. Similarly, the textile industry is exploring biodegradable materials (organic cotton, recycled fibers, natural dyes) and natural dyes, and the cosmetics industry is developing natural formulations, eco-friendly packaging, and sustainable alternatives.

In this sense, population growth exacerbates the demand for food and natural resources, while increasing food and industrial waste production. According to the Food and Agriculture Organization of the United Nations (FAO) report, around 828 million people were affected by hunger in 2021, and nearly 3.1 billion people could not afford a healthy diet in 2020 (3). Over 931 million tons of food are wasted annually, 61 % of which comes from households, 26 % from food service, and 13 % from retail (4). A significant portion of this waste corresponds to by-products, including damaged raw materials, bagasse, leaves, seeds, peels, bran, oilseed cakes, molasses, and other food processing byproducts that have significant levels of dietary fiber and bioactive

compounds with greater nutritional value. Scientific publications addressing food waste and its impacts have increased exponentially, reaching 2,701 documents in 2022 (5). The scientific community is also focusing on utilizing agri-food and industrial by-products to generate new foods, natural and bioactive products, and innovative, sustainable approaches that make these processes economical and circular.

One of the most consumed products around the world is fruit and vegetables, which represent more than 44 % of all food waste (6). Fruit pomace, a by-product of fruit juice extraction and processing, is rich in polyphenols such as flavonoids and phenolic acids, which offer various health benefits, including cardiovascular diseases, and anti-inflammatory and antioxidant effects. Red grape pomace extracts, which contain anthocyanins, have long been used in food preparation and are approved as food additives. Anthocyanins are notable among polyphenols for their range of natural colors, from red and orange to blue and purple. Anthocyanin-based colorants are increasingly popular in pastries, fruit yogurts, and fruit-flavored dry mixes (7). However, their application in food matrices is often limited due to instability under various food processing and storage conditions, such as pH, temperature, enzyme activity, chemical interactions, and exposure to light and oxygen. To address this, several stabilizing strategies have been developed to enhance the color performance of anthocyanins, which is crucial for their use in food, cosmetic, and medicinal applications. The shift from synthetic to natural colorants has driven extensive research in this area. The growing demand for sustainable practices and natural products aligns with the need for innovative approaches to utilize food by-products and develop stable, natural colorants.

Other valuable byproducts include lycopene from tomato processing waste, which adds color to foods and has antioxidant capacity (8). Carbohydrates such as pectin are derived from citrus or apple juice production and are used in the pharmaceutical, cosmetic, and food industries (9). Wine by-products contain biomolecules such as fiber, lipids, proteins, antioxidants, and phenolic compounds, making them suitable for nutritional supplements. Protein hydrolysates and collagen peptides can be extracted from fish and meat processing, with benefits such as antioxidant, antihypertensive, and antimicrobial activities, and improved skin, joint, and bone health (10, 11). Grain processing residues like wheat and rice bran are high in dietary fibers that aid digestive health, weight management, and blood sugar regulation, and act as prebiotics (12).

Pineapple plant waste leaves are used to create traditional clothing, reducing the need for additional environmental resources (13). Lignocellulosic biomass, a by-product of agriculture, food processing, and forestry, can be transformed into biochemical, biofuel, and polymer products. Lignin, an aromatic polymer from wood or agricultural residues, can be converted into value-added products like enzymes, polyhydroxyalkanoates, microbial lipids, and vanillin (14).

With the growing global population, the demand for food and innovative bioproducts has increased, driving companies to harness woody biomass for alternative proteins, food or feed additives, and novel foods. Despite these efforts, the global economy's circularity is only 7.2 %, where 90 % of materials are wasted, lost, or unavailable for reuse (15), highlighting the need for sustainable and inventive alternatives.

OBJECTIVES

The main purpose of this PhD work was to explore and develop high-value applications for natural compounds that can be derived from byproducts, focusing on two main areas: the extraction, chemical characterization, and potential technological applications of lignin as a byproduct to enhance circularity and sustainability in industrial practices, and stabilization of anthocyanin-based extracts as natural colorants and antioxidants for food applications.

1. A promising study that integrated the wine industry and lignin valorization proposes using vine shoots as lignocellulosic biomass for lignin extraction. This sustainable practice aimed to reuse a byproduct while obtaining a value-added biopolymer with broad technological applications. Optimization of isolation conditions using environmentally friendly methods, analysis of lignin's final chemical composition impact, and preparation of nanoparticles aimed to extend their applicability in environmental and agricultural contexts.

2. Due to their high molecular weight, adsorption capacity, and different functional groups in their structure, three types of lignin were explored as potential modulating agents to enhance wine quality. The research aimed to assess the performance of these lignin types in addressing issues affecting wine stability, clarity, texture, taste,

and production efficiency, utilizing Bentonite as a commercial fining agent for comparative purposes.

3. Investigate lignosulfonates as potential stabilizing agents for the red color of anthocyanins through the formation of lignin-anthocyanin complexes. A combination of ITC, UV-Vis, fluorescence, voltammetry, and FTIR techniques was employed to study the chemical properties of the complex and evaluate lignosulfonates' effects on the color and oxidative properties of cyanidin-3-*O*-glucoside.

4. Evaluate the impact of acyl groups on the chemical stability of anthocyanins, particularly focusing on their chromatic properties for incorporation into food matrices as replacements for synthetic dyes; analyze the performance of the extracts when exposed to different factors associated with the food production, including pH, temperature, and the presence of bisulfite and investigate matrix effects on final colors.

5. Explore the chemical stability and degradation mechanisms of malvidin-3-O-glucoside (M3G) and malvidin-3,5-O-diglucoside (M3,5diG), particularly in the transition pH range between the acidic and basic medium. Given M3G's potential incorporation into diverse food matrices, it is crucial to understand the chemical species present in the solution and their degradation rates.

CHAPTER I

GENERAL INTRODUCTION

1. POLYPHENOLS

Phenolic compounds, commonly known as polyphenols, are a class of naturally occurring molecules produced by the secondary metabolism of plants. They are important elements of various foods having physiological and morphological significance. They can be found in plants, fruits, vegetables, and beverages including tea, coffee, and wine (15). Polyphenols are recognized for their antioxidant properties, contributing to their possible health benefits such as anti-inflammatory, antibacterial, antidiabetic, cardioprotective, neuroprotective, and vasodilator effects (16). Dietary polyphenols are known to have powerful antioxidant capabilities that protect against reactive oxygen species and cellular oxidative stress (OS), potentially avoiding OS-related pathological illnesses or diseases (17, 18). According to current studies, polyphenols may be an efficient source of skin protection against ultraviolet (UV) radiation (UVA and UVB) (19). Polyphenols have received special attention in scientific research due to their extensive biological activity and possible medical applications. In addition, food polyphenols have steadily made their way into industrial production and cosmetic applications as food science and technology have advanced. Chemically, polyphenols are distinguished by the existence of a phenolic ring system with one or more hydroxyl groups and a wide structural diversity of molecules with various methoxylation and glycosylation patterns (20). Generally, polyphenols are divided into two classes, non-flavonoids and flavonoids (Table 1). Non-flavonoids include phenolic acids like hydroxycinnamic acids (for example chlorogenic acid, ferulic acid, caffeic acid, etc.) and hydroxybenzoic (represented by gallic acid, protocatechuic acid, etc.), as well as other derivatives like stilbenes. Flavonoids are molecules that have a low molecular weight and a common C6-C3-C6 skeleton called the flavanic nucleus, which is composed of two benzenic rings (A and B) and a heterocyclic pyran ring C. These include anthocyanins, flavanones, flavones, flavonols, isoflavones, and flavan-3-ols (21), and are widely found in foods. Depending on the phenolic class, the molecules exhibit diverse structural characteristics and, as a result, distinct biological functions (22).

Table 1 – General chemical structures of the most common non-flavonoids and flavonoids along with examples of their natural sources.

NON-FLAVONOIDS	HYDROXYCINNAMIC ACIDS 	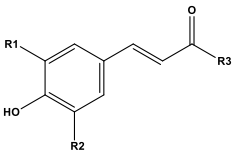	R1=R3=OH; R2=H: CAFFEIC ACID R1=OCH_3; R2=H; R3=OH: FERULIC ACID R1=R2=H; R3=OH: *p*-COUMARIC ACID R1=R2=OCH_3; R3=OH: SINAPIC ACID R1=OH; R2=H; R3= $C_7H_{11}O_6$ CHLOROGENIC ACID
	HYDROXYBENZOIC ACIDS 	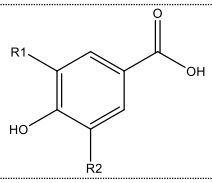	R1=R2=OH: GALLIC ACID R1=R2= OCH_3: SYRINGIC ACID R1=H; R2= OCH_3: VANILLIC ACID R1=R2=H: *p*-HYDROXYBENZOIC ACID R1=H; R2= OH: PROTOCATECHUIC ACID
	STILBENES 	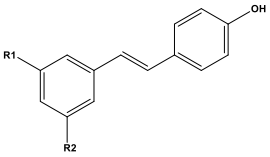	R1=OH; R2=OH: RESVERATROL R1= OCH_3; R2=OCH_3: PTEROSTILBENE
FLAVONOIDS	FLAVONOLS 	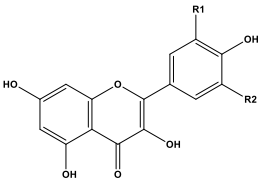	R1=H; R2=H: KAEMPFEROL R1=OH; R2=H: QUERCETIN R1=OH; R2=OH: MYRICETIN
	FLAVONES 	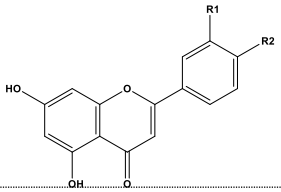	R1= H; R2= OH: APIGENIN R1= OH; R2= OH: LUTEOLIN
	FLAVANOLS 	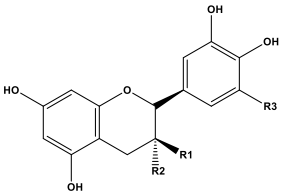	R1= OH; R2= H; R3= H: CATECHIN R1= H; R2= OH; R3= H: EPICATECHIN R1= OH; R2= OH; R3= OH: GALLOCATECHIN
	ISOFLAVONES 	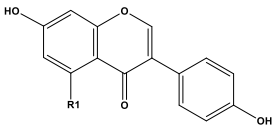	R1= H: DAIDZEIN R1= OH: GENISTEIN
	FLAVANONES 	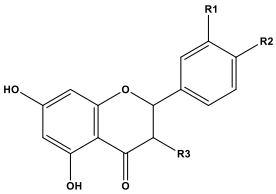	R1= H; R2= OH; R3= H: NARINGENIN R1= OH; R2= OCH_3; R3= OH: HESPERETINE
	ANTHOCYANIDINS 	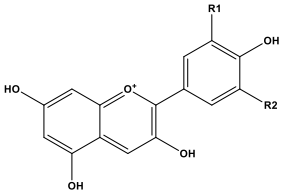	R1= H; R2= H: PELARGONIDIN R1= OH; R2= H: CYANIDIN R1= OH; R2= OH: DELPHINIDIN R1= OCH_3; R2= OH: PETUNIDIN R1= OCH_3; R2= H: PEONIDIN R1= OCH_3; R2= OCH_3: MALVIDIN

2. ANTHOCYANINS

Anthocyanins (from the Greek terms *Anthos* meaning flower and *kyanos* meaning blue) are natural water-soluble pigments present in diverse fruits, vegetables, and flowers, giving them colors ranging from red to orange, purple, and blue. They accumulate in the vacuoles of various cells and tissues and have a crucial role in processes like pollination and seed distribution. They can also act as antioxidants, phytoalexins, and as antibacterial agents. Furthermore, because of their high light absorption, anthocyanins protect the plant tissues from UV-induced damage such as photo-inhibitory and photo-oxidative effects (23, 24). In addition to their physiological functions in plants, polyphenols are commonly found in the human diet, notably as a result of the ingestion of colored fruits (grapes, blackberries, raspberries, strawberries, cherries, etc.) and dark-colored vegetables (red cabbage, beans, red onion, red radish, purple potato, etc.). Anthocyanins exist in different amounts depending on the type of fruit or vegetable, and in the case of vegetables, these compounds have a more complex structure than those present in fruits, with one or two acyl groups. Mediterranean countries are prominent consumers of anthocyanins due to their diet rich in reddish berries and other red and blue fruits and vegetables, as well as red wine (25). In Europe, the consumption of anthocyanins ranges from 18.4 mg/per day (Spain) to 64.9 mg/per day (Italy). In the United States of America, Australia, and Asian countries, the intake is approximately 12.5, 24.2, and 37 mg per day per person, respectively (26). Several types of research have been conducted to employ anthocyanins as natural colors in the food industry, with a synergistic approach based on their biological characteristics and bioactivities, which translate into positive benefits on human health (such as anti-inflammatory, antimicrobial, and antiproliferative properties) (27).

2.1. CHEMICAL PROPERTIES OF ANTHOCYANINS

Chemically, anthocyanins are distinguished by their flavylium cation structure, which derives from various glycosylation, hydroxylation, and methoxylation patterns of a 2-phenyl-1-benzopyrylium moiety. As well as in the aglycone form, known as anthocyanidins, the structure comprises two aromatic rings (A and B rings) linked by a heterocyclic pyranic ring (C ring) (28, 29) (Table 2). The locations of the hydroxyl groups, and the nature, position, and number of sugar moieties linked to the structure core, as well as the nature and number of aliphatic or aromatic acids bonded to the sugars,

contribute to the diverse chemical structures of anthocyanins (28, 30). Glycosylation and acylation of anthocyanins influence their physical and chemical properties, specifically the polarity and molecular size of the molecule, which affect the stability and reactivity of these compounds. The low solubility and stability of the aglycone form make that these structures practically do not exist in nature. The most common six anthocyanidins found in nature from which 95 % of anthocyanins are derived are delphinidin, cyanidin, petunidin, peonidin, pelargonidin, and malvidin which differ in the hydroxylation and methoxylation pattern on ring A and B, changing the color from orange-red to purple-blue at acidic pH (Table 2). The addition of hydroxyl groups in ring B promotes a bathochromic shift in the maximum absorption wavelength, whereas methylation causes a hypsochromic shift (31). For acidic conditions, the maximum absorption wavelength of anthocyanins is typically located at 465 − 550 nm (visible region) and 270 − 280 nm (UV region). In nature, the most prevalent non-methylated anthocyanidins are cyanidin, delphinidin, and pelargonidin glucosides, which are distributed in 80 % of pigmented leaves, 69 % of fruits, and 50 % of flowers. The six anthocyanidins are distributed in different amounts in the edible parts of flowers cyanidin (50 %), pelargonidin (12 %), peonidin (12 %), delphinidin (12 %), petunidin (7 %), and malvidin (7 %), being the cyanidin-3-*O*-glucoside is the most common anthocyanin in the natural sources (32). More than 27 anthocyanidins with the same carbon-C15 skeleton and 635 anthocyanins have been reported (33).

Table 2 - Chemical structures of the most common anthocyanidins found in nature and the respective maximum absorption wavelength observed in methanol acidified with hydrochloric acid.

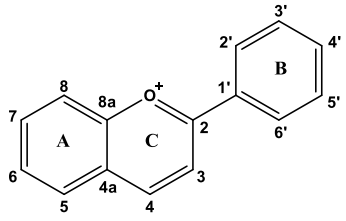

Anthocyanidin	Substitution pattern							λ_{max} (nm)	Color
	3	5	6	7	3'	4'	5'		
Cyanidin	OH	OH	H	OH	OH	OH	H	535	Magenta
Pelargonidin	OH	OH	H	OH	H	OH	H	520	Red
Peonidin	OH	OH	H	OH	OMe	OH	H	532	Magenta
Delphinidin	OH	OH	H	OH	OH	OH	OH	546	Purple
Petunidin	OH	OH	H	OH	OMe	OH	OH	543	Purple
Malvidin	OH	OH	H	OH	OMe	OH	OMe	542	Purple

The glycosylation enhances the anthocyanin stability by creating an intramolecular H-bonding system within the anthocyanin molecule (34). Generally, the most prevalent anthocyanins are both 3-*O*-glycosides and 3,5-*O*-diglycosides; however, glycosylation of the C-7, C-3', and C-5' has also been verified. Glucose, rhamnose, galactose, xylose, and arabinose are the most common sugars in anthocyanin structure (Table 3) and can occur as monosaccharide, disaccharide, and trisaccharide (30, 34). Anthocyanins can occur in nature as acylated anthocyanins, particularly in edible pigmented vegetables and tubers. Sugar units can establish a covalent ester bond with one or more aliphatic or aromatic acids, including aliphatic acids (e.g. acetic, malonic, oxalic, and succinic acids) and aromatic acids (e.g., caffeic, coumaric, ferulic, hydroxybenzoic, and sinapic acids - Table 3). Acyl substituents are often linked to the C3 sugar, esterified to the 6-OH, or, less frequently, to the 4-OH group of the sugar (35). Cinnamic acids can contain glycosidic sugars, and aromatic and aliphatic acylation can happen within the same molecule, resulting in a polyacylated structure. In the same way that glycosylation promotes some modifications in the properties and reactivity of anthocyanins, the addition of acyl groups in the anthocyanin structure also affects these compounds. Depending on the position and number of acyl residues different arrangements of anthocyanin molecules can be observed (36). Contrarily to the glycosylation, the addition of acyl groups reduces polarity, leading to a reduction in water solubility. (35, 37). On the other hand, the acylation with cinnamic acids produces a bathochromic shift in the maximum absorption wavelength of the anthocyanin coupled with a strongly increased absorptivity (hyperchromic effect) (27). In general, the increase in the complexity of the anthocyanin structure by different glycosylation and acylation patterns demonstrates remarkable stability to modifications in pH, temperature, and light exposure (38, 39). This can be explained by the occurrence of intra- and intermolecular copigmentation and/or self-association phenomenon (35, 40).

Table 3 - Chemical structure of the most common sugars and aromatic and aliphatic acyl units present in anthocyanins.

SUGARS UNITS	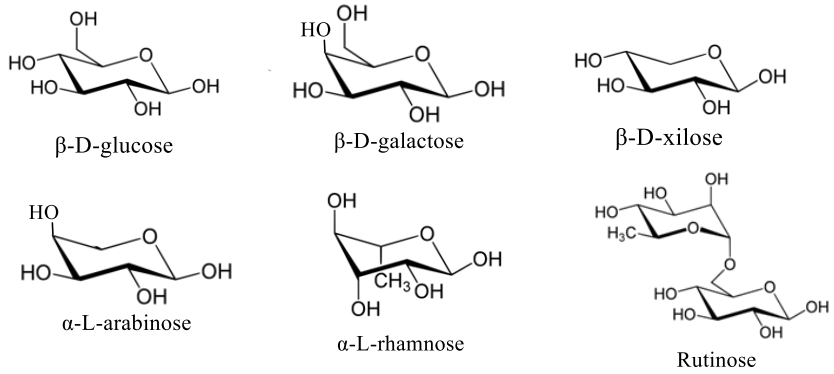
ACYL UNITS	ALIPHATIC ACIDS 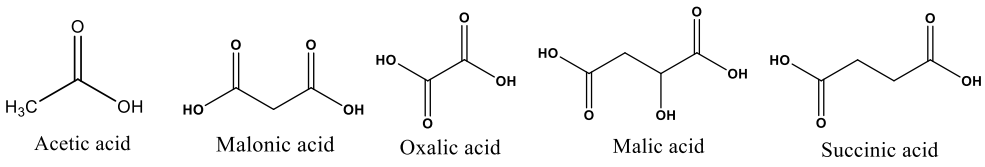 AROMATIC ACIDS 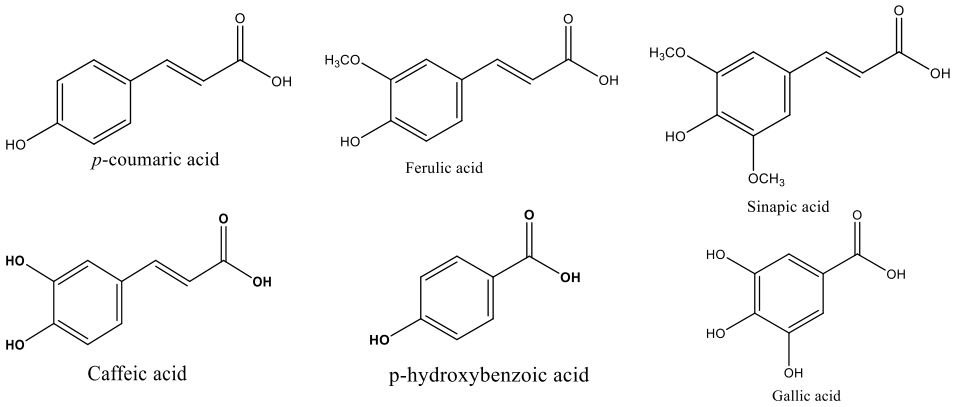

2.2. REACTIVITY OF ANTHOCYANINS

The reactivity of anthocyanins is determined by the type of ring in their structure, particularly due to their unique pyrylium nucleus (C-ring). The presence of an unsaturated central ring in all flavonoid classes, except flavanols (monomers and polymers - tannins), which have a saturated central ring, increases electron delocalization, resulting in a higher maximum absorption wavelength ranging from yellow for flavones and flavonols to red and blue for anthocyanins (41). In addition, the

central pyranic C-ring tends to have a natural cationic charge for the flavylium forms of anthocyanins, delocalized on positions C2 and C4. Therefore, C2 and C4 of the C-ring react as a hard and soft electrophilic center (Figure 1), respectively, and undergoes nucleophilic addition (36, 41). As a result, they react with hard (O-centered) and soft (S- and C-centered) nucleophiles, driven by local charge and interactions between the frontier molecular orbitals (HOMO of nucleophiles and LUMO of electrophiles), respectively (36).

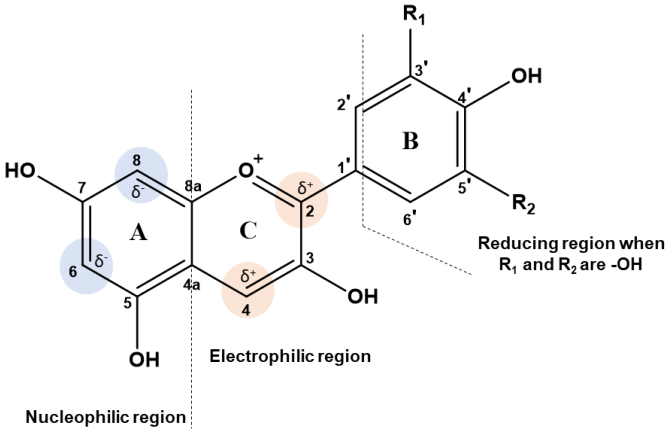

Figure 1 - General reactivity scheme on anthocyanins (anthocyanidin structure).

In the case of the C2 position, the most reported reaction for anthocyanins is the nucleophilic attack of water on flavylium cation giving the hemiketal (uncolored species), while on the C4 position, the reaction with the bisulfite (SO_2) which is used as an antimicrobial and anti-browning agent in food industry thus yielding colorless adducts (Figure 2) (36, 42). Another type of reaction observed at C4 involves the cationic form of anthocyanins, forming new pigments known as pyranoanthocyanins. This reaction entails the creation of a second pyranic ring. It is mediated by the electron-deficient C4 and the 5-hydroxyl group of the anthocyanin interacting with compounds possessing a polarizable double bond (43-46). On the other hand, anthocyanins can act as nucleophiles and undergo electrophilic aromatic substitutions at positions C6 and C8 in the A-ring due to hydroxyl groups at C5/C7 (Figure 2). The hydrogens at C6 and C8 assumed particular positions that undergo hydrogen-deuterium nuclear exchange with deuterium in deuterated solvents, which does not occur for the hydrogens of rings B and C that are directly bonded to carbon skeleton (47). Phenolic OH groups of the flavylium cation at C4′, C5, and C7 are fairly acidic because of conjugation with the electron-withdrawing pyrylium ring (36). Ring B possesses a catechol-type structure, and depending on the pattern of hydroxylation this nucleus works mainly as a reducing

agent. Once oxidized, it can undergo either coupled oxidation or Michael addition as a strong electrophile, to recover the catechol structure. The presence of at least two adjacent hydroxyl groups on the B-ring, such as cyanidin and delphinidin which contain 3',4'-dihydroxyl groups, allow a readily ions metal chelation exhibiting bathochromic shifts in the visible spectrum. Related to their antioxidant activity, anthocyanins containing ortho-dihydroxyl groups can scavenge hydroxyl radicals by inhibiting HO• production and preventing iron-induced lipid peroxidation. At physiological pH ranges, the ortho-dihydroxyl group facilitates the formation of anthocyanin-metal copigment complexes with organic compounds like ascorbic acid. Conversely, the presence of a methoxy group at the ortho position 4 on the B ring of malvidin diminishes its ability to form complexes with metal ions (48).

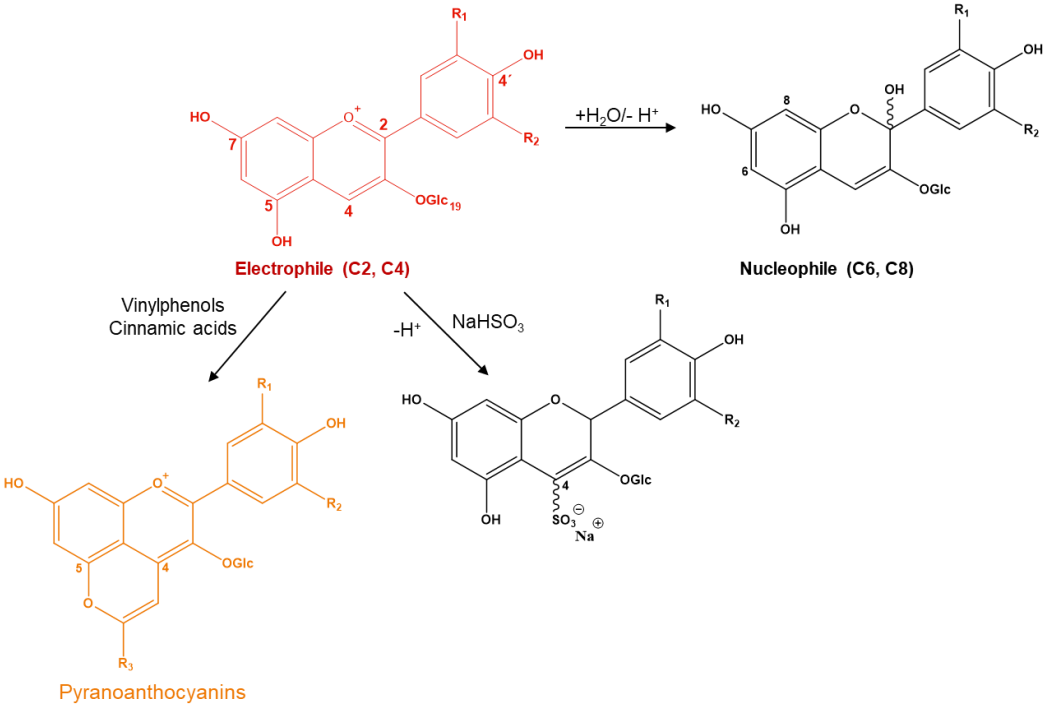

Figure 2 - General chemical reactivity sites of anthocyanins. Adapted from (49).

2.3. STABILITY OF ANTHOCYANINS – DRIVING FACTORS

Regarding the natural color palette associated with anthocyanins and the increased water solubility due to the presence of sugar moieties, these compounds are proposed as prospective candidates for natural colorants to replace synthetic dyes employed, particularly in the food industry. Nonetheless, anthocyanin stability is affected by many exogenous factors, including the pH and temperature of the manufacturing and storage

medium, anthocyanin concentration, light and oxygen exposure, solvents, and the presence of metabolites such as enzymes, ascorbic acid, sulfur dioxide, and other reactive compounds (41). The low stability of anthocyanins to various chemical and enzymatic reactions can lead to degradation or changes in their chemical structure through three mechanisms: cleavage, derivatization, and polymerization. In general, these reactions result in colorless or browned products, which restricts their application in food matrices. This phenomenon can impact the appearance, functionality, and biological activity of foods containing anthocyanins (50). One of the problems in the food industry is developing novel processing technologies that efficiently reduce anthocyanin losses or adequately handle anthocyanin reactions to provide more stable and appealing colors.

2.3.1. pH AND EQUILIBRIUM FORMS OF ANTHOCYANINS

The pH of anthocyanin solutions is an important factor component that affects their stability. Anthocyanins exhibit a pH-dependent equilibrium where their structure and color adapt to varying pH conditions (Figure 3) (51, 52). At very acidic conditions (pH < 2), the predominant species is the red flavylium cation (AH^+), which is positively charged. As pH increases to 3 − 4, the flavylium cation participates in two simultaneous reactions: (I) proton-transfer reaction to form the quinoidal base (A) and (II) hydration reaction at position C2 or C4 yielding the non-colored hemiketal (B). Subsequently, the hemiketal undergoes a tautomerization process (opening of the pyranic ring) forming *cis*-chalcone (C*c*) followed by an isomerization mechanism giving the *trans*-chalcone (C*t*), both with a yellowish color. Although the proton transfer reactions occur more rapidly than nucleophilic attacks from water, the species B, C*c*, and C*t* in equilibrium are more stable. At pH values higher than 7, the quinoidal base can be deprotonated to originate the anionic bases (A^-, and A^{2-}) with purple and blue colors. The molar fraction of the different structures coexistent in solution over time is dependent on the pH, anthocyanin structure, temperature, concentration, and time.

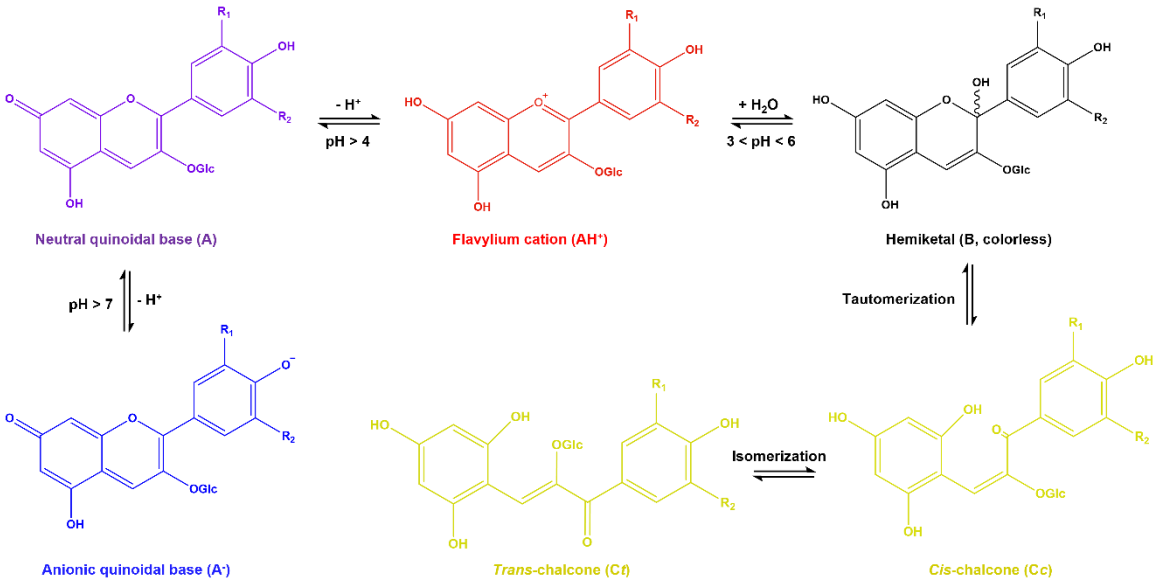

Figure 3 - Representative scheme for anthocyanins chemical equilibrium forms in aqueous solution. The substituents R1 and R2 can be OH and/or OCH_3 groups depending on the type of anthocyanin.

2.3.2. TEMPERATURE, OXYGEN, AND LIGHT EXPOSURE

Temperature is a crucial factor in the food manufacturing and storage processes. Thermal processing is the most common method for commercial fruit juice manufacturing and is employed in mixed milk juice beverages to assure microbiological safety and preservation without refrigeration. In some beverages, the pasteurization process can reach temperatures of 100 ºC (53). In general, the stability of anthocyanins decreases as the temperature rises (first-order kinetics), and the great loss of anthocyanins is correlated with the degradation reaction during the heating process (54). In a pH range between 2 − 4, the higher temperatures shifted the equilibrium for the formation of *trans*-chalcone seeing a paler anthocyanin solution after heating (55). Subsequently, the higher temperatures promote the hydrolysis of sugar moieties forming unstable anthocyanidins which can be degraded into uncolored and dangerous substances for human health (56, 57).

The presence of oxygen is another factor with the capacity to degrade anthocyanins, as the combination of heat and oxygen content was determined as the most specific accelerating agent responsible for the deterioration of anthocyanins color during storage (54, 58). This degradation by the oxygen can occur by two mechanisms, namely, through direct and/or indirect oxidation, where the anthocyanins react with the oxidized components of the medium to yield colorless or brown products (59).

Light has a double role in anthocyanins. It promotes anthocyanin biosynthesis by the occurrence of photoreactions, while simultaneously accelerating its degradation (54). Studies demonstrate that photochemical degradation products of anthocyanins are similar to degradation products obtained in thermal degradation processes (60). In addition, it is reported that the degradation promoted by the light is dependent on the anthocyanin structure since acylated methylated anthocyanidin diglycoside displayed the greatest stability against light in wines followed by nonacylated diglycoside and the monoglycoside as the least stable (61).

2.3.3. CONCENTRATION AND MOLECULAR STRUCTURE

The concentration of pigment significantly influences the color stability and intensity. Higher anthocyanin concentration improves the chromatic properties (27). The self-association of anthocyanins enhances stability by shielding the molecules from the hydration reaction that leads to a colorless carbinol-chalcone system, causing a reduction in absorbance at the maximum absorption wavelength in the visible spectrum (62, 63). Studies for cyanidin-3,5-diglucoside found that increasing the pigment concentration from 10^{-4} to 10^{-2} produces a 300-fold increase in color intensity (63, 64).

Although concentration is important, molecular structure also plays a significant role in the stability and color of these molecules. The simple structure of anthocyanidins is influenced by the B-ring substituents. The presence of hydroxyl and methoxyl groups contributes to reducing the aglycone stability in neutral conditions (65). For anthocyanins, methylation stabilizes the phenolic B ring, lowering the reactivity of the overall molecules, and enhancing the color characteristics (66). Opposite to aglycones, anthocyanin monoglycoside, and diglycoside are rather stable at neutral pH. The presence of sugar moieties inhibits the breakdown of unstable intermediates into phenolic and aldehyde chemicals (65). The common substitution of hydroxyl groups of glycosyl units of anthocyanins by organic acids via ester bonds to produce acylated anthocyanins also increases molecular stability. The increase in the complexity of anthocyanin structure makes them more resistant to various physicochemical and biochemical factors than their nonacylated analogs, namely the color loss with rising pH (27). This happens due to the stacking of the acyl groups, especially the aromatic ones, with the pyrylium ring of flavylium cation (intramolecular copigmentation), where the steric hindrance reduces the possibility of the nucleophilic attack from water with a consequent formation of colorless species (67, 68).

Substituents on the C-ring, particularly at C4 of the flavylium cation, play a crucial role in modifying the charge distribution across the ring, as observed in the synthesis of pyranoanthocyanins. This modification reduces the reactivity of positions C2 and C4 towards hydration reactions, resulting in enhanced stability of these anthocyanin derivatives across a broader pH range. Consequently, they exhibit greater resistance to bisulfite bleaching and display higher color intensities compared to similar anthocyanin glucosides (45).

2.4. STRATEGIES TO STABILIZE ANTHOCYANINS

As previously mentioned, the stability of the quinoidal base (A) in simple anthocyanins is very low, and its formation is often transient, resulting in the formation of multiple uncolored species. Additionally, at pH > 2, the flavylium cation (AH^+) undergoes a hydration reaction, leading to the development of the B species. Considering that the pH inside the plant's tissues could be as low as 2.0 in citrus fruits (69), and as high as 7.7 in some flowers (70), the typical colorful forms achieved suggest the presence of protective strategies over A and AH^+ species responsible for numerous blue tones and the flavylium cation of red hues in plants. The anthocyanin´s-colored forms are stabilized through complex mechanisms including intramolecular and intermolecular interactions with other molecules that naturally exist in plant cells alongside anthocyanin. The interaction of anthocyanins with different molecules to produce color intensification and an improvement of stability is known as copigmentation. The copigmentation can occur at intra- and intermolecular levels, englobing metallic complexation self-association phenomena. On the other hand, encapsulation approaches such as microencapsulation, spray/freeze-drying, emulsification, liposomes, and nanoparticles have shown a high potential for reducing anthocyanin instability due to environmental conditions.

2.4.1. COPIGMENTATION

Copigmentation is regarded as the primary and most successful method for increasing anthocyanin stability. It is an anthocyanin-specific phenomenon that has not been reported in any other polyphenol family or nonphenolic chemical class. This phenomenon comprises physical and chemical processes that lead to the formation of transient non-covalent molecular complexes based on hydrogen-bind interactions and hydrophobic π–π molecular interactions (vertical stacking) between a planar anthocyanin structure and another additional anthocyanin structural components or

external medium molecules (copigment) (71). Copigmentation occurs when a pigment is added to a mildly acidic anthocyanin solution, resulting in color intensification and spectrum changes. UV-vis absorption spectroscopy can identify hyperchromic effects caused by the formation of the π-π complex through molecular interactions that stabilize the colored form of anthocyanins and prevent their degradation and bathochromic shifts which require copigment-to-pigment charge transfer (72). Copigmentation plays a crucial role between pH 2 − 5, due to the formation of substantial quantities of colorless hemiketal (B) and chalcone forms (*Cc* and *Ct*). These forms can reversibly convert into flavylium cation and quinoidal bases by the creation of copigmentation complexes. Besides pH, copigmentation is influenced by factors such as temperature, concentrations, solvents, and molecular structures (40, 64). Copigment is a molecule that interacts with anthocyanin and can be a metal, ion, or another organic component such as flavonoids, amino acids, polysaccharides, proteins, organic acids, or another anthocyanin. Copigments are often colorless or yellowish colored, and they must be a π-conjugated system capable of promoting de π-π stacking interactions or a hydrogen bond developer (64). Copigmentation can be characterized in various ways, depending on the type of copigment that interacts with the chromophores (Figure 4). Intramolecular copigmentation happens when the copigment is part of the anthocyanin structure. Intermolecular copigmentation occurs when another molecule interacts with the anthocyanin to generate a π-π stacking. On the other hand, anthocyanins can interact with one another by self-association, and the copigment can also be a metal, resulting in a metal-anthocyanin complex. Copigmentation can be observed by UV-visible absorption spectroscopy and ^{1}H NMR methods, which allows us to identify some details such as the formation of a 1:1 vertical stacking complex between pigment and copigment molecules (72).

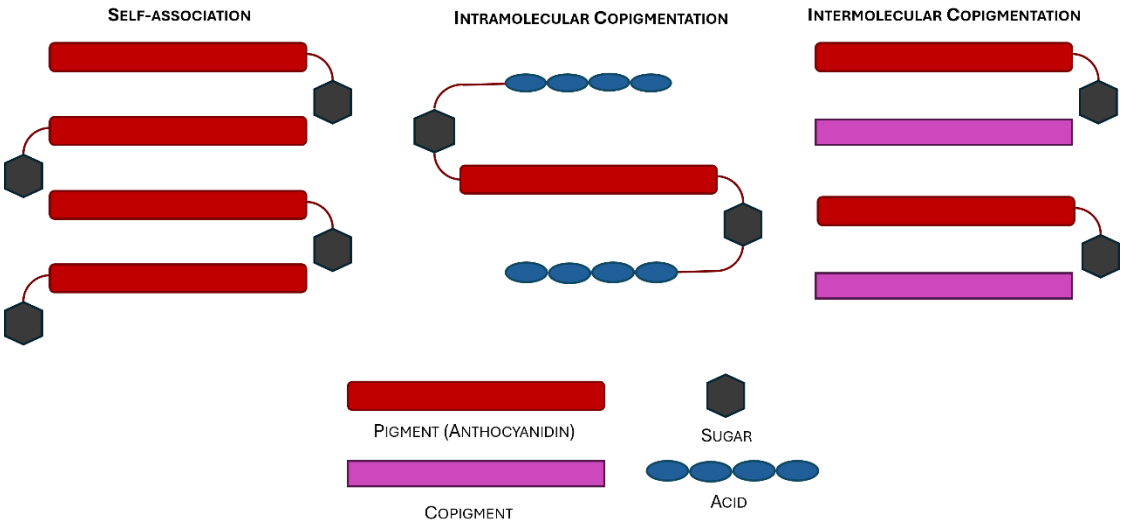

Figure 4 - Copigmentation mechanism in anthocyanins: Self-association, Intramolecular copigmentation in acylated anthocyanins, and Intermolecular copigmentation. Adapted from Trouillas et al. (40).

2.4.1.1. INTRAMOLECULAR COPIGMENTATION

The intramolecular copigmentation is more evident in acylated anthocyanins in which the anthocyanin´s chromophore (aglycone) and the copigment (phenolic acids) are covalently linked to the same sugar residue. Acylated sugars play a crucial role in stabilization, as this effect does not occur when the acyl group is directly attached to the flavylium backbone (73). Intramolecular copigmentation is achieved by the alignment of aromatic acyl units of acylated anthocyanin with the anthocyanidin core structure driven primarily through van der Waals forces and hydrophobic effects (74, 75). The protective effect is based on the steric hindrance of the nucleophilic attack of water at the C2 or C4 positions of the flavylium cation (76), contributing to the color stability of anthocyanins. The efficiency of the intramolecular copigmentation is determined by the π-π interaction between the acyl group and the aromatic backbone of the anthocyanidin and the alignment of both molecule parts which is allowed by the saccharides that act as “linkers” or “spacers” between the acyl group and the anthocyanidin core. The presence of two or more monosaccharide units enhances stabilization by allowing the acyl aromatic rings to fold over the planar pyrylium ring, protecting it from hydration reactions. Acylated and poly-acylated anthocyanins with two or more aromatic acyl units are more stable than their nonacylated precursors due to the formation of sandwich-type structures, where the anthocyanidin nucleus is positioned between two acyl moieties. (68). The number and structure of acyl groups, as well as the position at which they are attached to the sugar moiety, affect the efficiency of the intramolecular copigmentation (75). In addition,

at higher pH values the (poly)acylation of anthocyanins is responsible for blue-shifted hues as a consequence of the stabilization of the quinoidal base species as observed in some flowers including the butterfly pea flower (*Clitoria ternatea*).

2.4.1.2. INTERMOLECULAR COPIGMENTATION

Intermolecular copigmentation occurs when the colored multi-state species of anthocyanin interact with other colorless molecules that are not bound to the anthocyanin molecule and are called copigments (73). Hydrogen bonds and hydrophobic interactions (π-stacking interactions and/or charge transfer complex) are considered the main mechanistic driving forces between the planar polarizable nuclei of the different forms of the anthocyanin multi-state (flavylium cation, AH^+, and neutral quinoidal base, A) and the copigment (64, 68). The protective effect, similar to intramolecular copigmentation, is due to steric hindrance, which blocks water's nucleophilic addition through the interaction of two distinct molecules. Color stabilization is less efficient than intramolecular copigmentation since the latter has the entropic advantage of binding the copigment to the anthocyanidin nucleus, eliminating the need to mix chromophores and copigments, and consequently, the interactions are stronger (72). Copigmentation is an exothermic process that is preferred at lower temperatures and decreases at higher temperatures, becoming insignificant at temperatures close to the boiling point of water (71, 77). Depending on the type of copigment, the formation constants are not greater, indicating the presence of weak molecular interactions that allow for a chemical equilibrium between the complexed and non-complexed forms. In food science, intermolecular copigmentation has been intensively studied by adding different phenolic compounds as copigments to wine, juices, and food products to improve color stabilization during food processing and storage (78, 79).

2.4.1.3. SELF-ASSOCIATION

The structure and color of anthocyanins can be stabilized via self-association, which occurs when two or more anthocyanin molecules join with one another. The mechanism is similar to the vertical stacking-like interactions, where aromatic rings establish hydrophobic interactions blocking the hydration reaction and thus the formation of colorless species such as hemiketal and chalcone forms (64). The occurrence of self-association between anthocyanins is highly dependent on the anthocyanin concentration in the medium and can be observed through various methodologies.,

namely by UV-Vis spectroscopy, NMR, and circular dichroism (64, 80, 81). In contrast to intermolecular copigmentation, anthocyanin self-association causes a hypsochromic shift in the maximum absorption wavelength (64), and NMR analysis reveals a chemical shift of aromatic protons to the shielded field as anthocyanin concentration increases, indicating the presence of hydrophobic interactions. The diffusion coefficient can also be used to predict the self-association of anthocyanins into bigger molecular structures because it decreases as anthocyanin concentrations increase (82). Gonzalez-Manzano et al., (83) studied the self-association process in wine-like model solutions containing various grape anthocyanins, and the results showed that there was an influence on the apparent hydration constants, which had a favorable effect on anthocyanin color and stability. In addition to the self-association between the flavylium cation forms of anthocyanins, Houbiers et al., (84) had previously reported malvidin-3-*O*-glucoside the occurrence of this phenomenon between the flavylium cation and *trans*-chalcone, which was explained by the planar structure of the *trans*-chalcone form, which favors closer packing of the flavylium cation.

2.4.2. INTERACTION WITH MACROMOLECULES

In addition to phenolic compounds used as copigments to stabilize anthocyanins, researchers have also explored other macromolecules. Proteins, carbohydrates, and macrocycles are promising options for preserving the color of anthocyanins. The food industry has focused on the effect of polysaccharides on anthocyanin stabilization since these pigments are bio-synthesized in a polysaccharide-rich media, which may result in extensive contact between these molecules. Anthocyanins are primarily found in plant cells' vacuoles, where they can interact with other cell wall constituents such as pectin during fruit and vegetable processing, affecting their stability, bioavailability, extractability, and color properties. Several studies have been conducted in this sector to evaluate the influence of pectin on anthocyanin stability. Fernandes et al. (85) used saturation transfer difference (STD) NMR spectroscopy and molecular dynamics simulation to investigate the interaction of pectin with two anthocyanins (cyanidin-3-*O*-glucoside and delphinidin-3-*O*-glucoside). The results showed that the interaction is most likely caused by hydrogen bonding and hydrophobic interaction, being significantly greater in the presence of flavylium cation species than in the anthocyanin hemiketal form (weak interaction). The effect on thermodynamic and kinetic constants was minimal, resulting in a little rise in the hydration constant in the presence of pectin. The number of hydroxyl groups in the anthocyanin structure also altered the extent of this

interaction, as seen in prior publications related to the stabilization of strawberry anthocyanins with various pectins (86). Later, the same authors investigated the effect of low methoxylated pectic polysaccharide from citrus fruit on copigmentation interactions between malvidin-3-*O*-glucoside and a common copigment, catechin. The results suggest that both catechin and pectic polysaccharides strongly bind to anthocyanin, increasing its color and acting as copigment components; however, the concurrent presence of two copigments promoted a competing behavior in the complexation reaction (87). The binding constants were significantly affected by the degree and the type of esterification of each pectic fraction, with those having a higher degree of methyl esterification showing lower binding affinities (88). All of these studies confirmed that pectin improved the color stabilization of anthocyanins, where the thermodynamic parameters revealed the formation of a complex by weak noncovalent interactions. Other types of polysaccharides such as gums have proven their potential to interact and stabilize anthocyanins namely xanthan gum (89), and arabic gum (90), which are used as emulsifiers in food and beverage systems.

Cyclodextrins are cyclic oligosaccharides composed of several glucopyranose units joined by α-(1,4) linkages. They are naturally formed through enzymatic starch modification. These macrocycles can interact with anthocyanins through a host-guest interaction pathway. β-cyclodextrin has been shown to protect anthocyanins from oxidation, heat degradation, and digestive damage (91, 92). These macrocycles inhibit copigmentation by selectively incorporating and stabilizing colorless anthocyanins in the β-cyclodextrin cavity (93).

Proteins, like carbohydrates, are dietary polymers that have been examined for their ability to form complexes with anthocyanins and stabilize them through various chemical interactions such as hydrophobic and hydrophilic interactions, van der Walls forces, and hydrogen bonds. Once again, the effectiveness of the complex anthocyanin protein is influenced by parameters such as protein structure, amino acid content, pH, and temperature. Using β-lactoglobulin (94) and milk α- and β-casein (95) to stabilize malvidin-3-*O*-glucoside resulted in the development of a complex anthocyanin-protein, which improved anthocyanin's thermal, oxidation, and photostability while preventing color fading and degradation. Chung et al., (96) demonstrated that both heat denatured and native whey protein can significantly improve the stability of the color of anthocyanin in model beverages during storage. The formation of an anthocyanin-protein complex reduces the anthocyanin degradation caused by the ascorbic acid (through

condensation or oxidation) during storage. McClements and coworkers (97) found that the color of purple carrot anthocyanins in model beverages containing citric acid and ascorbic acid at pH 3 was stabilized by aromatic amino acids (tryptophan, phenylalanine, and tyrosine) and a polypeptide (ε-poly-L-lysine), with tryptophan having the greatest effect. Cahyana used a fluorescence quenching method to study how pH and anthocyanin structure affect binding affinity to human serum albumin (HSA). Four anthocyanidins were analyzed over a pH range of 4-7.4, and the constants for binding to HSA ranged from 1.08×10^5 to 13.2×10^5 M^{-1}. The binding affinities were found to be usually higher at pH 4 which was associated with the presence of higher fractions of quinoidal and ionized quinoidal bases at higher pH values, and, on the other hand, to the increasing hydrophobic nature of HSA at pH = 4 (98). A growing number of studies have demonstrated the applicability of several proteins as copigments to stabilize anthocyanins (99, 100).

Some studies in the literature report the use of lignin to stabilize anthocyanins and derivatives. Araújo et al., (101) investigated the first evidence of this interaction by evaluating the effects of lignosulfonates on the thermodynamic and kinetic parameters of malvidin-3-*O*-glucoside at pH 1, revealing a positive effect on anthocyanin color stabilization. They also explored the interaction between lignosulfonates and pyranoanthocyanins, including portisins and pyranoanthocyanin dimers. The findings indicated that the concentrations of both compounds influenced the interaction, with a cooperative stacking of the dye at lower macromolecule concentrations due to the binding of multiple dyes to adjacent binding sites. A redistribution of the dye to more distant binding sites was observed at higher polymer concentrations. This interaction modulated the color of natural bluish dyes and improved their solubility in aqueous systems (102). In terms of industrial applications, studies in a wider pH range may validate the strong applicability of this polymer to form stable complexes with anthocyanins.

3. LIGNIN

After cellulose, lignin is the second most abundant biopolymer in nature. Alongside cellulose and hemicellulose, it forms the most abundant renewable lignocellulosic biomass, making it an attractive source of bioenergy and biobased chemicals (Figure 5). This natural polymer confers strength and rigidity to the plant cell walls and contributes to 40 % of the energy content of lignocellulosic biomass (103). The lignin content and composition depend on the species and morphological parts of the plant. Lignin concentration can range from 18 − 33 % in softwoods and 15 − 35 % in hardwoods (104). Non-wood fiber crops often have a lower percentage, ranging from less than 5 % in cotton to 15 % to 25 % for grasses such as cereal straws, bamboo, and bagasse (104, 105).

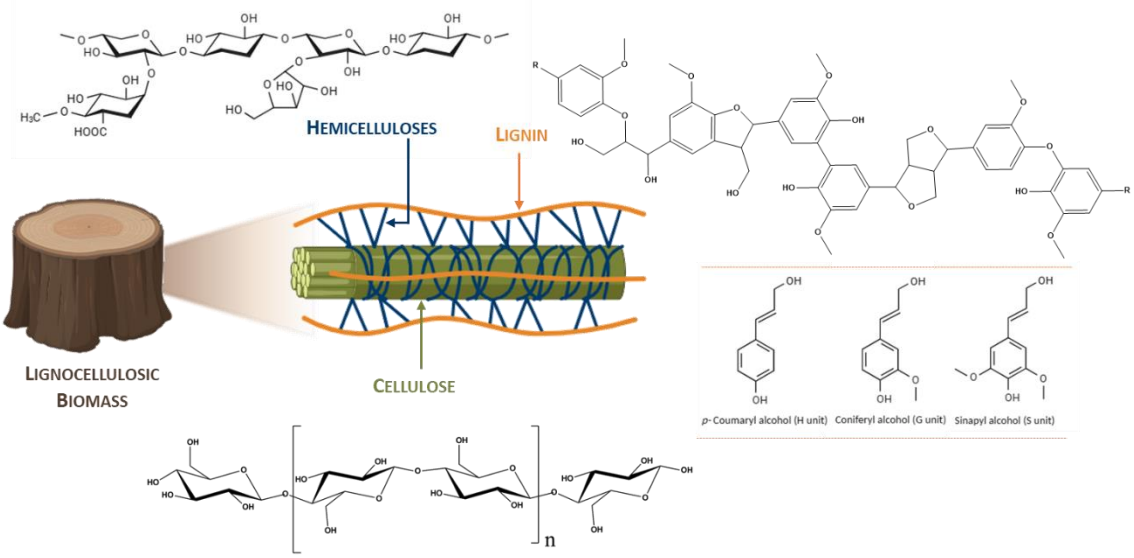

Figure 5 – Lignocellulosic components in the plant cell wall's microfibrillar framework, including cellulose, hemicellulose, and lignin. Chemical structure of the three lignin basic units (monolignols). Lignin structure adapted from (106).

3.1. LIGNIN STRUCTURE

Lignin is a complex three-dimensional amorphous structure comprised of three basic phenylpropanoid monomers: p-coumaryl, coniferyl, and sinapyl alcohols. These monolignols form the three basic units of lignin: *p*-hydroxyphenyl (H), guaiacyl (G), and syringyl (S) when incorporated into its structure, which differ in the methoxylation pattern of the aromatic nuclei (Figure 6). The proportion of these units depends on the plant

source and species, such as grass, hardwood, or softwood, and the extraction method (107). Softwood lignin mainly comprises guaiacyl units (G – type lignin) while hardwood lignin contains an equal proportion of G and S units (G/S − type lignin). On the other hand, lignin of herbaceous, grass, and angiosperm plants (non-wood crops) contain a higher proportion of H units about S and G units (G/S/H − type lignin) (108). The phenylpropane units are linked through aryl ether linkages (β-*O*-4, α-*O*-4, 4-*O*-5) and carbon-carbon bonds (5-5', β-5, β-1, β-β) which are less readily degraded identified as "condensed" units (Figure 6) (107, 109). Linkages β-*O*-4 and α-*O*-4 are known as "uncondensed structures", which are easily cleaved during the pulping in industrial processes given the monomers. The complexity of lignin arises from the numerous possible linkages between its monolignol units. The most abundant linkage is the β-*O*-4 type accounting for more than 50 % of the linkages between the units of lignin; however, once again the percentage of each inter-unit's linkage depends on the lignin nature (107, 110, 111). The degree of condensation (DC) is one of the important characteristics of lignin. According to the literature, DC determination is useful for distinguishing the uncondensed from the condensed structures, indicating the extent to which the lignin is broken down under specific conditions. However, its definition is unclear and often depends on the method used for its analysis. The more accepted concept for DC is related to the lignin portion linked with the C-C bond with other units of lignin via C2 or C6 positions in the aromatic ring of S units, C2, C5, or C6 positions for the G units and the position C_3 for the H units. The most common condensed structures are 5-5', β-5, and 4-*O*-5', which are more resistant to chemical degradation (111). The higher percentage of condensed structures in the G type of lignin (Table 4) justifies the higher condensation degree of softwood lignin compared to the hardwood and herbaceous lignin having consequences on lignin reactivity.

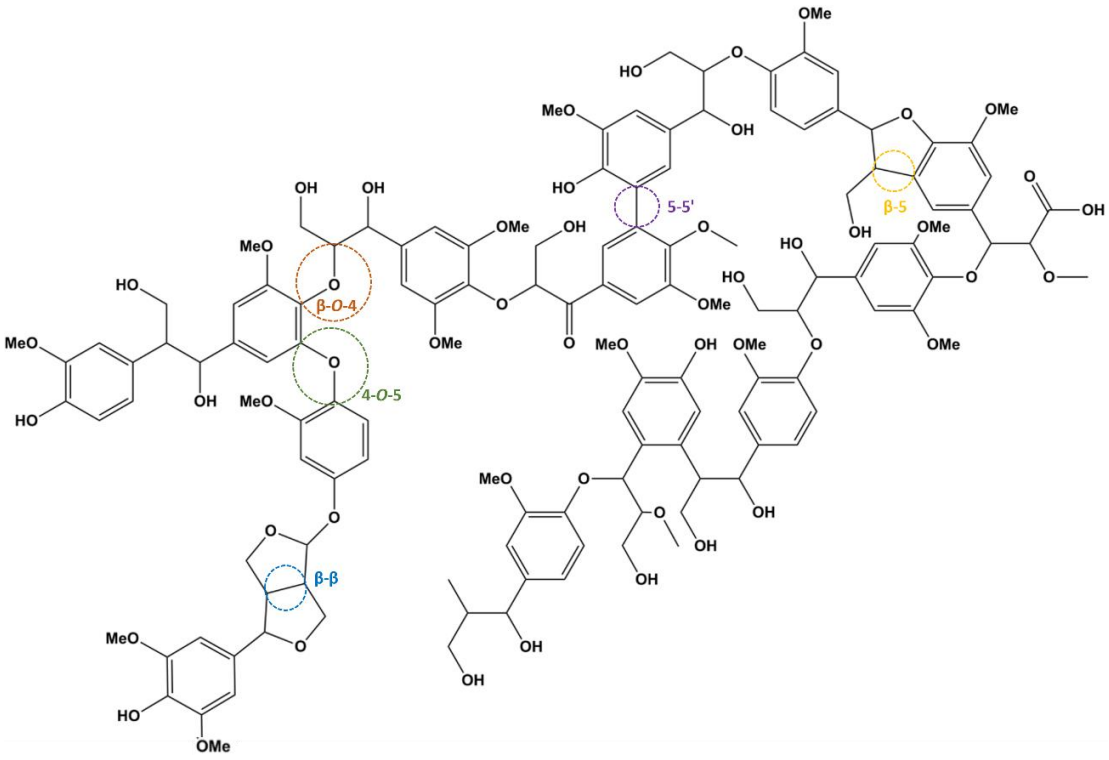

Figure 6 – Chemical structure of lignin. Main ether and C-C linkages in the lignin structure.

Table 4 - Incidence of the different types of linkages (wt.%) in softwood and hardwood lignin (107, 109).

Linkage type	(wt.%)	
	Softwood	Hardwood
C-O-C linkage		
β-*O*-4	45−50	50−65
4-*O*-5'	4−8	6−7
α-*O*-4	6−8	4-8
C-C linkage		
β-5	9−12	4−6
5-5'	10−25	4−10
β-1	3−10	5−7
β-β	2−4	3−7

3.2. ISOLATION METHODS

As already mentioned, the nature and method used to isolate lignin affects the physical-chemical features of this complex biopolymer. Variations include the ratio S/G/H units, the type and amount of un- and condensed structures, and the content of functional groups on lignin structure, specifically carboxylic groups and the phenolic and aliphatic hydroxyl groups. Biomass delignification is a complex process that involves the breakdown of bonds between lignin and hemicellulose, which are covalently bonded to form lignin-carbohydrate complexes. Partial depolymerization of lignin is also essential to separate them from the biomass. Depending on the temperature range, the employing time, and many other variables applied in the delignification process, it is possible to obtain different types of technical lignin, namely the Lignosulfonates (LS), Kraft lignin (KL), Organosolv lignin (OL) and Soda lignin (SL) (Figure 7). In a transition toward a more circular and sustainable economy, lignin can be obtained as a by-product from the industrial processes, namely, the pulp and paper industries. The pulp and paper industries are the primary sources, generating lignosulfonates and kraft lignin, making up 97% of global technical lignin production. In contrast, biorefineries produce organosolv lignin, which accounts for only 2% of total lignin production worldwide (112).

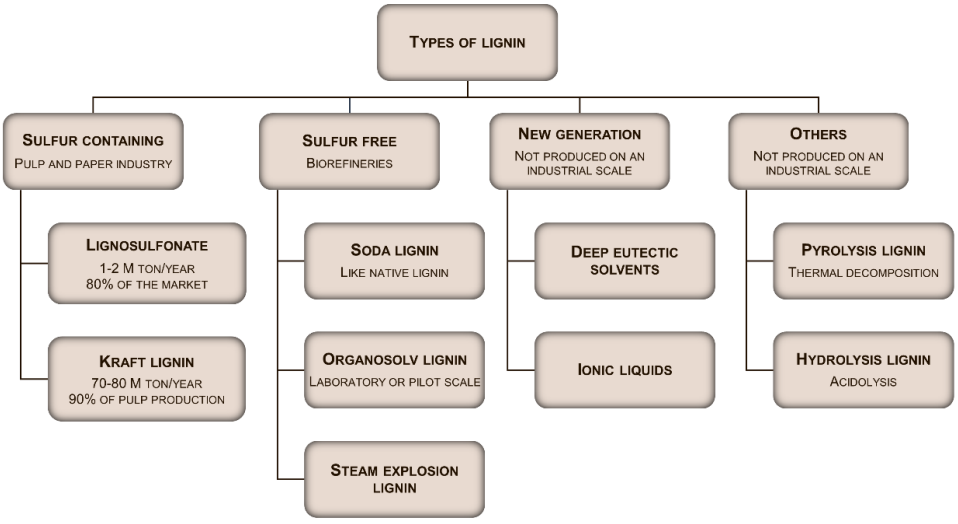

Figure 7 - Identification of the most common types of lignin. Diagram and data adapted from (113, 114).

3.2.1. THE PULP AND PAPER INDUSTRY

Wood is a three-dimensional composite composed of an interconnected network of sugar-based polymers (cellulose and hemicellulose, 65 − 75 %) and lignin (18 − 35 %), with a minor amount of extractives and inorganics. In the paper industry, chemical

pulping removes the lignin from lignocellulose, and the resulting cellulose fibers may be used for paper production. Lignin results as a byproduct in the pulping process, which is directly converted into fuel to generate heat and electricity due to its high calorific power. Only 1 − 2 % of industrially produced lignin is isolated for other uses, including the production of dispersants, adhesives, surfactants, and other value-added lignin-derived products (115). However, the amount of technical lignin produced each year is extremely high, accounting for a worldwide production of 100 million tons/ year valued at USD 732 million in 2015, which is expected to reach USD 913 million by 2025 with a compound annual growth rate (CAGR) of 2.2 % (112). Sweden (31.2 %) and Finland (30.2 %) are the leading pulp producers, with Europe accounting for 25.3 % of global pulp production (116, 117).

.

3.2.1.1. SULFITE PROCESS

LS are produced during the sulfite pulping process, where appropriately sized wood chips (15 − 25 mm long) are cooked at high temperatures (125 − 150 °C) for 3 to 7 hours under pressures ranging from 500 to 700 kPa. This cooking process occurs in a digester filled with a cooking liquor consisting of sulfur dioxide (SO_2) dissolved in water to form sulfurous acid (H_2SO_3). The process can occur under acidic, neutral, or alkaline conditions, with the pH of the digestion controlled by the type of salt used (such as sodium, ammonium, calcium, or magnesium), as well as its solubility and dissociation characteristics. The process occurs in two types of reactions, namely the sulfonation and the hydrolysis reaction. During sulfonation (ideally at acidic pH), the cleavage of an ether bond or the removal of a hydroxyl group leads to the formation of a quinone methide intermediate. This intermediate then establishes a linkage with the sulfite ion. The presence of ionizable sulfonate groups in the lignin structure makes them very soluble in water, with sulfur content around 6 − 8 %. The hydrolysis reaction breaks down the ether bonds between the phenylpropane units and the linkages between lignin and carbohydrates, resulting in a decrease in lignin's molecular weight. However, it occurs slower than the sulfonation reaction. Considering that in the liquor there are other components like residual cellulose and hemicellulose, and some inorganic molecules that are dissolved throughout the pulping process, it is performed a filtration step to accumulate the lignin in the spent liquor (50 − 80 wt.%). One of the main disadvantages of LS is the considerable amount of impurities where up to 30 wt.% of carbohydrates, ash, and other inorganic materials (≈10 wt.%) which contributes to the higher molecular weight of lignosulfonates (between 1000 and 150,000 g/mol) (118) and polydispersity

index. Membrane ultrafiltration can be used to reduce the wide distribution of molar mass (119), obtaining more homogeneous and purified LS and facilitating their physicochemical characterization. Additionally to the sulfonate groups, other functional groups are present in the LS structure including phenolic and aliphatic hydroxyls, carboxylic acids, and methoxy groups in various combinations. In general, lignosulfonates have more sulfur groups than Kraft lignin and consequently, a higher sulfonation degree. The presence of these sulfonated groups confers an anionic charge to the LS and high solubility in water enhances the use of this type of lignin to create value-added products (118).

The world's commercial production (excluding bioenergy production) of technical lignin totaled roughly 1.65 Mt/y, with lignosulfonates dominating nearly 80 % of the market (114). They have a wide range of applications, especially as dispersants and binders, improving the efficiency and performance of some products used in agriculture, animal feed, construction, and ceramics industries (120). Related to their dispersant properties, they are used in agriculture to facilitate the distribution of pesticides and fertilizers, and as components of drilling fluids for oil recovery. One of the biggest applications is the production of animal feed pellets that due to their ability to bind the particles make the final product more consistent. Lignosulfonates are bio-based surfactants widely used in the chemical industry as emulsion stabilizers (121). In the construction industry, LS are used as additives in concrete mixtures acting as water-reducing agents and improving the workability of the cement (122). In the case of ceramic production, namely in the molding and extrusion processes, the presence of LS functions as binders and plasticizers.

3.2.1.2. KRAFT PROCESS

The delignification of biomass by kraft process is considered the principal pulp process in the industry accounting for circa 80 – 90 % of the pulp production (123). In this process, wood chips are treated in a digester with aqueous solutions of sodium hydroxide (NaOH) and sodium sulfide (Na_2S), conducted at high temperatures (160 – 180 ºC) and pressures (around 800 KPa). The process involves three steps, namely the initial phase, the bulk, and the final phases. The pulp is separated from the black liquor obtained during the process (containing 35 − 45 % lignin), which is concentrated and precipitated with acidic solutions of H_2SO_4 or CO_2 to obtain the kraft lignin. The closed-loop cycle (Figure 8) enhances the environmental sustainability of the kraft process, making it more favorable than sulfite pulping and reinforcing its dominant role in the

paper industry (124). The molecular weight of kraft lignin ranges from 200 to 200,000 g/mol with a residual sulfur content of around 1 – 3 %. This sulfur is typically found in the thiols form bonded to the aliphatic chains of lignin, contributing to its characteristic smell. Furthermore, it contains a higher number of phenolic hydroxyl groups due to the extensive cleavage of β-aryl linkages in the pulping process and some impurities such as carbohydrates from hemicellulose and fatty acids. At an industrial scale, the LignoBoost process was developed to isolate relatively pure kraft lignin powder with minimal residual impurities. Lignin at alkaline pH (9.5) is precipitated with isolation yields about 85 %; however, although different companies produced kraft lignin following this approach only 2 % is used to create added-value products. It is mainly used as a fuel but has recognized dispersant and emulsifying properties to be applied for crop protection products formulated in tablets, microcapsule suspensions, wettable powders, and spray drying. The production of blends and composites, adhesives, epoxy resins, and polyols are other possible applications of kraft lignin. Additionally, it has shown significant potential as a precursor for producing bio-based aromatics through catalytic or oxidative depolymerization of lignin. With ongoing advancements in lignin chemistry, kraft lignin has also been utilized to create nanoparticles for drug delivery in medical applications (125, 126).

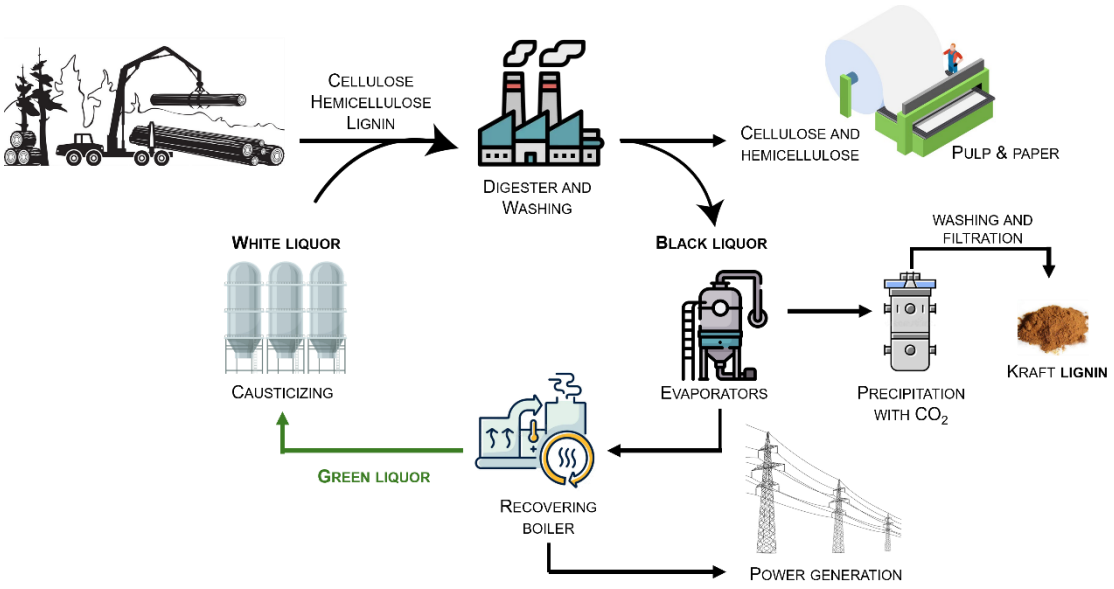

Figure 8 - Simplified scheme of the Kraft process highlighting lignin recovery from the black liquor.

3.2.2. BIOREFINERY PROCESSES

Biorefineries are a key element in the transition towards more sustainable production and bio-based value chains. This type of infrastructure uses the lignocellulosic biomass as feedstock, providing from non-food feedstock such as agriculture residues or wood, to produce biofuels, biochemicals, bioenergy, and other added-value bioproducts using several conversion and advanced technologies like enzymatic hydrolysis, combustion, and biochemical and thermochemical processes. This way, it plays a crucial role in addressing global energy and climate changes by harnessing the untapped potential of abundant and diverse biomass resources, providing a cleaner and more sustainable alternative to conventional fossil fuels. Contrarily to the pulp and paper industry, where the lignin is only a by-product, in the case of the biorefineries an integral valorization of the biomass to produce the bio-based products is performed. Several techniques are utilized for lignin separation, with the most common methods including alkaline and organosolv methodologies, steam explosion, and dilute acid hydrolysis.

3.2.2.1. ALKALINE PROCESS

The alkaline method, also known as the soda process, closely resembles the kraft process but utilizes a sulfur-free cooking liquor, resulting in a higher purity of extracted lignin. The feedstock is heated (140 − 175 ºC) and digested inside a pressurized reactor using an alkaline aqueous solution typically composed of sodium hydroxide (NaOH), potassium hydroxide (KOH), or calcium hydroxide (CaOH). The process involves an alkaline delignification related to the saponification of intermolecular ester bonds between lignin and carbohydrates, and also a depolymerization of lignin with a cleavage of α and β aryl ether bonds in phenolic and non-phenolic units. The treatment parameters and biomass type influence the efficiency of alkaline delignification, with higher isolation yields obtained for biomass with low lignin content and nonwoody lignocellulosic biomass, namely annual crops such as flax, bamboo, bagasse, or wheat straw. The recovery of soda lignin is very similar to the procedure discussed in the kraft pulping process, which is based on acid precipitation.

Most soda lignin has a low molecular weight (800 − 3000 Da), is insoluble in water, and is isolated with minimal sugars and ash impurities, distinguishing it from lignosulfonates. In addition to the guaiacyl and syringyl moieties, as well as the considerable amounts of *p*-hydroxyl phenolics found in non-wood fibers, soda lignin is characterized by the presence of a greater number of carboxylic acids derived from the

aliphatic hydroxyl groups oxidation (127). As a result, they are less hydrophobic than kraft wood lignin, and considerable content of silicate and nitrogen. Lignin derived from non-wood biomass has different structural characteristics relative to wood lignin. As previously mentioned, soda lignin is sulfur-free and closely resembles native lignin, offering advantages and greater applicability in biological fields, such as animal feed and nutrition. It has been proposed for the control of gastrointestinal disorders in ruminants and monogastric animals. Unmodified soda lignin has been employed as a dispersant for biological slime management in industrial water circuits and as a concrete addition due to its dispersion capabilities. Other applications include the production of phenol-formaldehyde resins, where soda lignin serves as a partial substitute for phenol as a binder in plywood (128, 129).

3.2.2.2. ORGANOSOLV PROCESS

The recovery of lignin and other extractives using organic solvents is regarded as a more environmentally friendly technique since the organic solvents used in the process are often recycled minimizing the environmental effect and reducing costs. The most frequent solvents employed in this procedure are organic solvents such as ethanol, methanol, and acetone, which can be coupled with mineral acids as catalysts (e.g. HCl, $MgCl_2$, or H_2SO_4), which improve delignification yields; however, isolated lignin is more degraded, limiting its use as a coproduct. Even without additional catalysts, the process can be considered self-catalyzed. This is because acetic acid, released from hemicelluloses during the process, initiates acid hydrolysis of lignin. This hydrolysis results in the formation of phenolic hydroxyl and carbonyl groups within the lignin structure (130). Common feedstocks include wood, agricultural residues, and other plants rich in lignocellulosic biomass. Ethanol is employed as the solvent, and the biomass undergoes a pulping phase that may entail high pressures and a broad range of cooking conditions: temperatures from 100 to 250 ºC, durations across 30 to 90 minutes, solvent concentrations ranging from 35 to 70 wt.%, and solid-liquid ratios of 1:4 to 1:10 (w/w) (131). During the organosolv treatment, the breakdown of lignin-cellulose linkages and lignin is solubilized, the glycosidic bonds in hemicellulose are cleaved into soluble sugars and sometimes the cellulose, as previously mentioned, suffers acid-catalyzed monosaccharides degradation. By using a fractionation approach, organosolv lignin is removed from the final combination and recovered as a soluble fraction in the organic solvent, but cellulose and the remaining solid wastes remain insoluble (130, 131). Unlike other procedures, the reaction media successfully solubilizes lignin without

requiring structural alterations; hence, organosolv pulping might be regarded as a more efficient choice for preserving the natural structure of lignin during extraction (132). Organosolv pulping has been demonstrated to provide better isolation yields (> 70 %) than typical pulping processes, and the lignin obtained is of high purity. As a result, organosolv lignin has reduced molecular weights and polydispersity indexes of 800 − 16,000 g/mol and 1.5 − 10, respectively (133, 134). Isolated lignin can be used for various purposes, including as a bio-based feedstock for added-value chemicals and materials such as the formulation of glues and binders in polymer substitutions, as well as a sustainable energy source. Despite its benefits (sulfur-free, low ash content, greater ability to be derivatized, and high purity), organosolv pulping is not frequently used due to the inferior quality of the pulp and considerable corrosion of the equipment caused by the organic solvents used.

3.2.2.3. STEAM EXPLOSION

One of the thermochemical processes used to separate the lignin is steam explosion, which includes the use of high-pressure steam to break down the structural components of lignocellulosic biomass. To make the biomass structure more accessible for subsequent treatment, this lignocellulosic biomass is pretreated to reduce size and increase surface area. There are two steps to the procedure (135). The biomass is impregnated with steam under high pressure (1 − 3.5 MPa) and temperature (180 − 240 ºC) in the first stage, known as autohydrolysis, which leads to the rupture of glycosidic linkages in hemicellulose and lignin-hemicellulose (136, 137). The hydrolysis of hemicellulose is catalyzed by acetic acid produced from the acetyl groups within hemicellulose. After 1 − 20 minutes, depressurization (second stage) occurs, promoting the separation of the internal components of the biomass, including lignin, while the acidic medium promotes the autohydrolysis of ether linkages in lignin (136). The following stages such as precipitation and filtration are used to isolate lignin; nevertheless, the major shortcoming of this approach is the low extraction yield, allowing only a small fraction of lignin to be solubilized. Steam explosion is widely used for cellulose production, which is then used for bioethanol conversion. The key advantages of the steam explosion method are that it uses less dangerous chemicals, is more energy efficient, and has a minimal environmental impact (138).

3.2.3. NEW ALTERNATIVES IN LIGNIN EXTRACTION PROCEDURES

From an economic and sustainability perspective, the fundamental advantage of traditional industrial processes is the use of lignin as a by-product (low cost associated), which is generated in vast quantities, and many efforts and studies have been made to create added-value products. However, due to the needed temperature and pressure conditions, these procedures involve extensive processing times, considerable solvent and reagent usage, and can be energy-intensive. Moreover, industrial operations often prioritize pulp production without focusing on the quality of the extracted lignin, which may have a high molecular weight and contain a substantial amount of contaminants. Recently, research has switched toward more environmentally friendly approaches, such as utilizing novel alternative solvents like ionic liquids (ILs) and deep eutectic solvents (DES) (139), as well as employing efficient isolation techniques such as microwaves and ultrasound. These methods are more selective and environmentally beneficial (140). Compared to other techniques, ILs and DES have emerged as leading trends for biomass delignification and lignin extraction due to their ability to achieve significant yields of pure lignin with minimal alteration or degradation of its structure. This purity and structural integrity make lignin extracted using ILs and DESs suitable for a wide range of high-value applications (141). The use of ILs can address some of the disadvantages of the organosolv procedure, such as the high volatility, explosiveness, and difficulty in recovering them. Avoiding these limitations may encourage the technique to be implemented on a larger scale (142). DESs offer the advantages of being nontoxic (natural origin), biodegradable, easily accessible, and inexpensive, making them more suitable for large-scale procedures. Microwaves and ultrasounds appear to lower these two factors and reduce solvent consumption, making the lignin extraction process less expensive and less harmful to the environment (143). Using microwave radiation for biomass pretreatment offers several advantages. It allows precise control over the rate at which biomass temperature increases, which enhances process efficiency. This approach leverages the unique properties of microwave radiation to facilitate efficient and controlled biomass treatment, enhancing the overall efficacy of lignin extraction processes (144-146). Other methodologies like supercritical fluid extraction (SFE) and subcritical water extraction (SWE) are beginning to be developed and explored for lignin extraction (147, 148).

3.3. METHODS FOR CHARACTERIZING THE CHEMICAL STRUCTURE OF LIGNIN

The structure of lignin is extremely complex resulting from the diverse combinations of three basic units linked through several linkages in a three-dimensional network. This complexity impacts its reactivity, and the undefinition structure limits its application, particularly in producing value-added products. The structure of lignin is characterized by considering some specifications such as the condensation degree, the relative abundance of S, G, and H units, the principal functional groups present in the structure and their distribution and amount, and information about the common lignin-carbohydrates and linin-lignin linkages present in the structure; however, other variables like as the molecular weight and the total lignin content are important to define the lignin sample (149). Various methodologies have been investigated to achieve the major structural properties of lignin. These approaches are classified as destructive and non-destructive. The destructive method requires the lignin decomposition into low-molecular-weight compounds and comprises a selective cleavage of a specific fraction of lignin which limits the characterization of whole lignin structure. These include nitrobenzene oxidation (150), permanganate oxidation (151), ozonation (152), hydrogenolysis, thioacidolysis (153), cupric (II) oxidation (154), and derivatization followed by reductive cleavage (155). Nondestructive approaches, such as spectroscopic methods, are widely employed to characterize lignin structure because they allow for a complete investigation of the entire lignin structure as well as a direct recognition of the lignin moieties and functional groups present in the structure. Nuclear magnetic resonance (NMR), UV-spectroscopy, X-ray photoelectron spectroscopy (XPS), and Fourier transform infrared spectroscopy (FTIR), Raman spectroscopy are the reference methods used to elucidate the lignin structure, being that the NMR techniques include the carbon (^{13}C), phosphorus (^{31}P), proton (^{1}H), and 2D heteronuclear single quantum coherence (HSQC) NMR (149, 156). Because of its aromatic nature, the lignin absorbs strongly in the UV area, with a distinctive band at 280 nm corresponding to the benzene ring substituted with hydroxyl and methoxyl groups. In the presence of unconjugated phenolic groups and α-conjugated phenolic structures in alkaline environments, the UV-Vis spectrum has two additional bands at 300 and 370 nm, respectively (157). The FTIR spectrum of lignin exposes certain significant structural properties, mostly related to the presence of functional groups (e.g. hydroxyl, carboxylic, and ketone groups) and subunits, as well as relevant information about lignin purity. Lignin is often characterized in the mid-infrared region, corresponding to electromagnetic radiation with wavenumbers between 4000 and 400 cm^{-1} (156).

Although the structure of lignin is dependent on the source and isolation method, lignin has common absorption bands such as a broad absorption band at 3600 − 3200 cm^{-1} suggesting the presence of O-H stretching vibrations of hydroxyl groups, an absorption band at 3000 − 2800 cm^{-1} associated to the C-H vibrations in aliphatic groups of lignin, strong absorption in the aromatic region at 1600 − 1500 cm^{-1} related to the aromatic C=C stretching vibrations which reflects the aromatic nature of lignin, an absorption band around 1730 cm^{-1} due to the presence of C=O stretching vibrations of ketones and aldehydes and a typical band at 2900 and 1460 cm^{-1} attributed to the methoxyl groups. Nonetheless, other variations in the FTIR spectrum appear related to the lignin structure (158). NMR is a comprehensive technique that provides detailed and advanced information about lignin structure. The subunits (e.g. syringyl and guaiacyl) and the absolute content of β-O-4, β-β, and β-5 substructures are frequently identified by the two-dimensional ^{1}H and ^{13}C correlation HSQC NMR. ^{31}P NMR is also a promising tool widely used because through this technique it is possible to quantify the amount of aliphatic and hydroxyl phenolic groups as well as carboxyl groups in lignin. The method requires a phosphitylation step of these functional groups with 2-chloro-4,4,5,5-tetramethyl-1,3,2-dioxaphospholane (TMDP) to be quantified (159).

3.4. LIGNIN APPLICATIONS

As already discussed, lignin has a complex structure and variable composition that is extremely dependent on the biomass and the extraction processes. The low-purity standards of existing commercial lignin, the non-uniform structure, and the intense brown color are the major drawbacks to the valorization. Moreover, the potential of lignin is directed towards the production of low-grade fuel for electricity and heat generation (Figure 9), leading to resource waste and environmental pollution, while hindering its commercialization. Despite numerous efforts to make lignin value-added products scientifically and economically viable, there is still significant resistance to valorizing this biopolymer. Only about 2 % of the total lignin produced globally is commercially used for value-added products, such as dispersants, adhesives, and surfactants. However, lignin's abundance and the diverse functional groups in its structure make it an attractive precursor for emerging applications. Technologies focused on lignin depolymerization (such as hydrogenolysis, pyrolysis, oxidation, and hydrolysis) are being developed to leverage its potential. Additionally, lignin can be used in the synthesis of chemically active sites through reactions like hydroxyalkylation, amination, nitration, and sulfonation. Functionalization of hydroxyl groups via processes such as alkylation,

phenolation, urethanization, and etherification is also explored, along with the production of lignin graft copolymers. These approaches aim to unlock the full value of the lignin and expand its applications beyond traditional uses.

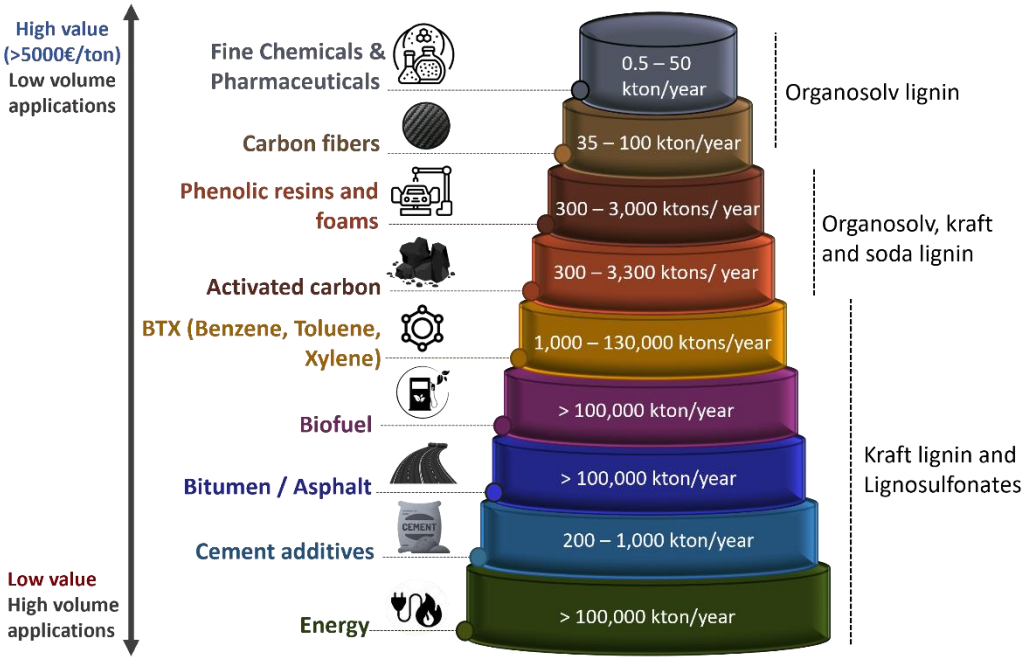

Figure 9 - Potential lignin applications and the corresponding market volume, with the most appropriate type of lignin. Diagram and data values were adapted from the literature (104, 105, 160, 161).

According to the literature, lignin has been used to produce carbon materials. Lignin is an abundant carbon-rich biomass (50 − 60 % in carbon). Based on scientific evidence lignin-based carbon fibers were produced using kraft lignin from hardwood and softwoods (162, 163), and some research institutes (Plasan, Ford Motor (USA), BASF & SGL (Germany), DowAska (Netherlands)) have attempted to produce high-quality carbon fiber using lignin (112). Carbon fiber can be used in sports and aerospace industries, with promising results in the automotive industry to replace steel. Because of its low cost and availability, lignin is an appealing precursor for the production of a variety of carbon materials, such as activated carbon, activated carbon fibers, graphitic carbons, or carbon black to be used in different fields like environmental protection (purifying gas an aqueous media from organic pollutants or heavy metals), catalysts, absorbent materials, production of electrodes for electrochemical applications, in energy storage, or as reinforcing components in advanced composite materials (164-167). In the case of energy storage devices, the lignin enhances efficiency and significantly contributes to reducing toxicity and cost, while promoting the development of more eco-

friendly devices. Lignin has been considered for the production of superconductors and supercapacitors since the activated carbon materials are derived from an abundant and renewable source through sustainable processes (167, 168). Furthermore, studies demonstrated that lignin-derived by-products may significantly improve surface ion accessibility and electronic conductivity to assist the electrochemical process (168).

The oxidation of lignin yields high-value compounds such as vanillin and other aldehydes, vanillic acid, dimethyl sulfoxide (DMSO), aromatic and aliphatic acids, and cyclohexane (169, 170). Of all the compounds possible to obtain from the oxidation of lignin, vanillin is the one that assumes the greatest importance and its production process has been extensively investigated and optimized, due to its wide application in various industries. Vanillin, the primary component of natural vanilla extract, is widely used to flavor food, beverages, and pharmaceuticals. Currently, 80 % of vanillin is derived from crude oil, while 20 % comes from lignin (171), which can be obtained by oxidizing kraft lignin in an alkaline medium (172, 173). Benzene, toluene, and xylene (BTX) are important chemicals that can be derived from lignin. These aromatic compounds have numerous applications with a potential focus in the chemical industry representing 24 % of the total petrochemical market (174). The main advantage is that the lignin-based BTX is identical to petroleum-based BTX, allowing it to be used as a direct substitute (171). Other organic compounds that can be obtained from lignin depolymerization include phenols (175). Phenol derivatives have a wide range of applications, including the preparation of cosmetics (sunscreens, hair coloring, and skin lightening), the manufacture of plastics, phenolic adhesives, fine chemicals, food additives, and the perfumery industry. Lignin phenol-formaldehyde resins have been synthesized to replace phenol-formaldehyde resins (176), polyurethane foams, and polyurethanes for the automotive sector (173, 177). However, over 90% of the world's phenol is derived from petroleum-based benzene, sourced from fossil fuels, contributing to environmental degradation. The generation of phenol from lignin by various methods (hydrolysis, pyrolysis, or alkaline oxidation) can result in clean phenol production from a renewable feedstock and a competitive market price (178, 179). Aromatic amines for pharmaceutical applications (167) or *p*-hydroxyl acetophenone (180) for drug production and perfume synthesis are other chemicals isolated from lignin.

Over time, lignin has gained special attention for its potential application in the textile industry. In addition to the sustainable and environmental concerns related to the use of natural and renewable biomass in substitution of synthetic and non-degradable materials, it is reported that the incorporation of lignin into textile improved strength, UV

resistance, and antibacterial properties in linen fabrics in the form of lignin nanoparticles (181), the filtration and antimicrobial effect of fabric coated with lignin (182) and act as a fire retardant and dying on textiles (183).

Lignin is increasingly incorporated into cosmetic formulations to replace synthetic components, offering a more environmentally and health-friendly alternative. The presence of different functional groups in the lignin structure gives some skin benefits including photoprotection, anti-aging, and skin-whitening properties (184). Some studies have already reported the use of lignin as an ingredient in cosmetic formulations, particularly its usage in the manufacture of natural sunscreen to replace dangerous commercial chemical and physical ultraviolet (UV) filters (185). The results described lignin as a promising natural UV protection element in broad-spectrum (UVA and UVB) sunscreen, with UV-blocking properties improved when low molecular weight fractions and lignin as micro- and nanoparticles were used (186, 187). However, this application is still in its early stages most likely due to issues related to the typical dark brown color of lignin, the non-uniform molecular structure, and some impurities.

In food applications, there are still limited scientific studies exploring the use of lignin in food matrices. The researchers from the VTT Technical Research Center of Finland highlighted that wood-derived products like lignin can be used as texture enhancers, thickening agents, and stabilizers for emulsions and foams in specific foods such as yogurt, baked goods, and meat products (188). However, according to EFSA, the incorporation into food matrices requires more detailed studies to determine the safety of lignin and establish an acceptable daily dose. On the other hand, lignin properties such as antioxidant activity and antimicrobial effects can be extremely beneficial in scavenging free radicals and extending the shelf life of food products, as well as acting as a food preservative, potentially reducing reliance on synthetic preservatives and increasing food safety (189). Lignin is already used in food packaging. Studies reported that when lignin is mixed with chitosan, it results in controlled water permeability, better water resistance, and increased antibacterial activity (190, 191).

Over the years, lignin composites have gained popularity in biomedical applications including drug delivery carriers, tissue engineering scaffolds, wound dressing materials, biosensors, biomedical imaging, and anticancer therapy. This includes the use of lignin-based nanomaterials such as nanoparticles (NPs) and hydrogels (Figure 10). In recent years, there has been a growing number of publications on the preparation of lignin

nanoparticles (LNPs) with controlled particle size and morphology, highlighting the strong expectation for their potential applications (192).

The excerpt described below was revised from the chapter of the book written by the author about methods for preparing lignin nanoparticles for biomedical application (Adapted from: Ana Rita Pereira, Victor de Freitas, Joana Oliveria; Chapter 7—Development of lignin-based nanoparticles: Fabrication methods and functionalization approaches, 2021).

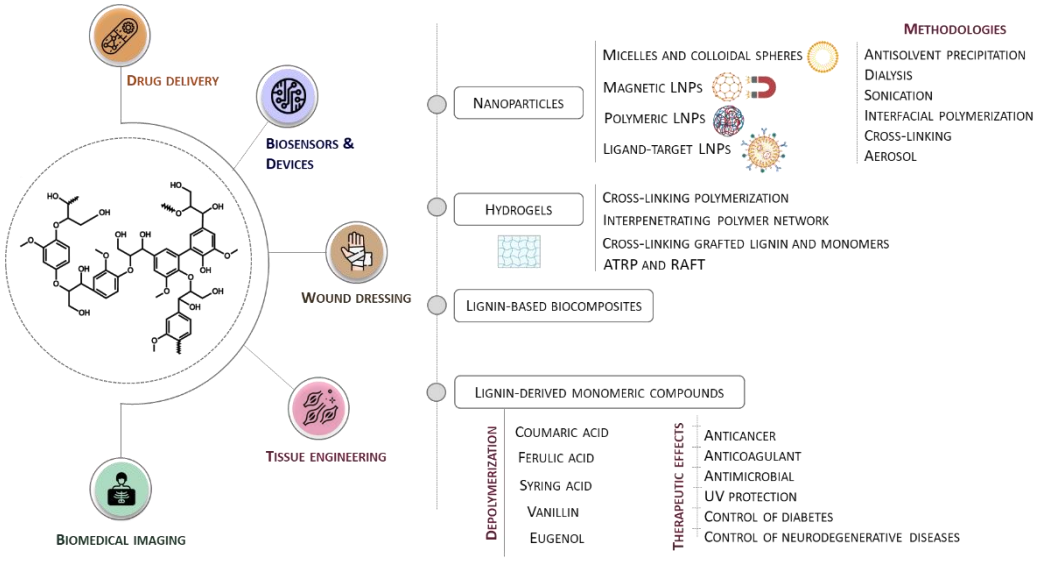

Figure 10 – Potential biomedical applications and therapeutical effects of lignin and lignin derivatives. Evidence of the different methodologies applied to obtain lignin nanoparticles and lignin-based hydrogels (ATRP - atom transfer radical polymerization) and RAFT - reversible addition-fragmentation chain transfer polymerization).

Considering all the promising features such as increased stability, efficiency, and effectiveness of the drugs used, NPs are the most common nanostructures used in biomedical applications, including vesicle-based carriers (e.g., micelles and colloidal spheres), inorganic NPs (e.g., metallic NPs), polymer-conjugates, and polymeric NPs. NPs synthesized from lignin are relatively nontoxic, highly biodegradable, stable, and inexpensive, which makes them promising for biomedical applications (193). LNPs demonstrated the ability to load different drugs and the possibility of being modified with targeting molecules, such as pH-sensitive polymers and targeting ligands, allowing a pH-responsive drug release and an increased cellular interaction with specific cells, respectively (194). To maximize their performance, especially to increase the treatment effectiveness, reduce side effects, and overcome drug resistance, the size, shape, and surface properties of NPs can be optimized and functionalized to obtain modified or

functional NPs (195). LNP can be prepared using different methods including antisolvent precipitation, solvent exchange, aerosol process, supercritical solvent precipitation, ultrasonication, and interfacial polymerization/ cross-linking. Generally, antisolvent nanoprecipitation methods are currently the most popular methods for LNPs production from technical lignin. They are facile and simple methods, easy to perform with minimal experimental setup (196). Solvent exchange via dialysis has been reported as an easy method to prepare LNPs and has been considered economically feasible on a large scale. However, this method has some limitations: it is time- and reagent-consuming, the stability of the drug may be compromised during dialysis, and the generated NPs have a heterogeneous size distribution (197). Methods for producing lignin particles through cross-linking and polymerization often involve toxic and hazardous agents, such as epichlorohydrin, hydrogen peroxide, and toluene diisocyanate. However, these production methods show particular advantages for encapsulating active substances due to the straightforward cross-linking process in mini and macroemulsions (198). The production of lignin nanostructures using supercritical fluids (SCF) allows precise control over the size and shape of the nanomaterials. However, a major limitation of this technique is the solubility of compounds in carbon dioxide, along with the high costs associated with sophisticated laboratory facilities and maintenance (199).

To improve the accumulation of the nanomedicines at the target site (e.g., tumor) with increased therapeutic effects, LNPs can be modified to respond to certain stimuli (e.g. changes in pH, temperature, magnetic field, ultrasound intensity, and light) (200) or using active-targeting ligands (e.g., antibodies, engineered proteins, nucleic acid aptamers, and peptides) (201). LNPs with superparamagnetic behavior are also promising vehicles for cancer therapy and diagnosis, such as magnetic targeting and magnetic resonance imaging. Examples of them include the preparation of Fe-LNPs and Fe_3O_4-LNPs using a solution of iron (III) isopropoxide [$Fe(OiPr)_3$], where the results showed the superparamagnetic behavior makes them promising vehicles for delivery of drug molecules to a specific target in the body by using a magnetic field. The authors concluded that as a result of their surface structure, LNPs can next be modified with targeting moieties to increase the cellular uptake into specific cells for cancer therapies (126).

The preparation of pH-responsive lignin nanoparticles (LNPs) is a promising strategy, particularly for drug delivery systems where controlled release of therapeutic agents is essential. Lignin is first modified by amination (202) or carboxylation (203) to increase the number and the reactivity of the functional groups, and then prepare lignin conjugates or nanostructures (204) that exhibit the ability to respond to changes in pH

allowing the release payloads selectively in specific acidic or basic environments related to diseases sites. Furthermore, the biodegradability of lignin nanoparticles fits with the growing demand in the biomedical industry for eco-friendly and biocompatible materials. The pH-responsive nature of lignin nanoparticles holds enormous promises for increasing precision medicine and improving therapeutic outcomes as research continues to discover and exploit their potential.

CHAPTER II

LIGNIN: TRANSFORMING BYPRODUCTS INTO TECHNOLOGICAL INNOVATIONS

Chapter II of this Ph.D. dissertation focuses on lignin-related studies and is organized into three parts.

Part A: Valorization of vine shoots as a source of valuable extracts and stable lignin nanoparticles for multiple applications.

This section explores the isolation of dioxane lignin from vine shoots and includes detailed physicochemical characterizations. It also investigates the production of dioxane lignin nanoparticles for potential applications. This research was a collaborative effort with ALiCE, an associate laboratory in chemical engineering at the University of Porto's Faculty of Engineering.

Part B: Exploring the lignin valorization as a promising agent to modulate the physicochemical properties of wine.

This work investigates lignin's potential as a modulating agent of the physicochemical properties of wine. Through the assessment of various parameters, we performed an in-depth study on how this biopolymer impacts the structural elements and sensory characteristics of wine.

Part C: pH-dependent complexation of cyanidin-3-O-glucoside with lignosulfonates.

Lignosulfonates, a by-product of the pulp and paper industry, were investigated for their ability to form complexes with anthocyanins. It aimed to assess the effectiveness of lignosulfonates in enhancing color stability and oxidative protection, demonstrating their potential to improve the quality and longevity of anthocyanin-based products for various technological applications.

PART A

VALORIZATION OF VINE SHOOTS AS A SOURCE OF VALUABLE EXTRACTS AND STABLE LIGNIN NANOPARTICLES FOR MULTIPLE APPLICATIONS

SYNOPSIS

This work proposes the full valorization of vine shoots, which is an annual residue produced at a large scale, focusing on the extraction of lignin by mild acidolysis for the preparation of nanoparticles. The effect of the pretreatment solvents (ethanol/toluene, E/T, and water/ethanol, W/E), on the chemical and structural features of lignin, was evaluated. The chemical analysis suggests similar composition and structure regardless of the pretreatment solvent, although lignin isolated after pretreatment of biomass with E/T showed a higher content of proanthocyanidins (11 %) compared with W/E (5 %). Lignin nanoparticles (LNPs) presented an average size ranging from 130–200 nm and showed good stability for 30 days. Lignin and LNPs showed excellent antioxidant properties (half maximal inhibitory concentration, IC_{50} 0.016–0.031 mg/mL) when compared to commercial antioxidants. In addition, extracts resulting from biomass pretreatment showed antioxidant activity, with W/E presenting a lower IC_{50} (0.170 mg/mL) than E/T (0.270 mg/mL), correlated with the higher polyphenol content of W/E, with (+)-catechin and (−)-epicatechin being the main compounds detected. Overall, this work shows that the pre-treatment of vine shoots with green solvents can yield (i) the production of high-purity lignin samples with antioxidant properties and (ii) phenolic-rich extracts, promoting the integral reuse of this byproduct and contributing to sustainability.

This chapter was adapted from the following paper: ***Pereira, A.R.****; Costa, C.; Mateus, N.; de Freitas, V.; Rodrigues, A.; Oliveira, J. Exploring the Potential of Vine Shoots as a Source of Valuable Extracts and Stable Lignin Nanoparticles for Multiple Applications. Manuscript accepted in International Journal of Molecular Sciences. Doi: 10.3390/ijms24065165.*

Except for the ^{13}C NMR, GPC, and the determination of lignin content and inorganic material, the experimental design and work described in this chapter were carried out by the author.

1. INTRODUCTION

The European Union (EU) produced 165 million liters of wine in 2020, and by this measure, the wine industry is one of the most important food industries in the world. According to the International Organization of Vine and Wine (205), Portugal ranks 11th among major wine producers and exporters worldwide. With this, every year, millions of tons of organic waste (grape pomace, grape stems, lees, and vine pruning material), wastewater, and inorganic residue are produced, which contributes to significantly increasing greenhouse gas emissions. For instance, it has been estimated that the Portuguese wine industry generates between 1.2 and 3.5 t/ha of waste or co-products annually during the vintage season (206). In 2019, around 3.4×10^5, 5.8×10^6, and 1.3×10^7 t of vine shoots were produced in Portugal, Europe, and the world, respectively (207). Due to their high calorific value, these residues are typically left in the vineyard or used as domestic fuel, resulting in the release of greenhouse gases such as N_2O, CO, CH_4, and NO_2 into the atmosphere (208, 209). To reduce the impact of these co-products on the environment and increase the value of the winemaking process, new green strategies to reuse, recycle, and recover these residues - especially organic residues - are constantly being developed. Vine shoots are a complex matrix with structural components such as cellulose (32 – 40 %), hemicellulose (5 – 27 %), and lignin (16 – 39 %) (210-212), with other minor compounds such as lipids, vitamins, and more simple phenolic compounds. Due to their antioxidant properties and beneficial effects on human health, including cardioprotective, anticancer, anti-inflammation, antiaging, and antimicrobial properties, phenolic compounds have received the most attention, particularly from the industry (213, 214). It has been suggested that vine shoots could be used as a source of sugars that could be turned into bioethanol, xylitol, lactic acid, and biosurfactants (215, 216). In addition, it has been investigated whether this co-product could be applied in the production of various materials such as particle boards, biochar, and paper (217-220).

Lignin is a natural aromatic biopolymer that can be used as a raw material in various materials. It is inexpensive, stable, relatively nontoxic, and highly biodegradable. Several methods have been developed in the industrial sector to convert lignin directly into heat or electricity, bio-oil, or combustible biogas (221). Due to its complex and varied structure and low solubility, lignin has been used in several little-known applications, including surfactants, adhesives, and dispersants. Drug delivery vehicles, scaffolds for tissue engineering, materials for dressing wounds, lignin-based nanoparticles (NPs), and hydrogels are just a few examples of biomedical uses for lignin composites (222). Natural

lignocellulosic fibers from crops have found applications in many industries due to their low cost, lightweight, superior mechanical properties, and abundance (223, 224). Furthermore, since they are eco-friendly, non-toxic, and biodegradable, natural fiber-reinforced polymer composite materials have largely replaced synthetic carbon-based materials, particularly in plastics, electronics, packaging (225), and the automotive industry (226). There are three fundamental phenylpropanoid monolignols in the composition of lignin: sinapyl, coniferyl, and *p*-coumaryl alcohols. These subunits are the precursors of the main moieties of lignin structure: syringyl (S), guaiacyl (G), and p-hydroxyphenyl (H), which differ in the methoxylation of the aromatic units. Moreover, the structural units of lignin can comprise several functional groups. The most frequent ones are primary and secondary aliphatic hydroxyl, aromatic methoxyl, and phenolic hydroxyl, and in minor amounts, the carbonyl (aldehydes and ketones), and carboxyl groups (107). The plant species (softwood, hardwood, or grass), the morphological part of the plant, and the delignification process determine the structural characteristics (functional groups and type of linkage) and composition of lignin (107). It is essential to select a process that has a low impact on native lignin structure, such as dioxane and “milled wood” lignins to avoid extensive lignin structural changes caused by the isolation required for the characterization of lignocellulosic biomass (227). The extraction and structural characterization of lignin from various herbaceous plants, such as rice (228), cotton, corn stalks and roots, sugarcane, and tobacco, have been described in the literature (227). In the first case, the authors used ultrasound-assisted extraction in an alkaline medium to promote the extraction of lignin and cellulose from rice straw, and their yields increased with sonication time from 10 to 30 min (228). Esteves et al. (227) used mild acidolysis to extract lignin from two morphological parts (stalks and roots) of different sources to produce added-value products, such as vanillin and syringaldehyde, in the perspective of a biorefinery. Prozil and coworkers (229) reported the extraction of lignin from grape stalks using a modified acidolytic procedure with various steps and organic solvents.

Most of the works concerning the valorization of by-products focused on one class of compounds, overlooking the others. This work proposes the total extraction of bioactive and structural compounds (lignin), aiming for the full valorization of vine shoot residues. For that, a mild acidolysis methodology was used to obtain lignin (with little structural modifications) that was used to produce stable nanoparticles with the potential to be used in different technological applications (food, cosmetic, and pharmaceutical industries). Moreover, because of biomass pretreatment, phenolic compound-rich extracts were obtained with important antioxidant properties, contributing to the economy and sustainability.

2. MATERIALS AND METHODS

2.1. PREPARATION OF VINE SHOOTS

First, 250 g of vine shoots from the Vinhão variety (*Vitis vinifera*) were collected after pruning at Fradelos, Vila Nova de Famalicão, Vinhos Verdes Region, Portugal. The dry material was milled on a cross-beater millSKl (Retsch, Haan, Germany), and sieved to 0.250 – 0.425 mm sawdust (35 – 60 mesh).

2.2. BIOMASS PRE-TREATMENT AND LIGNIN ISOLATION

The biomass was submitted to a pre-treatment extraction with two different solvent mixtures (ethanol/toluene, E/T (4:1, v/v), or water/ethanol, W/E (4:1, v/v)). About 15 g of vine shoots (35 – 60 mesh fraction) were extracted in a Soxhlet extractor using 500 mL of a solvent mixture. The solvent was heated to the boiling point, and the extraction was performed for 6 h. The solvent was removed through roto-evaporation under vacuum, freeze-dried, and stored at −20 °C until chemical analysis. The pre-treated biomass was left to dry at room temperature overnight for further isolation of lignin by mild acidolysis, following the procedure previously described in the literature with some modifications (230). The pre-treated dried vine shoots were placed in contact with the dioxane/water (9:1, v/v) mixture containing HCl 0.2 M under nitrogen and reflux for 40 minutes. This procedure was performed two more times but in the last extraction, the HCl was not added to the dioxane/water mixture. Lignin was precipitated in cold water after the concentration of the previous fractions by evaporation under a vacuum. The precipitated lignin was removed by centrifugation, washed with water until neutral pH, and freeze-dried. Lignin samples were submitted to dialysis (membrane dialysis cutoff 12-14 kDa, Spectrum Labs) at a concentration of 2 mg/mL for 24 h, replacing the water several times. Lignin samples after precipitation, washing, and lyophilization were submitted to dialysis (membrane dialysis cutoff of 12–14 kDa, Spectrum Labs) for 24 h. Samples were coded as LET - lignin sample pre-treated with ethanol/toluene; LETD - lignin sample pre-treated with ethanol/toluene and dialyzed; LWE - lignin sample pre-treated with water/ethanol; and LWED - lignin sample pre-treated with water/ethanol and dialyzed.

2.3. Chemical Characterization of Extracts Obtained from Biomass Pretreatment

2.3.1. Total Polyphenol Content

The total polyphenol content (TPC) of the extracts obtained from the pretreatment of biomass with E/T and W/E was determined through the Folin-Ciocalteu assay described in the literature, using gallic acid as a standard (231).

2.3.2. Identification of Phenolic Compounds

The low molecular weight phenolic compounds and proanthocyanidins were determined by liquid chromatography equipped with diode array detection and mass spectrometry (HPLC–DAD/MS), as previously described in the literature (232). For that, each sample was first dissolved in water (1 g/L) and then a microscale liquid-liquid extraction was performed using an ethyl acetate:acetonitrile (2:1) mixture. The organic phase was dried in a Labconco CentriVac Concentrator for 3 h at 37 °C. Samples were dissolved in water:methanol (1:1, v/v) and analyzed by HPLC-DAD/MS in the negative ion mode. Mass Spectrometry analysis was performed using a Finnigan Surveyor series liquid chromatograph, equipped with a reversed-phase C18 column (LIchrospher® 100) with 250 × 4.6 mm i.d., 5 µm thermostatted at 25 °C. The mass detection was carried out in the negative ion mode in a Finnigan LCQ DECA XP MAX (Finnigan Corp., San José, CA, USA) mass detector with an API (Atmospheric Pressure Ionization) source of ionization and an ESI (ElectroSpray Ionization) interface. Spectra were recorded in the negative ion mode between m/z 300 and 1500. The elution procedure was presented in Appendix 1 (Table 1A), using solvent A (1 % acetic acid in water) and solvent B (1 % acetic acid and 20 % acetonitrile in water) at different percentages.

2.3.3. Sugar Content

The sugar content of both samples was quantified by their derivatization with hexamethyldisilazane (HMDS) and through analysis by gas chromatography-mass spectrometry (GC-MS/MS), as described in the literature (233). GC-MS/MS was carried out with a Trace 1300 gas chromatograph equipped with a split–splitless injector, an autosampler 1310 Thermo Scientific, and an ISQ Single quadrupole MS (Thermo Fisher, Austin, TX, USA). A total of 1 µL of the sample was injected into the injector operating in

splitless mode. The temperatures of the injector and the MS-transfer line were 250 °C and 300 °C, respectively. Compounds were separated on a 30 m × 0.25 mm (i.d.) × 0.25 µm DB-17 capillary column (Agilent Technologies, CA, USA) operating at a constant helium flow of 1.5 mL/min. The column temperature was initially set to 110 °C, held for 5 min, increasing then at a rate of 6 °C/min to 300 °C and held for 5 min. Measurements were performed in SCAN mode with the m/z range set to 40 – 1100. The MS conditions were as follows: ion source temperature 280 °C and electron energy 70 eV, using glucose as standard for the calibration curve. Selected ion monitoring (SIM) conditions were used for the glucose, selecting the m/z 204. Glucose was used as a standard, and sugar content was expressed as mg of glucose by g of dried sample.

2.4. Chemical Characterization of Lignin Samples

2.4.1. Lignin Content

The amount of Klason lignin was calculated in the biomass after sulfuric acid hydrolysis according to the method described in the literature (227). A solution of 72 % (w/w) H_2SO_4 was added to 1.0 g of residue and after 2.5 h the mixture was diluted with water and hydrolyzed for 2 h under reflux. Then, the final material was filtrated, washed with water until neutral pH, dried, and weighed. For the quantification of acid-soluble lignin, 20 mL of the filtrate was adjusted to pH 9 and mixed with 50 mg of $NaBH_4$ and left stirring for 20 min. Following this, the solution was acidified, and diluted, and the absorbance at 280 nm was measured using a solution of 1.8 % H_2SO_4 as a reference. This estimate was adjusted for moisture content.

2.4.2. Inorganic Material and macronutrients Content

The inorganic material was quantified gravimetrically after lignin sample incineration at 550 °C for 6 h. For the carbohydrate content determination, 15 mg of material was dissolved in 2 mL of a methanol solution containing 2 M HCl and submitted to acid methanolysis at 100 °C for 4 h. After cooling, pyridine and sorbitol (internal standard solution) were added, and the mixture was evaporated under reduced pressure. The dried methanol derivatives were converted into trimethylsilylated products and the quantification was performed by gas chromatography with a flame ionization detector (GC-FID), as already described in the literature (234, 235).

Proanthocyanidins (PACs) were quantified by the acid butanol assay adapted from the method described by Porter et al. (236). Into pressure and temperature-resistant tubes, 500 µL of butanol reagent (butanol with 5 % (v/v) of concentrated hydrochloric acid) were mixed with 18 µL of ammonium iron (III) sulfate dodecahydrate solution (20 mg/mL) prepared in aqueous hydrochloric acid (2 M) and 82.5 µL of a methanolic solution of each lignin fraction (3.0 mg/mL: LET, LETD, LWE, and LWED). The mixture was incubated at 100°C for 50 min, and after cooling, the absorbance was determined at 520 nm was determined. The quantification was made using as standard a purified PACs fraction containing trimers and based on the calibration curve ($y = 1.7091x + 0.0519$, $R^2 = 0.9992$).

2.4.3. GEL PERMEATION CHROMATOGRAPHY

The molecular weight distribution of lignin samples was determined on a Shimadzu UFLC with a diode array (running at 280 nm wavelength) and refraction index detectors. It was used two Agilent gel columns (an OligoPore column 300×7.5 mm and a MesoPore column 300×7.5 mm) placed in series with a guard column Oligopore 50×7.5 mm. GPC analysis was performed at a flow rate of 0.8 mL/min using an isocratic gradient and dimethylformamide with 0.5 % w/v of lithium chloride as the mobile phase. The temperature of the columns was maintained at 70 °C during the acquisition. Polystyrene standards with molecular weights ranging from 162 to 55,000 g/mol and measured at 268 nm were used to calibrate the equipment before sample analysis. Solutions (5 mg/mL) of each polystyrene standard and each lignin sample were dissolved in dimethylformamide with 0.5 % w/v of lithium chloride, stirred, and filtered (0.2 µm) before injection.

2.4.4. ^{13}C NMR AND ^{31}P NMR

Quantitative ^{13}C NMR spectra were recorded in a Bruker AVANCE III 400 spectrometer operating at 400 MHz at a temperature of 318 K for 72 h. For that, 170 mg of dried lignin was dissolved in 500 µL DMSO-d6. ^{13}C NMR measurements were determined by a simple 1D pulse sequence, a recycling time of 12 s, 1400 scans, and a 1D sequence with power-gated coupling using a 90° flip angle. For the ^{31}P NMR analysis, LWED and LTED samples were accurately weighted (about 40 mg) and dissolved in 500 µL of a mixture of pyridine and deuterated chloroform (1.6:1, v/v) and left for a few minutes at room temperature until complete dissolution. Cholesterol (85 mg/mL, 100 µL)

and chromium (III) acetylacetonate (5.6 mg/mL, 50 µL) were used as internal standards and relaxation reagents, respectively, as previously described (237). The phosphitylation reagent (2-chloro-4,4,5,5-tetramethyl-1,3,2-dioxaphospholane) (100 µL) was added and the sample analyzed on a Bruker AVANCE III 400 spectrometer operating at 400 MHz at 298 K. The spectrum was acquired for 30 min with a relaxation time of 10 seconds.

2.4.5. Fourier-transform infrared spectroscopy (FTIR)

FTIR spectra of lignin samples were recorded on a Spectrum Two FTIR Spectrometer (PerkinElmer). Potassium bromide (KBr) discs of each sample were prepared by pressing a mixture of 100 mg of KBr and 1 mg of the sample under a vacuum. The spectra were recorded in the range of 4000 − 400 cm^{-1} with 4 scans in the medium-infrared area.

2.5. PREPARATION OF LIGNIN NANOPARTICLES

Lignin nanoparticles (LNPs) were prepared from lignin samples by nanoprecipitation or dialysis (222). For the nanoprecipitation method, each lignin sample (LET, LETD, LWE, and LWED at 10 mg/mL) was dissolved in a mixture of acetone:water (9:1, v/v) and filtered through a 0.22 µm filter. The filtrate was added to Milli-Q water (1:20) under constant stirring using a micro syringe and left stirring for 3 h at room temperature. The suspension was centrifuged at 1500 g (10 min at 20 °C) to remove aggregates. Regarding the dialysis method, lignin samples (2 mg/mL) were dissolved in tetrahydrofuran and introduced into a dialysis bag (flat width, 25 mm) with a 12 – 14 kDa cut-off (Spectra/Por ® 2 Standard RC Tubing, Spectrum Labs, USA), similar to what was described previously in the literature (238). Membranes were left submerged in de-ionized water (1:60) under slow stirring for 24 h at room temperature with the dialysis water being periodically replaced. LNPs were stored at room temperature and characterized (average particle size, Z-average; polydispersity index, PDI; and the average zeta (ζ)-potential) by dynamic light scattering (DLS) and electrophoretic light scattering (ELS) using a Malvern Zetasizer Nano ZS instrument (Malvern Instruments Ltd., UK). Samples were diluted 10 times with Milli-Q water and analyzed in triplicate. The stability of DLNPs over time (0, 7, 15, and 30 days) was assessed by following the changes in the average particle size, polydispersity index, and average zeta (ξ)-potential. Each experiment was performed in triplicate.

2.6. ANTIOXIDANT ACTIVITY

The antioxidant activity of extracts, LNPs, and lignin samples was performed using a 2,2′-diphenyl-1-picrylhydrazyl radical (DPPH) assay, a common spectrophotometric assay procedure for determining the antioxidant capacities of compounds. In a 96-well plate, 270 µL of DPPH solution (prepared in methanol at a concentration of 24.2 µg/mL) was mixed with 30 µL of antioxidant samples. Commercial antioxidants such as Trolox, ascorbic acid, and gallic acid were used as references. E/T and W/E extracts were dissolved in ethanol. LNPs were dispersed in water, while the reference antioxidants, including lignin samples (LET, LETD, LWE, and LWED), were dispersed in 50% (v/v) of ethanol, in a range of concentrations between 0 and 1 mg/mL. For each sample concentration, the radical scavenging reaction was monitored as a function of time by measuring the DPPH absorbance band at 517 nm (λ_{max}) on a plate reader (Biotek Powerwave XS), in the beginning, and after 30 min of reaction. IC_{50} values of test/reference compounds are represented as half of the maximum inhibitory concentration of DPPH radical scavenging activity. The antioxidant activity was expressed as the radical scavenging activity (RSA) by calculating the fitting peak area at 517 nm, using the following equation: $RSA\ (\%) = \frac{(Abs\ control - Abs\ sample)}{Abs\ control} \times 100$

2.7. STATISTICAL ANALYSIS

All data were reported as the mean standard deviation of at least three values. Statistical analyses were performed using GraphPad Prism 7 for Windows (GraphPad Software, version 7.04, San Diego, California; www.graphpad.com). Results were subjected to an analysis of variance (one-way or two-way ANOVA), and the differences between means were calculated using Tukey's and Holm-Sidak multiple comparison tests. They were considered significant when the p-values were below 0.05 ($p < 0.001$ and $p < 0.0001$).

3. RESULTS AND DISCUSSION

3.1. CHARACTERIZATION OF EXTRACTS RESULTING FROM THE PRETREATMENT

The biomass was pretreated before the delignification of vine shoots by Soxhlet extraction using ethanol/toluene (E/T) or water/ethanol (W/E), and the lignin was then isolated from the dried biomass by mild acidolysis (Figure 11). The chemical composition

analysis of vine shoots revealed that this material contained low amounts of inorganic compounds and other extractives (2.5 % and 4.9 %, respectively). Non-cellulosic carbohydrates represents 21 % of the weight of the biomass, and the lignin content (Klason lignin) is about 30 %. These numbers are in line with those that have been reported in the literature (210, 219). The yield of lignin isolation from the mild acidolysis procedure was about 30 %, calculated concerning the total lignin content (Klason and soluble lignin) determined in vine shoot samples.

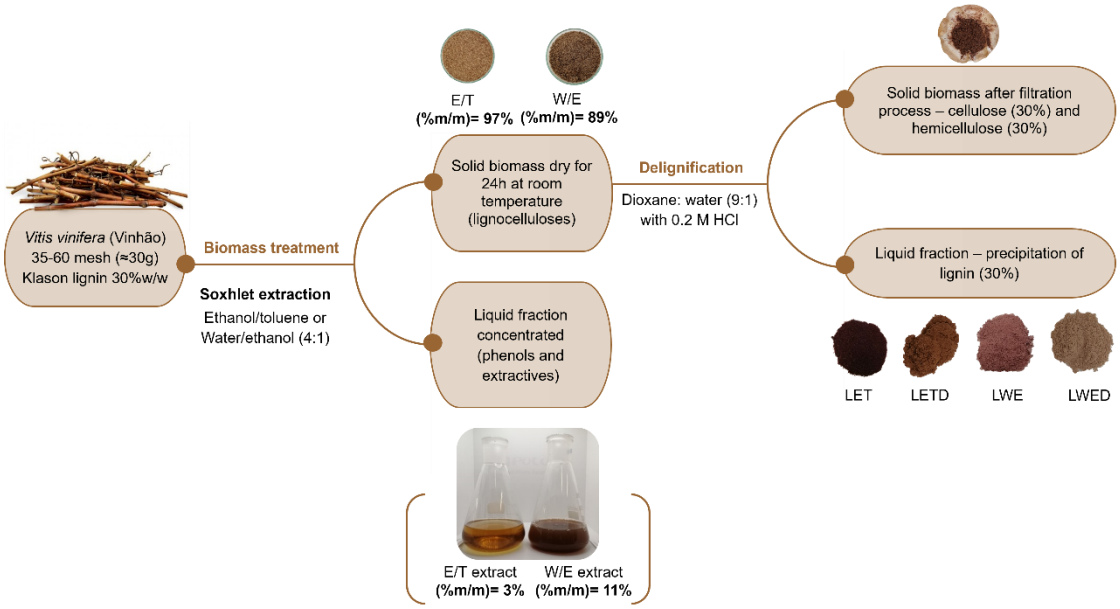

Figure 11 - Lignin content in the vine shoots and the yield of liquids and solids recovered after each procedure.

Compared to the 3 % obtained for the E/T extract, the W/E extract accounts for approximately 11 % of the initial biomass. This suggests that this solvent mixture has been more effective at removing the phenolic and other bioactive compounds from biomass, as previously documented in the literature (239, 240). When compared to the E/T extract, which had a total polyphenol (TP) of 82.8 ± 0.7 mg GAE (gallic acid equivalents)/g extract, the Folin–Ciocalteu method revealed a much higher value ($p < 0.001$) of TP content (328.9 ± 0.4 mg GAE/g extract). The antioxidant activity of W/E extract showed a similar pattern, with a lower IC_{50} value (IC_{50} 0.170 mg/mL) in comparison to a higher value for E/T extract (IC_{50} 0.270 mg/mL). This is a consequence of the higher phenolic content of this extract.

3.1.1. PROANTHOCYANIDINS

The phenolic compound composition of extracts W/E and E/T was determined by mass spectrometry coupled to diode array detection and mass spectrometry (LC-DAD/MS). The isomer monomeric units (+)-catechin (m/z 289) and (−)-epicatechin (m/z 289) were the main flavan-3-ols detected in both samples. Moreover, three B-type procyanidin dimers (m/z 577) were also identified in both extracts. The unequivocal identification of proanthocyanidins was achieved by their characteristic fragmentation (MS^2) patterns that include water loss (MS^2 407 and 559), heterolytic ring fission (HRF, MS^2 451), quinone methide (QM, MS^2 289) fission, and the retro-Diels-Alder (RDA, MS^2 425) (241, 242). Gallic acid esters of flavan-3-ol and PAS dimers were also identified: (epi)catechin-(epi)catechin gallate (m/z 729) and a 3-methyl epigallocatechin gallate (m/z 471). The first form produced ions (MS^2) at m/z 577, 559, and 407, which are typical fragments of B-type procyanidin dimers. The gallic acid ester position is fundamentally based on QM fission. Thus, the ions at m/z 441 were crucial in assigning the gallic acid ester to the bottom positions. Phenolic compounds detected in these samples were already reported in the literature to be present in vine shoots, being present in higher amounts in the WE extract (239, 240).

3.1.2. SUGARS

The analysis of the sugar content of both extracts showed that samples are mainly composed of glucose, with residual amounts of fructose and sucrose. As expected, the W/E extract resulting from Soxhlet extraction with water/ethanol (dark brown) exhibited a higher sugar content (681.3 ± 8.8 mg glucose/g extract) than the extract from the biomass treatment with ethanol/toluene (112.6 ± 7.6 mg glucose/g extract). The treatment with water allowed a more effective removal of sugars present in the biomass, which means that the isolated lignin will present a lower amount of this component. In this way, a sugar-rich extract is obtained using a combination of environmentally friendly solvents in the treatment of vine shoots. In other works, Jesus and coworkers (215) also detected the presence of xylose and arabinose in liquid fractions resulting from a sequential autohydrolysis treatment at 180 °C for 60 min of vine pruning residues. Then, bioethanol was produced by separate and simultaneous saccharification and fermentation. Rivas et al. (211) added the presence of galactose (2.5 ± 0.3 wt.% in oven-dry basis) and mannose (1.0 ± 0.1 wt.% in oven-dry basis) after the treatment of this biomass with aqueous solvent extraction at 130 °C. Independent of the biomass

treatment or extraction method used, these results show that vine shoots are a potential renewable source of sugars to produce value-added products for different industries.

3.2. Cellulose and Hemicellulose Fraction

Solid fractions containing 30 % cellulose, and 30 % hemicellulose were produced following the delignification process. These percentages are consistent with the literature descriptions, and depending on the extraction technique, different levels of polysaccharides may be obtained (211). Additionally, a variety of bioproducts can be produced by individually valorizing these fractions. The literature describes various fractionation techniques based on one-step fractionation with immiscible solvents, with 1-butanol (green solvent) being the solvent that allowed more favorable results (243). After fermentation, cellulose solids go through enzymatic hydrolysis to produce glucose solutions, which can be used as fermentation media to produce bioproducts such as bioethanol or biofuels (244). For hemicellulose, when exposed to acidic conditions, pentosan polysaccharides are converted into pentoses (xylose and arabinose) by dehydration, leading to the formation of furfural, whose excellent yields make this procedure a source of commercial production (245). In the same way, hexoses (such as glucose, galactose, or mannose) can be produced by hydrolyzing hexosans and then dehydrated to produce hydroxymethylfurfural. Furfural and hydroxymethylfurfural are significant platform chemicals that can be used to produce a variety of fuels and bioproducts (245, 246). Most of the byproducts produced during partial hydrolysis of hemicelluloses are polysaccharide fragments (low molecular polysaccharides and/or oligosaccharides). Oligosaccharides can be utilized as prebiotics, for instance, in the food and pharmaceutical industries due to their bioactivity (247).

3.3. Characterization of Lignin from Vine Shoots

3.3.1. Composition of the Isolated Lignin Samples

The chemical composition of the isolated lignin is depicted in Table 5. For the isolated lignin, a maximum of 1.2 % of inorganic content was found, while the content of co-extracted carbohydrates was between 4.2 and 6.9 %, accounting for a maximum of 7.2 % of the referred contaminants in the lignin pretreated with water/ethanol (LWE) sample.

Table 5 - Contaminant content (ashes, carbohydrates, and tannins-proanthocyanidins) in isolated lignin (dry weight). LET (lignin pretreated with ethanol/toluene); LETD (lignin pretreated with ethanol/toluene and purified by dialysis); LWE (lignin pretreated with water/ethanol); and LWED (lignin pretreated with water/ethanol and purified by dialysis).

Lignin	Ashes %w/w $_{lignin}$	Carbohydrates %w/w $_{lignin}$	Proanthocyanidins % w/w $_{lignin}$
LET	0.12	5.4	11.3 ± 0.02
LETD	0.19	4.2	9.95 ± 0.03
LWE	0.30	6.9	4.65 ± 0.01
LWED	1.17	5.1	3.38 ± 0.01

One of the main objectives of this work was to evaluate the influence of the solvent mixture used in the Soxhlet extraction (pre-treatment of the vine shoots) and the purification of the sample by dialysis in the final structure and composition of lignin. Based on the previous results, there are no significant differences in the composition of the different lignin samples, considering the inorganic material and the carbohydrates. It is also important to note that mild acidolysis gives rise to lignin with a low content of contaminants.

3.3.2. PROANTHOCYANIDIN CONTENT IN LIGNIN SAMPLES

According to the literature, the lignocellulosic biomass from the wine industry co-products presents a considerable percentage of proanthocyanins in its composition. It is described that grape stalks can have approximately 6 % of tannins (248, 249) although in some cases, their amount can reach ≈ 17 % (212). Considering that vine shoots are derived from the same plant, the evaluation of the presence of these compounds is essential. The undefined and complex structure of the lignin and its possible interaction with tannins was suggested to be the reason for the extremely difficult delignification of this type of biomass. Table 5 shows that samples LET and LETD present a higher percentage of proanthocyanidins with values around 11 and 9 %, respectively, when compared with the 5 and 3 % of proanthocyanidins that were obtained for LWE and LWED, respectively. This means that the pre-treatment with water/ethanol was more efficient in the elimination of tannins from the lignocellulosic biomass. The resulting liquor from this extractive process had a more intense brown color than the liquor obtained using ethanol/toluene. The literature states that water alone or water mixed with other solvents such as methanol, ethanol, acetone, or NaOH can effectively extract lignin free

of tannins. The ethanol-toluene mixture is better suited to remove waxes, fats, resins, and wood gums (250).

3.3.3. MOLECULAR WEIGHT AND POLYDISPERSITY OF LIGNIN SAMPLES

The molecular weight (Mw) and polydispersity (Mw/Mn) of the isolated lignin were determined by gel permeation chromatography (GPC). The values obtained are between 43 – 49 KDa (Table 6). The lignin resulting from the vine shoots pre-treated with ethanol/toluene (LET and LETD) have a higher molecular weight of 45,000 and 48,000 g/mol, respectively, when compared with the lignin resulting from the vine shoot pre-treatment with water/ethanol (LWE: 43, 000 g/mol and LWED: 47, 000 g/mol). Moreover, the lignin subjected to dialysis shows a higher molecular weight than the correspondent lignin not submitted to this purification step.

Table 6 - Molecular weight and evaluation of the polydispersity of the different lignin fractions. LET – lignin sample pre-treated with ethanol/toluene; LETD – lignin sample pre-treated with ethanol/toluene and dialyzed; LWE – lignin sample pre-treated with water/ethanol and LWED – lignin sample pre-treated with water/ethanol and dialyzed.

Lignin	Molecular weight (g/mol)	Polydispersity
LET	45,000	1.43
LETD	48,000	1.42
LWE	43,000	1.44
LWED	47,000	1.40

3.3.4. QUANTITATIVE CARBON-13 NUCLEAR MAGNETIC RESONANCE (^{13}C NMR)

The quantitative ^{13}C NMR spectra of the analyzed lignin, with the main assignments identified, are presented in Appendix 1 - Figure 1A. The assignments and quantification of each structure, linkage, and functional groups identified in the lignin structure were made based on reference spectra and data available in the literature (227). The ^{13}C NMR results, presented in Table 7, are reported as the ratio of the integration of a given carbon signal to one-sixth of the integral of aromatic carbons (Ar).

Table 7 - Assignments and quantification of the structure/linkages and functional groups identified by ^{13}C NMR in the different lignin samples.

Assignments (Spectroscopic Range)	Amount (Number per Ar)			
	LET	**LETD**	**LWE**	**LWED**
C_β in β-5 and β-β structures (δ 51.0–53.8 ppm)	0.11	0.12	0.14	0.12
Aromatic OCH_3 (δ 54.3–57.3 ppm)	1.29	1.21	1.50	1.43
Cγ in β-*O*-4 structures without Cα=O (δ 59.3–60.8 ppm)	0.39	0.36	0.42	0.39
Cγ in β-5, β-*O*-4 structures with Cα=O and β-1 (δ 62.5–63.8 ppm)	0.12	0.11	0.13	0.12
Cα in β-*O*-4 structures; Cγ in pinoresinol/syringaresinol and β-β structures (δ 70.0–76.0 ppm)	0.82	0.77	0.79	0.76
C_β in β-*O*-4 structures; Cα in β-5 and β-β structures (δ 80.0–90.0 ppm)	0.71	0.69	0.77	0.77
Aromatic C_{Ar}-H (δ 103.0–123.0 ppm)	2.28	2.25	2.16	2.16
Aromatic C_{Ar}-C (δ 123.0–137.0 ppm)	1.19	1.30	1.27	1.31
Aromatic C_{Ar}-O (δ 137.0–156.0 ppm)	2.42	2.37	1.47	2.44
C_4 in H units (δ 157.0–162.0 ppm)	0.11	0.08	0.10	0.09
CHO in benzaldehyde structures (δ 191.0–192.0 ppm)	0.02	0.02	0.03	0.02
CHO in cinnamaldehyde structures (δ 193.5–194.5 ppm)	0.02	0.03	0.04	0.03
CO in aldehydes and ketones (δ 195.0–210.0 ppm)	0.39	0.65	0.50	0.38

The quantitative data from ^{13}C NMR enables the determination of the main structural characteristics of isolated lignin (Table 8). The results confirm that lignin isolated by mild acidolysis after pre-treatment of the vine shoots with water/ethanol and purified by dialysis (LWED) has the highest content of non-condensed structures (β-*O*-4 structures, 65 per 100 aryl units) and the highest condensation degree. It was observed that the condensation degree increases in the following order: LET (9 %) < LETD (13 %) < LWE (19 %) < LWED (21 %). Moreover, there are no differences in the number of the main structural units, S, G, and H, between all the lignin types, confirming that the dialysis and the Soxhlet extraction do not influence lignin structure, resulting in lignin with a structure closer to the native one.

Table 8 - β-O-4 structures content (number per 100 aromatic rings), degree condensation (DC), S:G:H and S/G ratio determined for the lignin samples.

	β-*O*-4 structures	**DC %**	**S:G:H**	**S/G**
LET	60	9	54:36:10	1.48
LETD	57	13	54:38:08	1.45
LWE	63	19	55:35:10	1.55
LWED	65	21	54:37:09	1.47

3.3.5. PHOSPHORUS-31 NUCLEAR MAGNETIC RESONANCE (^{31}P NMR)

Lignin's properties are influenced by the aliphatic and phenolic hydroxyl groups ratio. To elucidate the amount and type of hydroxyl groups present in these samples, isolated lignin (LETD and LWED) were phosphitylated with 2-chloro-4,4,5,5-tetramethyl-1,3,2-dioxaphospholane and analyzed by quantitative ^{31}P NMR. The ^{31}P NMR spectra of the phosphitylated lignin and the respective quantification of the different hydroxyl groups are described in Appendix 1 (Figure 1B) and Table 9, respectively. Aliphatic hydroxyl groups are associated with signals between 149 and 146 ppm, while phenolic hydroxyl groups are associated with signals between 143 and 137 ppm. The content of phenolic OH in the lignin structure was 1.01 mmol/g of lignin for sample LETD and 0.84 mmol/g of lignin for sample LWED. In the phenolic hydroxyl region, the signals in the range of 143.1–142.5, 140.2 to 139.4, and 138.2 to 137.8 ppm are assigned to hydroxyl groups in non-condensed guaiacyl, syringyl, and p-hydroxyphenyl units, respectively. The presence of these signals in isolated lignin fractions suggests GSH-type lignin, which agrees with the results obtained from FTIR. Relative to the higher quantity of aliphatic hydroxyls (3.20 mmol/g lignin for LETD and 2.80 mmol/g lignin for LWED), these could be overestimated values once the residual carbohydrates present in the samples can undergo phosphorylation of the hydroxyl groups that are quantified by ^{31}P NMR as aliphatic OH groups, as described in the literature (227). In this sense, the aliphatic hydroxyl content was not considered for the total phenolic hydroxyls.

Table 9- Quantification of phenolic and aliphatic hydroxyl groups, and carboxylic acids in lignin LETD and LWED by ^{31}P NMR.

Assignments	Amounts (mmol/g $_{lignin}$)	
	LETD	LWED
Aliphatic OH	3.20	2.80
Carboxylic acids	0.05	0.07
Total phenolic units	1.01	0.84
S phenolic units	0.30	0.37
G phenolic units	0.48	0.41
H phenolic units	0.23	0.06

3.3.6. FOURIER-TRANSFORM INFRARED SPECTROSCOPY (FTIR)

Figure 12 displays the FTIR spectra of the different lignin samples. As observed, the spectra are similar for all lignin samples, with the same absorption bands and equivalent intensities.

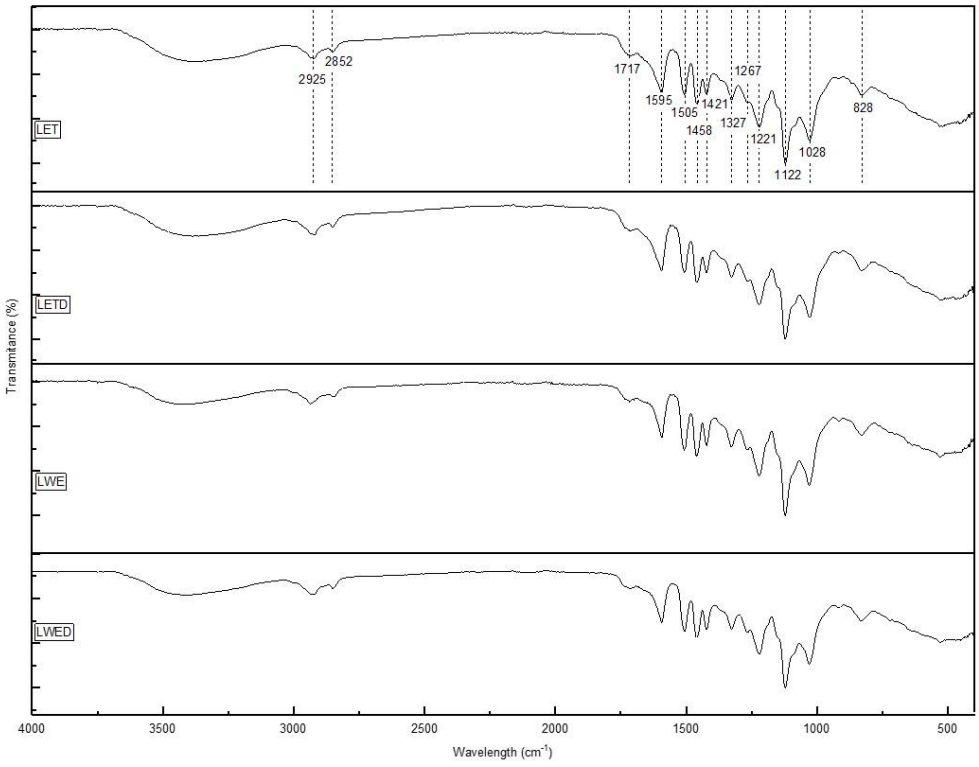

Figure 12 - FTIR absorption spectra for isolated lignin LET, LETD, LWE, and LWED.

Lignin has characteristic signals in the region between 700 and 1600 cm^{-1}, and typical chemical group stretching was observed between 2800 and 3500 cm^{-1}. Characteristic bands of the lignin structure at 1593, 1505, and 1422 cm^{-1} were assigned to the aromatic skeletal vibration. The presence of the three basic units of lignin was also evidenced, where the syringyl (S) ring absorption is observed at 1327 cm^{-1}, the guaiacyl (G) ring appears with a small shoulder at 1267 cm^{-1}, and for p-hydroxyphenyl (H) units, an absorption band is observed at 833 cm^{-1}. The presence of both absorption bands at 1267 and 833 cm^{-1} and a dominating peak at 1121 cm^{-1} are typical of S:G:H lignin (158, 251, 252). The absorption band at 1717 cm^{-1} in lignin indicates the presence of unconjugated C=O stretching (vibration of unconjugated ketones, ester, or carboxylic groups). The FTIR spectra also showed two peaks with low intensity at 2852 and 2925 cm^{-1}, which can be attributed to symmetric and asymmetric C-H stretching in the aromatic methoxyl group and the methyl and methylene groups of the side chain of lignin. On the other hand, according to the literature, these absorption bands also appear in the FTIR spectrum of proanthocyanidins (253, 254), causing a noticeable interference in all samples; even small amounts can contribute to the intensity of these peaks. Asymmetric C-H deformation in $-CH_2-$ and $-CH_3-$ groups can be found at 1461 cm^{-1}. The band at 1221 cm^{-1} is attributed to C-C plus C-O plus C=O stretch, whereby G condensed > G esterified (158, 251, 252), and the band at 1028 cm^{-1} is associated with C-H (in-plane) deformation of the guaiacyl ring plus deformation of primary C-O and in ether with contribution from the stretching of unconjugated C=O (252).

3.4. CHARACTERIZATION OF LIGNIN NANOPARTICLES

Attending to the increasing growth of lignin used in biological applications, such as nanoparticles and hydrogels, the four lignin samples (LET, LETD, LWE, and LWED) were used to produce lignin nanoparticles (LNPs) using nanoprecipitation or dialysis, and their physical-chemical properties were evaluated over time. By comparing the size and the polydispersity index of LNPs produced by nanoprecipitation and dialysis, the results show significant differences ($p < 0.001$) in the size of the LNPs produced by nanoprecipitation (120–200 nm) when compared with the ones obtained by dialysis (250 – 505 nm). A similar trend was observed for the polydispersity index (0.19–0.26 compared with 0.37 – 0.44, respectively). LET and LWE lignin samples yielded nanoparticles with larger sizes and polydispersity index compared to LNPs obtained from LETD and LWED (Figure 13).

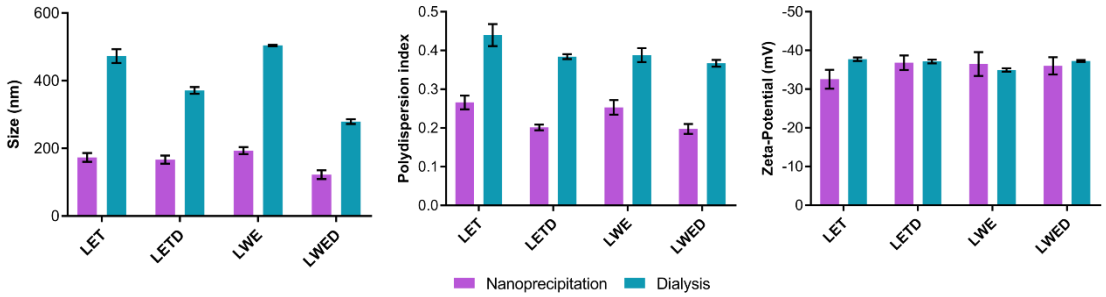

Figure 13 - Evaluation of physical properties (size, polydisperse index, and zeta-potential) of LNPs prepared by nanoprecipitation or dialysis.

Bearing all this, the stability of the LNPs prepared by nanoprecipitation was monitored over time. In a brief comparison between the different lignin samples (Figure 14), the results showed significant differences, especially in the particle size, with LNPs produced with LWED yielding lower values (LET: 173.3 ± 4.3 nm; LETD: 166.7 ± 4.0 nm; LWE: 193.3 ± 3.4 nm and LWED: 122.1 ± 4.3 nm). Depending on the target application, all samples present appropriate sizes as LNPs. Relatively to the polydispersity index, the values ranged between 0.1–0.4, which means that the samples are moderately dispersed. A similar trend was observed for the polydispersity index with LNPs prepared with LWED, showing lower values (0.18 ± 0.02) when compared with the other lignin samples: LET (0.24 ± 0.04), LETD (0.22 ± 0.04), and LWT (0.25 ± 0.02). The zeta potential was below −30 mV for all samples, which suggests a good physical-chemical stability of the nanosuspension due to the electrostatic repulsion of individual particles.

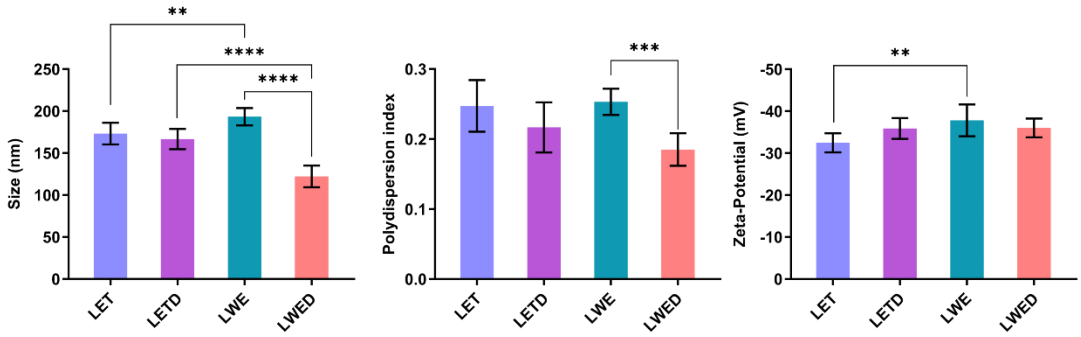

Figure 14 - Comparison of physical properties of lignin nanoparticles obtained by nanoprecipitation for different isolated lignin. Statistical analysis was made by ANOVA, followed by a Turkey's test. Different asterisks indicate a statistical difference: $p < 0.005$ (**), $p < 0.001$ (***), and $p < 0.0001$ (****). Errors bars represent the mean ± s.d. (n=9).

In general, LNPs were revealed to be stable for 30 days (Figure 15). When compared to the particle size on the first day, the size of the LETD increased to values of about 200 nm after 30 days. The results in the subsequent lignin samples remained remarkably

close to those observed on the first day, except for the LWED sample, in which a greater change in the polydispersity index values was observed, although it was below 0.4. The nanoparticles kept their negative charge on the surface in all samples, with the LWED sample experiencing a slight reduction to values below −30 mV after 7 days. In this sense, lignin from vine shoots demonstrated its potential for use in the production of stable LNPs.

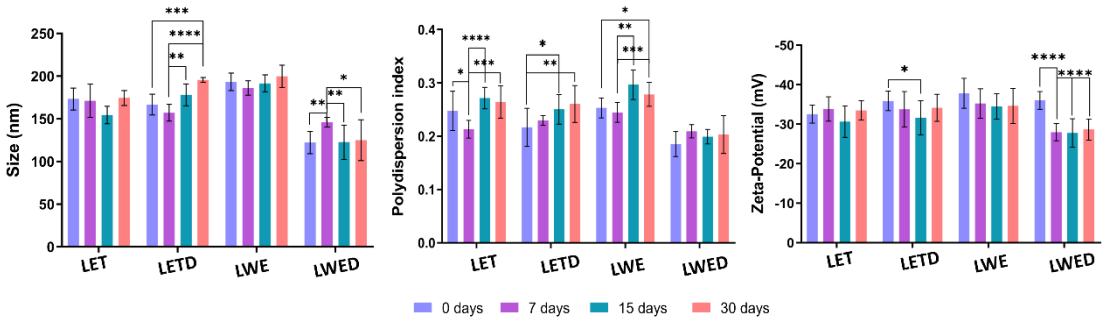

Figure 15- Evaluation of LNPs stability for 30 days for their size, polydisperse index, and zeta potential. Statistical analysis was performed by ANOVA, followed by Sidak's multiple comparison tests. Different asterisks indicate a statistical difference: $p < 0.05$ (*), $p < 0.005$ (**), $p < 0.001$ (***), and $p < 0.0001$ (****) Error bars represent the mean ± s.d (n = 9).

3.5. Antioxidant Activity of Soluble Lignin and Lignin Nanoparticles

The chemical structure of a molecule directly affects its antioxidant capacity. In this work, the antioxidant activity of lignin and LNPs was evaluated using a common colorimetric assay based on the elimination of the π-radical. Although there may be several reaction mechanisms for the scavenging, many radical scavengers react with DPPH (2,2-diphenyl-1-picrylhydrazyl) by giving one electron and one proton. The results of the antioxidant activity of lignin solutions and respective nanoparticles (Table 10) were expressed in terms of IC_{50}, which corresponds to the amount of the antioxidant required to reduce the initial concentration of the DPPH% radical by 50 %, and in terms of the radical scavenging index (RSI), which is the inverse of IC_{50}. This means that the lower the IC_{50} of an antioxidant, the higher its antioxidant efficiency and RSI value.

DPPH results showed a clear correlation between lignin concentration and antioxidant activity, increasing the inhibitory effect at higher concentrations for all samples. It was observed that the antioxidant activity of soluble lignin and LNPs was higher than some commercial antioxidants, such as BHT (butylated hydroxytoluene) and BHA (butylated hydroxyanisole), whereas it was lower than trolox, gallic, and ascorbic acids. The highest antioxidant capacity demonstrated by the soluble LET and LETD could be attributed to the presence of the highest phenolic content and the lowest carboxylic acid content

previously quantified by the ^{31}P NMR, which is described in the literature as factors that affect the antioxidant behavior of lignin (255-257). Impurities such as carbohydrates can also negatively affect antioxidant activity since the formation of hydrogen bonding with lignin blocks the formation of free radicals (258). The soluble lignin with higher carbohydrate content (around 6.9 %) in the LWE sample showed a lower antioxidant capability. By comparing the IC_{50} and RSI values obtained for lignin in solution, similar results for the antioxidant capacity of different types of lignin were found by other authors (185, 259). In general, the LNPs showed lower IC_{50} values when compared to the respective soluble lignin. However, it is important to highlight that LNPs were dispersed in water to avoid disintegration while the reference antioxidants and soluble lignin were dispersed in 50 % (v/v) of ethanol, which may influence the obtained results. In conclusion, the high antioxidant activity of the lignin samples suggests that they could act as potential antioxidants for the food, cosmetic, and pharmaceutical industries instead of using BHT.

Table 10 - IC_{50} values of the lignin and nanoparticles from vine shoots were obtained in the current study with other antioxidants described in the literature. For comparison, RSI values were computed (=1/IC_{50}).

Sample	**IC_{50} (mg/mL)**	**RSI (1/IC_{50})**
LET (Soluble lignin)	0.017	59
LETD (Soluble lignin)	0.016	63
LWE (Soluble lignin)	0.030	33
LWED (Soluble lignin)	0.026	38
LET Nanoparticles	0.031	32
LETD Nanoparticles	0.029	34
LWE Nanoparticles	0.029	34
LWED Nanoparticles	0.030	33
Commercial antioxidants		
Gallic acid	0.002 (In this work)	500
Trolox	0.003 (In this work)	333
Ascorbic acid	0.005 (In this work)	200
Vitamin E	0.0037 (255)	263
BHT	0.038 (259)	26
BHA	0.056 (259)	18

4. CONCLUSIONS

This work highlights a strategy to contribute to sustainability and a circular economy by reusing a very abundant by-product from one of the most important industries in the food sector. Furthermore, it was possible to obtain purified lignin using a simple procedure, which is increasingly used in different areas. The lignin obtained after a pre-treatment of the biomass with water/ethanol and purified by dialysis (LWED) showed a lower content of contaminants (around 9 %), mainly carbohydrates (5 %), and tannins (3 %), when compared with the sample pre-treated with ethanol/toluene and purified by dialysis (LETD), which contains ~14 % (10 % of tannins and 4 % of carbohydrates). The results obtained in the chemical composition of the lignin fractions were consistent with the results obtained in the characterization of the extracts resulting from the Soxhlet procedure since the lignin treated with water/ethanol showed a lower percentage of impurities such as proanthocyanidins (tannins) and the respective extract showed a higher phenolic content when compared with the extract resulting from the Soxhlet with ethanol/toluene. Furthermore, the extract W/E showed a high content of sugar, which could be converted into lactic acid, xylitol, bioethanol, and biosurfactants. As to the structure, the results were similar for all lignin samples, indicating that the pre-treatment and purification methodologies do not lead to modifications in lignin chemical composition. The lignin obtained showed a predominance of S over G units, with an S/G ratio between 1.45 and 1.55 and a high content of β-*O*-4 linkages. The content of phenolic hydroxyl groups was similar for both lignin samples analyzed, being 1.01 and 0.84 mmol/ g lignin for E/T dialysis and W/E dialysis, respectively. Nanoparticles proved to be very promising, with a very satisfactory size and polydispersity index. Additionally, it was very stable over time, and the antioxidant activity was higher than the ones typically reported for the commercial antioxidants BHT and BHA.

The data obtained in this study is an important tool for the design of processes to transform these agro-industrial waste materials into lignin-based high-added-value products and the production of bioactive compound extracts.

PART B

EXPLORING THE LIGNIN VALORIZATION AS A PROMISING AGENT TO MODULATE THE PHYSICOCHEMICAL PROPERTIES OF WINE

SYNOPSIS

Lignosulfonate (LS), Kraft (KL), and Organosolv lignin (OL) were evaluated as a potential modulating agent of the physicochemical properties of Port Wine at two different concentrations (25 and 100 g/hL) during 7 and 30 days. The type of lignin affects the wine composition differently. KL and LS demonstrated the ability to remove proteins, allowing a reduction of the content in 37 % after 7 days with KL and 57 % after 30 days of treatment with LS. LS also yielded a significant decrease in the tannin concentration, which can be important in modulating wine astringency. Wine clarification with LS and KL yielded a slight increase in anthocyanin concentration, probably due to the dissociation of anthocyanin aggregates from the polymeric fraction. Regarding the overall color, none of the lignin types yielded a significant color change ($0 < \Delta E < 2$), however, the yellowish color of KL and OL at 100 g/hL contributed to an increase of b* color coordinate value. Regarding wine aroma, the contact with lignin had a positive impact, especially with LS, since it yielded a decrease of circa 30 % in the concentration of some undesirable volatiles such as isoamyl alcohol (cheese and fusel descriptor) and 1-hexanol (resin descriptor), and, increased up to 60 % in some ethyl esters like ethyl octanoate and decanoate (brandy and fruit descriptors). The results suggest that lignin, especially LS, can be employed as a modulating agent, positively impacting wine's physicochemical properties. This valorization of a byproduct opens up new opportunities for the wine industry.

*This Part B was adapted from the paper: "**Pereira, A.R.**; Brandão, E.; Pinto, J.; Pinho, P.G.; Costa, C.; Rodrigues, A.; Michelin, M.; Soares, S.; de Freitas, V.; Mateus, N.; Oliveira, J. First insight into lignin valorization as a promising biopolymer for the modulation of the physicochemical properties of wine. Manuscript accepted in the Journal of Agricultural and Food Chemistry.*

Except for the astringency assays and the determination of volatile compounds, the experimental design and work described in this chapter were carried out by the author. The lignosulfonates and kraft lignin were provided by LSRE-LCM / ALiCE group and organosolv lignin by CEB/LABBELS group.

1. INTRODUCTION

Winemaking is a dynamic and interactive process responsible for transforming grapes into wine. During fermentation and aging, various solids and colloidal particles, such as grape skin, tartrate crystals, and microorganisms (yeast and bacteria cells) can form (260). These particles, solutes, and macromolecules can significantly affect the wine's stability, clarity, texture, taste, and production efficiency. Even after wine bottling, the presence of suspended and colloidal particles increases the turbidity due to denaturation or agglomeration of unstable proteins, tannins, carbohydrates, and other macromolecules (260, 261). Additionally, undesirable colors can appear as a consequence of reactions between wine components, or the oxidation of wine phenolic compounds (262, 263). Besides color, wine aroma significantly influences consumer acceptability. It is a complex mixture of volatile molecules present at various levels (ng/L up to mg/mL) in the wine, that exceeds the sensory threshold. A volatile compound may have a pleasant aroma at lower concentrations but can contribute to an unpleasant odor at higher concentrations. The occurrence of chemical reactions during wine aging can also form volatile compounds associated with off-odors (264, 265). Imbalance among astringency, bitterness, and acidity is the main factor related to the taste and tactile defects. Wine astringency is a consequence of the presence of proanthocyanidins (condensed tannins) responsible for sensations of drying and roughness (266). Among the several mechanisms proposed to explain astringency perception, the interaction between salivary proteins (SP) and tannins, with precipitation of the insoluble complexes, has been the most accepted one (267). All the referred phenomena generally reduce the quality and/or safety of wine, resulting in economic losses for the wine industry. To prevent their appearance, in addition to the natural sedimentation or filtration (262, 263), the use of fining agents is a more common and straightforward procedure including bentonite, colloidal silica, phenolic substance complexes, and synthetic polyamides such as polyvinylpyrrolidone (PVP) and polyvinylpolypyrrolidone (PVPP) (268). Extensive research suggests the application of animal proteins (bovine proteins, porcine gelatin, egg albumin, and casein); however, they have various disadvantages, including ethical and religious considerations, and they are well-known food allergens that can pose a risk to consumers (269). To overcome these issues, plant-based proteins (e.g., from grape seeds (270), potatoes (271), and vegetables (272)), as well as non-protein plant-based materials (e.g., cell wall polysaccharides (273, 274) and pomace materials (275)) have been the focus of research in this area. This work presents a new approach for the wine industry, using lignin as a putative agent to modulate the physicochemical properties of

wines. Lignin is a complex macromolecule found abundantly in nature (plant cells) and used as a raw material for several applications including the chemical industry. Depending on the plant species (hardwood, softwood, or herbaceous plants) and the extraction method, lignin can have different proportions of the chemical units, linkages, and functional groups, affecting their chemical and structural characteristics (276). This biopolymer has several advantages, including biodegradability, high stability, low cost, and low toxicity. The high molecular weight, the presence of several functional groups, and the structure with high adsorption area are crucial characteristics that can influence the efficiency of lignin to modulate the chemical composition and improve the wine quality. Various lignin types were applied, specifically lignosulfonate (LS), kraft (KL), and organosolv lignin (OL) determining their impact on the removal of colloids and unwanted particles, protein and tannin content, anthocyanin concentration, color stability, and aroma profile. By assessing these physicochemical properties, the study explores the feasibility of using lignin as a sustainable and effective alternative for improving wine quality while maintaining its inherent flavor and color characteristics.

2. MATERIALS AND METHODS

2.1. WINE SAMPLE

The wine used in this work was a ruby-style Port wine, produced from red grapes and supplied by Granvinhos, a company from the Douro region in Portugal. It was produced in the harvest of 2022 and was provided without any treatment six months after fermentation. The standard oenological parameters carried out by the company´s laboratory are summarized in Table 11. The pH of wine samples was also measured after contact with lignin (Appendix 2 – Table 2A).

Table 11 - Physicochemical analysis of the Port wine sample at 20 ºC.

Parameters	Values
Alcohol content (ABV)	18.5% (v/v)
Baumé degree	3.15
Density	1.02 g/L
Total acidity (tartaric acid equivalents)	4.14 g/L
Total sulfur dioxide	48 mg/mL
Volatile acidity	0.21 g/L
L-Malic acid	1.24 g/L
pH	3.62

2.2. LIGNIN SAMPLES

LS and KL, by-products from the pulp and paper industry, were supplied by Portuguese companies. LS was obtained from a softwood sulfite liquor (SSL, total solids, 11.3 % w/w liquor) by a mixture of 90 % of spruce (softwood material) and 10 % of beech (hardwood biomass). The liquor resulting from the delignification process in alkaline conditions was submitted to an ultrafiltration process using a Synder MT membrane with a molecular weight cutoff (MWCO) of 5 kDa performed in a G.E. Osmonics SEPA CF II crossflow filtration system. The solid retained in the membrane was freeze-dried with a lignin yield of around 53 %. More details about the composition and structure of LS are described in the literature (277). KL was isolated from industrial Eucalyptus globulus kraft liquor collected in a Portuguese pulp mill. The extraction procedure and chemical characterization are reported in the literature (278). OL was isolated from corncob supplied by a local farmer involving two stages: autohydrolysis and ethanol organosolv treatment. In a stainless-steel cylindrical reactor (Parr Instruments Company, Moline Illinois, USA) equipped with a Parr PID temperature controller (model 4848) were mixed 100 g of raw material (particle sizes from 1 to 1.6 mm) with distilled water at a solid-liquid ratio of 1:10. Then, the reactor was heated until a final temperature of 200 ºC for 30 minutes – the first step known as autohydrolysis or liquid hot water (LHW). The solid phase obtained in this process which contains cellulose and insoluble lignin (Klason lignin) was filtered, washed with distilled water at 70 ºC, and used in the second step – the organosolv. For that, this solid with 60 % ethanol at a solid-liquid ratio of 1:10 was mixed inside the reactor tube. The reactor was closed and heated at a temperature of 140 °C for 40 minutes. Then, the liquid resulting from filtering the material and washing the solid with 60 % ethanol was reserved for subsequent lignin precipitation by adding three volumes of acidic water (pH 2.0), prepared with sulfuric acid. This precipitation process was left overnight and the next day, the precipitated lignin was centrifuged at 10,000 rpm, 4 °C, for 10 minutes. The pellet (insoluble lignin) was recovered from bottles and placed in the freeze-dryer (Klason lignin with a purity of 95 %). More details about this OL´s experimental procedure and physicochemical properties are available in the literature (279).

The content of proanthocyanidins (PACs) in lignin samples was determined according to the procedure described in the literature with some modifications (236). Into Pyrex tubes, 500 µL of butanol reagent (butanol with 5 % (v/v) of concentrated hydrochloric acid) were mixed with 18 µL of ammonium iron (III) sulfate dodecahydrate solution (20 mg/mL prepared in aqueous hydrochloric acid (2 M)) and 82.5 µL of a methanolic solution

of each lignin fraction (3.0 mg/mL of LS, KL and OL). The mixture was incubated at 100 °C for 50 min. After cooling, the absorbance of each sample was recorded at 520 nm. The quantification was made using a purified PACs fraction containing trimers as a standard.

2.3. EXPERIMENTAL DESIGN

In this work, three types of lignin were studied as modulating agents, namely, the LS, KL, and OL at two concentrations (25 g/hL and 100 g/hL). These concentration values were chosen based on the amount of commercial bentonite used in the wine industry (40 g/hL), and two extreme values were selected to compare the effect. For that, 100 mL of Port wine was combined with the specific type and concentration of lignin in a sealed glass bottle. Then, the mixture was shaken and maintained in the dark at room temperature. The experiments were carried out in triplicates for each type of lignin and concentration. Wine samples were analyzed after 7 and 30 days of contact with lignin. After this time, the control and wine samples treated with lignin were centrifuged at 10,000 rpm for 12 minutes. Bentonite (40 g/hL) was also used as a reference since it is a widely used commercial fining agent. The experimental design is represented in Figure 16.

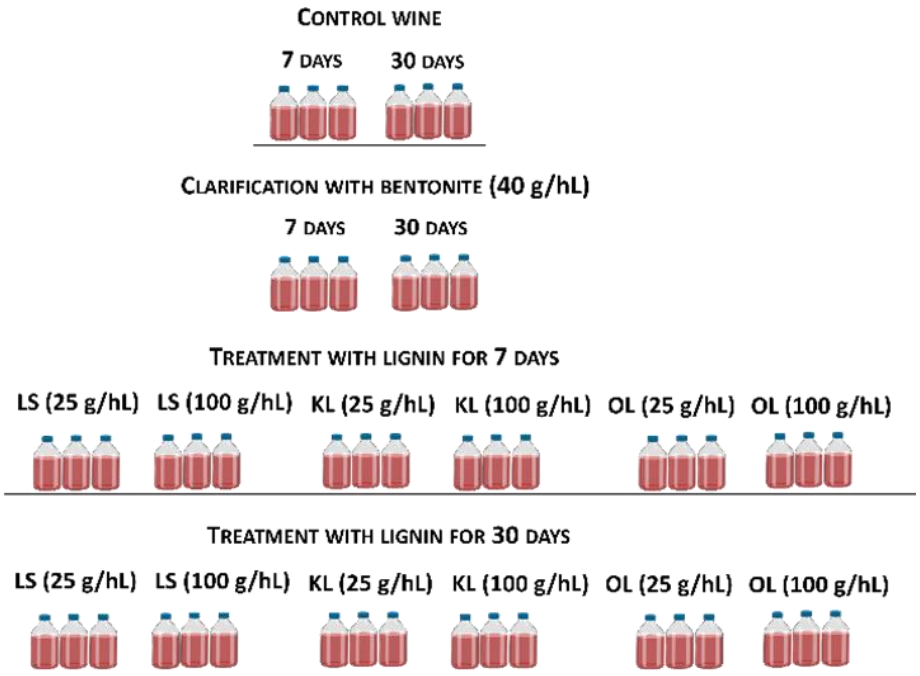

Figure 16 -The experimental design used to evaluate the potential of different types of lignin as improving agents for clarifying wine (LS: Lignosulfonate; KL: Kraft Lignin and OL: Organosolv Lignin).

2.4. PHYSICOCHEMICAL ANALYSIS

2.4.1. DETERMINATION OF WINE TURBIDITY

The assessment of wine turbidity allows us to confirm the presence of suspended solids in the samples, proving wine clarity. The turbidity of the samples was measured before and after the centrifugation step (10,000 rpm for 10 minutes) using a turbidimeter HACH 2100 N equipped with a cell adapter of 100 x 12 mm.

2.4.2. THERMAL STABILITY TEST

The heat test is a simple method to regulate the possibility of a wine becoming hazy. The samples were heated at 80 ºC for 2 hours to unfold the haze-forming proteins, followed by cooling at 20 ºC, for 3 hours. The turbidity of the samples was measured before and after heat treatment using a HACH 2100 N turbidimeter equipped with a cell adapter of 100x12 mm.

2.4.3. PROTEIN QUANTIFICATION

The concentration of proteins present in the wine samples was quantified using the bicinchoninic acid assay (BCA) and following the guidelines described by Thermo Scientific (280). It is based on the reduction of the copper cation in an alkaline medium by the proteins present in the samples, which results in a purple color formation by bicinchoninic acid. Before quantification, proteins were precipitated with 20 % (m/v) of trifluoroacetic acid (TCA) in acetone to eliminate interferences. Wine samples were mixed with the TCA solution (1:1), left for 1 hour at -20 ºC, and then centrifuged at 10,000 rpm for 10 minutes. Then, the pellet was removed, washed, and resuspended in water. In 96-well plates, 10 µL of each pellet solution or BSA standard solution were mixed with 200 µL of working reagent (50:1, Reagent A: B, Pierce™ BCA Protein Assay Kits). The plate was covered and incubated for 30 minutes at 37 ºC. Then, the mixture was cooled to room temperature, and the absorbance was recorded at 562 nm on a plate reader (Biotek Powerwave XS). BSA was used as a standard for the calibration curve (Appendix 2, Figure 2A) to quantify the protein content in wine control, wine clarified with bentonite, and wine samples with the different types of lignin.

2.4.4. PHENOLIC COMPOUNDS QUANTIFICATION

The total phenolic index (TPI) is based on the ability of benzenic rings to absorb UV light. The wines were diluted 20 times with a filtered wine model solution (12 % ethanol, v/v, 5 g/L tartaric acid at pH 3.5) before being measured in a quartz cuvette using UV-vis spectroscopy (Cary 60 – Agilent). TPI was calculated by multiplying the absorbance at 280 nm by the dilution factor. The total phenolic compounds were also estimated based on the Folin-Ciocalteu colorimetric method (281), where the intensity of the blue complex is proportional to the concentration of phenolic compounds. The wine samples were diluted 20 times and then mixed with the redox agents. The results were expressed as gallic acid equivalent per milliliter of wine (mg GAE/mL), considering the calibration curve in Appendix 2, Figure 2B.

2.4.5. QUANTIFICATION OF TOTAL PROANTHOCYANIDINS (CONDENSED TANNINS)

The concentration of PACs in wine samples was determined following the method described by Ribéreau-Gayon et al. (282). The total PACs were quantified based on their oxidative depolymerization in the acidic medium at a high temperature (100 ºC) to give colored anthocyanidin pigments (282). 4 mL of wine sample (diluted 50 times with a wine model solution), 2 mL of deionized water, and 6 mL of 37 % HCl (v/v) were added to a Pyrex tube. After that, the tubes were closed and heated at 100 ºC for 30 minutes. The tubes were then cooled in cold water and mixed with 1 mL of ethanol. These samples were prepared in triplicates. A solution with the same composition but without heating was done for each wine sample as a reference. Then, the absorbance of all solutions was determined at 520 nm using a glass cell with an optical path of 1 cm in a UV-visible spectrophotometer (Cary 60 Agilent). The concentration of condensed tannins was determined through a calibration curve (Abs = 0.0456 [PACs] + 0.0178) prepared by a mixture of oligomeric PACs and expressed in g/L.

2.4.5.1. TANNINS-SPECIFIC ACTIVITY

This methodology is characterized by the interaction of phenolic compounds, namely, tannins, with proteins resulting in the formation of aggregates that increase light diffraction. The protocol to determine the tannin-specific activity (TSA) is described in the literature (283) and it was performed with some modifications. For that, samples were

diluted 50 times with filtered wine model solution. Then, 4 mL of the diluted wine samples were placed in a glass tube and the turbidity (blank) was recorded using a turbidimeter HACH 2100 N equipped with a cell adaptor of 100 x 12 mm. Then, 150 µL of a solution of bovine serum albumin (BSA) at 0.8 g/L was added, mixed in the vortex, and left at room temperature in the dark for 30 minutes. After this time, the turbidity was determined. Data were expressed in turbidity units per milliliter of wine (NTU/mL), and determined using the expression: $Turbidity\ (NTU/mL) = \frac{(Sample\ turbidity - Blank\ sample)}{0.08}$, where 0.08 correspond to the dilution factor of wine.

2.4.6. INTERACTIONS OF SALIVA WITH SUPPLEMENTED WINE

To obtain the first insights into the possibility of different types of lignin being able to modulate salivary protein (SP) precipitation, the interaction between saliva and wine treated with lignin was studied. Bentonite, a commonly used fining agent, was used as a commercial standard to compare the effectiveness of different types of lignin in reducing SP interaction and, consequently, astringency perception.

Saliva was collected from 20 healthy volunteers (aged 25 to 45 years old) who received specific instructions to avoid food/beverage intake before saliva collection, as already reported (284, 285). Briefly, human saliva was collected at 2 p.m., pooled together (≈50 mL), and treated with TFA (final concentration 0.1 %) to inhibit intrinsic proteases and precipitate high-molecular-weight proteins. After centrifugation (8000 g, 5 min), the supernatant was recovered, and the final pH was adjusted to 6-7 to represent the biological pH of human saliva. Before saliva collection, all the participants signed an informed consent. This study was permitted by the Ethics Committee of the Faculty of Sciences of the University of Porto (EK84032011) and carried out according to the Declaration of Helsinki (The World Medical Association).

The interaction with wine before and after treatment (7 and 30 days) was carried out using a fixed volume of saliva (90 µL). After the addition of 30 µL of wine or wine model solution to saliva, the solutions were mixed and interacted for 10 min at 37 °C (286, 287). Then, they were centrifuged and the supernatant (SP that did not interact) was analyzed by HPLC. Ninety microliters of each supernatant were injected into a JASCO HPLC-DAD system (LC-4000) with a Vydac C8 column (150 x 2.1 mm, 5 µm particle diameter), and the detection was carried out at 214 nm. The eluents were 0.2 % TFA in H_2O (A) and 0.2 % TFA in ACN/ H_2O 80:20 (v/v) (B). The gradient was linear from 11 % to 70 % eluent B in 70 min at a flow rate of 0.3 mL/min. After each injection, a washing step was performed

with 100 % eluent B and then set to the initial conditions. Typical SP profile obtained by HPLC analysis with detection at 214 nm is represented in Appendix 2, Figure 2C.

2.4.7. ANALYSIS OF ANTHOCYANINS

2.4.7.1. TOTAL FREE ANTHOCYANINS

Free anthocyanins react with the bisulfite anion yielding the non-colored adduct which can be used to determine the concentration of free anthocyanins. The concentration of free anthocyanins was determined using the method described by Somers et al. (288) with some modifications. For that, a solution with 40 mL of 2 % HCl, 2 mL of ethanol, and 2 mL of wine sample was prepared. Then, 10 mL of this solution was added to four glass tubes. To three of them, 4 mL of 20 % (v/v) sodium bisulfite 20 % was added, and to the fourth, 4 mL of deionized water (blank). The mixtures were homogenized in a vortex and left in the dark for 20 minutes. Next, the absorbance was determined at 520 nm using a glass cuvette with an optical path of 1 cm in a UV-visible spectrophotometer (Cary 60 Agilent). The concentration of anthocyanins was determined by the difference between blank absorbance and the samples treated with sodium bisulfite. The values expressed in mg/L were obtained by a calibration curve of standard solutions of malvidin-3-*O*-glucoside.

2.4.7.2. QUANTIFICATION OF ANTHOCYANINS BY HIGH-PERFORMANCE LIQUID CHROMATOGRAPHY (HPLC-DAD)

Anthocyanins present in the wine samples were quantified using the HPLC-DAD (Thermo scientific – Dionex Ultimate 3000) on a reversed-phase C18 column (Agilent) with 250 × 4.6 mm i.d., 2.7 µm at 25 °C column chromatography. The solvents were A: H_2O/HCOOH (v/v) and B: HCOOH/CH_3CN (v/v), with a flow rate of 0.4 mL/min. The gradient consisted of 3 % to 30 % of solvent B for 31 minutes. Then, the column was washed with 100 % of B for 10 minutes and stabilized with the initial conditions for 10 minutes. 20 µL of each sample were analyzed by HPLC-DAD in triplicates. The concentration of anthocyanins was expressed in mg/mL using malvidin-3-*O*-glucoside as a standard.

2.5. CHROMATIC PROPERTIES

2.5.1. COLOR INTENSITY

The color intensity (CI) of the wine samples was determined by the sum of the absorbance at 420, 520, and 620 nm. For this experiment, the wine samples were filtered with a filter of 0.45 µm and then, the absorbance was determined in a UV-vis spectrophotometer (Cary 60 UV-vis Agilent) using quartz cells with a 1 mm optical path.

2.5.2. CIELAB COLOR COORDINATES

CIELAB color coordinates are a color system to quantify and measure the color of samples. The color is expressed by the three parameters, namely L* for perceptual lightness and a* and b* for the four unique colors of human vision: red (+a*), green (-a*), blue (-b*), and yellow (+b*). The values were obtained using Color software in a UV-vis spectrophotometer (Carry 60 Agilent). The CIELAB color coordinates of each sample were determined in triplicate using glass cells with an optical path of 2 mm. The illuminant condition D65 and an observer angle of 10º were used.

2.6. DIALYSIS INDEX

The dialysis index can be correlated with the structural complexity of the phenolic compounds present in the wine. It was performed according to the literature (289, 290) starting with the preparation of a reference solution using a volumetric flask (50 mL) to dilute 5 mL of wine control or wine-lignin sample with the model wine solution (D_0). At the same time, a dialysis membrane (cellulose, 6 mm i.d., cutoff 12-14 kDa) containing 5 mL of wine samples was placed inside the glass bottle of 50 mL with model wine solution (D). The bottles and the volumetric flasks were sealed, left at room temperature, and protected from the light for 24 hours. After this time, the absorbance at 280 nm was determined in a quartz cuvette with an optical path of 1 mm using the UV-visible spectrophotometer (Cary 60 UV-vis Agilent). Dialysis index (D.I.) was determined using the expression: $\mathrm{D.I.} = \frac{(D_0 - D)}{D_0}$.

2.7. ANALYSIS OF VOLATILE COMPOUND BY HS-SPME-GC/MS

2.7.1. CHEMICALS

Ethanol (99.9 %) was purchased from ERBA Reagents (Val de Reuil, France). 1-Hexanol (99.9 %), 3-hexen-1-ol (98 %), 5-methyl-2-furfural (99 %), benzaldehyde (≥99.5 %), diethyl succinate (≥99 %), ethyl 2-methyl butanoate (99 %), ethyl butanoate (99 %), ethyl decanoate (≥98 %), ethyl hexanoate (99 %), ethyl isobutanoate (≥98 %), ethyl isovalerate (98 %), ethyl nonanoate (≥98 %), ethyl octanoate (99 %), furfural (99 %), hexyl acetate (98 %), isoamyl acetate (≥99 %), isoamyl alcohol (98 %), linalool oxide (97 %), phenylacetaldehyde (90 %), phenylethyl acetate (99 %), phenylethyl alcohol (99 %), tartaric acid (≥99.5 %), β-damascenone (≥98 %), α-ionone (85 %), and β-linalool (80 %) were supplied by Sigma-Aldrich (Madrid, Spain).

2.7.2. ANALYSIS CONDITIONS

Volatile compounds present in wines were analyzed by headspace solid-phase microextraction coupled to gas chromatography-mass spectrometry (HS-SPME-GC/MS) as previously described (291), with some modifications. Briefly, 250 µL of each wine sample were placed in a 20 mL glass vial and incubated for 5 min at 45 °C under a stirring speed of 250 rpm, followed by volatile extraction using a divinylbenzene/carboxen/polydimethylsiloxane (DVB/CAR/PDMS) fiber (Supelco Inc., Bellefonte, Pennsylvania, USA) for 30 min at the same temperature and stirring speed. Then, the analytes were desorbed into the GC injector over 6 min at 250 °C. The separation and detection of volatile compounds was accomplished using a 436-GC model (Bruker Daltonics, Bremen, Germany) coupled to a SCION single quadrupole mass detector (SQ-MS) and a Bruker Daltonics MS workstation (version 8.2, Bruker Daltonics, Bremen, Germany). A fused silica Rxi-5Sil MS (30 m × 0.25 mm × 0.25 µm; Restek Corporation, U.S., Bellefonte, Pennsylvania, USA) was used and the carrier gas was high-purity helium (Gasin, Porto, Portugal) at a constant flow of 1 mL/min. The column temperature was 40 °C kept for 1 min, increasing to 250 °C (5 min), held for 5 min, followed by increasing to 300 ºC (rate 5 ºC/min). The SQ-MS was conducted in the electron ionization (EI) mode at 70 eV with temperatures of 250, 260, and 41 °C for the transfer line, ion source, and manifold. The data acquisition was performed in full scan mode considering a mass range of 40 to 400 *m/z* (500 ms scan time).

Standard compounds for volatile quantification were dissolved in a wine model solution and a range of known concentrations of each compound were analyzed under

the same conditions as wine samples by HS-SPME-GC/MS. The calibration curves were computed by the respective area of the peak versus concentration for each volatile compound. The recovery of the standard volatile compounds was assessed by spiking the wine model solution with known concentrations of each compound at three points within the calibration range (low, mid, and high). The spiked samples were analyzed by the same HS-SPME-GC/MS method as described for the wine samples. For reliable results, an acceptable recovery range of 80 − 120 % was considered. The recoveries are summarized in Appendix 2, Table 2B. The recoveries were calculated using the equation: $R(\%) = \frac{Measured\ concentration}{Known\ concentration} \times 100$.

2.8. STATISTICAL ANALYSIS

Statistical analyses were performed using GraphPad Prism 8 software (version 8.0.1, San Diego, California; www.graphpad.com). One-way and two-way ANOVA were used in the variance analysis and the differences between means were calculated using Tukey's and Holm-Sidak multiple comparison tests. They were considered significant when p-values were below 0.05 ($p < 0.001$ and $p < 0.0001$). In assays of volatile composition, the differences were evaluated using an ordinary one-way analysis of variance (ANOVA) between the control and each condition under study using the GraphPad Prism 9 software (version, 9.3.0, San Diego, CA, USA). The volatile concentrations were considered significantly different for p-values below 0.05.

3. RESULTS AND DISCUSSION

3.1. EFFECT OF CENTRIFUGATION AND HEAT ON WINE TURBIDITY

Solid particles suspended in the wine solution increase the turbidity, giving the wine a cloudy and undesirable appearance. It was determined the turbidity of the control wine, and the wine treated with different types of lignin and bentonite, to understand if the presence of this biopolymer contributed to the wine´s clarification process. The values are shown in Figure 17. Turbidity was measured before (blue bars) and after (pink bars) the centrifugation step because some particles accumulated spontaneously even without centrifugation.

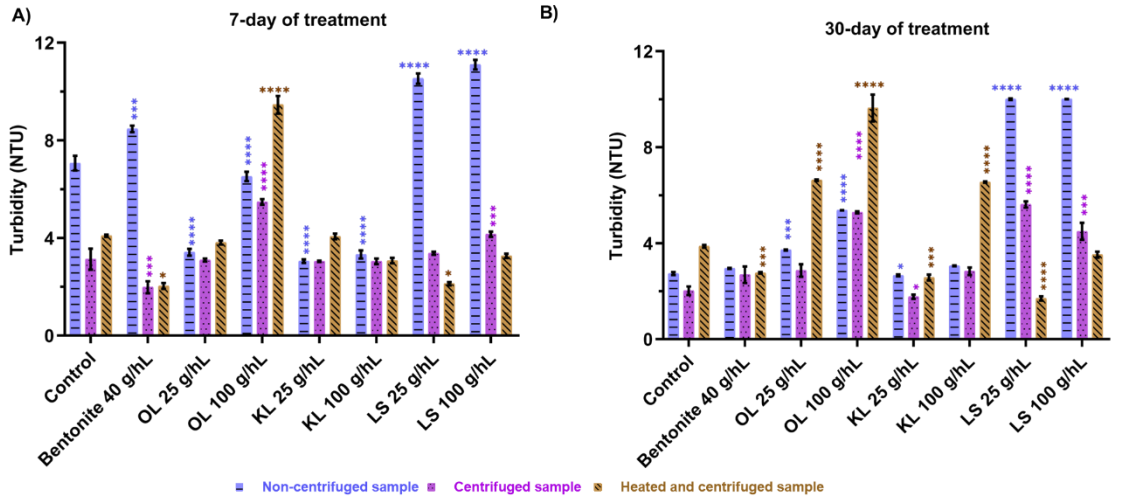

Figure 17 - Turbidity of wine samples measured using nephelometry before (blue bars) and after (pink bars) centrifugation, as well as after temperature treatment (brown bars). The results were determined after 7 (A) and 30 days (B) of lignin treatment (OL: Organosolv lignin, KL: Kraft lignin, and LS: lignosulfonate). The values are represented by the mean ± standard deviation (n=9). Asterisks indicate significant differences from the wine control (* – $p \leq 0.05$, ** – $p \leq 0.01$, *** – $p \leq 0.001$, **** – $p \leq 0.0001$).

The results for the 7-day lignin treatment indicated variations from the wine control. During this time, some solid particles were deposited by gravity; however, the addition of KL and OL significantly reduced the turbidity of the wine even without the centrifugation step (Figure 17 A blue bars). On the other hand, like with bentonite, LS at both concentrations (25 and 100 g/hL) causes an increase in turbidity, most likely due to the adsorption phenomena with suspended particles that do not settle due to gravity (Figure 17 A blue bars). After centrifugation, the bentonite revealed a significant decrease in wine turbidity, even though the centrifuge procedure alone helped to clarify the wine (Figure 17 A pink bars). KL outperforms LS and OL in reducing turbidity due to its higher molecular weight (69,000 g/mol (278)) and ability to deposit and drag suspended particles more effectively. The 30-day treatment resulted in a decrease in turbidity in the samples, including the control wine, even without the centrifugation process, as the samples had more time to settle the colloidal particles; however, the centrifugation step helped to remove suspended particles that caused turbidity, resulting in a reduction in turbidity (Figure 17 B pink bars versus blue bars). Regardless of the centrifugation procedure, kraft lignin reduced the turbidity of wine samples throughout 30 days.

3.1.1. THERMAL STABILITY OF WINES

The heat test is widely used in the wine industry to estimate haze-forming potential and protein instability. It is considered the most reliable tool for predicting sediment development in bottles during storage. Protein haze is a visual problem that results from the precipitation of grape proteins that are extracted during the winemaking process. This phenomenon can occur at any temperature but tends to form more quickly if wine is stored at high temperatures. Turbidity lower than 2 NTU, calculated by the difference between a heated (Figure 17 brown bars) and a non-heated sample (Figure 17 pink bars), indicates a stable wine. The results for the 7-day treatment revealed that the control wine tends to be stable because, after the treatment with temperature, the turbidity difference was less than 2 NTU. As expected, bentonite improved the stability by eliminating the colloidal content, with no variation in turbidity before and after the temperature experiment. Except for the OL at 100 g/hL, all types of lignin help in the stability of wine since the difference between the heated and non-heated samples is below 2 NTU and lower than the wine control. LS at both concentrations and KL at 100 g/hL had the best performance since the turbidity after the heat test was lower (around 40 % for LS) than the turbidity before the temperature treatment which means that this type of lignin prevents protein haze formation (Figure 17 A brown bars). The same trend was observed for the 30 days of treatment. The results demonstrated that LS at both concentrations and KL at 25 g/hL can help prevent turbidity increase after heating the samples (Figure 17 B, brown bars are smaller than pink bars).

3.2. DETERMINATION OF PROTEIN LEVELS

The protein levels for all wine samples are summarized in Table 12. Traditionally, wineries use fining chemicals such as bentonite to remove unstable proteins. The purpose is to use the lowest number of fining agents while simultaneously reducing unstable protein concentration to a level that prevents precipitation in the bottle. Bentonite is an absorbent clay that is widely utilized in the wine industry. As expected, it promoted a significant decrease (circa 80 %) in protein amount compared to the control wine. The type and concentration of lignin determined its effectiveness in removing proteins from wine samples. In the 7-day experiment, KL showed the highest potential for protein removal, decreasing protein content by 13 % at 25 g/hL and 37 % at 100 g/hL, compared to the control wine (67 mg/L BSA eq.). LS also significantly reduced protein content, decreasing 16 % at 25 g/hL and 90 % at 100 g/hL from day 7 to day 30. For OL

at 100 g/hL, protein content decreased by approximately 50 % after aging from day 7 to day 30. As reported in the literature (292, 293), proteins can adsorb onto the surface of lignin, leading to their precipitation and a consequent decrease in its levels.

Table 12 - Quantification of protein amounts in wine samples by the BCA method. Statistical differences were achieved by one-way ANOVA and represented by different letters: a (*), b (**), c (***) and d (****).

Samples	7 days (mg/L eq BSA)	30 days (mg/L eq BSA)
Wine control	67.1 ± 2.8	22.7 ± 1.4
Wine – Bentonite 40 g/hL	13.5 ± 0.3 [d]	9.9 ± 1.6 [d]
Wine - OL 25 g/hL	63.8 ± 3.2	21.6 ± 0.5
Wine - OL 100 g/hL	62.8 ± 3.9	30.7 ± 0.9
Wine - KL 25 g/hL	58.3 ± 2.3 [a]	25.8 ± 1.9
Wine - KL 100 g/hL	42.2 ± 2.4 [d]	23.3 ± 1.1
Wine - LS 25 g/hL	56.3 ± 4.0 [b]	19.8 ± 1.8
Wine - LS 100 g/hL	75.3 ± 5.8	5.6 ± 1.4 [d]

The values are represented by the mean ± standard deviation (n=9). Asterisks correspond to significant differences compared to the wine control. (* – $p \leq 0.05$, ** – $p \leq 0.01$, *** – $p \leq 0.001$, **** – $p \leq 0.0001$). n.d., not determined.

Compared with the results in Figure 17, LS showed a lower tendency to develop protein turbidity (the brown bar is lower than the pink bar in Figure 17), likely due to the reduction in protein content. For KL at 25 g/hL, the difference in NTU associated with turbidity was relatively similar to that of the control wine. However, at 100 g/hL, the difference between the heated and unheated samples was smaller than that of the control wine, suggesting that lignin helped control the increase in turbidity, which may also be associated with the decrease in protein over the 7 days. For OL, despite the reduction in protein content, no decrease in turbidity was observed from 7 to 30 days. This indicates that other molecules or colloids may have precipitated, suggesting a different interaction between OL and the wine matrix.

3.3. EVALUATION OF THE PHENOLIC COMPOUND CONTENT

The phenolic compounds in wines were quantified using the TPC index and the Folin-Ciocalteu assay. The results obtained for wines that undergo different treatments are presented in Figure 18.

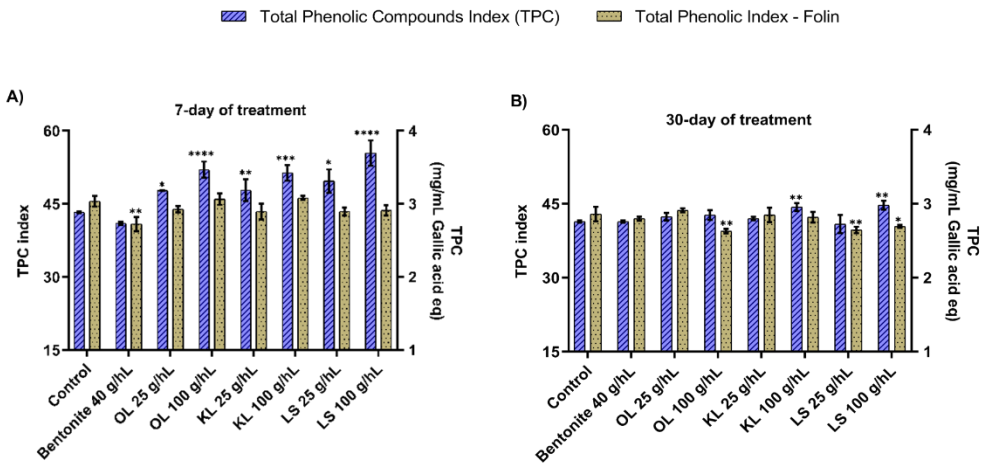

Figure 18 - Determination of the phenolic content by the total phenolic content index (blue bars) and the Folin method (brown bars) for the wine control and wine samples treated with different fining agents (bentonite, OL, KL, and LS) at two concentrations. Statistical analysis was made by one-way ANOVA. Asterisks (*) indicate a statistical difference (* – $p \leq 0.05$, ** – $p \leq 0.01$, *** – $p \leq 0.001$, **** – $p \leq 0.0001$) relative to the control wine. Bars represent the mean ± standard deviation (n=9).

The total phenolic compounds index was determined based on the ability of the aromatic rings to absorb in the ultra-violet region, with a maximum wavelength at 280 nm. As seen in Figure 18 A (blue bars), after 7 days of contact with the different lignin there was a significant increase in the total phenolic compounds index in wines that were in contact with the different types of lignin. This increase was more pronounced for concentrations of 100 g/hL, although the increase was also significant at lower concentrations. On the other hand, after 30 days, only the samples that were in contact with KL and LS at 100 g/hL presented values slightly higher than those of the control wine. Moreover, there was a decrease in the TPC index for all wine samples treated with lignin when compared to the 7-day process. These results evidence that the presence of lignin for the 7 days of contact has some influence on the values since lignin is a phenolic biopolymer composed of aromatic rings that can absorb at 280 nm which may contribute to higher values when compared to the control wine. Bentonite allowed a slight decrease in the total phenolic index (around 5 %) compared to the control wine.

In contrast to the results previously described in the total phenolic compounds index, there were no significant variations in the TPC (using the Folin Ciocalteu method) after 7 days for the samples treated with lignin (Figure 18 A brown bars). Based on the results obtained, it seems that the treatment with lignin does not interfere with the Folin-Ciocalteu reagent. The results obtained with bentonite agree with the ones reported previously in the total phenolic compounds index. When comparing the results obtained after 7 and 30 days, a decrease in phenolic compound content is observed, consistent

with the reduction noted in the total phenolic index. Increasing the exposure time of wines to the biopolymer may lead to greater adsorption and subsequent deposition of phenolic compounds, resulting in their reduced concentration in the wine over time. It is also important to remark that LS at 25 g/hL and OL at 100 g/hL allowed a slight decrease in the total phenolic compounds content which may be a positive point since some colloidal phenolic compounds are involved in oxidation, excess astringency, and bitterness that alter the organoleptic characteristics of wines.

3.4. QUANTIFICATION OF TOTAL PROANTHOCYANIDINS

The quantification of the total proanthocyanidins (condensed tannins) and the tannin activity measured by nephelometry are reported in Figure 19.

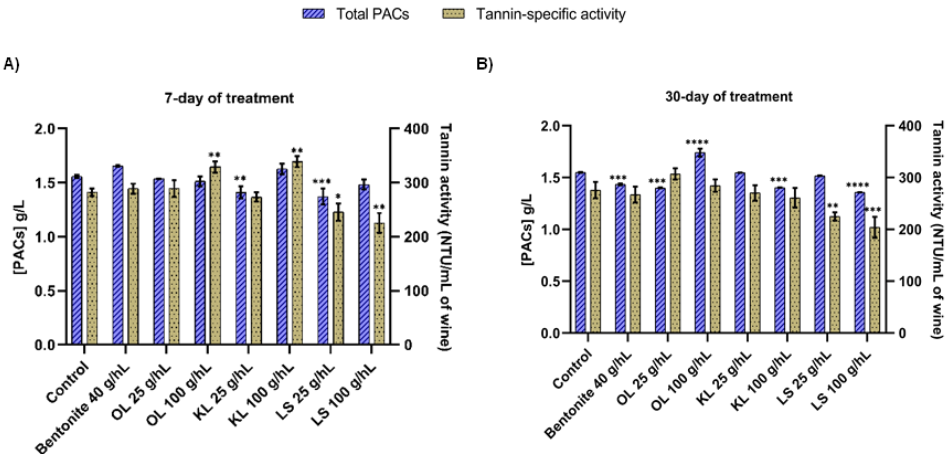

Figure 19 - Quantification of total proanthocyanidins (condensed tannins) present in control wine and wine treated with bentonite or lignin (blue bars) and determination of the tannin activity analyzed by nephelometry (brown bars). Statistical analyses were performed in one-way ANOVA, and the asterisk indicates significant differences between samples and wine control (* – $p \leq 0.05$, ** – $p \leq 0.01$, *** – $p \leq 0.001$, **** – $p \leq 0.0001$). Bars represent the mean ± standard deviation (n=9).

The content of PACs in all samples showed some differences when compared to the control wine ranging from 1.3 to 1.8 g/L (Figure 19 blue bars). After 7 days of interaction, the wine samples treated with the different types of lignin exhibited a decrease in proanthocyanidins, with a notable 12 % reduction for KL and LS at 25 g/hL (Figure 19 A). Regarding wines in contact with lignin for 30 days (Figure 19 B), the content of PACs in all wines, especially those treated with LS at both concentrations and KL at 25 g/hL, was reduced (maximum of 13 %) compared to the control wine. This reduction may be associated with interactions between lignin and tannins, leading to tannin condensation reactions and subsequent precipitation. Bentonite also reduces the level of

proanthocyanidins by 3 %. OL (100 g/hL) exhibited the opposite impact, significantly increasing the content of PACs. However, the lignin samples contain only negligible levels of PACs and hence do not contribute to the observed increases. (Appendix 2, Figure 2D).

3.4.1. TANNIN-SPECIFIC ACTIVITY

Tannins are compounds that confer structure and complexity to wines. These compounds can interact with salivary proteins (SP) forming insoluble complexes associated with astringency. The tannin-specific activity was evaluated using nephelometry and the BSA protein (bovine serum albumin) as a model. This methodology aims to explore the putative interaction of the compounds present in wine and proteins which increase the turbidity of the solution. The results obtained for all the samples are displayed in Figure 19 (brown bars). The type and concentration of lignin have an impact on the tannin-specific activity. OL and KL at 100 g/hL showed a significant increase in the turbidity of wines in the presence of BSA (7 days of contact) (Figure 19 A brown bars). In the case of KL, the increase can be attributed to a rise in PACs content. For OL at 100 g/hL, the increase may be due to the possible interaction of BSA with the lignin surface, especially since a decrease in condensed tannin content was observed (292-294). On the other hand, complex interactions between lignin and tannins may enhance tannin reactivity through selective binding, structural changes, or the formation of more active tannin complexes that justified this increase. More interesting was that LS resulted in a considerable decrease of turbidity for both concentrations (25 g/hL and 100 g/hL), which may be the first indication that this biopolymer can modulate the astringency of wines. This result is a consequence of the decrease in PACs concentration previously reported in Figure 19 (Blue bars). This is a relevant feature since higher amounts of tannins in wine give it rough or abrasive sensory characteristics. Also, many wineries try for a balanced level of astringency because it is one of the most recognized sensory properties in wine associated with quality. The decrease in the turbidity of wines in the presence of BSA is more pronounced after 30 days of contact with LS (Figure 19 B, brown bars), particularly at 100 g/hL.

3.5. EFFECT OF LIGNIN ON THE INTERACTION BETWEEN WINE PHENOLIC COMPOUNDS AND SALIVARY PROTEINS

The typical human saliva profile has been previously characterized by proteomic analysis (284). The chromatogram (Appendix 2, Figure 2C) is divided into different families of SP that have been widely associated with astringency perception, such as basic proline-rich proteins (bPRPs), glycosylated PRPs (gPRPs), acidic PRPs (aPRPs), statherin, P-B peptide, and cystatins (267). Since statherin and the P-B peptide are co-eluted, they were analyzed together. The effect of the addition of bentonite and lignin to wines on SP interaction and precipitation was evaluated. After centrifugation, the insoluble aggregates were removed, and the remaining part (SP that did not interact) was analyzed (Figure 20). The results of the SP were obtained by subtracting the area of the chromatographic peak corresponding to each SP family remaining in the solution after interaction from the initial concentration. Then, to evaluate and compare the reactivity towards different wines (with or without modulating agents), this latter value was divided by the initial concentration to obtain the final interaction value (%).

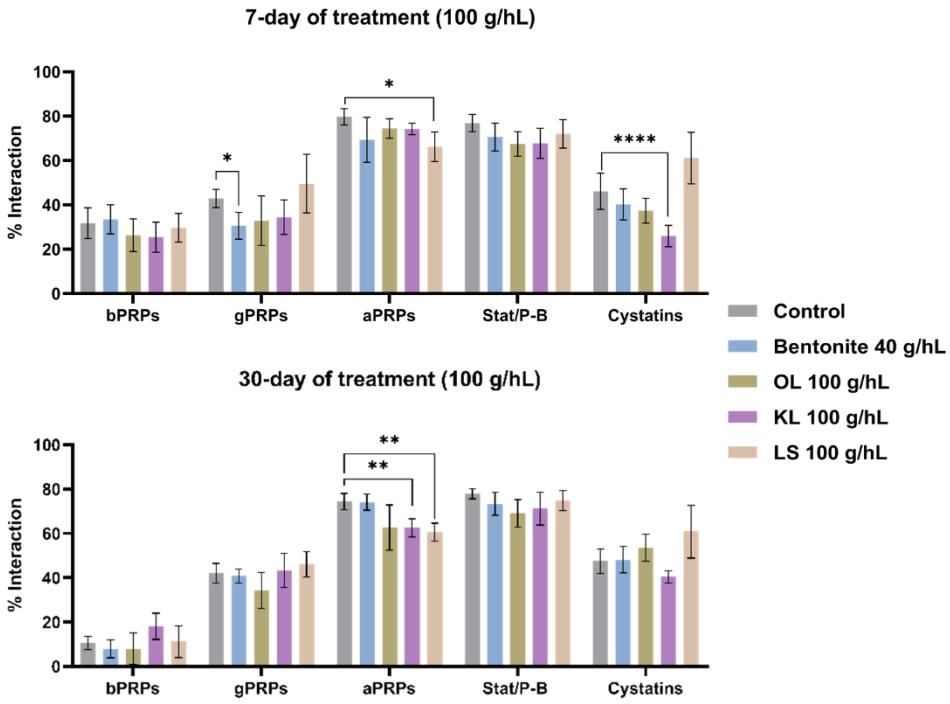

Figure 20 - Percentage of the interaction of the different SP families with each treated wine (bentonite at 40 g/hL and OL, KL, and LS at 100 g/hL) for both 7 and 30 days of treatment. Control conditions refers to the wine without modulating agents. Statistical analysis was made by two-way ANOVA. Asterisks (*) indicate a statistical difference (* – $p \leq 0.05$, ** – $p \leq 0.01$, **** – $p \leq 0.0001$) relative to the control wine. Bars represent the mean ± standard deviation (n=6).

In general, the results showed that some types of lignin were able to reduce the interaction and precipitation of specific families of SP. This effect seems to be specifically associated with the type, concentration, and days of treatment with lignin. Among the several types of lignin, LS showed the highest ability to reduce the interaction between aPRPs and wine phenolic compounds, one of the most important SP families involved in astringency perception. This effect was observed for the highest concentration (100 g/hL) both for 7 and 30 days of treatment. These results agree with the decrease of PACs concentration and tannin-specific activity previously reported (Figure 19), making it a promising candidate for being used as a modulating agent to balance wine astringency. On the other hand, KL at 100 g/hL also significantly reduced the interaction between aPRPs (significant only for 30 days of treatment) and cystatins with wine phenolic compounds. Comparing the days of treatment and concentration, the latter seems to be the most important factor affecting the higher efficiency of KL. Although the higher effect is observed at the highest lignin concentration (100 g/hL), it was also noted a significant effect of OL 25 g/hL on reducing the interaction of gPRPs and wine compounds (Appendix 2, Figure 2E). On the other hand, bentonite, a common fining agent, can reduce the interaction of gPRPs with wine polyphenols only for the 7-day treatment (Figure 20).

Fining agents are crucial for softening or reducing wine astringency and bitterness, as well as for stabilizing haze formation through physical or chemical reactions with wine compounds. However, fining can also potentially remove positive flavor characteristics. Therefore, new fining agents should avoid inducing drastic changes in wine compounds to mitigate the risk of over-fining. In this regard, LS and KL showed interesting results in reducing SP interaction and precipitation at a moderate level, turning them into suitable candidates for improving overall wine quality.

3.6. ANTHOCYANINS

Anthocyanins are responsible for the red color of wines, especially young red wines. The anthocyanin content was quantified by UV-visible spectroscopy and using the HPLC as a direct method. The results obtained are presented in Figure 21.

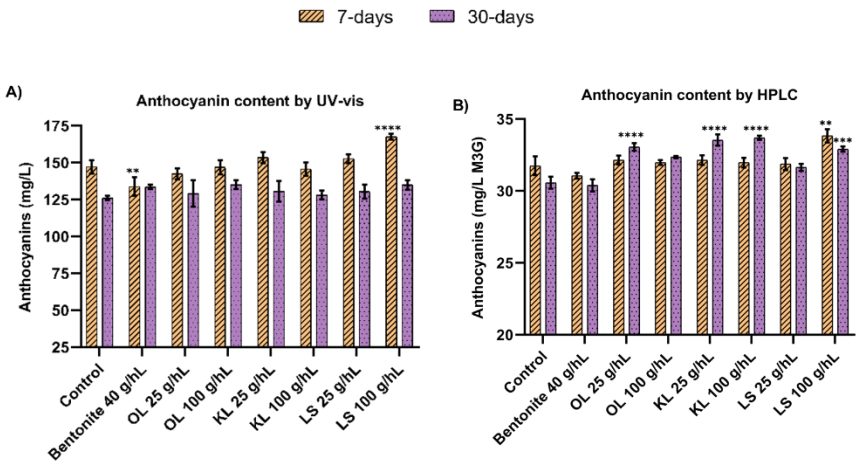

Figure 21 - Quantification of free anthocyanins by the reaction with bisulfite (A) and by HPLC (B) after 7 and 30 days represented by the orange and pink bars, respectively. Statistical differences were achieved by one-way ANOVA. Asterisks correspond to significant differences compared to the wine control (* – $p \leq 0.05$, ** – $p \leq 0.01$, *** – $p \leq 0.001$, **** – $p \leq 0.0001$). Bars represent the mean ± standard deviation (n=9).

As shown in Figure 21, the presence of lignin influenced the total amount of free anthocyanins. The results obtained by UV-vis spectroscopy after 7 days (Figure 21 A orange bars) had a greater variation when compared to the control. LS at 100 g/hL exhibited an increase in free anthocyanin levels (around 12 %). This can be due to the ability of LS to disaggregate anthocyanin aggregates formed during the production and aging, yielding the increase of solubilized free anthocyanins available to be decolorized by bisulfite. After 30 days of contact (Figure 21 B pink bars), the values did not show significant differences compared to the control wine. Moreover, comparing the results obtained after 7 days and 30 days of contact, it can be observed that over time the content of anthocyanins decreases with a reduction of approximately 14 %. However, in the presence of lignin, this decrease was less pronounced indicating that this biopolymer favors the stabilization of anthocyanins and thus the color of red wine. On the other hand, bentonite decreased in the concentration of free anthocyanins, which agrees with the significant decrease observed in the phenolic content previously discussed.

During red wine aging, anthocyanins undergo several reactions that result in the formation of new pigments. The quantification of anthocyanins and the identification of the anthocyanin-derived compounds formed during aging can be performed by HPLC-DAD coupled with mass spectrometry. Figure 21 B contains the results obtained in the quantification of anthocyanins by HPLC. As can be observed, there is a slight increase in the concentration of anthocyanins in wines that were clarified with the different types of lignin, similar to what was described previously in the bisulfite method and can be due

to the disaggregation of polymeric anthocyanin complexes. The increase was more pronounced for the 30 days and lignin concentrations of 100 g/hL; being that, in the case of LS, 7 days was enough to show a significant increase in the anthocyanins amount. Comparing both methods of Figure 21, it is observed that the concentration of these pigments is much higher when using the bisulfite method than obtained by HPLC-DAD, probably due to the presence of other colored pigments that are also discolored by bisulfite, being this method less accurate for the quantification of anthocyanins.

Regarding the chromatographic profile of the wine samples treated with bentonite or lignin, it can be observed that this was identical to the chromatographic profile of the wine without any clarification. The identity of each compound was achieved by the LS-MS considering the data reported in the literature (Appendix 2, Table 2C). Different phenolic compounds, especially anthocyanins, and their derivatives are observed in all samples. Malvidin-3-*O*-glucoside and Malvidin-3-*O*-coumaroylglucoside were the most abundant anthocyanins detected; however, peonidin-3-*O*-glucoside and petunidin-3-*O*-glucoside were also observed. Concerning the increase in anthocyanin content, malvidin-3-*O*-coumaroylglucoside showed a slight increase across the three types of lignin, ranging between 4 − 7 %. Malvidin-3-*O*-glucoside showed an increase of approximately 4 % only with lignosulfonates at a 100 g/hL concentration. Petunidin increased in wine samples treated with kraft lignin and lignosulfonates at 100 g/hL. Pyranoanthocyanins, such as A-type and B-type vitisins, were also identified in wine samples. These compounds are described to increase the color stability of red wines due to their higher stability towards hydration reactions and bisulfite bleaching. Other anthocyanin-derived compounds were also detected in all wine samples resulting from the reaction of anthocyanins with other phenolic compounds such as catechin, vinylphenol, or vinylcatechol. Hydroxybenzoic acids, catechins, epigallocatechins, and procyanidins trimers were also found in wine samples, with coumaric and cinnamic acids being the major phenolic compounds. Wine samples treated with KL showed an increase in coumaric acid, whereas aging with OL led to an increase in cinnamic acid. Treatment with LS resulted in a slight decrease in all identified phenolic compounds. The results indicated that the content of each phenolic compound depends on the type and amount of lignin used.

3.7. CHROMATIC PROPERTIES

The chromatic properties of red wines are associated with the presence of anthocyanins and all their derivatives which are directly correlated with wine quality. The

chromatic properties of wines were evaluated by determining the color intensity (CI) and the CIELAB color coordinates.

3.7.1. COLOR INTENSITY

The CI of all wine samples was determined by the sum of the absorbances at 420, 520, and 620 nm. The results are presented in Figure 22 (blue bars). The yellow tones of lignin are one of the major drawbacks associated with the use of this biopolymer, as its addition to some matrices, can change the color of the finished product. Depending on the extraction method and purification degree, lignin can range from pale yellow to brown.

The results obtained demonstrate that the presence of lignin has an impact on the color of the wine. Regarding the wines that were clarified with lignin for 7 days, especially for KL and OL at both concentrations (Figure 22 A, blue bars), it was observed an increase in the color intensity related to the intensification of the absorbance at 420 nm which can be due to the contribution of the yellow color of lignin. Bentonite yielded a decrease in the wine color intensity due to the reduction of the absorbance at 520 and 620 nm. These results are correlated with the decrease in anthocyanin concentration as these pigments absorb at 520 nm. Regarding the wines that were in contact with lignin for 30 days (Figure 22 B blue bars), two conditions yielded a significant decrease in CI, the wine treated with OL at 100 g/hL and LS at 25 g/hL. In the case of OL, the reduction was due to the decrease in the absorption at 620 nm. In the case of LS, the decrease was due to the reduction of the absorption at 420 and 620 nm.

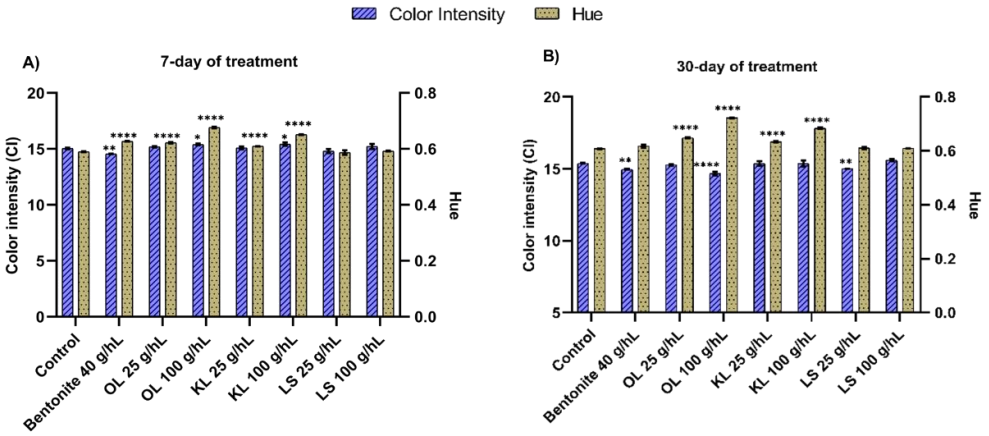

Figure 22 - Color intensity (CI) of wine samples treated with bentonite and different types of lignin at different contact times (blue bars) and determination of the hue for all samples (brown bars). Statistical analysis was made by one-way ANOVA. Asterisks (*) indicate a statistical difference (* – $p \leq 0.05$, ** – $p \leq 0.01$, *** – $p \leq 0.001$, **** – $p \leq 0.0001$) relative to the control wine. Bars represent the mean ± standard deviation (n=9).

The hue of the wine samples was assessed and compared to the control wine. This hue is calculated as the ratio between the absorbance at 420 and 520 nm (Figure 22 brown bars). Except for the LS, the clarification of wines with OL and KL yields the increase of the yellow character of the final wine, due to the darker color of these lignin samples, which remained brown in the aqueous solution, and caused the increase of color intensity for the 7 days experiment, as previously described. The same was observed during the 30-day experiment (Figure 22 B brown bars), with higher values, most likely due to the longer period in contact with the wine. In the case of bentonite, an increase in the hue of the wine was observed after 7 days of treatment due to the decrease in absorbance at 520 nm as a result of the decrease in anthocyanins concentration as already discussed above.

3.7.2. CIELAB COLOR COORDINATES

The CIELAB coordinates of the wine samples were determined to evaluate the color change of wine during the treatment with the different types of lignin for 7 and 30 days (Table 13).

Table 13 - CIELAB coordinates for wine control and wine clarified with bentonite and lignin for 7 and 30 days. Statistical differences were assessed concerning the wine control and evaluated by one-way ANOVA reported using different letters: a (*), b (**), c (***), and d (****).

Samples	CIELAB color coordinates - 7 days			
	L*	a*	b*	ΔE
Control	63.4 ± 0.1	38.5 ± 0.1	5.31 ± 0.09	----------
Bentonite 40 g/hL	63.06 ± 0.08	38.44 ± 0.08	8.68 ± 0.08 [d]	3.39
OL 25 g/hL	63.34 ± 0.08	37.80 ± 0.07 [b]	6.1 ± 0.1 [a]	1.08
OL 100 g/hL	63.4 ± 0.1	36.68 ± 0.03 [d]	7.5 ± 0.1 [d]	2.92
KL 25 g/hL	63.56 ± 0.04	37.9 ± 0.2 [a]	5.88 ± 0.07	0.89
KL 100 g/hL	63.2 ± 0.3	37.1 ± 0.3 [d]	7.4 ± 0.1 [d]	2.56
LS 25 g/hL	63.4 ± 0.2	38.5 ± 0.3	5.03 ± 0.02	0.42
LS 100 g/hL	62.9 ± 0.6	38.8 ± 0.7	4.9 ± 0.2	0.93

	CIELAB color coordinates 30 days			
	L*	a*	b*	ΔE
Wine control	61.79 ± 0.07	39.81 ± 0.06	7.92 ± 0.02	----------
Bentonite 40 g/hL	62.54 ± 0.05 [a]	38.87 ± 0.08 [c]	7.70 ± 0.04 [a]	1.22
OL 25 g/hL	62.3 ± 0.1 [a]	38.5 ± 0.1 [c]	8.89 ± 0.07 [d]	1.15
OL 100 g/hL	64.2 ± 0.2 [d]	35.6 ± 0.2 [d]	10.5 ± 0.1 [d]	1.62
KL 25 g/hL	62.1 ± 0.3	38.8 ± 0.3 [c]	8.8 ± 0.1 [d]	4.74
KL 100 g/hL	62.6 ± 0.4 [b]	37.5 ± 0.3 [d]	10.6 ± 0.2 [d]	4.60
LS 25 g/hL	62.43 ± 0.04 [a]	39.3 ± 0.3	7.64 ± 0.09 [a]	0.94
LS 100 g/hL	61.2 ± 0.1 [a]	40.3 ± 0.2	7.5 ± 0.1 [c]	1.07

The values are represented by the mean ± standard deviation (n=9). Asterisks indicate significant differences from the wine control (* – $p \leq 0.05$, ** – $p \leq 0.01$, *** – $p \leq 0.001$, **** – $p \leq 0.0001$).

According to the results presented in Table 13, the lightness (L*) values for the 7 days were similar for all samples, indicating that lignin does not interfere with the sample transparency. After 30 days, there was an increase of L* in wine samples treated with OL at 100 g/hL. Regarding the colorimetric coordinates a* and b*, it was observed that for a* parameter, there is a decrease for KL and OL (independent of the contact time) when compared to the control wine, indicating a decrease in the red color contribution. Considering the b* values, the samples in contact with OL and KL showed higher values of this color coordinate when compared with the control wine. This indicates a higher contribution of the yellow color to the overall color of wine due to the yellowish color of lignin. This has already been discussed above in the analysis of the red wine hue (Table 13). This effect was directly correlated with the concentration of lignin. On the other hand, the light brownish-yellow tone of LS has a low contribution to the wine color change, and the decrease of values of the b* coordinate shifted to the blue axis agrees with the increase of the absorbance at 620 nm. Bentonite also demonstrated a strong influence on wine color, particularly for the yellow-blue coordinate. Regarding the ΔE values, a dependence on the type and quantity of lignin was observed. After 7 days of treatment, OL and KL at 100 g/hL demonstrated ΔE values of approximately 2.5 and 2.9, respectively, indicating that an inexperienced observer could notice the difference. However, the bentonite showed a higher color difference compared to lignin. After 30

days of treatment, only kraft lignin exhibited an ΔE value of around 4.5, indicating clear differences detectable by observers (295).

3.8. DIALYSIS INDEX

The dialysis index determines the structural complexity and molecular weight of the chemicals found in wine. Based on the results obtained (Appendix 2, Figure 2F), the clarification process does not affect the complexity of the wine, except when LS is used at 100 g/hL during 7 days of contact time, yielding a significant decrease in the wine complexity. This decrease could be related to the decrease in the PACs content, as previously described. Overall, after 30 days of contact with the different types of lignin, there are no significant differences in the complexity of the wine compounds when compared with the control wine.

3.9. QUANTIFICATION OF VOLATILE COMPOUNDS BY HS-SPME-GC/MS

Volatile compounds, including terpenes, phenols, alcohols, esters, aldehydes, ketones, and lactones, play an important role in the sensory characteristics of wines. They can be generated during the fermentation and aging processes, or they can come directly from the grape berries. This work evaluated the volatile profile of the control wine and the impact of lignin during a 7-day clarification process. The levels of 23 volatile compounds were determined in all samples (Appendix 2, Table 2D), of which 6 of them showed significant differences, Figure 23.

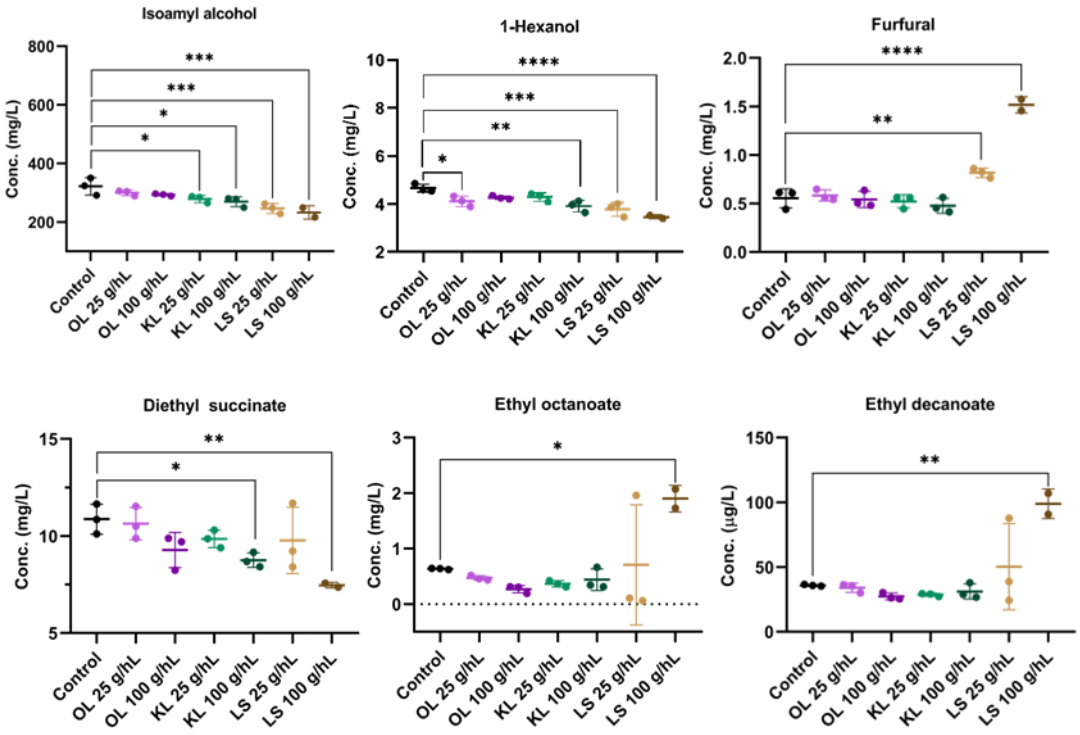

Figure 23 - Volatile compounds with significant differences in the groups under study compared with the control group. Statistical analysis was made by one-way ANOVA. Asterisks (*) indicate a statistical difference (* – $p \leq 0.05$, ** – $p \leq 0.01$, *** – $p \leq 0.001$, **** – $p \leq 0.0001$) relative to the control wine. Bars represent the mean ± standard deviation (n=9). Sample LS 100 g/hL is representative of an n=2, as the third triplicate had to be excluded due to a low chromatogram signal.

The presence of some volatile compounds might have a negative connotation since some of them confer the wine's unwanted odors and flavors. Isoamyl alcohol is an example, it is associated with descriptors like cheese and fusel (296). In this study, the Port wine employed as a control had a high concentration of isoamyl alcohol (approximately 350 mg/L) which is above the olfactory perception threshold (30 mg/L) (140, 297). The application of lignin as a clarifying agent, during the 7 days was very positive since there was a decrease of up to 27 % in the case of LS at 100 g/hL. For LS concentration of 25 g/hL or using KL, it was possible to observe significant differences with decreases between 13-16 % of this volatile compound. The presence of 1-hexanol confers odors that evoke newly cut grass or hay, as well as resin (296), and has a negative connotation as it usually refers to grapes that have not reached an optimal level of maturity before being harvested. The results obtained for the samples analyzed in this study were lower than the olfactory perception threshold (8 mg/L) (140, 297); nonetheless, the three types of lignin allowed for a significant decrease in this volatile following wine clarification. Furfural belongs to the aldehyde class, and it is usually found in red wine at levels below their odor thresholds (14 mg/L) (140, 297). This compound may be involved in polymerization reactions with polyphenols, and it is associated with

descriptors like almonds, bread, caramelization products, and sometimes dried wood (296). The results of this work demonstrated that furfural concentrations were much lower compared to the odor threshold, but for the wines treated with lignosulfonates, it was observed a significant increase in furfural concentration. The sulfite liquors that produce the lignosulfonates contain some traces of pentoses, an undesirable constituent that could be the furfural source. The LS used in this work underwent an ultrafiltration process, which can be insufficient to remove traces of furfural, which may lead to the increase that is shown in Figure 23. Still, the concentration values obtained are much lower than its olfactory perception threshold. Esters are chemical molecules found in wine that contribute to its fruity aroma. The diethyl succinate and ethyl decanoate concentrations found in the control wine were relatively low compared to the odor thresholds of 200 mg/L and 200 µg/L (140, 297), respectively. In the first case, there was a decrease in KL and LS at 100 g/hL compared to the control wine. Regarding the ethyl decanoate, in which its presence is associated with brandy and fruit descriptors (296), there was a significant increase in levels of circa 64 %. Finally, the concentration observed in control wine for ethyl octanoate was near to, and in some cases, greater than, the odor threshold (0.6 mg/L) (140, 297). The wine treated with LS at 100 g/hL showed the greatest rise in ethyl octanoate when compared to the other types of lignin. This increase may result in a sweeter aroma directed towards the pineapple flavor as these are the descriptors associated with this volatile compound. Overall, lignin had no negative influence on the aroma of the wine (at least that was detectable by smell), and it also helped to minimize the presence of volatiles associated with unpleasant descriptors.

4. CONCLUSIONS

The present work reports the first insight into the potential of different types of lignin on the modulating process of a Port wine. It was observed that the different types of lignin can affect wine's chemical composition and therefore, it can be used to modulate their composition. LS demonstrated better performance with the ability to reduce the tannin content, which can be useful in modulating astringency. LS also led to a decrease in the undesirable aromas (isoamyl alcohol and 1-hexanol) of wine and a reduction in the concentration of proteins after 30 days of treatment. Furthermore, an increase in anthocyanin content was observed, suggesting that lignin can assist in the depolymerization of aggregated anthocyanin fractions. The presence of lignin did not change the final color of the wine ($\Delta E<5$), even though the yellow color of lignin is one of the major limitations of its use in the creation of added-value products. This work opens up innovative approaches like exploring other possibilities using different lignin sources, and their combination with other non-animal fining agents. Furthermore, it contributes to new applications for lignin, the second most abundant biopolymer in nature. This sustainable approach addresses a significant challenge in the wine industry, showcasing lignin as a promising solution to enhance the overall quality of the wine. Furthermore, chemical modification of lignin can contribute to improved performance and adsorption efficiency for colloids and other compounds.

PART C

pH-DEPENDENT COMPLEXATION OF CYANIDIN-3-*O*-GLUCOSIDE WITH LIGNOSULFONATES

SYNOPSIS

Anthocyanins have limited application as natural colorants and antioxidants due to their loss of color and instability under certain conditions. This research explores the formation of a complex between lignosulfonates (LS) and cyanidin-3-*O*-glucoside (C3G) using a multi-technique approach as well as the effect on C3G's red color and oxidative stability in acidic mediums. All data revealed pH-dependent LS-C3G interactions. Thermodynamic parameters showed that at pH 1 the LS-C3G complex is formed mostly by electrostatic interactions between the flavylium cation of C3G and the sulfonate groups of LS. At pH 3 hydrophobic interactions arose from the different C3G species in the equilibrium, demonstrating a higher association constant at this pH. Fourier-transform infrared spectroscopy and Zeta-potential experiments further corroborate evidence of these LS-C3G interactions. Fluorescence quenching and lifetime experiments revealed static and dynamic quenching at pH 1 and 3, respectively. UV-visible spectroscopy demonstrated a bathochromic shift upon complex formation and a hyperchromic effect at pH 3 and 4, causing an enhancement of the red color of C3G. Electrochemical results suggested that at pH 3 the LS also enhances C3G stability by protecting its oxidizable moieties over time. C3G was stabilized using LS, an often-discarded byproduct of the paper industry, thus promoting the sustainable use of environmentally friendly resources.

*This chapter was adapted from the following paper: "**Pereira, A.R.**; Bravo, C.; Ramos, R.M.; Costa, C.; Rodrigues, A.; de Freitas, V.; Mateus, N.; Dias, Soares, S.; Oliveira, J.; New insights into pH-dependent complex formation between lignosulfonates and anthocyanins: Impact on color and oxidative stability. Manuscript submitted to the International Journal of Agriculture and Food Chemistry.*

Except for the ITC and voltammetry assays, as well as the processing of fluorescence results, the experimental design and work described in this part were conducted by the author. The lignosulfonates used in this work were provided by the LSRE-LCM/ALiCE group.

1. INTRODUCTION

Anthocyanins are biologically active phenolic compounds responsible for the orange, red, purple, and blue hues observed in different fruits, vegetables, and flowers (298, 299). Cyanidin-3-*O*-glucoside (C3G) is the most abundant anthocyanin widely distributed in natural sources, especially in fruits such as blackberries, cherries, and red grapes (32). These compounds are characterized by the flavylium cation or 2-phenylbenzopyrylium core structure, with variable methoxylation and hydroxylation patterns in the aromatic ring B. They can have acylated groups and sugar moieties connected to different places, which confers good water solubility facilitating the incorporation of these dyes into food matrices (298). In addition to the food and beverage processing industry, anthocyanins find wide applications as colorants and antioxidant agents in cosmetics, textiles, and food packaging industries (300). However, the stability of these natural compounds is affected by pH, temperature, oxygen, and light (301) which limits their use as colorants due to color modification or color loss. In addition, oxidation can lead to the deterioration and loss of the nutritional, commercial, and organoleptic quality (302).

Various strategies have been adopted to improve anthocyanin stability by forming stable complexes with carbohydrates, proteins, and macrocycles. Hydrogen bonding and hydrophobic effects are the main driving forces for creating the complexes observed with carbohydrates and proteins, particularly in the presence of flavylium cation species (303, 304). Polysaccharides such as pectin have gained special attention as both compounds co-exist in plant cell vacuoles and can interact with anthocyanins, thus improving their stability, bioavailability, extractability, and color stability (85, 87, 88). Through hydrogen bonds, xanthan (89) and arabic gums (90) improved black rice anthocyanins' color and thermal stability. Proteins, including β-lactoglobulin (94) and milk α- and β-casein (95), have also shown potential to improve anthocyanin's photostability while preventing color fading and degradation. Macrocycles such as natural cyclodextrins incorporate ACNs inside their cavities, demonstrating higher affinity to the hemiketal, *cis*- and *trans*-chalcone forms of the anthocyanin multistate equilibrium, a phenomenon leading to the shifting of the pigment hydration equilibrium towards the formation of more colorless forms (92, 93).

More recently, it has been reported the first evidence of the impact of commercial lignosulfonate on the thermodynamic and kinetic parameters of malvidin-3-*O*-glucoside at pH 1 using UV-visible spectroscopy (101). Lignosulfonates (LS) are anionic polyelectrolyte polymers with an irregular three-dimensional macromolecular structure, primarily composed of three phenylpropanoid units (p-coumaryl, coniferyl, and sinapyl

alcohols) (305). Due to the abundance of ionizable functional groups, including sulfonate groups, this lignin presents the advantage of being water-soluble. The skeletal lignin structure contains hydrophobic groups, consisting of aromatic and residual aliphatic units, and certain oxygen-containing groups. Their behavior in aqueous solution is largely determined by the proportion of hydrophilic (ionizable) and hydrophobic groups (306). Depending on the pH, LS can present different surface charges and interact with anthocyanins in various ways.

This work provides new insights into the red color stabilization and oxidative protection of C3G in the acidic pH range by a softwood lignosulfonate from the pulp and paper industry. The interaction between LS and C3G as well as the complex characteristics were achieved using a calorimetric and spectroscopic-based multi-technique approach namely, isothermal titration calorimetry (ITC), UV-visible and fluorescence spectroscopy, voltammetry, Fourier-transform infrared spectroscopy (FTIR) and electrophoretic light scattering (ELS).

2. MATERIALS AND METHODS

2.1. REAGENTS

Lignosulfonates (average molecular weight of 48,550 g mol^{-1}) were obtained from a softwood sulfite liquor (total solids, 11.3 % w/w liquor), supplied by a pulp mill of a local company, as a mixture of 90 % spruce (softwood material) and 10 % beech (hardwood biomass). This liquor was submitted to an ultrafiltration process and the obtained retentate was freeze-dried to yield a golden-brown powder. Specific conditions of this isolation process are described by Casimiro et al. (277). Hexadecyltrimethylammonium bromide (CTAB, ≥ 98 %) was purchased from Sigma. Commercial cyanidin-3-*O*-glucoside chloride was purchased from Extrasynthese (≥ 98 %). Milli-Q water was used for the preparation of all solutions.

2.2. pH DETERMINATION

The pH of all solutions was recorded (and if necessary adjusted using 1 M HCl or 1 M NaOH) in a WTW pH 320 or 508 (Weilheim, Germany) with a CRISON 5209 combined glass electrode of 3 mm diameter (Barcelona, Spain), previously calibrated with buffer solutions (pH 4.00, 7.00 and 10.00).

2.3. QUANTIFICATION OF NEGATIVE GROUPS

The quantification of negative groups in the LS structure followed the established method described by Li et al (307). LS (1 $g.L^{-1}$) and CTAB (0.01 M) stock solutions were prepared in Milli-Q water. Then, 10 mL of the LS solution was mixed with increasing volumes of the CTAB stock solution, ranging from 0.5 to 2.5 mL (in intervals of 0.1 mL), at each pH value (1 to 11). Water was then added to bring the total volume to 25 mL. Then, 1.5 mL of the resulting solution was centrifuged at 14,000 rpm for 10 minutes, and the absorbance of the supernatant was measured at 280 nm by UV-visible spectrophotometry using a 1 mm quartz cell. The number of negative groups, N (mmol. g^{-1}) was determined considering the CTAB volume corresponding to the minimum absorbance and following Equation 1:

$$\text{Negative groups, N} = \frac{\text{CTAB volume (L)} \times \text{CTAB concentration (mol.L}^{-1})}{\text{LS volume (L)} \times \text{LS concentration (g.L}^{-1})} \quad \text{Equation 1}$$

2.4. STUDY OF THE SURFACE CHARGE OF LIGNOSULFONATES

LS solutions (1 µM) were prepared in Milli-Q water across a pH range of 1 – 11, with the pH adjusted to the desired values using NaOH or HCl stock solutions. The solutions were filtered through a 0.22 µm filter, allowed to equilibrate for 1 hour, diluted 10-fold with deionized water, and transferred to a capillary cell. Stock solutions of C3G (100, 500, and 1000 µM) were prepared in 0.1 M HCl for pH 1 experiences and in deionized water with pH adjustment for pH 3 studies. Solutions of the complex LS-C3G keeping the biopolymer concentration at 1 µM and changing the concentration of C3G (100, 500, and 1000 µM) were also prepared in the same solvents of the stock solutions depending on the pH of the experience. After 30 minutes of stabilization, the samples were transferred to the capillary cells, and the zeta-potential values were determined. The average zeta (ζ)-potential was measured by an Electrophoretic Light Scattering (ELS) using a Malvern Zetasizer Nano ZS instrument (Malvern Instruments Ltd, UK).

2.5. LS-C3G INTERACTIONS BY ISOTHERMAL TITRATION CALORIMETRY

A MicroCal-PEAQ-ITC (Malvern Panalytical) controlled by MicroCal-PEAQ-ITC Analysis Software (version 1.41, Malvern Panalytical) was used to conduct isothermal titration calorimetry (ITC) experiments. Solutions of LS (150 µM) and C3G (5 mM) were prepared in a 10 mM citrate buffer for the experiments at pH 3 and 0.1 M HCl for the

experiments at pH 1. Then, 240 µL of the LS solution was loaded on the sample cell and the injection syringe was loaded with C3G solution. After reaching baseline stability, the C3G solution was injected (2 to 3 µL/injection) into the sample cell 19 – 22 times. Samples were stirred continuously at 1,500 rpm to ensure full mixing. The time between injections (250–300 s) was optimized to allow reaching the baseline before subsequent injections. Raw data from a plot of heat flow vs injection number were fitted by the MicroCal-PEAQ-ITC Analysis Software to find the binding constants, stoichiometry, and thermodynamic parameters for the LS-C3G interactions studied using the one-site binding model. Blank experiments of C3G titration into 10 mM citrate buffer and 0.1 M HCl were performed and were subtracted from sample experiments.

2.6. FOURIER-TRANSFORM INFRARED SPECTROSCOPY

The Fourier-transform infrared (FTIR) spectra were recorded with an FTIR Spectrum (PerkinElmer) spectrometer equipped with a universal attenuated total reflectance (ATR) sampling device. Spectra were recorded in transmission mode over a wavenumber interval from 4000 to 600 cm^{-1} (64 scans at a resolution of 2 cm^{-1}). Analyses of the LS and LS-C3G complex were performed in a solid state after lyophilizing the solutions used in UV-vis experiments at pH 3.

2.7. FLUORESCENCE SPECTROSCOPY

Fluorescence quenching was measured using a Fluoromax-4 fluorimeter (Horiba Scientific). The emission spectra were recorded from 300 to 500 nm (scan rate 10 $nm.s^{-1}$) at two different excitation wavelengths (285 and 315 nm – maximum fluorescence peaks of LS). Both slit widths were set to 5 nm. The experiments were performed at pH 1 and 3 using 0.1 M HCl and 10 mM citrate buffer as solvents, respectively. The LS concentration was kept constant (0.82 µM), while the concentration of C3G varied between 0 – 4.25 µM. The final concentrations of LS and C3G were optimized to guarantee adequate fluorescence intensity values while avoiding inner filter effects (UV absorbance at 285 and 315 nm under 0.1) (308). Absorbance measurements are summarized in Appendix 3 (Figure 3A). The stock solutions were filtered (0.22 µm filter) and maintained at 20 °C in a thermoshaker at 200 rpm (MSC-100 Cooling Thermoshaker Incubator) protected from light. The quenching mechanism was described by the Stern-Volmer equation (Equation 2):

$$\frac{F_0}{F} = 1 + k_q \tau_0 [Q] = 1 + K_{SV}[Q] \quad \text{Equation 2}$$

where F_0 and F are the fluorescence intensities of LS before and after the addition of the quencher (C3G), respectively; k_q is the bimolecular quenching constant; τ_0 is the lifetime of LS fluorophore; [Q] is the C3G concentration; K_{SV} is the Stern-Volmer quenching constant.

In the 3D excitation-emission matrix (EEM) measurements, emission spectra (300 – 550 nm) were recorded at 2 nm increments of excitation wavelength between 250 – 350 nm at a scan rate of 20 nm s^{-1}. The EEMs parallel factor analysis (PARAFAC) was used to quantify the effects of C3G on the LS fluorescence individual components and was conducted using the drEEM toolbox (https://dreem.openfluor.org/) in MATLAB. More details of the EEM-PARAFAC analysis are described in Appendix 3 (Text 3A and Figure 3B).

Time-resolved fluorescence measurements were performed with a TemPro 01 system (Horiba Jobin Yvon, USA). The samples were excited at 290 nm (NanoLED light source) and the emission was set to 376 nm (bandpass of 16 nm). Time-resolved experiments were recorded using a window of 4024 channels (time calibration of 0.055 ns/channel). To optimize the S/N ratio, 10,000 photon counts were collected at the peak channel.

2.8. MULTISTATE OF C3G SPECIES BY UV-VISIBLE SPECTROSCOPY

The pseudo-equilibrium and equilibrium constants for C3G were determined by UV-visible spectroscopy using aqueous solutions ranging from pH 0 to 6. A stock solution of C3G (2.6 mM) was prepared in 0.1 M HCl, and different stock solutions of LS (90 µM) were prepared in water at pH values ranging from 0 to 6 with a pH tolerance of ± 0.2. For pH 0, the stock solution of C3G was prepared in 1 M HCl. In each experiment, 981 µL of water at the desired pH, 500 µL of the LS solution (previously filtered with a 0.22 µm filter), and 19 µL of C3G stock solution were added into a plastic cuvette (10 x 10 mm). A control experiment without LS was performed by replacing the volume of LS with water. The absorption spectra of all solutions from 200 − 800 nm were recorded in a Cary 60 UV-visible spectrophotometer (Agilent) after 30 minutes (pseudo-equilibrium, pK^a) and

one day (equilibrium, pK'a). The fittings for the pK^a and pK'a were carried out using the Solver tool in Microsoft Excel.

2.9. UV-VISIBLE TITRATION EXPERIMENTS FOR LS-C3G COMPLEX

The association constants between C3G and LS were determined at pH 1, 3, and 4 using UV-visible spectroscopy. For pH 1, the experiment was performed using 0.1 M HCl as the solvent, while for pH 3 and 4, Milli-Q water with pH adjusted with HCl (12 M) was used. Two solutions were prepared for each pH value: solution A containing C3G (26 µM) and solution B containing C3G (26 µM) and LS (30 µM). Small volumes of solution B were then added to solution A to obtain solutions with increasing concentrations of LS (from 0.30 µM to 24 µM). The absorption spectrum from 350 to 700 nm was recorded for all solutions in a quartz cell (10 × 10 mm). The values of the apparent association constants (nK_a) were determined using the solver tool in Microsoft Excel, by fitting the obtained data from the graphical representation of the maximum absorption wavelength as a function of LS concentration. It used a mathematical model that considers the number of functional groups in LS (n) available to interact with C3G and the concentration of LS ([LS]) in each point (101). This model assumes that the interactions are mainly electrostatic and the flavylium cation is the predominant species interacting with LS, with Equation 3:

$$\mathrm{Abs} = \mathrm{Abs}_0 + \Delta\mathrm{Abs}\frac{\mathrm{nK[LS]}}{(1+\mathrm{nK[LS]})} \qquad \text{Equation 3}$$

where Abs represents the absorbance, Abs_0 is the initial absorbance, ΔAbs is the change in absorbance, n is the number of functional groups in LS available for interaction, and K is the association constant.

2.10. ELECTROCHEMICAL STUDIES

Square wave voltammograms (SWVs) were performed with a potentiostat driven (PalmSens4) by PSTrace software in a three-electrode cell consisting of a 3-mm glassy carbon working electrode (WE), an Ag|AgCl (3 M KCl) reference electrode and a Pt wire counter electrode (all from Basi, USA). The instrumental parameters used for the analysis were: square-wave frequency of 25 Hz, wave amplitude of 25 mV, and potential step of 5 mV (resulting in a scan rate of 125 mV s^{-1}). After each measurement, the WE

surface was renewed using 1.0 µm aluminum oxide on polishing pads, thoroughly rinsed with Milli-Q water, and dried. The cleaning procedure was necessary to avoid underestimating anodic currents due to the passivation of the WE. The linearity of each compound was verified by varying the concentration of LS (1–20.5 µM) and C3G (2–100 µM). For titration, the LS concentration remained fixed (8.2 µM), and increasing concentrations of C3G between 2 and 50 µM were added.

2.11. STATISTICAL ANALYSIS

Analyses were performed in triplicates and the results were expressed as mean values and standard deviation (SD). All experiments were performed at room temperature, being that for fluorescence studies the temperature was controlled at 20 ºC. Analysis of variance (ANOVA) was used to identify statistical significance, and differences were considered statistically significant at $p < 0.05$. GraphPad Prism 8.0 for Windows was used to process all statistical data.

3. RESULTS AND DISCUSSION

3.1. CHARACTERIZATION OF LS IN AQUEOUS SOLUTION

The LS used in this work were isolated from a sulfite liquor and characterized based on inorganic content, phenolic monomers, ^{13}C NMR, and molecular weight, as detailed in Appendix 3 (Table 3A). Considering the hypothesis of electrostatic interactions between the positively charged C3G and the negatively charged groups of LS, the number of ionizable groups and the overall LS surface charge were investigated from acidic to alkaline conditions. LS comprises ionizable groups such as sulfonate, carboxylic, and hydroxyl groups. According to the literature, the degree of ionization of LS in aqueous systems is influenced by the pH, with sulfonate groups ionizing at pH 1.5, carboxylic groups at pH 5.1, and hydroxyl groups at pH 10.5 (309, 310). The zeta-potential revealed two inflection points: one at pH 4.2, attributed to carboxyl groups, and the other at pH 8.1 related to phenolic hydroxyl groups that may start to deprotonate, further increasing the negative charge on the surface (Appendix 3, Figure 3C). Under acidic conditions (pH < 4), the zeta potential of LS decreased from -10 to -30 mV due to the successive ionization of sulfonic acid groups. Between pH 4 and 8 - where the ionization of carboxylic groups occurs - the zeta potential values remain constant, suggesting that these functional groups are not surface-exposed. At pH values higher than 8, the zeta potential became more negative due to the ionization of phenolic

hydroxyl groups. These results suggested that both sulfonic and phenolic hydroxyl groups are distributed on the LS surface, while carboxyl groups are concentrated in the polymer's core. Deprotonated sulfonic acid groups can directly interact with C3G within the studied pH range (between pH 1 and 4).

The CTAB precipitation method was used to determine the amount of negative groups in LS. Since CTAB is a cationic surfactant that establishes an electrostatic interaction with the negative groups of LS, the amount of CTAB required reflects the content of negative groups in LS (Appendix 3, Figure 3D (a)). As the pH increases, a higher amount of CTAB is necessary to neutralize the negative charge of LS, indicating the presence of more negative groups (Appendix 3, Figure 3D (b)). Up to pH 4, the content of negative groups increased from 1.00 mmol g^{-1} to 1.33 mmol g^{-1} of LS due to the neutralization of the deprotonated sulfonic acid and carboxylic groups. Between pH 5 and pH 9, the results showed a plateau, with the negative groups measuring approximately 1.53 mmol g^{-1} of lignosulfonate, suggesting that the ionization of the negative groups reached equilibrium. At pH values higher than 9, the content undergoes a clear increase from 1.60 mmol g^{-1} to 1.97 mmol g^{-1} of LS (pH 12) due to the ionization of the phenolic hydroxyl groups. These results support the previously obtained zeta potential values: up to pH 5 and after pH 9 the ionization of sulfonic and phenolic hydroxyl groups occurs.

3.2. LS-C3G COMPLEX FORMATION

3.2.1. THERMODYNAMIC CHARACTERIZATION OF LS-C3G INTERACTION

The binding affinity between LS and C3G was characterized by isothermal titration calorimetry (ITC). The enthalpy changes per mole of injectant (kcal/mol) were plotted against the molar ratio LS:C3G at pH 1 and 3 (Figure 24). The resulting binding isotherms were fitted by the MicroCal-PEAQ-ITC Analysis Software according to an independent site model. Due to their general shape, it could be assumed that anthocyanins interact non-specifically with lignosulfonates rather than binding to specific sites, as the binding isotherms do not exhibit the sigmoidal shape expected for a specific (311). From these curves, the dissociation constants (K_D) and the number of binding sites in LS for each interaction were determined and both are indicated in the graphs. The association constants ($K_a = 1/K_D$) and the thermodynamic parameters obtained from the analysis of the fitting of the ITC binding isotherms are summarized in Table 14.

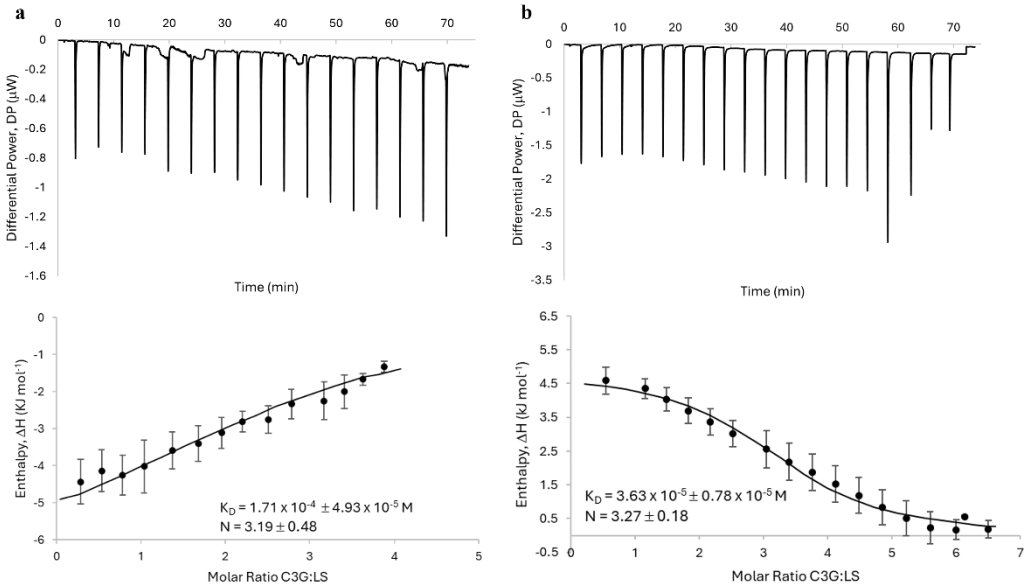

Figure 24 - ITC isotherms for the LS (150 µM) with C3G (5 mM) at pH 1 (left) and pH 3 (right): binding isotherm (points) and fitting curve (line).

Table 14 - Thermodynamic parameters (association constants, Ka, enthalpy, ΔH, Gibbs energy, ΔG, and entropy, -TΔS) determined for the LS-C3G interaction. Presented data were obtained by subtracting C3G titration into the buffer used for each experiment and results from at least three independent experiments. Data with different letters are statistically different ($p < 0.05$).

pH	K_a (M^{-1})	ΔG^o (KJ mol^{-1})	ΔH^o (KJ mol^{-1})	$-T\Delta S^o$ (KJ mol^{-1})
1.0	$6.1 \times 10^3 \pm 1.6 \times 10^3$	$-21.5^d \pm 0.1$	$-23.1^f \pm 2.6$	$0.61^g \pm 0.04$
3.0	$2.8 \times 10^4 \pm 5.5 \times 10^3$	$-25.4^e \pm 0.5$	$20.2^e \pm 0.9$	$-45.6^h \pm 0.8$

The association constant (K_a) obtained by the ITC demonstrated a pH dependency, with the highest K_a value observed for the interaction between LS and C3G at pH 3 ($K_a = 2.8 \times 10^4$ M^{-1}). Anthocyanins exhibit different forms in equilibrium depending on the pH of the medium. At strongly acidic conditions (pH ≤ 1), the flavylium cation (AH^+) is the predominant species, responsible for the red color of anthocyanins. As the pH increases, the flavylium cation undergoes two simultaneous reactions: rapid deprotonation to generate the neutral quinoidal base (A, blue form), and a slower hydration process at carbon 2 resulting in the colorless hemiketal B (thermodynamically more stable than A). This form then undergoes ring opening (tautomerization) to produce cis-chalcone (Cc) which further isomerizes in trans-chalcone (Ct) (Figure 3) (51). At pH 3, about 50 % of

the anthocyanin is likely to occur as flavylium cation (AH^+) and the other 50 % corresponds to other species as neutral hemiketal form (B) (312). Although electrostatic interaction is an important mechanism for the LS-C3G binding between the flavylium cation and the sulfonate groups of LS, the presence of other species can promote different types of interaction such as hydrophobic effects or π-π interactions between the aromatic rings of C3G and LS and explain the higher binding affinity at pH 3. Furthermore, the higher concentration of C3G used in the ITC experiments (5 mM) also induces self-association phenomena which prevent the hydration reaction and favor the presence of flavylium cation in solution available to interact with LS (312). At very acidic conditions such as pH 1, flavylium cation is the only species in solution. This positively charged species interacts mainly with the negative groups of LS, which are the deprotonated groups in the structure of the polymer (pK_a 1.5). However, due to the presence of aromatic rings on the C3G and LS structures, π-π stacking interactions and hydrophobic effects can also occur between the molecules, as observed in copigmentation between ACNs and flavonoids or hydroxycinnamic acids

The negative Gibbs free energy ($\Delta G^o < 0$) in both systems (Table 14) indicated that the interactions between LS and C3G are thermodynamically favorable, and as expected, the quite weak Gibbs energy observed for both pH´s (-21 to -25 KJ mol^{-1} at pH 1 and 3, respectively) suggested the presence of non-covalent interactions. Further thermodynamic analysis indicated that at pH 1 the LS-C3G interaction is exothermic (negative enthalpy, $\Delta H^o < 0$) driven primarily by enthalpy with negligible entropy (ΔS^o) changes. Conversely, at pH 3, the interaction is endothermic ($\Delta H^o > 0$) and entropy-driven (higher contribution for $-T\Delta S^o$ parameter). In general, in systems with negative enthalpy (ΔH) and positive entropy (ΔS), as observed at pH 1, the interaction is essentially mediated by electrostatic forces, including hydrogen bonds between ionized groups (313). This occurs between the negative sulfonated groups of LS and the flavylium cation (AH^+) of C3G. Nevertheless, due to the chemical structure of both molecules, π-π interactions between the aromatic rings of LS and C3G can also favor the complex formation. The formation of these favorable interactions releases energy (negative enthalpy), and positive entropy indicates an increase in disorder, which can be attributed to the rearranging of the molecular structure during complex formation. At pH 3, the interaction is entropically driven, with a larger negative entropy ($-T\Delta S < 0$) and a positive ΔH, indicating that hydrophobic effects dominate this endothermic complex (314). At this pH, neutral forms of C3G such as the hemiketal are in equilibrium with the flavylium cation and can create π-stacking interactions with macromolecules like LS,

particularly in nonpolar or hydrophobic environments. However, the possibility of electrostatic interactions occurring between the ionizable groups of LS and the [AH^+] form of C3G cannot be dismissed. The interaction requires energy from the surroundings to occur, indicating the production of a less stable complex; nonetheless, the negative entropy suggests the formation of a more well-organized structure or complex between LS and C3G.

3.2.2. SURFACE CHARGE AND MOLECULAR STRUCTURE OF LS IN THE COMPLEX LS-C3G

The study of the surface charge of LS molecules corroborated the results observed in the thermodynamic parameters, revealing more pronounced electrostatic interactions at pH 1, which resulted in a significant variation in surface charge. Considering that these interactions primarily occur on the surface of molecules, particularly in the case of LS, which has been shown to have ionizable groups on the structure's periphery, the surface charge of LS was evaluated with various concentrations of anthocyanin (0 – 1 mM). Experiments were carried out at pH 1 and 3 as LS has variable surface charges because of the successive ionization of sulfonate groups as the pH of the medium increases. At pH 3, the zeta value of LS is more negative (around -30 mV) compared to the value for pH 1 (-19 mV), indicating more deprotonated functional groups (sulfonated groups). At both pHs, higher concentrations of C3G made the zeta potential less negative, which means that the negative groups are unavailable due to the interaction with the positive charges from the flavylium cation of the anthocyanin (Figure 25).

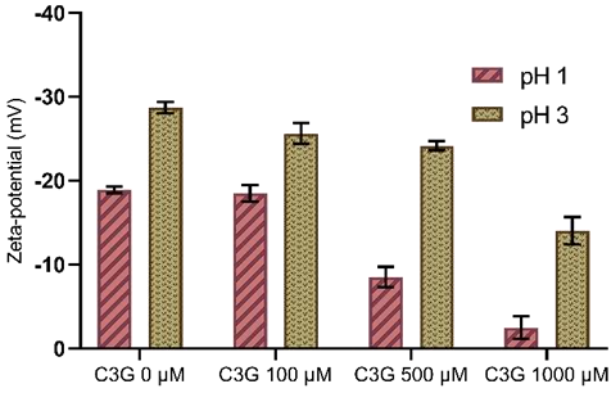

Figure 25 - Variation in LS's zeta-potential (mV) with increasing C3G concentrations at pH 1 and 3.

This modification was more evident at pH 1 corresponding to a variation of 83 % for the highest concentration of C3G (1000 µM), while for pH 3 the increase of the zeta potential was around 41 %. At pH 3, although the hydrophobic effect was found to be the major mechanism for C3G-LS complex formation, the presence of electrostatic forces must be considered due to negative and positive charges in the solution that can interact and promote the complex formation. It was also detected that these modifications result from the electrostatic interactions between C3G and LS and not from a synergic effect by adding positive charges.

FTIR was used to perform complementary analysis on functional group modifications in LS molecules on the complex at pH 3. The data showed that the interactions with C3G resulted in some intensity variations in the aromatic region, without showing any shift in the peak positions (Appendix 3, Figure 3E). In agreement with literature data (315-317), LS has characteristic wavenumber and corresponding vibration types (Appendix 3, Table 3B), since the most characteristic IR regions of LS are the C=C aromatic skeletal vibrations around 1500–1650 cm^{-1}, and the sulfonic acid groups around 1150–1200 and 1030 cm^{-1}. The intensity ratio between the peaks at 1600/1650 cm^{-1} increased in the presence of C3G, suggesting that the aromatic rings of LS are the most prone to interact with the anthocyanin molecules through π-π interactions already mentioned in the ITC results. Furthermore, slight modifications on the band at 1200 cm^{-1} characteristic of the sulfonate group (S=O) suggest possible interactions of this functional group with the C3G.

3.2.3. FLUORESCENCE EVIDENCE

The formation of the LS-C3G complex and the conformational changes of LS upon binding with C3G were followed by fluorescence. One of the intrinsic features of LS is its autofluorescence, attributed to fluorophores within the LS structure. While benzene rings, prevalent in all lignin monomers, largely contribute to fluorescence emissions, distinct side chains and substitutions on these rings can alter the emission spectrum, indicating the presence of multiple fluorescent structures within the lignin molecule (318). To the best of our knowledge, this is the first study investigating the quenching mechanism between LS and phenolic compounds. Similar studies only examined the binding mechanisms of LS with metal(oid)s, like Fe, Ag, and Hg (319, 320).

In all experiments, the chosen concentration of LS (0.82 µM) was in the linear range of concentrations with fluorescence (Appendix 3, Figure 3F). The 3D EEM spectrum of LS at pH 3 (Figure 26 a) revealed the presence of two main peaks: peak 1 at λex / λem of 315/385 nm, and peak 2 at a lower excitation wavelength (λex / λem of 285/380 nm). The fluorescence quenching studies were performed for both peaks (Figure 26, b-e). The interaction between LS and C3G was highly affected by the solution pH. Probably, because LS molecules are formed by different ionizable groups, the increase in the pH can promote the formation of negative charges responsible for electrostatic repulsion, which expands the molecule structure and favors the interaction with other molecules (321). These modifications on the LS structure resulted in different fluorescence behaviors, since at pH 3, as seen in Figure 26 c and e, was observed a linear Stern-Volmer equation, while at pH 1 a clear trend was not observed (Figure 27). Consequently, it was possible to only calculate the K_{sv} and k_q values at pH 3 (Figure 26 e). The K_{SV} values found in this study were similar to those reported for C3G binding with proteins (322). The higher values of the bimolecular quenching constant (k_q), which could mean a quenching efficiency or fluorophores' accessibility to the quencher, compared to the diffusion-controlled limit (1.0×10^{10} M^{-1} s^{-1}) suggest an interaction (308).

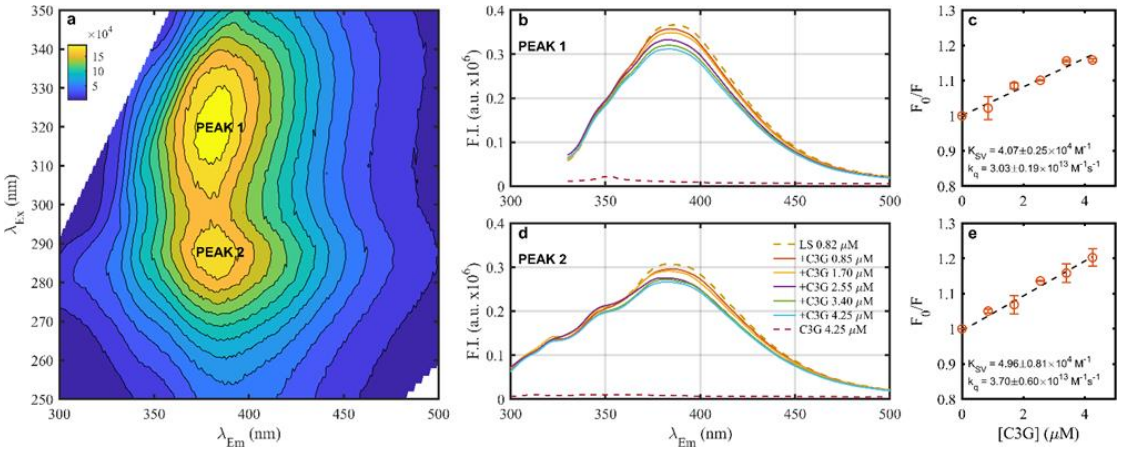

Figure 26 - (a) 3D EEM fluorescence spectrum of a 0.82 µM LS solution at pH 3. Emission spectra of LS Peak 1 (b) and Peak 2 (d) in the presence of increasing concentrations of C3G (0.42 – 4.25 µM) and corresponding Stern-Volmer plots with the quenching and binding constants for C3G binding to LS (c, e). In plots b and d, the intrinsic fluorescence of C3G is reported as red dotted lines. The measured τ_0 value of 1.34 ns was considered for the calculation of the binding constant.

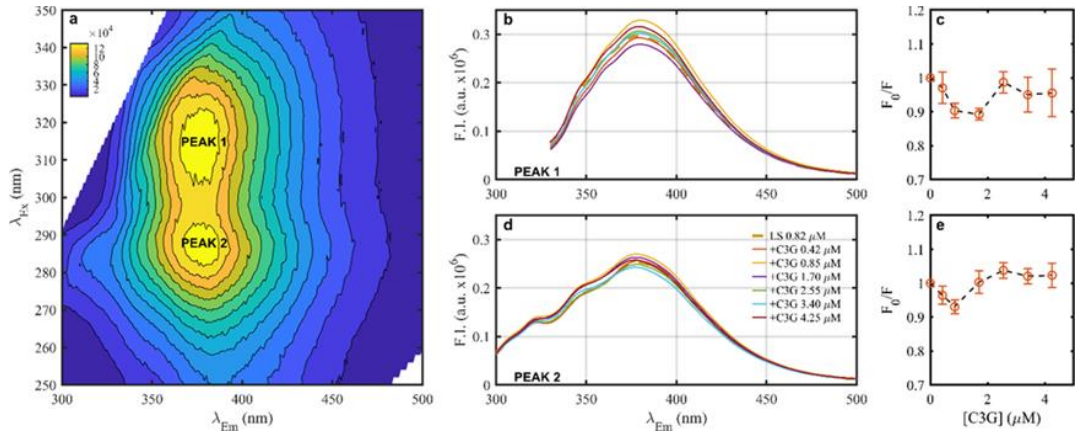

Figure 27 - (a) 3D EEM fluorescence spectrum of a 0.82 µM LS solution at pH 1. Emission spectra of LS Peak 1 (b) and Peak 2 (d) in the presence of increasing concentrations of C3G (0.42 – 4.25 µM) and corresponding Stern-Volmer plots with the quenching and binding constants for C3G binding to LS (c, e). In plots b and d, the intrinsic fluorescence of C3G is reported as red dotted lines. The measured τ0 value of 1.34 ns was considered for the calculation of the binding constant.

However, to understand the type of quenching involved in these interactions, time-resolved fluorescence experiments were performed using a similar approach to the one taken for steady-state fluorescence. The complex structure with random and disorganized linkages as well as branches makes the fluorescence lifetime of lignin very short in a range of sub- to nanoseconds. Furthermore, the fluorescence of LS is strongly dependent on the biomass nature and the applied pretreatment (323). In agreement with the literature (324, 325), very small values for the lignin lifetime at both pH 1 and 3 were measured. While no significant changes in the fluorescence lifetime (τ) of LS were observed at pH 1 after the interaction of C3G, at pH 3 there was a slight decrease in the τ value (Figure 28). These data can help to distinguish between static quenching at pH 1 and dynamic quenching at pH 3.

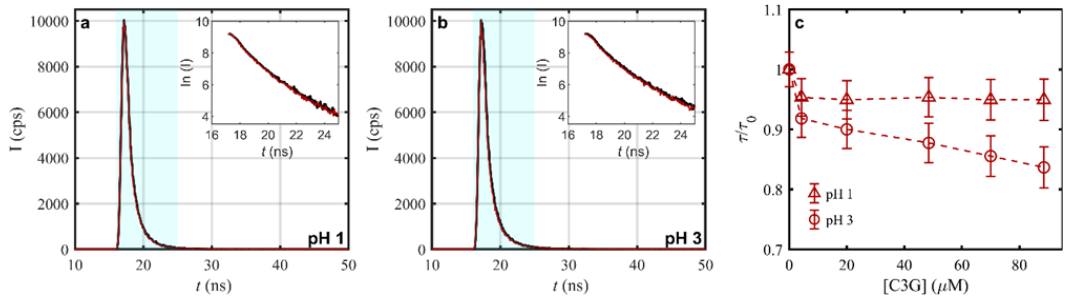

Figure 28 - Fluorescence intensity decay was recorded at pH 1 (a) and pH 3 (b) of 0.82 μM. LS solutions in the absence (black traces) and presence (red traces) of 88.5 μM C3G. The ratio of τ/τ0 versus the C3G concentration is reported in (c).

In static quenching, a nonfluorescent complex is formed, where the ratio of the fluorescence lifetimes in the absence and presence of the quencher (τ_0/τ) equals 1, indicating that the fraction of non-complexed fluorophores remains unperturbed. Electrostatic interactions suggested as the driving forces for the formation of the LS-C3G complex at pH 1 may promote the binding between the fluorophore and the quencher to form a nonfluorescent ground-state complex. On the other hand, collisions between the fluorophore and the quenching agent induce dynamic quenching, which is characterized by a decrease in the τ of the excited state (308).

All EEM spectra of LS samples at pH 1 and pH 3 measured in the absence and presence of C3G are shown in Appendix 3 (Figures 3G and 3H). Coherently with 2D results, the addition of C3G affected the fluorescence behavior of LS only at pH 3. Thus, only the EEM spectra at pH 3 were analyzed by PARAFAC (Figure 29). Split-half analysis, residual analysis, and visual inspection identified that three components were appropriate: C1 (Ex/Em 310/360 nm), C2 (Ex/Em 330/390 nm), and C3 (Ex/Em 285/315-400 nm) (Figure 29 c).

PARAFAC analysis provided additional quantitative information describing the distribution of the three components with increasing concentrations of C3G (Figure 29 d), showing that only component 2 was affected by the interaction with C3G. On the other hand, C1 and C3 did not show any significant decrease in intensity, highlighting the selectivity of the C3G interaction with LS.

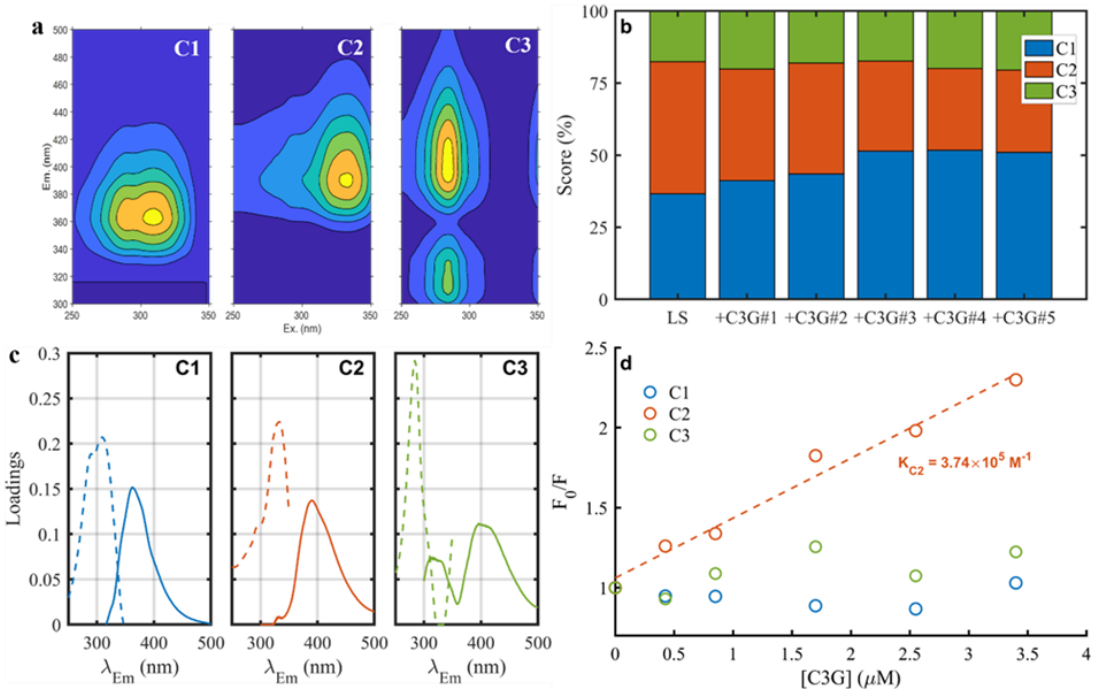

Figure 29 - Fluorescence components detected in excitation-emission matrices and modeled by PARAFAC analysis of LS sample in the presence of increasing concentrations of C3G at pH 3 (a) and their relative score in each sample (b); (c) Excitation (dotted lines) and emission (continuous lines) loadings of each component; (d) Stern-Volmer plots of each component vs. C3G concentrations.

3.3. CHROMATIC CHARACTERISTICS OF LS-C3G COMPLEX

3.3.1. IMPACT OF LS ON THE MULTISTATE OF SPECIES OF C3G AT ACIDIC CONDITIONS

To evaluate the effect of LS in the multistate of species of C3G, C3G in the presence of LS was titrated across a pH range of 0 to 6 and the pseudo-equilibrium (pK^a) and equilibrium (pK´a) constants were determined. The UV-visible spectrum of each solution (C3G and C3G with LS) was recorded after 30 min (pseudo-equilibrium) and 1 day (equilibrium) (Figure 30). This time scale allows for the establishment of equilibrium between AH^+, B, and Cc forms at pH below ≈ 5, and Ct formation over a longer period. Up to pH 6, there is a significant decrease in absorbance at 519 nm, corresponding to the disappearance of the AH^+ species to form B, Cc, and Ct. Acidity constants were determined from the graphical representation of the maximum absorbance (519 nm) as a function of the pH. As shown in Figure 30 (insets), the pK^a value closely aligned with pK´a in the absence (Figure 30 a and b) or presence of LS (Figure 30 c and d) indicating that the contribution of the trans-chalcone form to the overall multistate species is below 10 % in both cases. In the presence of LS, both acidity

equilibrium constants showed a significative increase of approximately 1 unit, highlighting the LS's role in stabilizing the AH^+ form of C3G.

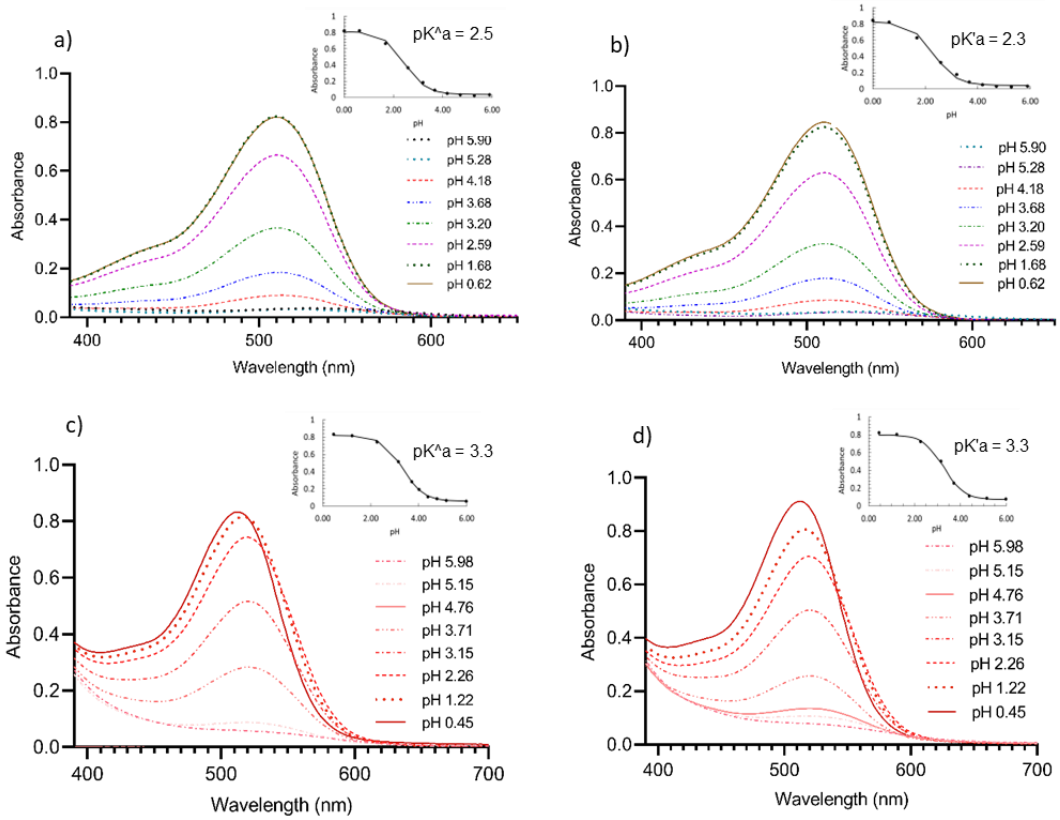

Figure 30 - UV-vis spectra for C3G in the absence (a and b) or presence of LS (c and d) with the respective fitting (insets) for the pseudo-equilibrium (a) and (c) and equilibrium (b) and (d), respectively.

3.3.2. DETERMINATION OF LS-C3G ASSOCIATION CONSTANT BY UV-VISIBLE SPECTROSCOPY

UV-visible spectroscopy was used to assess the interaction of C3G with LS. At all pH values investigated, there is a bathochromic shift in the maximum wavelength of C3G in the presence of LS (Figure 31). A hypochromic effect was also detected with increased LS concentrations at pH 1. This behavior has also been observed with other macromolecules such as dendrimers (326) and curcubit[n]urils (327). Conversely, at pH 3 (Figure 31 b) and 4 (Figure 31 c), the bathochromic shift was coupled with an increase in the absorbance intensity for the maximum wavelength (hyperchromic effect). At these pH values, the LS polymer interacts with the flavylium cation and pseudo-base present (pKh ≈ 3.5, which means that at pH 3.5 there is 50 % of flavylium cation and 50 % of hemiketal), shifting the equilibrium towards the formation of more flavylium cation. This

suggests that the presence of the LS reduces the formation of non-colored species during equilibrium, preserving the red color. However, the color stabilization was more efficient at pH 3 than pH 4 since the amount of flavylium cation decreased with increasing pH value (10 % at pH 4). The complex's apparent association constant (nK_a) was determined by the graphical representation of the maximum absorption wavelength as a function of LS concentration (Figure 31 d). The results showed a higher binding affinity between LS and C3G at pH 3 (2.27×10^5 M^{-1}) compared to pH 1 (1.04×10^5 M^{-1}), and pH 4 (6.58×10^4 M^{-1}). When the number of functional groups in LS (n) available to interact with C3G was included in the mathematical model to calculate the true values of the association constant (K_a), the same trend in values and magnitude difference was found for all three pH values (Appendix 3, Table 3C). This means that, for pH 1, there is a greater fraction of flavylium cation and a smaller amount of ionizable sulfonate groups, while for pH 3, although there is a larger amount of negative groups in the lignosulfonate structure, the molar fraction of flavylium cation is smaller. However, the results show a shift in the equilibrium towards the formation of the flavylium cation at this pH, enhancing the red color of the anthocyanins.

Experiments over time demonstrated that at pH 1 the complex forms immediately after LS addition and remains stable since the C3G is only in the chemical form of flavylium cation which interacts with LS. At pH 3, the formation of a stable LS-C3G complex is achieved after 40 minutes, and in the first 30 minutes, it was observed a decrease in the absorbance (≈ 8 %) until it stabilizes (Appendix 3, Figure 3I); this behavior was associated with the presence of different C3G species in solutions that can interact with LS taking longer time to reach equilibrium.

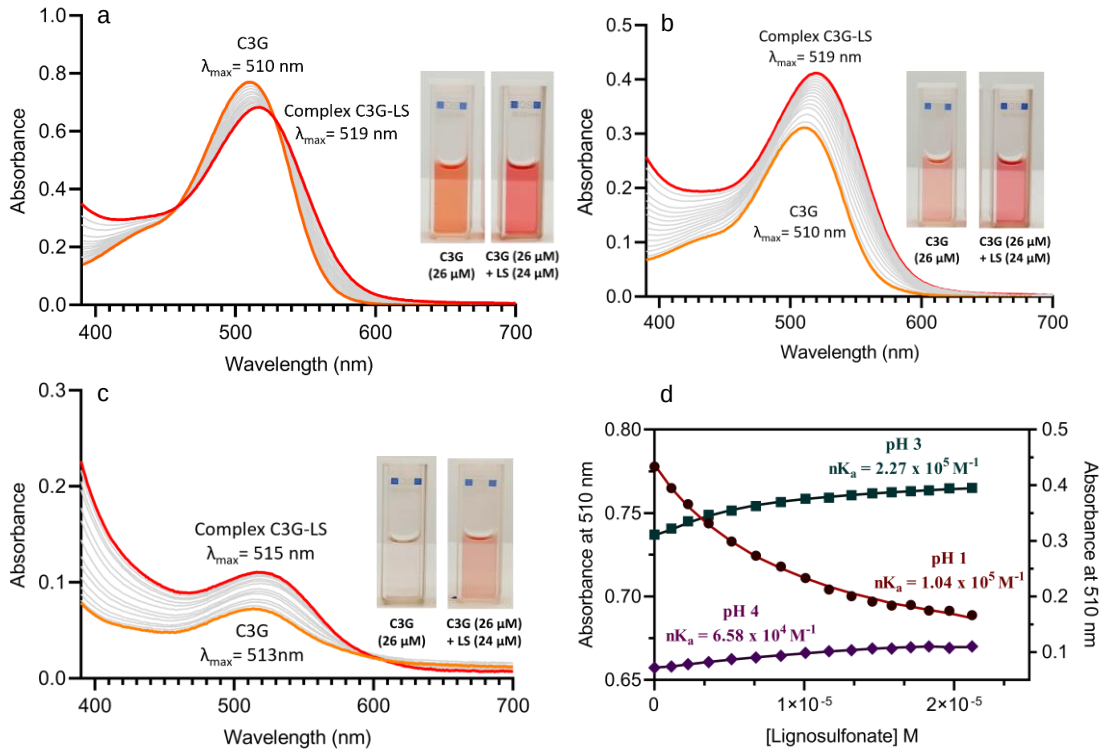

Figure 31 - Absorption spectra of free C3G (26 µM, orange line) with successive increases in LS concentrations (gray lines) until a maximum concentration of 24 µM (red line) at acidic conditions including pH 1 (a), pH 3 (b) and pH 4 (c). The apparent association constants (nK_a) are determined by fitting the results of the graphic representation of absorbance at 510 nm as a function of LS concentration (d).

3.3.3. OXIDATIVE PROTECTION OF C3G THROUGH VOLTAMMETRIC RESPONSE

The stability of anthocyanins can be compromised in aerobic conditions because these compounds undergo oxidation processes, resulting in the formation of colorless or brown degradation products that reduce the intensity and change the hue of the pigment (7). Electrochemical studies were conducted to elucidate the redox behavior and interfacial properties of the LS-C3G interactions, providing insights into the mechanism and kinetics of their electrochemical interaction. Square wave voltammetry (SWV) was employed to study the redox behavior of C3G and LS and evaluate possible changes induced by their interaction. SWVs were recorded at pH 1.0 (0.1 M HCl) and 3.0 (10 mM citrate buffer) in solutions containing: i) only LS; ii) only C3G; iii) C3G with increasing concentrations of LS.

As represented in Figure 32, both LS and C3G showed oxidative processes during the anodic scan (either at pH 1 or pH 3), meaning that they can be oxidized at the

working electrode (WE). Due to their polyphenolic nature, LS can be readily (electro)chemically oxidized. The main electroactive subunit is a substituted phenylpropane (C9) group, where methoxyphenol moieties undergo irreversible oxidation to form quinones (Appendix 3, Scheme 3A) (328, 329) .C3G has two oxidizable centers, the catechol group on ring B being more easily oxidized than the resorcinol group on ring A (330). Consequently, the observed oxidation peak at E = 610 mV (at pH 1) corresponds to the oxidation of the catechol moiety, 3',4',-dihydroxyl groups at ring B to the corresponding o-quinone (331). At pH 3, a second redox process is observable as a shoulder at more positive potentials (around 650 mV), probably involving the opening of the C-ring of the hemiketal form, as previously reported by other authors (332).

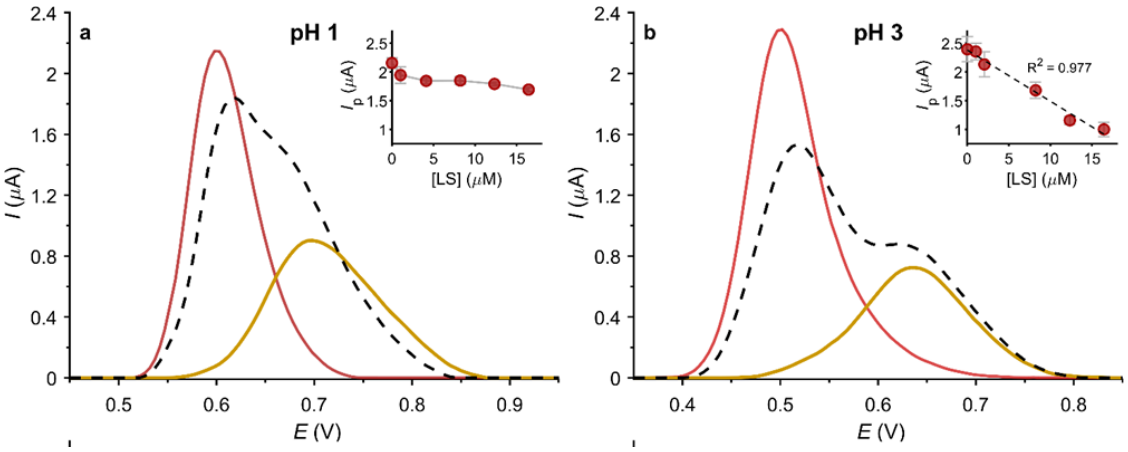

Figure 32 - SWVs of 20 μM C3G (red trace), 8.2 μM LS (yellow trace), and the mixture of the two recorded at pH 1 (a) and pH 3 (b). Insets: Decrease of C3G anodic peak current with increasing concentrations of LS.

The effect of C3G and LS concentrations on their voltammetric response was traced from 2–100 μM and 1 – 20.5 μM, respectively (Appendix 3, Figure 3J). A negative deviation of the anodic peak current response occurred at high concentrations (insets in Appendix 3, Figure 3J). At pH 3, this effect was also coupled with a positive shift of the peak potential. At both pHs, LS showed a wider and less intense peak compared to C3G, indicating that electron exchange involves an extensive range of oxidizable moieties with a wide distribution of overlapping redox potentials. On the other side, C3G showed higher anodic currents and a lower peak potential, suggesting that it is more prone to oxidation compared to LS (333). The formation of a poorly electroactive film on the electrode surface occurred for both LS and C3G and was confirmed by the decrease of the anodic

currents with consecutive scans (data not shown), demonstrating the importance of the WE cleaning procedure.

SWV was also used to evaluate the reaction and complex formation in the system. The formation of a complex with LS caused a decrease in the anodic peak current of C3G coupled with a positive shift of the peak potential of ca. 10 mV (Figure 32). At pH 1 the presence of LS caused a decrease in the C3G peak current (Ip, - 21.5 % at the highest LS concentration), without any clear correlation pattern. On the other side, at pH 3 the Ip decreased linearly with LS concentration (R^2 = 0.977) up to -58.2 % at the highest LS concentration. This suggests that, at pH 3, LS enhances C3G stability by protecting its oxidizable moieties. Results of LS voltammetric titration by increasing concentrations of C3G (Appendix 3, Figure 3K) confirm that the interaction mechanism is pH-dependent. The electrochemical stability of the lignosulfonate-cyanidin complex was also investigated for one hour, showing no modification of successive voltammograms (Appendix 3, Figure 3L). These results corroborated the formation of a stable complex that protects C3G oxidative stability under standard conditions.

4. CONCLUSIONS

This work demonstrated that the formation of the LS-C3G complex occurs spontaneously and is dependent on pH. At pH 1, the complex forms mainly through electrostatic interactions and hydrogen bonds, while at pH 3, hydrophobic effects coupled with electrostatic interactions are the primary driving forces. The interaction with LS significantly improves two key physicochemical properties of C3G: color and antioxidant capacity. A bathochromic shift in the maximum absorption wavelength, accompanied by a significant increase in absorbance intensity at pH 3 and 4, enhances the red color. Additionally, the formation of the LS-C3G complex, particularly at pH 3, reduces the oxidative degradation of C3G, which is a major limiting factor in the application of ACNs. Improving anthocyanin stability is critical for their use in textiles, cosmetics, and food products. However, it is essential to consider the practical challenges required in scaling up the use of the LS-C3G complex in industrial processes. Lignosulfonates, as by-products of the paper industry, offer a cost-effective and sustainable solution. On the other hand, factors such as structural heterogeneity, variable reactive group content, impurities, and the presence of sulfur must be considered when using this type of lignin in real-world applications. In cosmetics, lignin is commonly used as a natural antioxidant and UV stabilizer, with a safety profile supported by its non-toxic and biodegradable properties. Regulatory approval in cosmetics is often more flexible, requiring proof of non-irritation and stability. However, in food applications, lignin faces stricter regulatory challenges due to its interaction with ingestible products. Food-grade lignin must undergo rigorous safety evaluations, including toxicity tests, allergenicity assessments, and compliance with food safety standards set by agencies such as the FDA or EFSA. While lignin holds promise for both industries, its use in food is subject to more stringent oversight to ensure consumer safety.

CHAPTER III

CHEMICAL PROPERTIES AND STABILITY PROFILES OF ACYLATED AND GLYCOSYLATED ANTHOCYANINS

Chapter III of the current Ph.D. dissertation is organized into two parts.

Part A: Exploring the potential of acylated anthocyanin-based extracts as natural colorants for the food industry.

This section delves into the challenging field of anthocyanin-based extracts, focusing on their color stability under various conditions, including pH, temperature, and the presence of bisulfite. By analyzing these physicochemical parameters, a clear activity-structure relationship was established. The anthocyanin-based extracts were subsequently applied in developing food formulations, emphasizing their potential as natural colorants in the food industry.

Part B: Degradation pathways of Malvidin mono- and di-glycoside: Insights into pH-dependent reactivity and product formation.

This study investigated the degradation mechanisms of mono- and di-glycosylated anthocyanins under neutral to slightly basic conditions. This research highlights the crucial role of glycosylation in anthocyanin stability, offering deeper insights that could influence future applications and preservation strategies. The investigation was conducted in collaboration with Professor Fernando Pina's group from the Nova School of Science and Technology of Lisbon (FCT NOVA).

PART A

EXPLORING THE POTENTIAL OF ACYLATED ANTHOCYANIN-BASED EXTRACTS AS NATURAL COLORANTS FOR THE FOOD INDUSTRY

SYNOPSIS

This work explores the potential of three anthocyanin-based extracts (hibiscus calyxes – HC, red cabbage – RC, and butterfly pea flower - BPF) as natural alternatives to synthetic dyes used in the food industry. As a proof of concept, these extracts were obtained from fresh raw materials; however, they could be extracted from by-products of the food supply chain. LC-MS analysis revealed different acylation patterns in the extracts where non-acylated anthocyanins are present in HC, mono- and diacylated in RC, and polyacylated anthocyanins for BPF. Anthocyanin content in extracts ranged from 5 % in HC to 15 % in BPF. Analyses in a pH range for food applications (pH 2–7) revealed higher color stability for the BPF extract across pH values, keeping vibrant colors over the 7-day at room temperature. At pH 3 and 100 ºC, the BPF extract behaved more stable, suggesting a loss of half of the initial concentration of anthocyanins after 14 hours, while RC and HC occurred after 7 and 2 hours, respectively. The bisulfite bleaching followed a second-order reaction for HC (K_1= 1.75x10^{-2} and K_2= 3.94 x 10^{-2}) and RC (K_1= 8.32x10^{-2} and K_2= 2.84x10^{-3}), and a first-order reaction for BPF (K= 2.39x10^{-2}), suggesting a minor effect of the bisulfite on the BPF discoloration. The results revealed a correlation between chromatic stability and the complexity of the chemical structure of anthocyanin, with BPF > RC > HC. Incorporating these extracts into porcine protein gelatins and agar-agar formulations produced consistent products with appealing hues, particularly the blue and purple colors of BPF and RC. The extracts' chemical composition, food safety, and antioxidant activity were also assessed.

This part A was adapted from the paper: ***Pereira, A.R.****; Fernandes, V. C.; Delerue-Matos, C.; de Freitas, V.; Mateus, N.; Oliveira, J.; Exploring Acylated Anthocyanin-Based Extracts as a Natural Alternative to Synthetic Food Dyes: Stability and Application Insights. Manuscript accepted in the Food Chemistry.*

The author conducted the experimental design and work detailed in this part A, except for contaminant determination performed by Dr. Virginia Fernandes from ISEP - Porto School of Engineering.

1. INTRODUCTION

Organoleptic properties are an important sensory component of foods that influences their commercial success. Consumers frequently use color as an indicator of food product attributes including flavor, safety, and nutritional content (334). Not long ago, synthetic dyes (*e.g.,* azo dyes) dominated the large majority of industries, as they allowed the production of countless colorful products at low costs and conferred on them a brighter appearance, and more vivid colors, making the products more desirable. However, due to health issues related to synthetic dyes (335, 336), these colorants are being replaced by natural dyes. Nowadays, consumers are more conscious about the ingredients in their food and beverages, favoring natural alternatives over artificial additives. Consequently, the global market for natural extracts was valued at eleven billion in 2021 and is expected to grow at an annual rate of 9.2 % through 2030 (337). Significant technological advancements have led to a diverse range of natural colorants that enhance quality, stability, and color, enabling the industry to shift towards healthier options. However, challenges remain in maintaining product consistency and achieving vibrant shades in the complex world of natural dyes. In addition, the assessment of contaminants (e.g., pesticides, plastics additives, persistent organic pollutants) in natural product extracts become paramount due to their origin, amplifying the necessity to ensure their purity and safety for use in the food industry, safeguarding consumer health and upholding product quality standards (338).

Anthocyanins are the most important group of natural water-soluble pigments, responsible for the vibrant red, purple, and blue colors observed in fruits, vegetables, flowers, leaves, roots, etc. Additionally as previously mentioned, anthocyanins present minimal to no toxicity and several health benefits have been described in the literature including antioxidant and anti-inflammatory, anticancer, antimicrobial, and anti-obesity properties, as well as prevention of cardiovascular diseases (339, 340). Although anthocyanins can be used as an alternative to synthetic dyes, their color is particularly sensitive to different physicochemical parameters such as pH, temperature, oxygen, and light. Consequently, they present low chromatic stability under several processing, formulation, and storage conditions. They may be involved in several chemical and enzymatic reactions that degrade into colorless products or alter their structure (50). Apart from water, other nucleophiles can cause color loss in commercial food processing, including bisulfite (a common food preservative) and hydrogen peroxide which can be generated during the autoxidation of oxygen-sensitive molecules (341). One of the current challenges in food science is to find innovative approaches that efficiently

mitigate anthocyanin losses and manage anthocyanin reactions to generate more stable and attractive colors. It has been reported that increasing anthocyanin structural complexity through acylation yields more bluish hues and higher color stability due to intramolecular copigmentation and self-association (40). Intramolecular copigmentation is achieved by the arrangement of aromatic acyl units of acylated anthocyanin with the anthocyanidin core structure driven primarily through van der Waals forces and hydrophobic effects (75). The stacking of acyl groups with the pyrylium ring of the flavylium cation protects the chromophores from nucleophilic attack by water, preventing the formation of chalcone or pseudo-base. The acid-base equilibrium shifts to the presence of the blue-colored quinoidal base form, inducing a bathochromic shift (40). Acylated anthocyanins occur naturally in many vegetables and edible flowers, but they can also be obtained by chemical and enzymatic acylation in vitro (342).

Considering the increase in anthocyanin stability and the demand for natural colorants, this work proposes the preparation of three models of anthocyanin-based extracts (HC, RC, and BPF) with different acylation patterns and evaluate their performance as natural alternative colorants for the food industry. Color stability at several pH values (pH 2 − 7) and temperatures (60 and 100 ºC), along with the influence of sodium bisulfite bleaching, were studied over time and related to the anthocyanin structures in each extract. These anthocyanin-based extracts were incorporated into porcine protein gelatin and agar-agar formulations to show their potential as natural colorants evaluating the colors and compared to synthetic blue dye. The chemical composition was also estimated to fully characterize the extracts and correlate with their color and stability.

2. MATERIAL AND METHODS

2.1. REAGENTS

A universal buffer of Theorell and Stenhagen (343) used in the aqueous solution preparation at different pH values was achieved by dissolving 2.25 mL of phosphoric acid 85 % (w/w), 7.00 g of monohydrated citric acid, 3.54 g of boric acid, and 343 mL of a 1 M NaOH solution in Millipore water until 1 L (ionic strength of 0.7263 M).

2.2. PLANT MATERIAL AND EXTRACTION PROCEDURE

Three edible sources containing anthocyanins with different acylation patterns were used in this work. Fresh red cabbage (*Brassica oleracea var. capitata f. rubra*) was purchased from a local grocery store in Porto, and cut by mechanical means to reduce particle size, freeze-dried, and stored at -20 ºC until the extraction procedure. Butterfly pea flower (*Clitoria ternatea*) was acquired from Lamuntea (amazon.es) as dry flowers and Hibiscus calyxes (*Hibiscus sabdariffa*) were purchased as dry flowers from a local supermarket in Porto, Portugal. Since the flowers were small, mechanical disruption of the tissues was not performed. The preparation of the natural extracts was conducted via conventional infusion extraction (1:20, w/v) by adding boiled water (≈ 80 ºC) to the dried plant material, which quickly decreased to 50 ºC, 40 ºC and 35 ºC after 10, 20, and 30 min, respectively, eventually stabilizing. The extraction time was estimated until the total loss of color of the raw material was visible (approximately 1 hour). The pH of red cabbage and butterfly pea flower was between 5 – 6, whereas hibiscus calyxes had a more acidic pH (3 – 4) demonstrating that certain fruits and flowers provide some acidic environment. The resulting solutions were then filtered using a glass fiber filter, concentrated by rotary evaporation under vacuum, and freeze-dried to produce the HC, RC, and BPF extracts.

2.3. IDENTIFICATION OF PHENOLIC COMPOUNDS BY HIGH-PERFORMANCE LIQUID CHROMATOGRAPHY-MASS SPECTROMETRY ANALYSIS

For the identification of anthocyanins and other phenolic compounds, the extracts of HC, RC, and BPF were prepared at 1 g/L in Milli-Q water and filtered using a 0.45 µm syringe filter (Chromafil PET - 45/25). The chromatographic profile of a commercial dye (Rojo BLC-12) purchased from Coralim (Spain) was also evaluated at a concentration of 10 g/L in Milli-Q water. The samples were analyzed by liquid chromatography coupled with mass spectrometry (LC-DAD/ESI-MS) using a Finnigan Surveyor series liquid chromatography, equipped with a reversed-phase C18 column (Agilent) with 250 × 4.6 mm i.d., 2.7 µm at 25 °C. Mass detection was carried out in a Finnigan LCQ DECA XP MAX (Finnigan Corp., San José, CA, USA) quadrupole ion trap mass detector with an API (Atmospheric Pressure Ionization) source of ionization and an ESI (ElectroSpray Ionization) interface. Spectra were recorded in the positive ion mode between m/z 300 and 2000. The solvents used in the elution process were HCOOH/H_2O

(1/99, v/v) and HCOOH/CH_3CN/H_2O (1/30/69, v/v/v) (344). The elution gradient was performed from 35 to 80 % B for 65 min at a flow rate of 0.4 mL/min. After 66 min, the column was washed with 100 % B for 10 min and then, it stabilized with the initial condition for 10 min. The quantification was performed by HPLC-DAD using the same conditions described in the mass spectrometry analysis. The results were determined using the majority anthocyanin standard isolated from the respective extract by preparative HPLC and expressed in g per 100 g of dry weight using the external standard method (Calibration curve for HC: Area = 979.86 [Anthocyanin mg/mL] – 29.925, R^2=0.9992; Calibration curve for RC: Area = 1992.4 [Anthocyanin mg/mL] – 2.9058, R^2=0.9987; Calibration curve for BPF: Area = 374.08 [Anthocyanin mg/mL] + 8.633, R^2=0.9964). Non-anthocyanin phenolic compounds in HC, RC, and BPF extract were also quantified by HPLC-DAD using the kaempferol-3-glucoside as an external standard.

2.4. DETERMINATION OF CHEMICAL COMPOSITION

Since the chemical composition can influence the performance of the anthocyanin-based extracts, the content of different macronutrients, namely, protein, lipids, free sugars, and polysaccharides was determined using specific methods. Although these extracts were purchased at a grocery store, the presence of possible contaminants was determined to ensure food safety when applied in food applications. Details about the methods are reported in Appendix 4 (Section I).

2.5. CHROMATIC STABILITY AT DIFFERENT pH VALUES

The chromatic stability of each anthocyanin-based extract (HC, RC, and BPF) was evaluated in aqueous solutions at different pH values by UV-visible spectroscopy (Cary 60 - Agilent). For that, 500 µL of universal buffer at each pH value ranging between 2 – 7, 500 µL of NaOH 0.1 M, and 500 µL of each extract prepared in 0.1 M HCl were added to plastic cells (10 x 10 mm). The spectrum of each solution was recorded between 250-800 nm along with the CIELAB color coordinates every day for 7 days using the Agilent Color software (Cary WinUV Color software from Agilent). Parameters such as illuminant (CIE D65) and observer angle (10 degrees) were considered for the experiments. The solutions were kept at room temperature (≈ 20 ºC) and protected from light during the study. pH values of the solutions were checked at the beginning and end of the experience in a WTW pH 320 or 508 (Weilheim, Germany) with a CRISON 5209 combined glass electrode of 3 mm diameter (Barcelona, Spain), previously calibrated

with buffer solutions (pH 4, 7, and 10). The pH tested was close to the desired values, allowing a variation of ± 0.2 units.

2.6. EVALUATION OF THERMOSTABILITY OF THE ANTHOCYANIN-BASED EXTRACTS

To determine the thermostability, the extracts (1 g/L) were dissolved in 10 mM citrate buffer at pH 3 in a glass vial with a sealed screw cap and placed in a bath at 100 ºC for approximately 5 hours. The same experiment was also performed at 60 ºC to compare the temperature effect on the degradation rate. Over time, some aliquots were collected, which were immediately placed in an ice bath for 1 min to stop the degradation, and then the absorbance was recorded by UV-Vis spectrophotometry. The spectrum was recorded at room temperature from 200 to 700 nm using a plastic cell cuvette with 1 cm of optical path. Considering that the predominant phenomenon is color degradation, and the degradation kinetic studies of anthocyanins typically follow a first-order reaction (345) it was determined the first-order reaction rate constants (k) and the time needed for 50 % degradation of anthocyanins denominated as the half-life time ($t_{1/2}$) using the equations:

$\ln\left(\frac{A}{A_0}\right) = -kt$ and $t_{1/2} = \frac{-\ln 0.5}{k}$, where A is the absorbance after treatment in a certain time (t), A_0 is the initial absorbance, k is the kinetic constant and $t_{1/2}$ is the half-life time. The results were compared to an anthocyanin-rich commercial dye (Rojo BLC-12 from Coralim, Spain) prepared in the same conditions.

2.7. BISULFITE (SO_2) BLEACHING ASSAY

The bleaching action by SO_2 was evaluated by UV-vis spectroscopy. Different aliquots of a sodium metabisulfite solution between 0 and 1.05 x 10^{-3} M were added to a stock solution of anthocyanin extracts prepared at 1 g/L using the universal buffer of Theorell and Stenhagen at pH 2. The absorbance spectrum from 300 to 700 nm was recorded immediately after adding the bisulfite solution using a 1 cm path-length cell. The bleaching constant (K_{SO2}) was determined by calculating the fitting of the color intensity curve of absorbance (at λ_{max}) as a function of SO_2 concentration.

2.8. PREPARATION OF FOOD MATRICES

The anthocyanin-based extracts (HC, RC, and BPF) obtained in this work were used to prepare food formulations with both animal-based gelatin (porcine protein from Vahine) and plant-based (agar-agar from Mix) gelling agent. Each natural extract was prepared in hot potable water at 10 g/L and then diluted to final concentrations of 1 g/L, 3 g/L, or 5 g/L when mixed with the gelatin preparations. Both gelatin matrices, without the addition of extracts, were prepared at a concentration of 12.5 g/L in a final volume of 16 mL for each extract and concentration. The preparation process was as follows: 1) weigh approximately 200 mg of gelatin powder into multiple containers; 2) add 8 mL of cold water to each container to facilitate the complete dissolution of the gelatin powder, and 3) add the remaining amount of hot water (8 mL) comprising the natural extract to each container. For the animal-based gelatin, the mixture was placed in the refrigerator to jellify since for the plant-based gelling agent, the mixture was boiled for 2 minutes before being placed in the fridge to jellify. The pH of gelatin formulations was also confirmed by a previously calibrated CRISON 5209 combined glass electrode of 3 mm diameter (Barcelona, Spain). Another experiment was carried out for the RC and BPF extracts, adjusting the pH values of the gelatin preparations with 10 mM citrate buffer to values between 5 and 5.5 and registering the CIELAB coordinates.

2.9. DETERMINATION OF ANTIOXIDANT ACTIVITY

Standard DPPH assay was performed according to the literature (346). In a 96-well plate, 270 µL of DPPH solution (prepared in methanol at 60 µM) was mixed with 30 µL of the antioxidant sample. For each extract, a range of concentrations was tested, and the radical scavenging reaction was monitored over time by measuring the DPPH absorbance band at 517 nm (λ_{max}) on a plate reader (Biotek Powerwave XS) at the beginning (t_0) and after 30 min of reaction (t_{30}). IC_{50} values of test/reference compounds are represented as half of the maximum inhibitory concentration of DPPH radical scavenging activity. The antioxidant activity was expressed as the radical scavenging activity (RSA) by calculating the fitting peak area at 517 nm, using the following equation: $RSA\ (\%) = \frac{Abs\ control - Abs\ sample}{Abs\ control} \times 100$, where Abs control and Abs sample is the absorbance of the control at t = 0 min and the tested sample at different incubation times, respectively.

2.10. STATISTICAL ANALYSIS

The experiments were performed in triplicates and the final results were expressed as mean values and standard deviation (SD). All statistical data were processed using GraphPad Prism 8.0 for Windows.

3. RESULTS AND DISCUSSION

3.1. CHEMICAL COMPOSITION OF THE EXTRACTS

3.1.1. IDENTIFICATION OF PHENOLIC COMPOUNDS BY LC/DAD/MS

The profile of phenolic compounds of each extract was established using HPLC-DAD coupled with mass spectrometry. The identity of phenolic compounds was made using the ion mass, the respective fragmentation patterns, the UV-visible spectra, and a comparison with data already reported in the literature. The respective chromatographic profiles are presented in Appendix 4 (Figures 4A, 4B, and 4C). The extract from HC mainly comprises non-acylated anthocyanins, namely disaccharides (Figure 33 A), including delphinidin-3-sambubioside and cyanidin-3-sambubioside (347, 348). The typical fragmentation pattern in these anthocyanins involves the loss of the sugar moiety with the ion mass corresponding to the anthocyanidin moieties (*m/z* at 303 and 287) being detected in the MS^2 spectra. Other phenolic compounds, namely quercetin derivatives, were also detected in this natural extract (Appendix 4, Table 4A). Given its non-acylated nature, HC was chosen as a control to evaluate and compare the effect of acylation on anthocyanin stability as a natural colorant. Furthermore, cyanidin and delphinidin nuclei are present in the acylated extracts of red cabbage and butterfly pea flower, respectively.

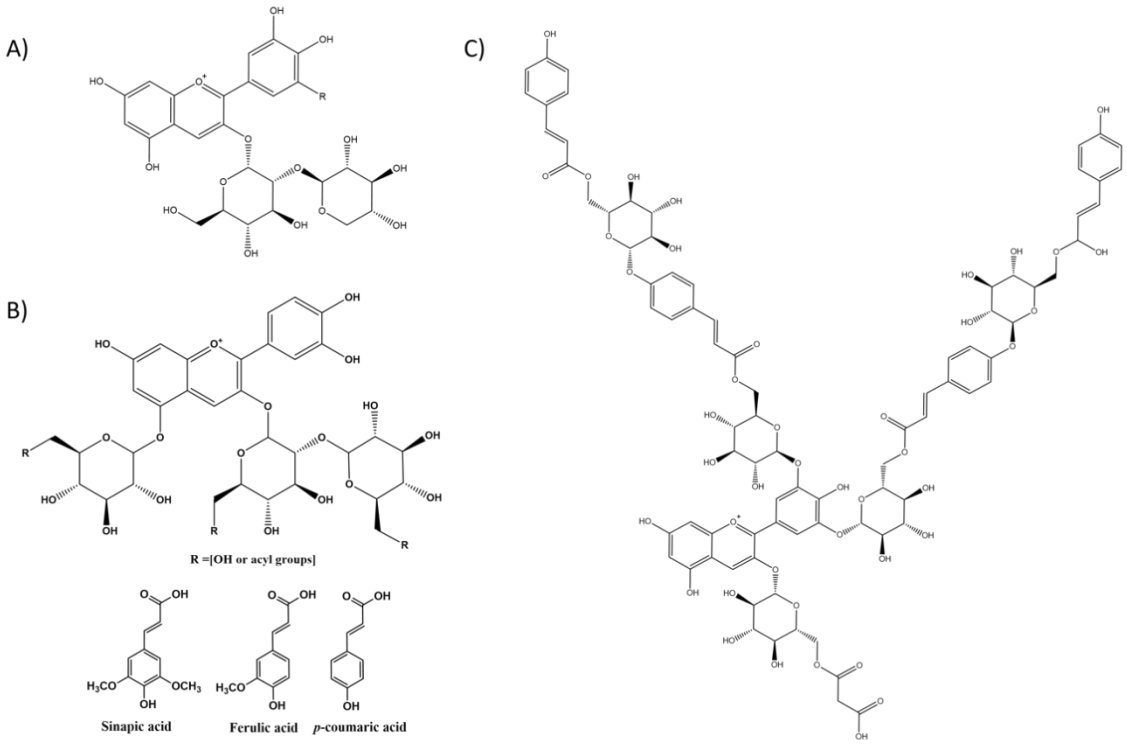

Figure 33 - (A) Core structure of anthocyanins found in HC extract; R= OH, delphinidin-3-sambubioside or R=H, cyanidin-3-sambubioside; (B) Basic nucleus of anthocyanins detected in RC extract (cyanidin-3-diglucoside-5-glucoside) that can be acylated in different OH positions of glucose units (R) by sinapic, ferulic and p-coumaric acids; (C) Ternatin D1, one of the main polyacylated anthocyanin identified in the BPF extract.

Concerning the RC extract, fourteen anthocyanins were identified by comparing the UV-visible spectra and MS/MS fragmentation pattern with data reported in the literature (349, 350). Cyanidin-3-diglucoside-5-glucoside is the basic nucleus of the anthocyanins present in RC, displaying several acylation patterns (non-, mono-, and diacylated) with phenolic acids such as sinapic, ferulic, and *p*-coumaric acids (Figure 33 B). The nonacylated anthocyanin presents a molecular ion $[M]^+$ at 773 and a fragment at *m/z* 287 corresponding to the cyanidin moiety and the fragments agree with the loss of three glucose units (Appendix 4, Table 4A). The presence of six monoacylated anthocyanins with acyl groups attached to the diglucosides and triglucosides of cyanidin present at the hydroxyl group in carbon 3 was also detected. The characteristic fragmentation pattern includes the loss of the glucose moiety (162 a.m.u.), ferulate (176 a.m.u.), sinapoyl (206 a.m.u.), and *p*-coumaroyl unit (146 a.m.u.). Two isomers of the monoacylated cyanidin-3-diglucoside-5-glucoside bearing the sinapoyl moiety in different sugars (*m/z* 979), cyanidin-3-(sinapoyl)-diglucoside-5-glucoside and cyanidin-3-diglucoside-5-(sinapoyl)-glucoside were detected in RC. Furthermore, it was identified seven diacylated anthocyanins resulted from the combination of two phenolic acids with triglucoside and

diglucoside of cyanidin. Other non-anthocyanin compound derivatives from these phenolic acids were detected in the RC extract (Appendix 4, Table 4A). The LC-MS analysis of the BPF extract showed the presence of more complex anthocyanins, namely polyacylated anthocyanins denominated ternatins. Terahara and co-workers (351, 352) isolated from mature flowers nine ternatins (A1, A2, A3, B1, B2, B3, B4, D1, and D2) and showed that the chemical structure of these compounds is based on a malonylated delphinidin 3,3‘,5‘-triglucoside having a series of 3‘,5‘-side chains with alternating D-glucose (G) and *p*-coumaric acid (C) units (Figure 33 C). Ternatins C (C1-C5) had no *p*-coumaroyl residue(s) on one (5‘-) side chain (353). The identified compounds present in the extract prepared from BPF are summarized in Appendix 4 (Table 4A). A total of eleven ternatins were identified and the fragmentation patterns are given by the loss of glucose units (162 a.m.u.), which can reach a loss of up to 4 units in the case of ternatins B2 and B3. The loss of glucose can occur along with fragments of coumarate and malonate, which can also occur individually as is the case of the first fragmentation of ternatins C2 and D3. Other phenolic compounds were also identified and should correspond to the quercetin 3-(2G-rhamnosylrutinoside) and kaempferol derivatives due to the typical fragments at m/z 594 correspondent to the $[M\text{-rhamnosyl}]^+$ and m/z 448 for $[M\text{-2rhamnosyl}]^+$, and also considering the main fragment with m/z 287 which correspond to kaempferol. The maximum absorption wavelength at circa 350 nm is also in agreement with the typical absorption of flavonols.

The concentration of anthocyanins in HC, RC, and BPF extracts was expressed in terms of g per 100 g of dry extract, corresponding to 6.6 ± 0.6 %, 5.1 ± 0.8 %, and 14.9 ± 1.6 %, respectively. Delphinidin-3-sambubioside, cyanidin-3-diglucoside-5-glucoside, and ternatin D1 were the external standards for the quantification of anthocyanin content in HC, RC, and BPF, respectively.

3.1.2. DETERMINATION OF MACRONUTRIENTS AND FOOD SAFETY

In addition to the anthocyanin content, which is directly related to the objective of this work in producing natural and stable food colorants, the number of other macronutrients that can influence the behavior and colors obtained from the three extracts was determined including proteins, lipids, free-sugar and polysaccharides (Appendix 4, Table 4B). Briefly, BPF extract presented the highest protein content (1.35 ± 0.02 g BSA eq./ 100 g extract) when compared to HC (0.20 ± 0.08 g BSA eq./ 100 g extract) and RC (0.15 ± 0.04 g BSA eq./ 100 g extract). HC, RC, and BPF showed lipid contents of 0.64

± 0.05, 0.41 ± 0.04, and 0.31 ± 0.04 g palmitic acid/ 100 g extract, respectively. RC extract showed the highest content of free sugar (0.22 ±0.03 g glucose/ 100 g extract), with values 4−5 times higher than BPF and HC extracts, and also the highest total carbohydrate content (67 %) when compared with 24 % of BPF and 18 % of HC.

The screening of 38 contaminants showed that none of the three extracts present pesticides, BDE (Brominated Diphenyl Ethers), and PCB (Polychlorinated Biphenyl) in their composition by comparison with a standard solution of a mixture with the halogenated compounds (organochlorine and pyrethroid pesticides, PCB and BDE) and organophosphorus pesticides (Appendix 4, Figure 4D).

3.2. UV-VISIBLE SPECTRAL ANALYSIS AND CIELAB COORDINATES

The analysis of the color modifications over time helps to determine the color stability and by this the potential of anthocyanin-based extracts to be used as natural dyes. UV-visible spectra and CIELAB coordinates were recorded at room temperature (20 ºC) over time in the pH range 2-7 and the results are presented in Figure 34.

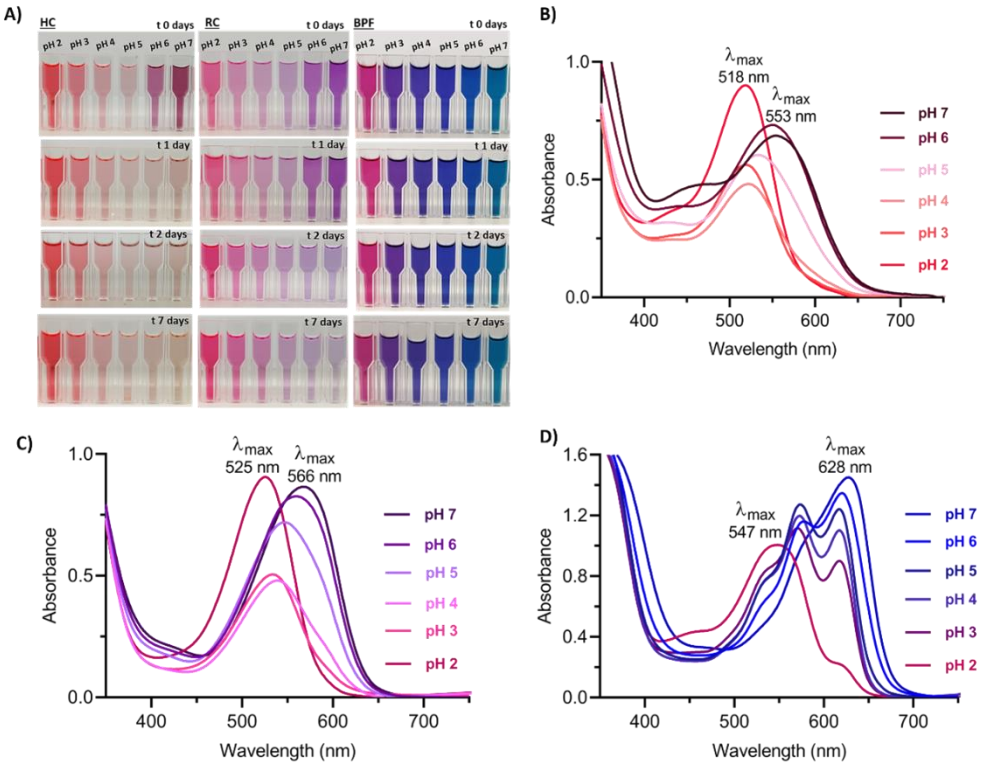

Figure 34 - Aqueous solutions of each anthocyanin-based extract at different pH values (2-7) after preparation (t 0 days) and after 1, 2, and 7 days (t 7 days) (A). UV-visible spectra for B) hibiscus calyxes (HC), C) red cabbage (RC), and D) butterfly pea flower (BPF) extracts in a pH range within different food applications at room temperature. These spectra were recorded immediately after the preparation of each solution.

At acidic conditions (pH 2) all extracts exhibited the a* coordinate related to the red color (Appendix 4, Tables 4C, 4D, and 4E), characteristic of the flavylium cation form, as seen in Figure 34 A by the reddish-orange and pink colors. The various colors result from the anthocyanin complex acid-base equilibrium which exists in different forms in solution depending on the pH (Figure 3). Concerning the HC extract, the red color present at acidic conditions changes to light pink (presence of non-colored hemiketal form) and then brownish hues (presence of quinoidal and chalcone forms) near neutral conditions (36). RC extract displays a reddish-purple hue in acidic conditions that shifts to a more bluish-purple in neutral conditions. Regarding BPF, this anthocyanin-based extract exhibits a vivid red-purple color at low pH values that shifts into blue-green as pH increases up to neutral pH conditions (Figure 34 A). As observed in UV-visible spectra (Figure 34 B and C), between pH 3 − 5, the absorbance intensity decreases for HC and RC, even at the initial time, resulting in a loss of color of the aqueous solutions and an increase of the lightness (L*). For the less complex anthocyanins, such as the diglycosylated anthocyanins present in HC extract, when the pH increases, the flavylium cation undergoes a hydration process, yielding the hemiketal species (colorless form), which is responsible for the increase in lightness values (about 20 %). The presence of acyl groups in the RC and BPF extracts protects the flavylium cation from water attack due to steric hindrance resulting mainly from intramolecular copigmentation and self-association, reducing the extension of the hydration reaction, and in the case of the BPF extract, inhibiting it (354). The UV-visible spectrum of BPF at pH 3 (Figure 34 D) shows a maximum absorption wavelength at 575 nm and two shoulders at 547 and 628 nm, suggesting the presence of the flavylium cation, the neutral and anionic quinoidal bases at this pH. With the increase of pH, the shoulder corresponding to the flavylium cation (λ_{max} at 547 nm) disappears, and the one at 628 nm increases up to pH 7. At pH 7, the UV-visible spectrum shows a maximum absorption wavelength of 628 nm, suggesting that the anionic quinoidal base is responsible for the intense blue color (Figure 34 A). These results are also supported by the more negative b* coordinate (bluish hues) with increasing pH (Appendix 4, Table 4E). At pH 7, diacylated cyanidin from RC is a mixture of neutral and anionic bases (pKa_2 = 7.0 – 7.3), adopting persistent anionic forms that slow down the water addition (loss of color only after 2 days) (355, 356)

Increasing the pH for neutral conditions, b* coordinate (Appendix 4, Tables 4C and 4D) for HC and RC shifted towards the negative axis, resulting in a light pink and purple color (Figure 34 A), respectively, due to the appearance of the neutral quinoidal base; however, for these extracts, after 4 and 7 days respectively, at pH 5 and 6 the b* values shift towards yellow tones, suggesting the presence of the chalcone form in the chemical

equilibrium. For RC, this happens but due to OH^- attack in the basic medium, although it appears to happen to a lesser extent than HC extract. In general, the ΔE values (Appendix 4, Tables 4C, 4D, and 4E), which allow us to conclude about the perception of color change, were very low ($0 < \Delta E < 2$) for the pH range analyzed, except for pH 6 and 7 in HC and RC extracts where the color change was noticeable to the Human eye with ΔE values > 5 (295).

Comparing the samples for the same pH after 7 days, the glycosylated anthocyanins in the HC extract showed lower stability, resulting in absorbance decreases of 2 % for pH 2, 33 % for pH 3, and 70 – 80 % after 4 days for neutral pH. For RC, the color intensity remains constant, with only a 25 % decrease observed after 4 days at pH 3. At pH 4 and 5, absorbance decreases by 45 % and 50 % after 7 days, while at pH 6 and 7, it decreases by approximately 75 % after 4 days. However, it is crucial to note that for HF and RC extracts between pH 3 and 5, the colors of the initial solution (t 0) are less colored due to the presence of acid-base equilibrium that results in colorless species such as hemiketal (B). For BPF extract over the experiment's duration, the color intensity at pH 3 decreases by around 24 % after 7 days, reaching a maximum reduction of 30 % for pH 3 and 36 % at pH 4 for 7 days, and 45 % for pH 5 and 6 after 4 days. The BPF extract showed much greater chromatic stability over time, since the efficient enhancement of the stability of the anthocyanins resulting from the stacking effect of the aromatic acyl groups with the benzopyrylium ring of the anthocyanin flavylium cation mainly by intramolecular copigmentation and self-association (35).

3.3. THERMOSTABILITY OF ANTHOCYANIN-BASED EXTRACTS

The thermostability of the three anthocyanin-based extracts was studied at pH 3 (citrate buffer) at 100 ºC. These conditions were chosen as they mimic the pH of some food matrices where these extracts can be employed as natural colorants such as beverages. Moreover, the temperature of 100 ºC was considered based on the temperature of the food pasteurization process. The thermal stability over time of the different anthocyanin-based extracts is presented in Figure 35. The linearity observed in the graphical representation of Ln (A/A_0) as a function of time confirms that the degradation of anthocyanin's color follows a first-order reaction and allows the determination of values of the kinetic parameters Table 15.

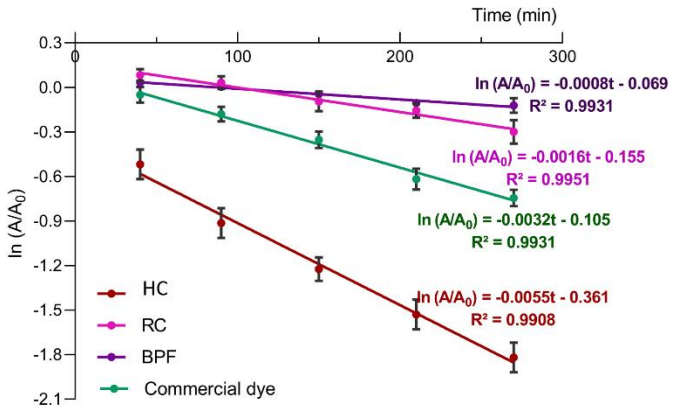

Figure 35 - Thermostability of anthocyanin-based extracts (HC, RC, and BPF) at pH 3 and 100 °C. An anthocyanin-based commercial dye (Rojo BLC-12) was used as a control.

At 100 ºC, the anthocyanin-based extract from BPF showed the highest color stability over time, with a degradation constant of 8 x 10^{-4} min^{-1}. This indicates that half of the initial concentration of anthocyanin is lost after 14 hours at 100 ºC (Table 15). Regarding the RC extract, the rate of color degradation has doubled, which indicates that half of the color is lost after 7 hours. These results suggest that the degree of acylation affects anthocyanin stability since the extract containing polyacylated anthocyanins (BPF) demonstrated the highest stability when compared with RC (mono- and diacylated) and especially with HC (nonacylated) extract. Acylated and polyacylated anthocyanins increase color stability, which proposes a protective effect mainly by intramolecular copigmentation. The water's nucleophilic attack on the anthocyanin molecule, which results in colorless carbinol (hemiketal) and chalcone forms, is thus reduced. Furthermore, compared to the HC extract, RC and BPF extracts present higher levels of carbohydrates and phenolic compounds, respectively, which can influence the chemistry of the anthocyanins due to the intermolecular copigmentation phenomena, protecting anthocyanins from degradation. Quercetin and kaempferol identified in the extracts are examples of copigments used to stabilize the anthocyanins (357). When compared to the commercial dye of black carrot, an extract rich in glycosylated and monoacylated anthocyanins (Appendix 4, Figure 4E), which had a significantly higher degradation rate (k = 3.2 x 10^{-3} min^{-1}) and a color shift after only one hour of temperature treatment, BPF and RC extracts demonstrated better thermal behavior to be incorporated in different food matrices. On the other hand, the extract isolated from HC had the highest rate of degradation (5.5 x 10^{-3} min^{-1}) and after 2 hours of the experiment, there was a loss of 50 % of the initial concentration of anthocyanins. As shown in Table 15, this instability causes color variations ranging from red to yellow.

Table 15 - Color stability of HC, RC, and BPF extracts at pH 3 and 100 ºC. A commercial dye was used as a control.

	Kinetic parameters at 100ºC		Color variation over time (hours)
	Degradation rate constant (k x 10^{-3}, min^{-1})	Half-life time ($t_{1/2}$, min)	T0 T1 T2 T3 T4
HC	5.5 ± 0.8	126.0 ± 0.8	
RC	1.6 ± 0.3	433.2 ± 0.3	
BPF	0.8 ± 0.2	866.4 ± 0.2	
Commercial dye	3.2 ± 0.5	216.6 ± 0.5	

As confirmed by LC-MS data, the HC extract is composed of nonacylated anthocyanins, which undergo hydration at this pH. This suggests that thermal degradation is associated with the hydrated form of anthocyanins, identified to be less stable than flavylium cation. Non-acylated anthocyanins, such as those present in HC extract, degrade via sugar loss, resulting in the formation of aglycones (anthocyanidin), which subsequently breaks into a phenolic acid from ring B and an aldehyde from ring A (358). The aldehyde will be common to the two principal anthocyanins in HC extract: phloroglucinaldehyde; in the case of cyanidin-3-*O*-sambubioside, it will generate protocatechuic acid; in the case of delphinidin-3-*O*-sambubioside, gallic acid. Depending on their chemical structure, anthocyanins can be degraded by oxidation during heat processing (37). To assess the temperature dependence of anthocyanin stability, the same experiment was conducted on the HC extract at 60°C, yielding a degradation rate (k) of 0.5 x 10^{-3} min^{-1} and a half-life ($t_1/_2$) of 23 hours. Detailed information is presented in Table 16, but it was demonstrated that decreasing the temperature from 100 ºC to 60 ºC reduces the degradation rate 11 times, with higher color stability of the aqueous solutions. This tendency agrees with results already reported in the literature for the HC extract (347, 358).

Table 16 - Thermostability of extract isolated for hibiscus calyxes at pH 3 for 270 minutes at 60 °C. Influence of temperature on the kinetic parameters and conception of color change.

	Kinetic parameters for heating at 60ºC for hibiscus extract		Color variation over time (hours)
	Rate constant (k x 10^{-3}, min^{-1})	Half-life time ($t_{1/2}$, min)	T0 T1 T2 T3 T4
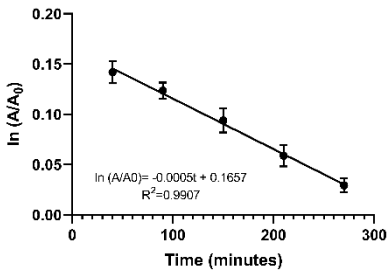	0.5 ± 0.1	1386.3 ± 0.1	

3.4. BISULFITE BLEACHING RESISTANCE

The performance of the three anthocyanin-based extracts in the presence of increasing concentrations of sodium metabisulfite (antioxidant and antibacterial preservative in food matrices) was evaluated. BPF extract demonstrated the highest resistance to the discoloration promoted by the metabisulfite compared to the RC and HC extracts. The UV-vis spectrum (Figure 36) showed a small decrease in the color intensity for BPF extract, around 5 % for 5.26 x 10^{-5} M, and 20 % for the maximum bisulfite concentration (1.05 x 10^{-3} M). Note that, according to EFSA, the maximum levels of sulfites can range from 5.0 x 10^{-5} to 1.0 x 10^{-2} M, depending on the food category (EFSA, 2008). RC and HC solutions became slightly noncolored with decreases circa 15 % and 10 % for 5.26 x 10^{-5} M and 55 % and 65 % for 1.05 x 10^{-3} M, respectively (Figure 36 A and B). In the UV-Vis spectrum of RC, a bathochromic shift was observed with the increase of bisulfite concentration. Furthermore, as well as for the HC, the fitting of the graphic representation of the absorbance at the maximum absorption wavelength as a function of the bisulfite concentration showed to be a second-order reaction while for the BPF it was obtained as a first-order reaction. For each extract, the respective bleaching constants (K_{SO2}) were calculated. The values obtained for the RC were K_1= 8.32 x 10^{-2} and K_2= 2.84 x 10^{-3} and for HC, K_1= 1.75 x 10^{-2} and K_2= 3.94 x 10^{-2}. A rapid flavylium bleaching occurs immediately after the addition of low concentrations of bisulfite (around 1.32 x 10^{-4} M), while for higher concentrations (between 2.64 x 10^{-4} M and 1.05 x 10^{-3} M) the nucleophilic addition to the flavylium cation is slower, especially for the RC in comparison to the HC (lower K_2 for RC). This means that the additional color loss slows down as you continue to increase bisulfite concentration. The BPF extract demonstrated the lower discoloration constant (K= 2.39 x 10^{-2}), verifying a slight effect of the bisulfite for lower nucleophile concentrations and then, a stabilization of the color (plateau) for higher concentrations (between 2.64 x 10^{-4} M and 1.05 x 10^{-3} M). The nucleophilic attack of anionic bisulfite occurs at the positively charged C−2 and preferentially at C−4 of the anthocyanin structure, which is available in all the extracts since the glycosylation and acylation occur in other OH groups (42). However, due to the greater complexity of the structure of the polyacylated anthocyanins that make up the BPF extract, the anthocyanin nucleus is more protected from SO_2 bleaching due to steric hindrance and the occurrence of intramolecular copigmentation (39). Besides that, BPF showed a higher phenolic content (non-anthocyanins) quantified by HPLC-DAD that can interact with the polyacylated anthocyanins by hydrophobic interactions and hydrogen bonding

(intermolecular copigmentation) stabilizing the chemical structure and consequently, the color.

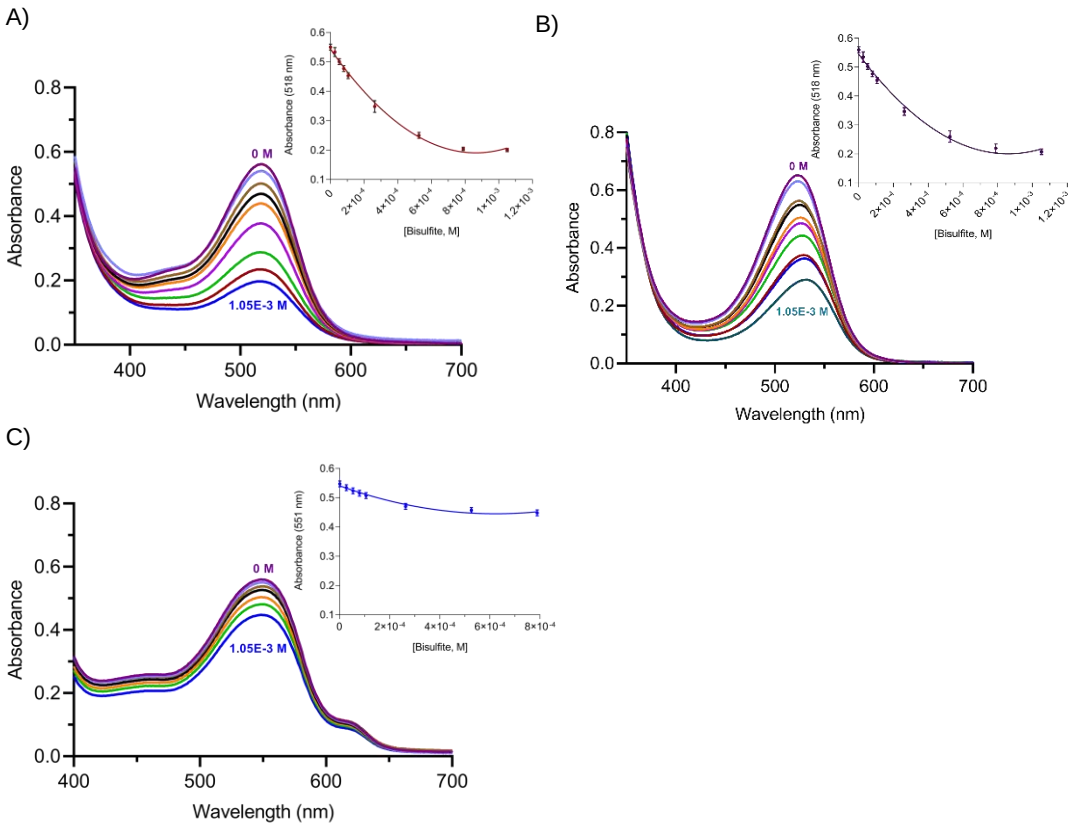

Figure 36 - UV-vis spectra of HC (A), RC (B), and BPF (C) extracts prepared in universal buffer at pH 2.0 with increasing amounts of bisulfite (0 – 1.05x10^{-3} M).

3.5. PREPARATION OF COLORED GELATINS – FOOD APPLICATION

The HC, RC, and BPF extracts obtained in this work were used to prepare colored gelatins to study the behavior of these compounds in animal and plant-based gelatin food matrices and verify the potential of these natural colorants to replace synthetic ones. The results demonstrated that it is possible to obtain consistent products with vibrant colors. The visual distribution of colors related to the gelatins prepared with the various extracts is illustrated in Figure 37 A, obtained by the correlation with the a* and b* CIELAB coordinates. CIELAB coordinates are reported in Appendix 4, Table 4F. The gelatins showed a higher lightness (L* values closer to 100) for lower extract concentrations, resulting in a higher transparency of the formulations. Animal-based gelatins with the same concentration of RC and BPF extracts as plant-based gelling agent showed a higher lightness. About the color coordinates a* and b*, it was observed

that in formulations containing animal-based gelatin, HC and RC extracts showed positive values of a* coordinate (values between 24 and 30 for concentrations of 5 g/L – Appendix 4, Table 4F), indicating a redder hue, which was especially noticeable for the HC extract resulting in their red color. The values for the BPF extract were negative, indicating a greater contribution of the green color to the solutions. The b* coordinate was strongly negative for the animal gelatin with BPF extract, as expected, due to the intense blue color of this formulation. The colors found in plant-based gelling formulations differed significantly from the colors reported in the animal-based gelatin formulations, namely for the RC and BPF extracts. In the case of gelatins made with HC extract, the colors were very similar to animal-based gelatin, although the intensification of the red color and a more positive a* coordinate, especially at a concentration of 5 g/L of extract was observed. In contrast to the purple and blue colors obtained in animal-based gelatin formulations, plant-based gelling formulations produced with RC and BPF extracts showed a bluish-green color. Real images of gelled food formulations are also presented in Figure 37, with animal-based gelatins visible in Figure 37 B and plant-based gelling formulations visible in Figure 37 C.

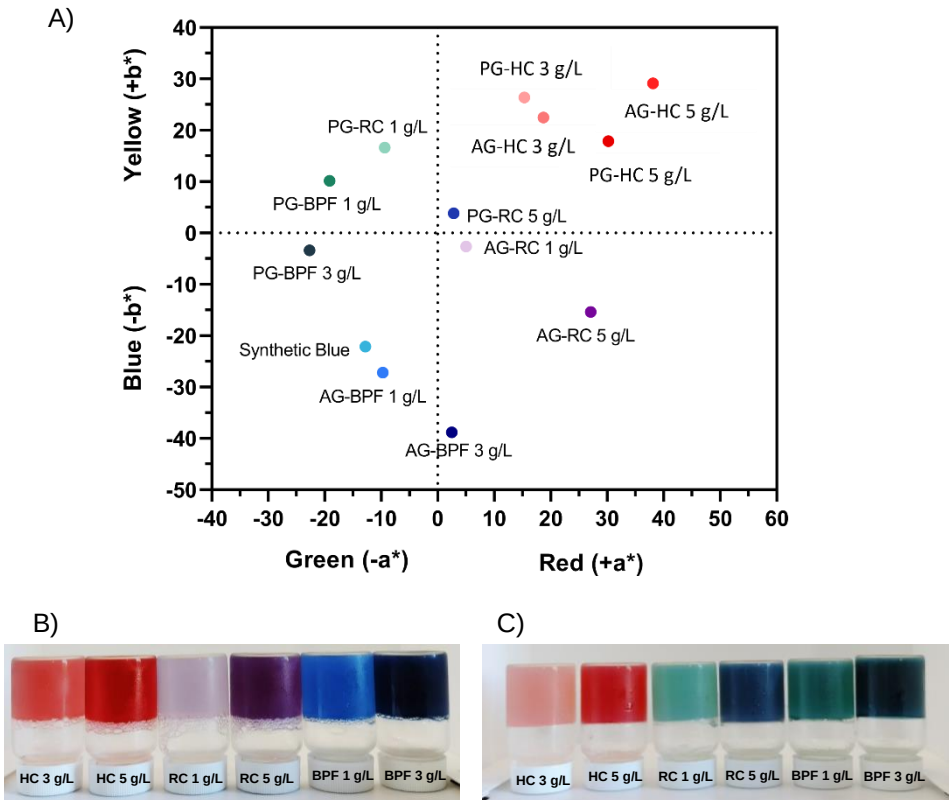

Figure 37 - (A) Graphic distribution of the colors observed in food formulations prepared by mixing gelatin with edible extracts at different concentrations, where AG means animal gelatin and PG plant-based gelling formulations. (B) Gelatins from animal origin and (C) vegetable gelling formulations with the different extracts isolated in this work at two distinct concentrations.

The color differences can be attributed to some factors, including the pH of the extracts. Depending on the extracts, different pH values were obtained for the gelatin food formulation prepared with them. HC extract showed a pH of 3.73 and 3.41 in animal gelatin and 3.35 and 2.79 in plant-based gelling formulations for concentrations of 3 g/L and 5 g/L, respectively. These pH values explain the red hue acquired in both instances, with greater intensity in the case of plant gelling agent at 5 g/L because their negative charges suggest the flavylium cation stabilization responsible for the red color. Gelatin food formulations containing RC extract had a higher pH value of 5.32 and 5.25 for animal-based gelatin, and 7.94 and 6.61 for plant-based gelling formulations for concentrations of 1 g/L and 5 g/L, respectively. The higher pH values in agar-agar formulation may be related to the higher pH reported in this matrix. The purple color found in animal gelatin is associated with the presence of neutral quinoidal bases at these pH values, as demonstrated by the colorimetric features of the extracts (Figure 34). The blue-green hues in agar-agar formulation are due to the anionic quinoidal bases, which occur in neutral - mildly alkaline conditions and are characteristic of the intense blue color. An identical correlation can be established for gelatins containing BPF extract, with animal gelatins having pH values of 5.71 and 5.69, and agar-agar formulations with pH values of 8.06 and 7.21 at the lowest and highest extract concentrations, respectively. In the case of gelatins containing animal protein, the blue color is caused by the presence of anionic quinoidal bases, which appear at lower pH ranges due to greater stabilization of the flavylium cation which inhibits the occurrence of hydration reactions, yielding only proton transfer reactions. The greener color of plant-based gelling formulations suggests the existence of other species in solutions, namely the di-anionic quinoidal bases characteristic of this pH range.

For both cases, RC and BPF extracts, when the pH of the plant-based matrix was adjusted with citrate buffer to values ranging from pH 5 − 6, the colors obtained in the gelatin food formulations were similar to those reported for animal-based gelatins (Figure 38 A − B and E − F). Furthermore, the colors remained unchanged after 5 hours of the experiment (Figure 38 B − D and F − H), suggesting that the different colors are primarily attributed to the matrix pH. Slight color changes mainly in RC extract at 5 g/L are plausible due to the possible effect of the matrix components since animal-based gelatin is mainly composed of porcine protein (359), and plant-based formulation (agar-agar) by polysaccharides (360). CIELAB coordinates also reported some statistically significant differences (Appendix 4, Table 4F) between the colors of animal-based gelatin and plant-based gelling formulations after pH correction for the respective extracts. RC extract and especially the BPF extract (polyacylated anthocyanins) demonstrated the potential for

obtaining more intense colors even at lower concentrations (1 g/L and 3 g/L). Compared to the commercial synthetic blue used in food matrices, also represented in the CIELAB graphic in Figure 37 A, the BPF extract demonstrated a potential to get the blue color with different shades. The biggest challenge for industries is to replace the blue color, which is why this anthocyanin-based extract proved to be a great source.

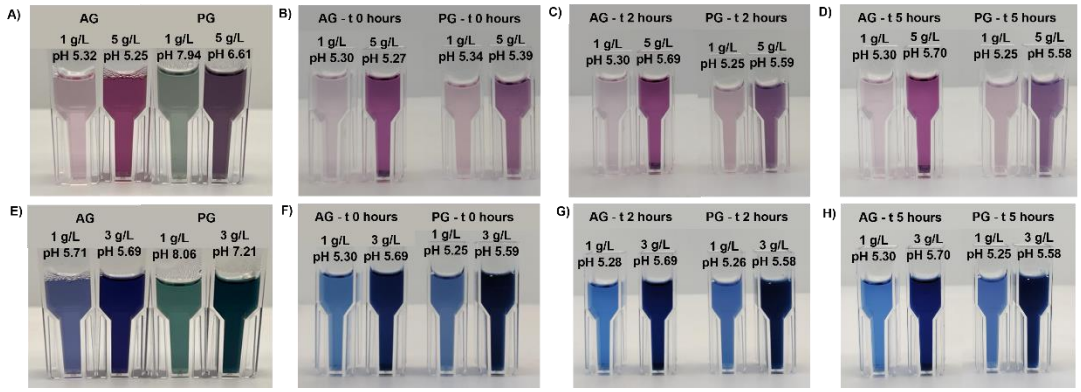

Figure 38 - Animal- (AG) gelatin and Plant-based (PG) gelling food formulations for RC (A − D) and BPF (E − H) extracts. Adjusted the pH values for the red cabbage extract (comparison between A and B) and butterfly pea flower (comparison between E and F). Color evolution for five hours for both extracts (B − D, for red cabbage and F − H for butterfly pea flower).

3.6. ANTIOXIDANT ACTIVITY OF HC, RC, AND BPF EXTRACTS

In this study, we went beyond the usual role of synthetic dyes as colorants, evaluating anthocyanin-based extracts for their antioxidant activity using the DPPH assay. The IC_{50} for each extract was obtained from the graphical representation of the radical inhibition percentage as a function of concentration after 30 minutes of incubation in the dark. RC extract showed significant activity against DPPH radical with a lower IC_{50} (0.135 ± 0.009 g/L), followed by HC (0.141 ± 0.020 g/L), and then BPF (0.231 ± 0.010 g/L) (Table 17). Considering that HC and RC extracts have lower phenolic compound content (including anthocyanins and non-anthocyanins), these results suggest that the antioxidant activity can be correlated with the complexity of the structure of the anthocyanins (361, 362), where the non-acylated and acylated anthocyanins exhibited superior antioxidant ability compared to the polyacylated anthocyanins found in BPF extracts. The presence of *p*- and *o*-phenolic groups in HC and RC extracts significantly contributes to the scavenging of reactive oxygen species (ROS). Hydroxyl groups present at carbons C3' and C4' on the B ring have a strong contribution to the antioxidant capacity of these compounds due to the ability to form ortho-semiquinones and subsequently ortho-quinones by two

consecutive single-electron transfer reactions. Hydroxyl groups present at carbons C5, and C7 on the ring A can be oxidized to form pseudo-semiquinone species and stabilize the formed radicals (363). In the case of polyacylated anthocyanins, these phenolic hydroxyl groups can be linked to sugars and hydroxycinnamic acids which decreases the reaction with DPPH radical reducing the antioxidant activity. Furthermore, considering the existence of other phenolic compounds such as caffeoylquinic and hydroxycinnamic acids in the HC and RC extracts, the presence of methoxy and carboxylic acids groups in their structure also has an important contribution to the antioxidant ability of the extracts (364).

Compared to the literature, the IC_{50} values obtained in this work are within the same range of concentrations, except for the RC extract, which revealed a stronger antioxidant activity. Commercial antioxidants commonly used in the food and cosmetic industries, such as ascorbic acid, trolox, and gallic acid, exhibit strong antioxidant activity; however, the anthocyanin-based extracts reported in this study demonstrated comparable antioxidant efficiency relative to the butylhydroxytoluene (BHT) and butylated hydroxyanisole (BHA) (Table 17).

Table 17 - The antioxidant activity of the anthocyanin-based extracts expressed in terms of IC_{50}, corresponding to the antioxidant concentration required to reduce the initial concentration of the DPPH% radical by 50 %. Comparison with commercial antioxidants.

Sample	IC_{50} (g/L)	RSI ($1/IC_{50}$)	Reference
HC	0.141±0.020	7.1	This work
Ethanolic leaf extract of *Hibiscus sabdariffa*	0.185	5.4	(365)
Hibiscus sabdariffa ethanolic extract	0.125	8.0	(366)
RC	0.135±0.009	7.4	This work
Red cabbage (Soxhlet extraction methanol 24h)	0.700	1.4	(367)
BPF	0.231±0.010	4.3	This work
Clitoria ternatea water extract	0.195	5.1	(368)
Clitoria ternatea flower extracts (methanol extraction 72h)	0.200	5.0	(369)
Commercial antioxidants			
Ascorbic acid	0.005	200	This work
Trolox	0.003	333	This work
Gallic acid	0.002	500	This work
BHA	0.100	10	(370)
BHT	0.170	5.9	(367)

4. CONCLUSIONS

This work demonstrated the potential of polyacylated extracts as natural colorants, offering an alternative to synthetic dyes. Increasing the degree of complexation enhanced color stability in aqueous solutions, particularly between pH 3 and 6, suitable for food applications. Thermostability studies at 100°C showed greater stability for the BPF extract compared to the RC and HC extracts. Bisulfite bleaching tests indicated quicker color loss for HC and RC extracts for low SO_2 concentrations, followed by a less intense color decline at higher concentrations (second-order reaction). BPF extract showed a smaller loss (one-order reaction) even at higher bisulfite concentrations. Gelatin-based formulations with these extracts produced vibrant hues, with BPF and RC yielding intense blue and purple colors, respectively. The pH of gelatin significantly influenced the resulting color. In addition to the colorimetric properties, these extracts, showing promising antioxidant activity compared to commercial antioxidants, highlight their potential as natural alternatives, aligning with the industry's growing interest in replacing synthetic additives with more sustainable, health-conscious options.

PART B

DEGRADATION PATHWAYS OF MALVIDIN MONO- AND DI-GLYCOSIDE: INSIGHTS INTO pH-DEPENDENT REACTIVITY AND PRODUCT FORMATION

SYNOPSIS

The objective of this study was to investigate the mechanisms and degradation rates of malvidin mono- and di-glucoside in basic conditions. While anthocyanin chemistry in acidic environments is well understood due to its food applications, its behavior in basic conditions has received less attention. They are separated by a range of transition pHs where irreversible processes occur more rapidly than hydration and OH^- nucleophilic addition. These transition pHs include the physiological pH (7.4), important for bioavailability and health benefits, and the pH of some flower and fruit vacuoles, which contribute to their natural blue color.

For the diglucoside, the anionic quinoidal base equilibrates within seconds with a kinetic product $B4^{2-}$ (kinetic reservoir), which is identified by its kinetic signature in UV-Vis spectroscopy and ^1H NMR, thereby slowing the overall equilibration rate. At the transition pHs of the monoglucoside, only quinoidal bases are found, and their degradation rates exceed those of hydration and OH^- nucleophilic addition, preventing the system from reaching equilibrium. Aside from the minor degradation route involving the loss of glucose to produce the more unstable aglycone, HPLC-DAD-MS and NMR experiments have identified degradation products originating from the initial formation of colored malvidin-3-*O*-glucoside dimers, which subsequently form oligomers. The transition pH range of the diglucoside is narrower than that of the monoglucoside. The kinetics toward equilibrium coexist with the degradation processes and are influenced by the equilibrium formed with $B4^{2-}$.

*This Part B was adapted from the paper: Seco, A.; **Pereira, A.R.**; Pina, F.; Camuenho, A.; Oliveira, J.; Dias, R.; Brás, N.; Basílio, N.; Parola, A. J.; Lima, J.; De Freitas, V. Comparing the Chemistry of Malvidin 3-O-Glucoside and Malvidin 3,5-O-Diglucoside Networks: A Holistic Approach to the Acidic and Basic Paradigms with Implications in Biological Studies. Manuscript accepted in the Journal of Agricultural and Food Chemistry. 2024. https://doi.org/10.1021/acs.jafc.4c00552*

The author carried out the HPLC-DAD, LC-MS, and NMR experiments, and also some of the UV-visible studies described in the scientific article, which will be the results presented in this part.

1. INTRODUCTION

Anthocyanins are the molecules responsible for the colors in most angiosperms, giving orange-red to purple-blue hues. Besides their functions in plants, such as attracting pollinators and seed dispersers or behaving as photoprotective agents by absorbing excess visible and UV light, the consumption of anthocyanin-rich foods has been associated with numerous beneficial health effects (23, 24, 27). They can be extracted from sources such as grape skins, blackberries, and purple carrots and incorporated into a range of food matrices including juices, jams, yogurts, and baked goods as natural colorants or nutritional additives. However, anthocyanins are intrinsically unstable and can react in vivo with other biological compounds or metals (371, 372), and decompose due to enzymatic processes (373), within other possible decomposition routes.

Anthocyanins acquire a diversity of chemical species that are interconnected by pH-dependent equilibrium. Most of the studies carried out on anthocyanins in the last decades are focused on their behavior in acidic mediums considering the wide applicability in the food industry (production of juice fruits or other food processing). In addition, it is the pH domain of the vacuoles where anthocyanins are located in most flowers and fruits responsible for their red, orange, or pink colors (69, 374). Understanding the degradation pathways is crucial to preserving the color and nutritional integrity of anthocyanin-rich foods and beverages. In very acidic conditions, anthocyanins are represented by the respective flavylium cation since all species in the medium converge towards the flavylium cation, increasing the concentration of protons, which becomes the only species (49). The hypothetical degradation pathway for anthocyanins includes several reactions, namely hydrolysis which involves the cleavage of glycosidic bonds between the sugar moiety and the aglycone (anthocyanidin) portion of the molecule (375, 376). Anthocyanins containing carboxylic acid groups are susceptible to decarboxylation in acidic environments with the loss of carbon dioxide from the carboxyl group, resulting in the formation of corresponding colorless chalcones or flavonoids (377). Chalcones have been proposed to be intermediates in the irreversible degradation of anthocyanins at acidic pH (60), where rearrangement reactions generate diverse degradation products, including phenolics acids (gallic acid, protocatechuic acid, vanillic acid, syringic acid and p-coumaric acid) and aldehydes (2,4,6-trihydroxybenzaldehyde) (375, 378). Acidic environments can increase the oxidative degradation of anthocyanins when oxygen is present. The process involves the oxidation of the phenolic hydroxyl groups within the anthocyanin structure, which results

in quinones associated with polymerization processes. Quinones and polymerization products lead to color loss and the development of dark pigments in degraded anthocyanin-containing products (36, 379).

Understanding the processes that occur at neutral-basic pH is particularly important since physiological pH is included in this pH range and anthocyanins have potential beneficial properties for human health, such as high antioxidant potential, whose stability can affect bioavailability and efficacy. Furthermore, some flower and fruit vacuoles where anthocyanins are stored tend to have slightly basic pHs, giving them a vibrant color palette, including natural blue (70). In a neutral to basic medium, anthocyanins are extensively degraded. The increasing OH^- concentration may accelerate the degradation reactions, and the hydroxyl group in position C-3 in anthocyanidins makes them unstable. The few studies in this pH range indicate that the structure of the degradation products results from the combination of irreversible hydrolytic and autoxidative processes with the cleavage of the carbon bonds (36, 60). Dangles *et al*. (39) studied the degradation rates of the cyanidin-based anthocyanin extracted from red cabbage at pH 7 and 8, and used reverse pH jumps back to flavylium cation to control the anthocyanin degradation as a function of time. It was verified a combination of two distinct processes involving the cyanidin nucleus: reversible water addition and irreversible autoxidation. In the present work, Malvidin-3-*O*-glucoside (M3G) and malvidin-3,5-*O*-diglucoside (M3,5diG) were selected to compare the effect of the glycosylation pattern in the thermodynamics as well as the kinetics of the reversible and irreversible chemical processes, focusing essentially on neutral and slightly basic pH, including mechanistic clues about degradation pathways.

2. MATERIALS AND METHODS

2.1. pH DETERMINATION

The pH of all solutions was determined on a WTW pH 320 or 508 (Weilheim, Germany) with a CRISON 5209 combined glass electrode of 3 mm diameter (Barcelona, Spain), previously calibrated with buffer solutions (pH 4.00, 7.00, and 10.00).

2.2. DETERMINATION OF DEGRADATION KINETICS BY HPLC-DAD

The degradation of M3G at different concentrations ($3.33x10^{-5}$, $2x10^{-4}$, and $1x10^{-3}$ M) was followed over time at pH 7.4 and 8.1 by HPLC coupled with DAD. Stock solutions of M3G ($1x10^{-4}$, $6x10^{-4}$, and $3x10^{-3}$ M) were prepared in 0.1 M HCl. Then, 1 mL of NaOH

0.1 M, 1 mL of universal buffer at pH 7.4 or 8.1, and 1 mL of each stock M3G solution were added to a glass vial, and the solution was analyzed over time by HPLC-DAD on a Thermo Ultimate 3000 liquid chromatograph. The decrease of the concentration of M3G was followed over time during 7 days in a 250 × 4.6 mm i.d., 2.7 μm Poroshell 120 reversed-phase C18 column (Agilent) at 25 °C. The eluents used were (A) 7.5 % (v/v) formic acid in water and (B) 7.5 % (v/v) formic acid in acetonitrile at a flow rate of 0.4 mL/min. The gradient consisted of 3 % to 15 % of B in 11 min, then 25 % of B in 23 min, 30 % of B in 27 min, and then, isocratic for 4 min. Detection was carried out from 200 to 800 nm in a Thermo Accela PDA detector. Due to the low concentration of M3G (3.33×10^{-5} M) needed to avoid self-association and the low sensitivity of HPLC analysis when compared to UV-visible spectroscopy, several aliquots (1 mL) of the degradation kinetic (pH 8.1) were taken, lyophilized and then resuspended in 0.1 mL of 0.1 M HCl to be analyzed by HPLC to tentatively identify the degradation products. For M3,5diG, it was followed the same methodology to analyze the chromatographic profile using a stock solution of 1×10^{-3} M at pH 8.1 and 3×10^{-4} M at pH 7.4.

2.3. DEGRADATION RATES BY UV-VISIBLE SPECTROSCOPY

The irreversible process that conduces to the anthocyanin degradation in basic solutions was studied by a sequence of pH jumps as follows: *i)* direct pH jump from equilibrated solutions of flavylium cation to the desired pH, *ii)* stand the solution for a given time (delay time); *iii)* carry out a reverse pH jump to pH≤1 and wait the necessary time to the flavylium cation reach the equilibrium. The degradation for each delay time was measured using equation 1, where $A_{initial}$ is the initial absorbance of the flavylium cation, before step *i)* and $A_{after\ delay}$ the absorbance after step *iii)*:

$$\chi_{decomposition} = 1 - \chi_{AH^+ recovery} = 1 - \frac{A_{after\ delay}}{A_{initial}} \qquad \text{Equation 1}$$

2.4. COMPUTATIONAL STUDIES

The Maestro software (380) was used to do the conformational search of all conformers of both M3G and M3,5diG molecules. All geometries were optimized at the SMD(water)/B3LYP-D3/6-31+G(d,p) (381-384) level of theory, and using the Gaussian

09 program package (385)**.** The charge distribution was analyzed by applying the NBO formalism (386)**.**

2.5. NMR STUDIES

To evaluate the degradation process of M3G, a stock solution of commercial M3G chloride (Extrasynthese ≥95%, $6x10^{-4}$ M) was prepared in 0.1 M HCl. For sample preparation, 200 μL of 0.1 M NaOD, 195 μL of universal buffer (pH 8.1), 5 μL of internal reference TSP (2,2,3,3-d(4)-3-(trimethylsilyl) propionic acid sodium salt 98+ atom% D, 2 mg/mL) and 200 μL of the M3G stock solution were added to a 5-mm NMR tube. The final concentration of M3G was $2x10^{-4}$ M. The ^{1}H spectra of the M3G solution were recorded over time (256 scans) at 25.00 (± 0.01) °C.

NMR experiments were conducted on a Bruker Ascend 600 spectrometer, operating at a ^{1}H frequency of 600.13 MHz, and equipped with a 5 mm BBO Cryogenic Prodigy Probe. All measurements were performed with standard Bruker pulse sequences at either 5.00 or 25.00 (± 0.01) °C, and the spectra were processed by the Bruker Topspin software package. The concentration of M3G was set to 1.0 $x10^{-3}$ M and prepared in 20 mmol/L Tris-d11 buffer solution (in D_2O, pH 8.10 ± 0.01). The ^{1}H chemical shifts are given concerning the methyl protons of tetramethylsilyl propionate (TSP), which were arbitrarily set as 0 ppm. A similar experiment was performed at 25.00 (± 0.01) °C and 5 (± 0.01) °C using a concentration of M3G of $1x10^{-3}$ M.

The 1D and 2D spectra of D-glucose were also recorded as a control at 5.00 or 25.00 (± 0.01) °C. For that, a solution of D-glucose ($1x10^{-3}$ M) was prepared in Tris-d11 buffer at pH 8.1.

One-dimensional ^{1}H spectra were acquired with a shaped pulse to suppress the water resonance using the following parameters: spectral width, 12 ppm; shaped pulse duration, 2.0 ms; relaxation delay, 2.0 s; 90° nutation angle duration, 12.80 μs. For each spectrum, 128 scans were collected per FID, consisting of 32768 complex data points. ^{1}H diffusion measurements were made using a 2D LED experiment based on bipolar gradients and an eddy current reduction delay, with presaturation. A total of 64 scans of 16 data points were collected using a 90° pulse angle, a relaxation delay of 2.5 s, and a spectral width of 12 ppm. The maximum gradient strength produced in the z direction was 50 G/cm. The duration of the magnetic field pulse gradients (δ=2400 μs) and diffusion time (Δ=200 ms) were optimized to obtain a 5 % residual signal with the maximum gradient strength. The pulse gradients were incremented from 2 to 95 % of

the maximum gradient strength in a linear ramp. The temperature was set and controlled to 25.00 ± 0.01 °C with a gas flow of 500 L/h to avoid any temperature fluctuations due to the sample heating during magnetic field pulse gradients. T1 relaxation measurements were performed using an inversion recovery sequence with inversion times of 0.1, 0.25, 0.5, 1.0, 1.5, 2.0, 3.0, and 5.0 seconds. T2 relaxometry was performed using the Carr-Purcell-Meiboom-Gill (CPMG) sequence; ten-point measurements were acquired, with delay times of 1, 5, 10, 25, 50, 75, 100, 250, 500, and 750 milliseconds. Dynamics Center (from Bruker) was used to calculate both diffusion coefficients as well as T1 and T2 relaxation times.

2.6. IDENTIFICATION OF THE DEGRADATION PRODUCTS BY LC−MS/DAD

Selected aliquots during the M3G and M3,5diG degradation experiments were analyzed by LC-MS to tentatively identify the degradation products. Mass spectrometry (MS) analysis was performed using a Finnigan Surveyor series liquid chromatograph, equipped with a 250 × 4.6 mm i.d., 2.7 μm Poroshell 120 reversed-phase C18 column (Agilent) at 25 °C. The eluents used were (A) 1 % (v/v) formic acid in water and (B) 1 % (v/v) formic acid and 30 % (v/v) acetonitrile in water at a flow rate of 0.4 mL/min. The elution gradient was performed from 20 to 100 % B for 70 min, then, the column was washed with 100 % B for 10 min and stabilized with the initial conditions for 10 min. The mass detection was carried out in the positive ion mode in a Finnigan LCQ DECA XP MAX (Finnigan Corp., San José, CA, USA) mass detector with an API (Atmospheric Pressure Ionization) source of ionization and an ESI (ElectroSpray Ionization) interface. Spectra were recorded in the positive ion mode between m/z 300 and 1500.

3. RESULTS AND DISCUSSION

Malvidin mono- and di-glucoside present a pH range (transition pHs) between acidic and basic values, where degradation is faster than hydration and OH^- nucleophilic addition, and the equilibrium is not reached. In the case of diglucoside, this transition pH interval is narrower than the one of the monoglucoside (Figure 39). As previously mentioned, the behavior of anthocyanins in this transition pH range is not yet fully understood concerning the degradation mechanisms and consequently, the type of compounds formed. In this way, this work investigated the degradation of malvidin mono- and di-glucoside in the pH region signed by the red lines in Figure 39 through a series of

complementary studies including HPLC, UV-visible spectroscopy, NMR, and LC-MS analysis.

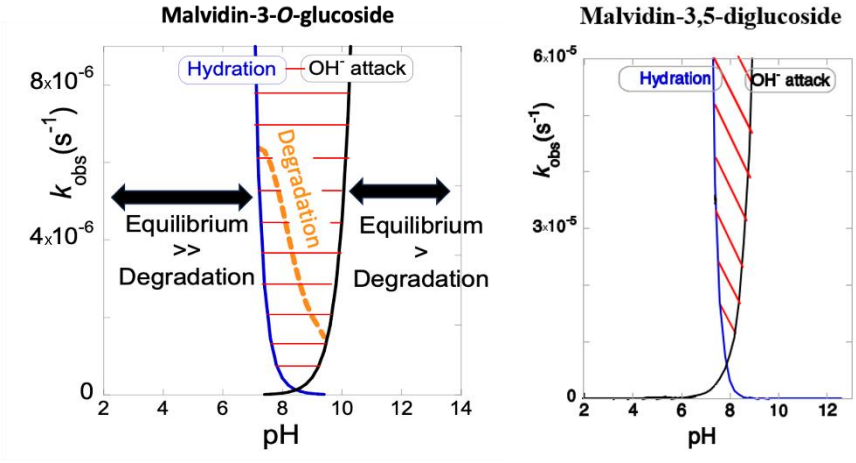

Figure 39 - Comparison between the hydration, OH^- attack, and decomposition rate constants for M3G in neutral−basic media. Degradation is faster than the other two processes for pH values between pH≈7.4 and 9.5.

As already mentioned, anthocyanins are chemical compounds that exist in different forms depending on the pH value. Except for more complex anthocyanins, at pH≤1 flavylium cation is the sole species. A convenient way to calculate the kinetics and thermodynamics constants of anthocyanins consists of adding base to equilibrated solutions of the flavylium cation (direct pH jumps) or acid to equilibrated solutions at higher pHs to regenerate flavylium cation (reverse pH jumps). When a direct pH jump is carried out (Figure 40) all the other species become thermodynamically more favorable, and this constitutes the driving force for the subsequent kinetics steps. Since proton transfer is by far the fastest kinetic step (sub microseconds), the quinoidal base is formed and equilibrates with flavylium cation. As discovered by Brouillard and Dubois (387), the quinoidal base does not hydrate in an acidic medium and behaves as a kinetic product that retards the hydration reaction, which occurs only via flavylium cation to form hemiketal. At the pH values reached by direct pH jumps, the hydration takes several minutes and the tautomerization seconds.

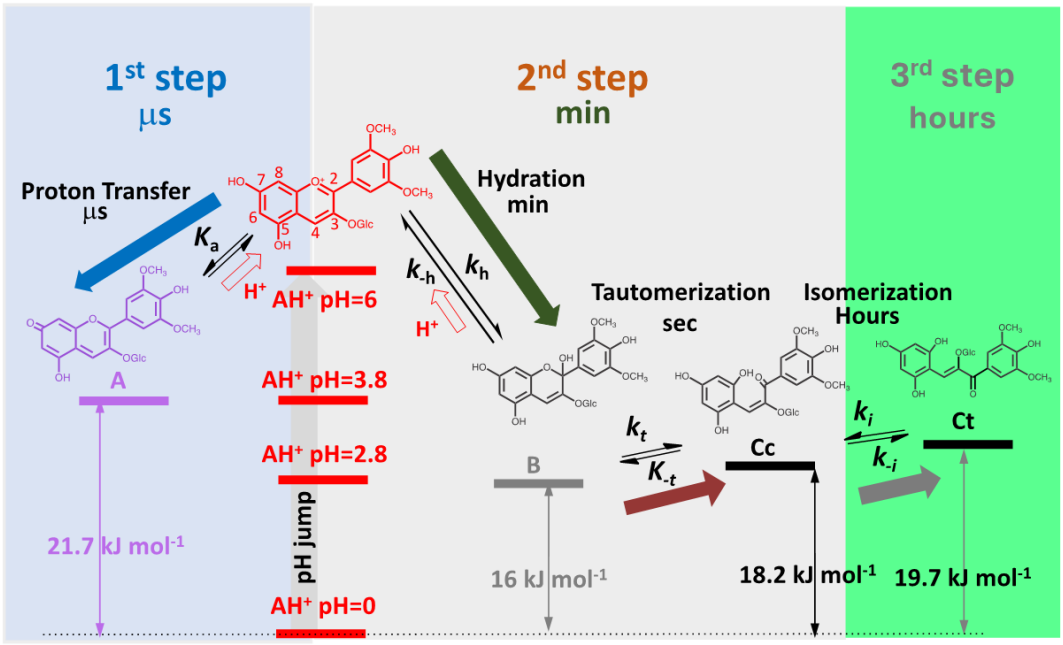

Figure 40 - Relative energy level diagram of the pH-dependent reversible reactions of M3G up to pH≈6. This system is conveniently studied upon the addition of base to equilibrated solutions of flavylium cation (direct pH jumps). Identical schemes are followed by all anthocyanins and related compounds.

The extension to the basic medium gives the possibility for the species reported in Figure 40, to deprotonate in the hydroxyl substituents. In Figure 41, all possible species that can appear as transients or at equilibrium are presented, and the respective equilibrium constants are defined. When a direct pH jump is extended to the basic region, the first step is still the formation of quinoidal bases, with a pH-dependent mole fraction distribution defined by the acid-base constants (Appendix 5, Tables 5A and 5B). The second step in the basic medium is due to the OH^- nucleophilic addition to the anionic quinoidal bases. The cis-trans isomerization is much faster than the OH^- nucleophilic addition, so in the basic medium, only these two steps are observed, exhibiting different kinetics in the mono- and di-glucosides. Except for the pH range between the acid and basic paradigms, as seen below, all these processes are accompanied by slower degradation kinetics.

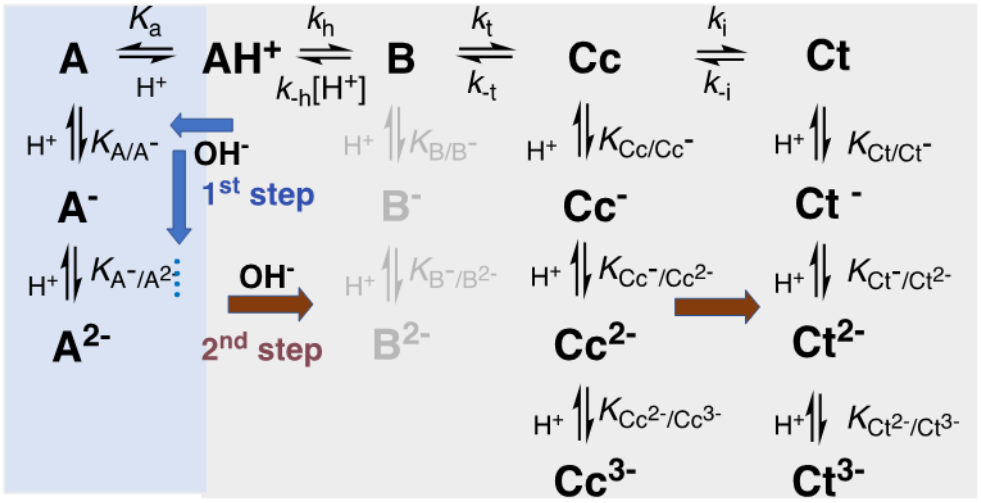

Figure 41 - General scheme of all possible anthocyanin species that can be formed as transients or at the equilibrium upon extending to basic pH values, together with the definition of the respective equilibrium constants. In the case of the diglucoside, the species A^{2-} cannot be formed. No spectral evidence of the hemiketal anionic forms at the equilibrium was obtained. The 2nd step is controlled by the OH^- nucleophilic addition since the *cis-trans* isomerization is much faster, see below.

3.1. Degradation kinetics of M3G and M3,5diG by HPLC-DAD and UV-Visible spectroscopy

Several aliquots of the aqueous solution of M3G and M3,5diG, $1x10^{-3}$ M at pH=7.4 were taken over time and analyzed by HPLC-DAD. The HPLC-DAD results provided critical and conclusive information, including the determination of the degradation kinetic constant and the evolution of the chromatographic profile over time.

The normalized area of the HPLC peaks of M3G and M3,5diG versus time after a direct pH jump to the physiological pH (7.4) is presented in Figure 42 A. The fitting was achieved with a mono-exponential rate constant of $9.1x10^{-6}$ s^{-1} for M3G and $9.8x10^{-7}$ s^{-1} for M3,5diG, indicating that the monoglucoside degrades much faster. In Figure 42 (B) an analog experiment was performed at pH=9.2. It is observed the inversion of stability of the two compounds in the basic medium. Fitting was achieved with mono-exponentials $5.6x10^{-6}$ s^{-1} and $3x10^{-5}$ s^{-1}, respectively for M3G and M3,5diG. It should be also emphasized that in contrast with acidic and transition pHs the degradation kinetics of the diglucoside in the basic medium is faster than the one of the monoglucoside, and after 50 h the M3G peak is reduced by 65 % while M3,5diG almost disappeared. A probable explanation for this behavior is the faster formation of the anionic chalcones of the diglucoside as well as the formation of another species ($B4^{2-}$ species identified by NMR

and UV-Vis spectroscopy, resulting from the OH^- attack in position 4 of the quinoidal base) which establishes a transient pre-equilibrium with an anionic quinoidal base.

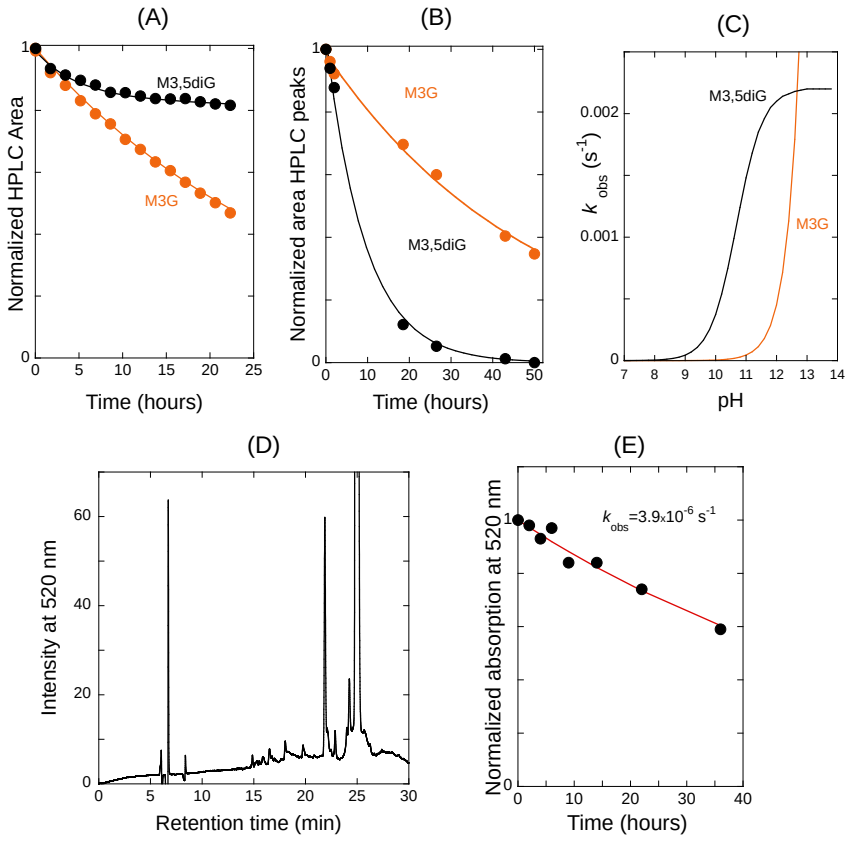

Figure 42 - (A) Normalized area of the HPLC peaks of M3G (orange points) and M3,5diG (black points) at the physiological pH (7.4), after 1 day. Fitting was achieved with a mono-exponential with rate constant 9.1x10^{-6} s^{-1} for M3G and biexponential with rate constants 8.9x10^{-5} s^{-1} (but only 12 % of the total amplitude) and circa 9.8x10^{-7} s^{-1} for M3,5diG; (B) The same of (A) for pH=9.2, with rate constants 5.5x10^{-6} s^{-1} for M3G and 3x10^{-5} s^{-1} for M3,5diG; (C) Rates of the two compounds toward the equilibrium versus pH in basic medium; (D) HPLC profile of the lyophilized sample of (3.3x10^{-5} M) after 2 days at pH=8.1; (E) Normalized areas upon integration of all peaks of (D) as a function of time.

When the HPLC areas of the lyophilized sample of M3G (3.33x10^{-5} M) after 2 days are integrated, Figure 42 (D) and (E), the observed rate constant (k=3.9x10^{-6} s^{-1}) of the colored forms is closer to the rate constant calculated through the assays carried out by UV-Vis spectroscopy (Figure 43 b, k= 4.6x10^{-6} s^{-1}). Representation of χ decomposition for different delay times, as exemplified in Figure 43 (a) for M3G, allowed the determination of the degradation rate represented in Figure 43 b and c, respectively for M3G and M3,5diG, black circles (●).

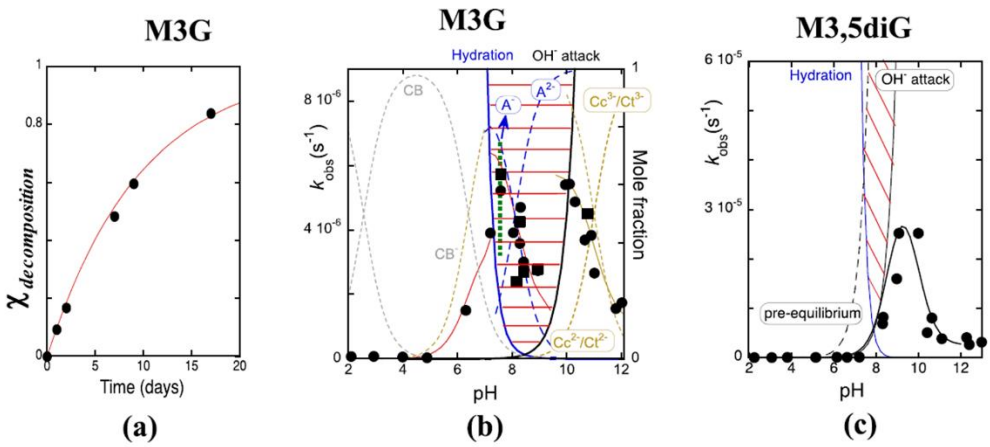

Figure 43 – (a) Mole fraction of the degradation processes upon a pH jump of M3G ($2x10^{-5}$ M) at pH=8.1 calculated at 520 nm. (b) (●) rate constants of the M3G colored species disappearance (includes the degradation products exhibiting absorption spectra similar to M3G) versus pH in acidic and basic medium (■) rate constant for the kinetics of quinoidal base disappearance. This figure completes and corrects a previous one reported in reference (388); (c) (●) degradation rate constants of M3,5diG ($1.3x10^{-5}$ M), calculated as in Figure 21 a.

Comparing the rate of M3G disappearance at the physiological pH with the rate reported for the studies carried out by the UV-vis spectroscopy (Figure 42 b), it is clear that the rates obtained from HPLC are higher than those monitored by UV-Vis spectrophotometry, which can be explained by the contribution of the degradation products exhibiting absorption spectra in the visible region and mitigate the color loss of M3G. Conversely, the rates of M3,5diG are similar for both techniques. When colored species (such as dimers and oligomers detected below by LC-MS) are formed in significant amounts, as in the case of M3G, the degradation rate is lower than the one measured by HPLC. This result can be explained if the mean average value of the mole absorption coefficients (ε Beer law) of the dimer and oligomers is similar to the one of the flavylium cation.

In this transition pH range, the equilibrium is not achieved, only anionic quinoidal bases are present (together with the respective irreversible products, some of them absorbing in the visible) and no trans-chalcone is detected, upon reverse pH jumps back to pH≤1.24. The fact that in the transition pHs of M3G, the degradation rates follow the mole fraction distribution of the species A^-, Figure 43 b, suggests that the degradation pathways are essentially initiated from this species. In the basic medium (out of the transition pHs), the degradation rate follows the mole fraction distribution of the anionic chalcones (the only observed species) suggesting an OH^- attack to these species, which is less efficient for the more negatively charged anionic chalcones due to the higher electrostatic repulsion.

M3,5diG behaves differently, Figure 43 c. The transition pHs, also delimited by the hydration reaction and the OH^- nucleophilic addition, are narrower in comparison with M3G. The transient equilibrium that forms a new species, $B4^{2-}$ (traced line in Figure 43 c), is reached in almost all this pH interval, and there is not a net separation between the kinetics towards the equilibrium and the degradation rate. On the other hand, above the transition pHs, the kinetics toward the equilibrium is always faster than the degradation, Figure 43 c, following the same trend of M3G.

It should be emphasized that in contrast with acidic and transition pHs, the degradation kinetics of the diglucoside in the basic medium is faster than the one of the monoglucoside, Figure 43 c (inversion of relative reactivity). This behavior was confirmed by following the kinetics by HPLC at pH=9. After 50 h the M3G peak is reduced by 65 % while M3,5diG almost disappeared, Figure 42 b. A probable explanation for this behavior is the faster formation of the anionic chalcones of the diglucoside, as observed in Figure 42 c, as well as the formation of $B4^{2-}$. Likely in an acidic medium, the disappearance of the monoglucoside at physiological pH is faster than the one of the diglucoside.

3.2. COMPUTATIONAL STUDIES

The question is why in the basic medium the OH^- attack occurs in A^- of M3,5diG but not in A^{2-} of M3G. To rationalize the above experimental observations, the molecular structures of the di-anionic quinoidal base of M3G and the mono-anionic M3,5diG have been analyzed using quantum mechanics calculations. Table 5C, in Appendix 5, summarizes the charge distribution of some key atoms as well as the HOMO/LUMO energy data for the most thermodynamically stable conformers of each molecule. Analysis of the charge distributions in the anthocyanins moiety indicates that the presence of the second glucose unit on the O-5 atom in M3,5diG increases (makes less negative) the charge of the O-5 and C-6 atoms by 0.274 and 0.127 au, respectively. Indeed, a significant difference is observed in the overall charge of the anthocyanins moiety in the diglucoside, which amounts to +0.476 au. This distinct charge distribution is remarkedly notorious in the comparison of the electrostatic potential energy maps for both molecules, Figure 44. Considering the proximity between the O-5 and C-4, the excess of negative charge in M3G disfavors the nucleophilic attack of the OH^- on C-4 and subsequent formation of the $B4^{2-}$. Noteworthy, no significant differences are observed in the HOMO/LUMO energies of the two compounds, which suggests that they do not significantly interfere with the different reactivities towards nucleophiles at the C-4 position.

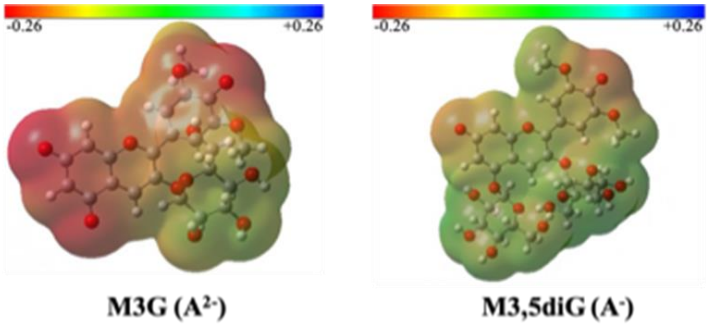

Figure 44 - The electrostatic potential energy (ESP) map of the thermodynamically most favored geometries of M3G (A^{2-}) and M3,5diG (A^{-}) obtained at the SMD (water)/B3LYP-D3/6-31+G(d,p) level of theory.

3.3. IDENTIFICATION OF DEGRADATION PRODUCTS FOR M3G

3.3.1. HPLC AND NMR ANALYSIS

The chromatographic profile of several aliquots of the M3G solution ($1x10^{-3}$ M at pH 8.1) was also examined throughout time by HPLC-DAD. Since the pH observed during the elution of the HPLC is very acidic (pH<1), quinoidal bases and cis-chalcone (independently of their protonated state) existents at pH 8.1 revert to the respective flavylium cation, while trans chalcones and all irreversible products appear in their protonated forms. It can be observed from the HPLC of Figure 45 that apart from M3G flavylium cation (peak 3) and petunidin 3-*O*-glucoside (already present in M3G standard, peak 2), new chromatic peaks in the visible region (λ_{max}=532 nm) of the spectrum start to appear after 2 hours (Figure 45 A). By increasing the incubation time to 24 hours, the number of peaks increases significantly, as shown in Figure 45 B. At this pH value, the anionic and di-anionic quinoidal bases are the only reversible species present in the solution ($pK_{A^-/A^{2-}}$ =8.1 (101)), and the pH dependence of the degradation curve achieved in this work by UV-Vis spectroscopy (data in scientific article) suggests that the mono-anionic quinoidal base is the main species responsible for the degradation. In this way, the formation of colored products at the physiological pH was corroborated during the disappearance of A^-. The chromatographic profile obtained by HPLC (Figure 45 A and B) reveals crucial information: some of the degradation products maintain the flavylium cation moiety and absorb at 520 nm.

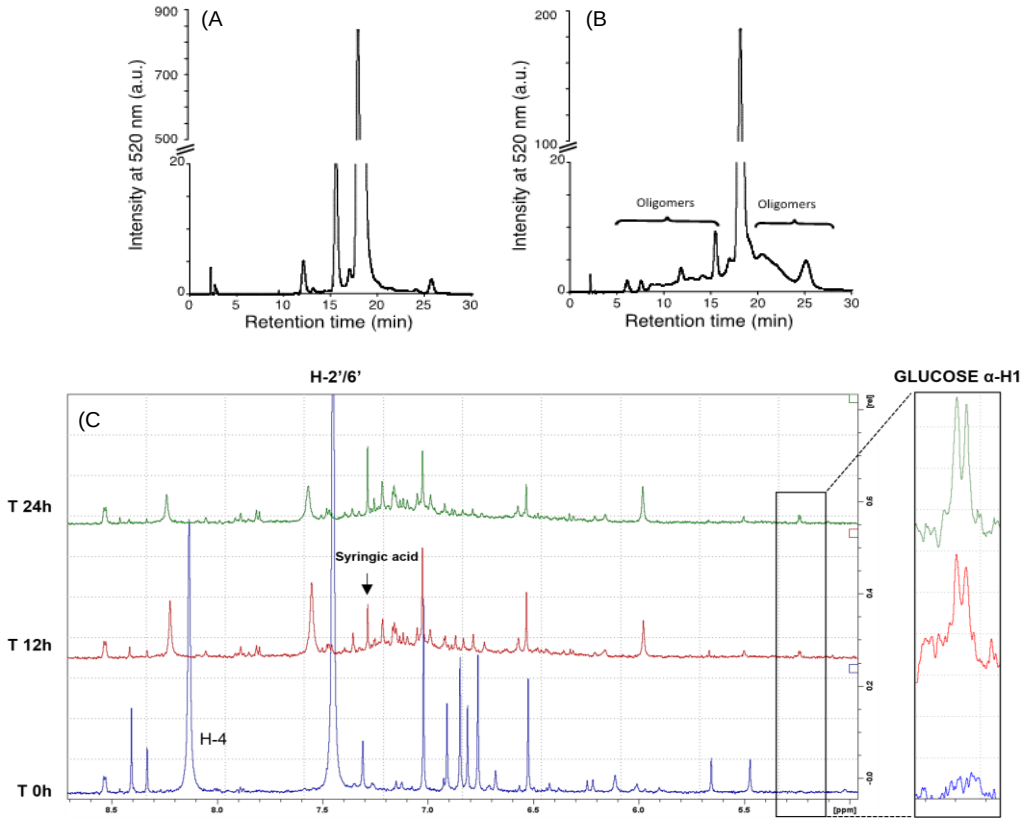

Figure 45 - HPLC chromatograms for representative transition pHs of (a) M3G solution ($1x10^{-3}$ M, pH 8.1) at the end of 2 hours; (b) and 24 hours. Peak 1 corresponds to the malvidin-3-*O*-glucoside dimer, peak 2 to petunidin-3-*O*-glucoside already present in M3G standard), and peak 3 to malvidin-3-*O*-glucoside; (c) ^{1}H NMR spectra in the aromatic region of M3G at $1x10^{-3}$ M, pH 8.1 versus time. Spectra were acquired at 25 °C.

^{1}H NMR studies have been reported to elucidate the different species resulting from the reversible equilibrium reactions of anthocyanins. However, they can be extended to the basic medium not only for the characterization of the reversible species but also for the degradation of products. Figure 45 C shows that right after the dissolution of M3G, $1x10^{-3}$ M, at pH=8.1, besides the signals assigned to the anionic quinoidal bases, several unidentified aromatic resonances appeared in the spectrum, which could not be attributed to either syringic acid or any other conventional degradation products. From the latter, only syringic acid was detected at the end of 12 h of incubation as did also the anomeric ^{1}H signal of free α-D-glucose. In detail, the degradation of M3G at $1x10^{-4}$ M at pH=8.1 was also monitored by ^{1}H NMR spectroscopy for 7 consecutive days (Figure 46). At time 0 (T0), three main proton signals were detected in the aromatic region. These were identified as corresponding to the H-4 (δ = 8.28 ppm), H-2',6' (δ = 7.63), and H-6 (δ = 6.22) of M3G ring C, B, and A, respectively. Over time, all proton signals were found to gradually become less intense, particularly within the first 72 hours,

when relative integrals reached 10 % of their initial value. For H-6,8, the behavior was somewhat different from the previous ones due to a hydrogen-deuterium (H/D) exchange effect, whose kinetics were faster than their chemical decay.

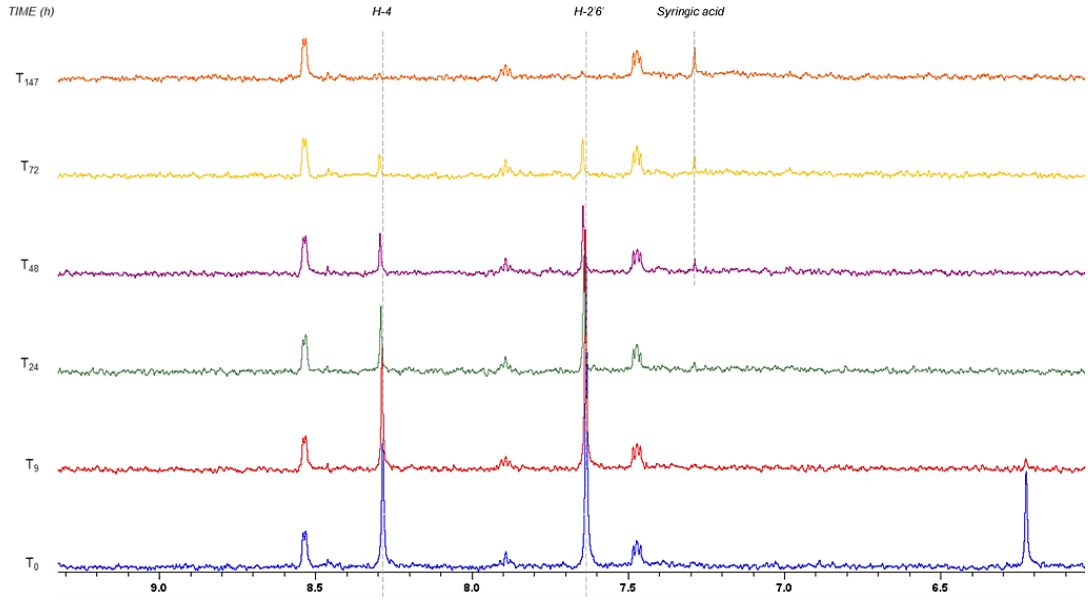

Figure 46 - ^{1}H NMR spectra in the aromatic region of M3G at 1x10^{-4} M taken at different time points. Spectra were acquired at 25 °C pH=8.1.

Of the four main by-products expected through the conventional degradation pathway, as mentioned only syringic acid and glucose were detected by 1D (Figure 46) and 2D NMR (Figure 47), respectively. Though non-quantifiable by ^{1}H NMR (when following the anomeric H-1 signal), glucose was found to be completely released from M3G at the end of 7 days, as confirmed by ^{1}H-^{1}H COSY spectroscopy (Figure 47). D-glucose was used as an external standard (at 1 mmol/L) allowing concentration measurements at each time point to be performed by the ERETIC method (Electronic REference To access In vivo Concentrations) monitored by the anomeric proton at 5.23 ppm. At the end of 12 h, glucose concentration was found to be around 0.080 mmol/L, further increasing to 0.137 mmol/L at the end of 24 h.

Due to the limited ^{1}H sensitivity of NMR spectroscopy at such a low M3G concentration, no reaction intermediaries or oligomerization phenomena could be detected, nor could other 2D approaches like DOSY be employed in a workable timeframe. It thus becomes clear that, though at pH 8.1 the anionic quinoidal base does become de-glycosylated and degraded into syringic acid, these pathways cannot entirely account for the rapid kinetic decay observed by both NMR and HPLC-DAD.

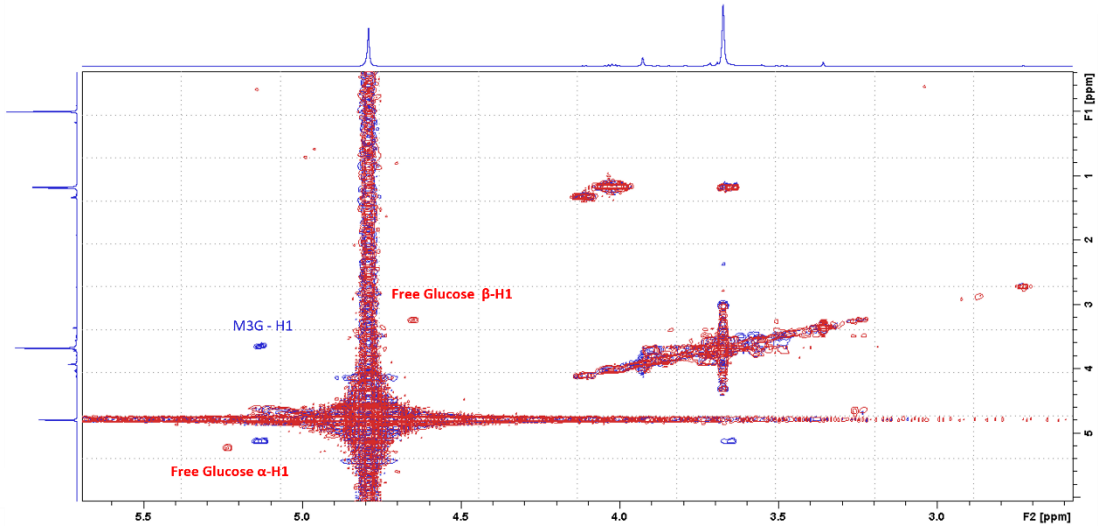

Figure 47 - Superimposition of M3G ^{1}H-^{1}H correlation spectra at T0h (blue) and T147h (red) highlighting the hydrolysis of glucose molecules from the parental structure into the solvent media. In solution, glucose can exist in two anomeric forms: α-D-glucose and ß-D-glucose. The presence of free glucose at that time point coincides with the appearance of ß-H1 and α-H1 correlations at the same 1H frequencies of D-glucose (δ = 5.238 ppm and 4.651 ppm respectively).

3.3.2. IDENTIFICATION OF DEGRADATION PRODUCTS OF M3G BY LC-MS/DAD

The analysis by LC-MS in the positive ion mode showed the presence of different ion masses, Table 18, comprising similar fragmentation patterns such as -162 and -18 a.m.u., corresponding to the loss of glucose moieties and water. Ion masses at m/z 985 and 1,001 were observed in the first stages of degradation. After 1 day at pH 8.1, ion mass at m/z 985, 1,001, 1,017, and 1,493 were detected. Based on the UV-visible spectrum, ion mass, and respective fragmentation pattern, the new peaks were assigned to oligomers formed during the compound degradation. This is not the first time that anthocyanin dimers and oligomers have been described as occurring in nature. Vidal et al., (389) Salas et al., (390), and Alcalde-Eon et al., (391) reported these anthocyanin-derivatives in grapes and wines based on the mass spectrometry data. Later, Oliveira et al., (392) using NMR confirmed the presence of an A-type trimer in a young red wine. The putative structures of the detected ion masses during M3G degradation are presented in Figure 48. Additional ion masses corresponding to hydrated and di-hydrated forms of dimers and trimers were also detected as degradation products. At low concentrations of M3G ($3.3x10^{-5}$ M), oligomerization still occurs, although to a lesser extent when compared with the more concentrated solution ($1x10^{-3}$ M). Typical anthocyanin degradation mechanisms involve the loss of glucose from M3G yielding to malvidin aglycone and then C3-C4 cleavage to give syringic acid (ring B) and 2,4,6-

trihydroxybenzaldehyde (2,4,6-THB) that in oxidative conditions can yield the respective acid (393)**.** The presence of 2,4,6-THB and syringic acid was observed during the degradation of M3G at slightly basic conditions. However, the concentration of syringic acid after the total degradation of M3G (~7 days) only corresponds to about 10 % of the initial concentration of M3G, which once more indicates that this pathway is not the main one involved in this irreversible process.

Table 18 - Ion masses in the positive ion mode of the degradation products formed during degradation at slightly basic conditions.

Compound	$[M^+]$	$[MS^2]$	$[MS^3]$	Possible identity
1	199	------	------	Syringic acid
2	985	823	661	Malvidin 3-*O*-glucoside dimer 1
3	985	823	661	Malvidin 3-*O*-glucoside dimer 2
4	1001	983; 839; 677	------	Monohydrated malvidin 3-*O*-glucoside dimer
5	1003	985; 823	------	Monohydrated malvidin 3-*O*-glucoside dimer
6	1017	855; 693	------	No identified
7	1511	1349; 1493; 1331	------	Di-hydrated malvidin 3-*O*-glucoside trimer
8	1491	1329; 1167; 1005	------	Monohydrated malvidin 3-*O*-glucoside trimer
9	1493	1331; 1169	------	Monohydrated malvidin 3-*O*-glucoside trimer

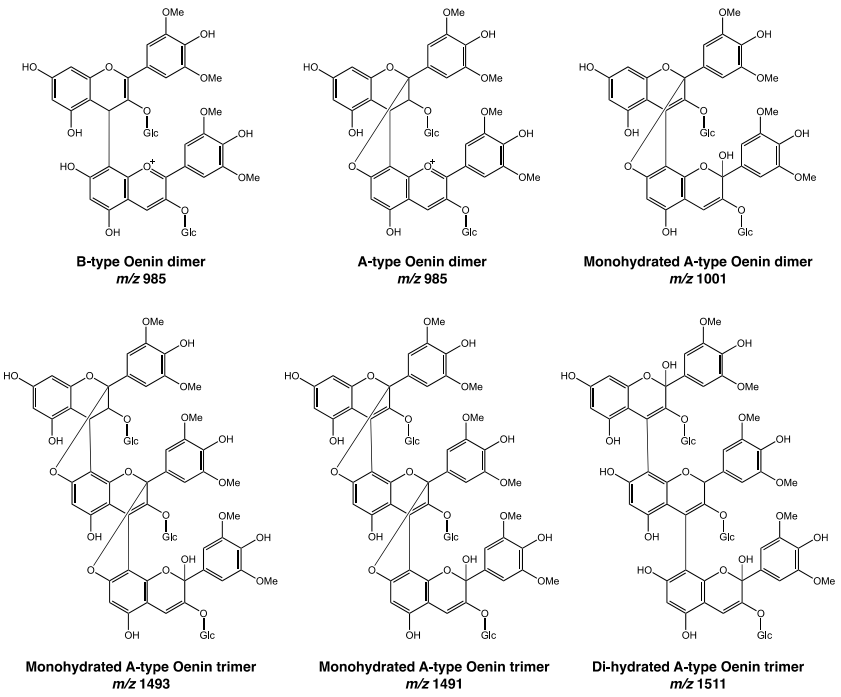

Figure 48 - Putative structures for degradation products of M3G (oenin) based on LC-MS/MS data.

3.4. IDENTIFICATION OF DIMERS

The formation and degradation of the dimer were further supported by kinetic experiments conducted at 5 ºC, which also show the formation and disappearance of different glycosylated and non-glycosylated intermediate species. The results of HPLC-DAD and NMR showed that the degradation process was delayed at lower temperatures, where it was possible to follow the formation and disappearance of the intermediate (malvidin 3-*O*-glucoside dimer). When the experiment is performed at room temperature, the maximum formation of the malvidin 3-*O*-glucoside dimer is impossible to determine. Fitting of the traces reported in Figure 49 is achieved with a biexponential with rate constants k1=1.0x10^{-4} s^{-1} and k2= 6.3x10^{-6} s^{-1}. The first process can be associated with the disappearance of malvidin 3-*O*-glucoside responsible for the appearance of the dimer. Further conclusions regarding the second-rate constant in this experiment are limited by its low accuracy. However, the data at 5 ºC permits rationalizing the results at room temperature, Figure 49 (B). The two first points remain from the dimer formation. The rest of the decay regards the disappearance of the monoglucoside, 1.5x10^{-5} s^{-1}, and dimer, 3.0x10^{-5} s^{-1}.

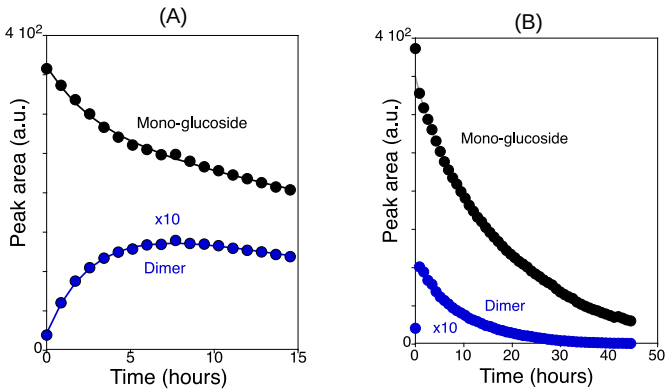

Figure 49 - (A) Degradation kinetics of malvidin 3-O-glucoside pH=8.1 (1x10^{-3} M) at 5 ºC (black) and formation of malvidin 3-O-glucoside dimer intermediate (blue); fitting of both curves can be achieved with a bi-exponential of rate constants k1=1.0x10^{-4} s^{-1} and k2= 6.3x10^{-6} s^{-1}; (B) the same of (A) at room temperature; neglecting the two first points the fitting can be achieved with a mono-exponential with rate constants for the monoglucoside and dimer respectively 1.5x10^{-5} s^{-1} and 3.0x10^{-5} s^{-1}.

The formation of any potential intermediate was also followed by ^{1}H NMR. Through analysis of the major spectral changes occurring in a 5-day window, and like was observed at 25 °C, several different intermediate species were found to gradually arise and decay over time - some glycosylated (Figure 50) -, though in these conditions 1 week wasn't still enough to get a spectral pattern as crowded as the one obtained at 25 °C at

T0. The decay of glycosylated intermediates (and subsequent glucose release) follows the decrease of the aromatic signals identified as H-4 and H-2'6' resonance signals from M3G dimers, suggesting that they represent the same compound. Moreover, the release of glucose appears to be secondary to the formation of malvidin-3-*O*-glucoside oligomers (slow process at NMR timescale). In addition, dimers seem to be in equilibrium with larger species, leading to larger peak width at half height and broader glucose signals.

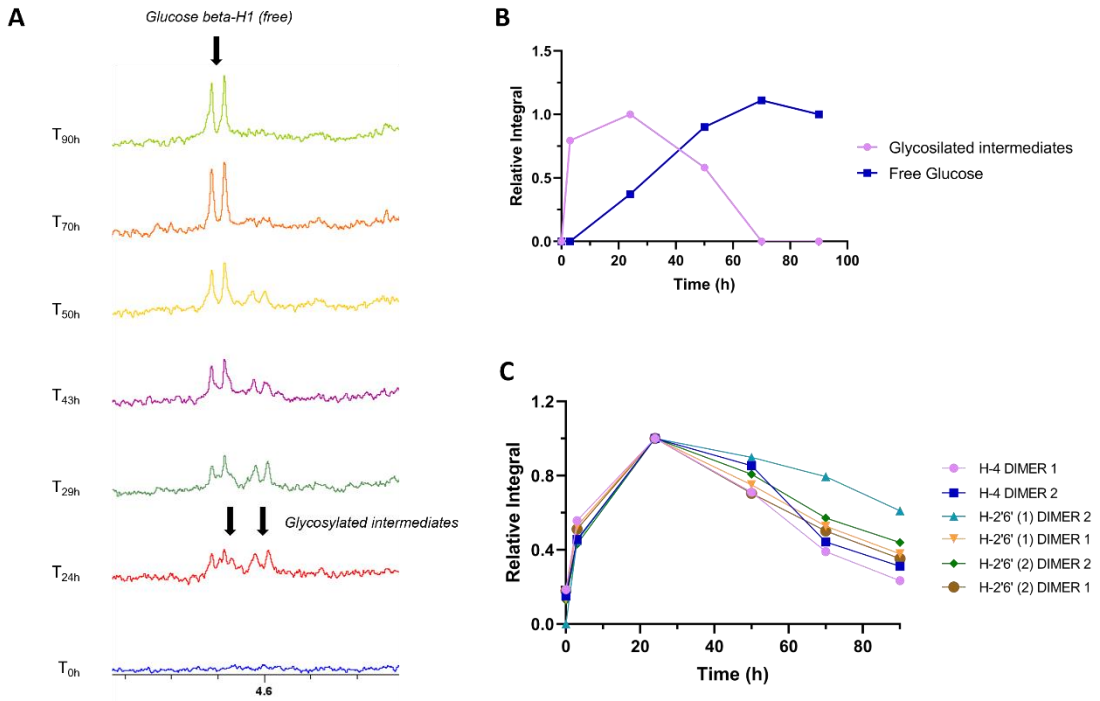

Figure 50 - a) Zoom-in of M3G NMR spectra (acquired at 5 °C) in the anomeric 1H region of D-glucose, where the appearance and disappearance of glycosylated intermediates were detected (b). The latter were found to correspond to type-A C4-C6 and C4-C8 M3G dimers whose kinetic decay accompanies the ones observed for their corresponding H-4 and H-2'6' aromatic signals (c).

A close inspection of Figure 51 (A) and knowing that two malvidin-3-*O*-glucoside dimers were detected by mass spectrometry in the positive ion mode (as described above), a tentative assignment of these intermediates was accomplished by 1D and 2D proton NMR. It can be observed in the ^{1}H NMR spectrum the appearance over time of two protons (in different ratios) corresponding to the protons H-4 of the terminal units of two malvidin-3-*O*-glucoside dimers. At 6.9-6.6 ppm, two sets of signals corresponding to protons H-2', and 6' present at the B-ring of the terminal, and the extension units of each malvidin-3-*O*-glucoside dimer were also found to occur. According to these results, two possible structures could be assigned to the malvidin-3-*O*-glucoside dimer as presented in Figure 48, the A and the B-type dimers. From the 2D analysis (COSY), it was possible

to observe two correlations at around 2.6 ppm with protons at 3.3 ppm that should correspond to protons H-3 and H-4 from ring C of the flavene extension unit (Figure 51 B), which indicates that the linkage between the two malvidin-3-*O*-glucoside units should correspond to an A-type linkage as previously described to occur in grapes and wines. The presence of two isomers should correspond to C-4/C-8 (major isomer) and C-4/C-6 (minor isomer) (Figure 51 B).

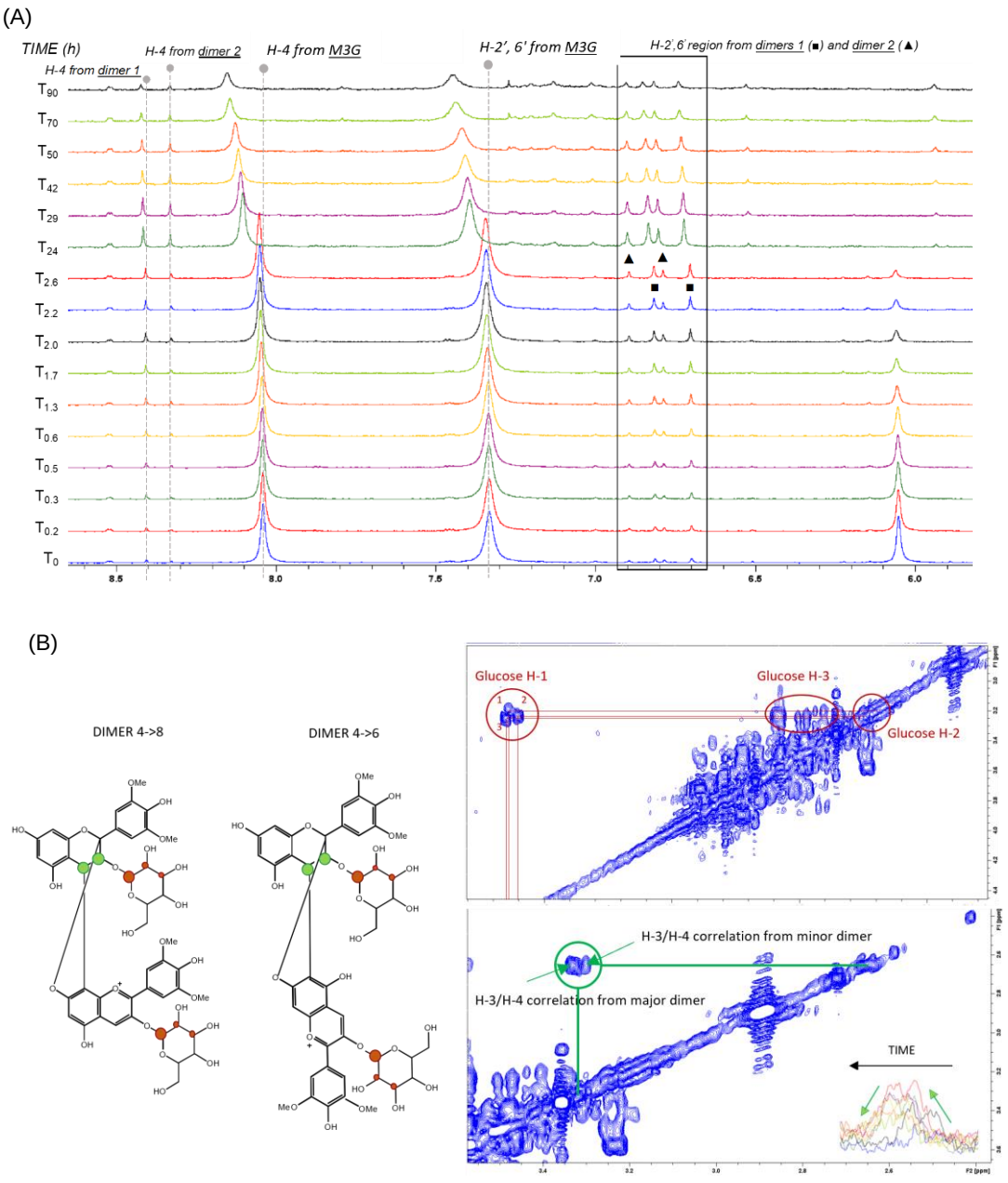

Figure 51 - A) ^{1}H NMR spectra in the aromatic region of M3G at 1x10^{-3} M taken at different time points. Spectra were acquired at 5 °C. B) COSY spectra showing H-3/H-4 correlation from ring C of the extension unit of dimers and correlations of anomeric proton H-1 and protons H-2 and H-3 from the glucose moiety. 1- Anomeric beta-H-1 from minor dimer (2 moieties); 2- Anomeric beta-H-1 from major dimer (2 moieties); 3- Anomeric beta-H-1 from glucose (by chemical shift referencing).

As expected, there is a temperature dependence of the M3G diffusion coefficient (Table 19). The signal(s) (i.e. moiety) identified before as the anomeric beta-H-1 of glucose from M3G dimers have a lower diffusion coefficient than glucose when freed, and therefore a higher molecular weight. Of note, diffusion coefficients were determined at T 24 h (where intermediate dimer signals reached their maximum intensity) except for D-glucose whose diffusion coefficient was calculated at T 90 h. Also, M3G appears to be in fast exchange with heavier structural conformers (with longer T2 values) characterized by a high degree of order (reflected by slow longitudinal (T1) relaxation) and these effects increase over time (Figure 52).

Bearing all this, it seems that M3G degradation at the transition pHs follows two different pathways; 1) condensation, followed by glucose hydrolysis, and 2) auto-association (which may be the first step) triggering condensation reactions. The formation of the dimer and respective oligomers in M3G increases dramatically along with the anthocyanin concentration.

Table 19 - Diffusion coefficients determined at 5 and 25 ºC for different protons signals during M3G degradation.

	5 °C		25 °C	
	Chemical Shift (ppm)	Diffusion coefficient (m^2/s)	Chemical Shift (ppm)	Diffusion coefficient at (m^2/s)
TSP	0.00	$3.98 \times 10^{-10} \pm 5.58 \times 10^{-12}$	0.00	$8.59 \times 10^{-10} \pm 6.17 \times 10^{-12}$
M3G H-4	8.04	$1.95 \times 10^{-10} \pm 3.69 \times 10^{-12}$	8.13	$3.54 \times 10^{-10} \pm 5.49 \times 10^{-12}$
M3G H-2'6'	7.33	$1.87 \times 10^{-10} \pm 3.42 \times 10^{-12}$	7.45	$4.30 \times 10^{-10} \pm 2.52 \times 10^{-12}$
M3G dimer 1 (H-2'6')	6.72	$1.74 \times 10^{-10} \pm 3.30 \times 10^{-12}$	---	---
M3G dimer 2 (H-2'6')	6.80	$1.85 \times 10^{-10} \pm 7.66 \times 10^{-12}$	---	---
Conjugated glucose	4.59	$1.50 \times 10^{-10} \pm 1.07 \times 10^{-11}$	---	---
(D)-Glucose	4.65 (ß)	$4.32 \times 10^{-10} \pm 4.62 \times 10^{-12}$	5.24 (α)	$8.26 \times 10^{-10} \pm 2.61 \times 10^{-11}$
(D)-Glucose Standard	---	---	5.24 (α)	$8.31 \times 10^{-10} \pm 3.55 \times 10^{-12}$

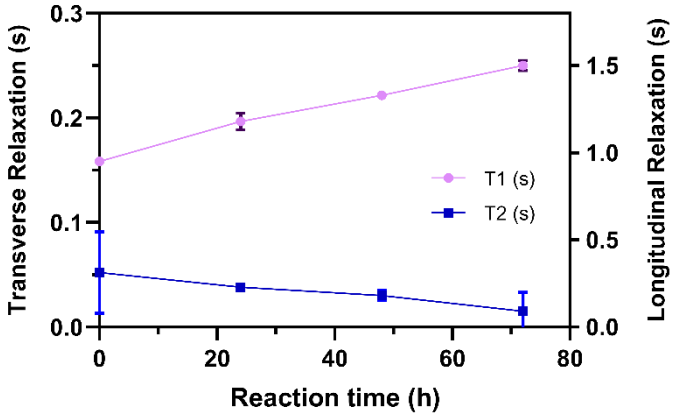

Figure 52 - T1/T2 relaxation measurements (determined for M3G H-4) over time.

3.5. M3,5diG – DEGRADATION PRODUCTS

Identical HPLC experiments were carried out for M3,5diG (Figure 53). In contrast to M3G, no clear evidence for the formation of colored dimers and oligomers was achieved. Moreover, the degradation rate of M3,5diG is much slowly than M3G, and after 7 days circa 33 % of the flavylium cation is recovered in contrast with circa 21 % in the case of M3G after 1 day. The slower degradation rates of M3,5diG in comparison to M3G are also observed in acidic medium. After standing M3G for 14 days at pH=4 its disappearance is circa 4 %, while M3,5diG in identical conditions is <1 %. This contrasts with the faster degradation rate of M3,5diG at higher pH values in comparison with M3G, as reported above in Figure 45 (explained by the higher instability of $B4^{2-}$).

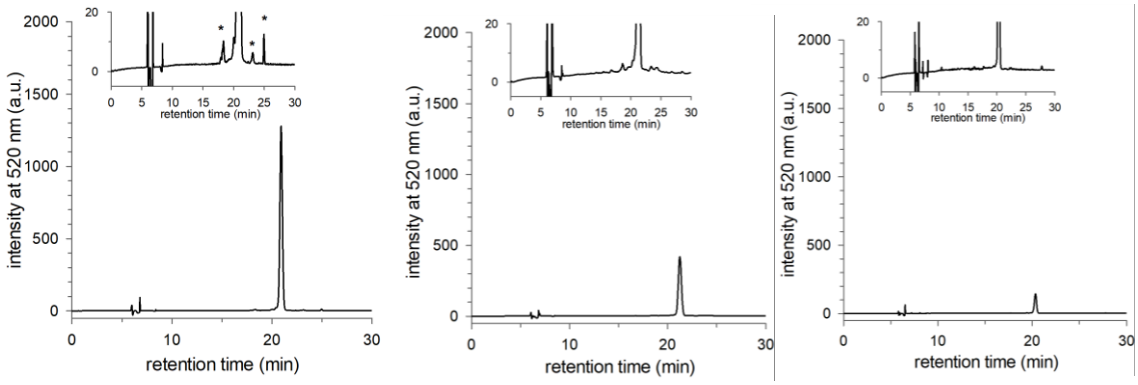

Figure 53 - HPLC chromatograms of M3,5diG solution for the representative transition pH 7.4 ($1x10^{-3}$ M) (a) after 2 hours; (b) after 7 days, and for pH 9 after 3 days for the same M3,5diG concentration (c) Unidentified impurities are marked with an asterisk (*) in the inset and exist in commercial stock.

The analysis by LC-MS in a positive mode of M3,5diG solution revealed the presence of different ion masses (Table 20). Diglucosylated (m/z 655) and monoglucosylated (m/z 493) forms of malvidin were detected, considering the typical fragmentation pattern characteristic of anthocyanins corresponding to the loss of glucose units (m/z 162), Figure 54. The cross-ring cleavage, which includes the breakdown of two C-ring bonds, is one of the anthocyanin fragmentation mechanisms common with other flavonoids. Type A fragments are the same for the majority of anthocyanidin species (just a few have different substituents on the A ring), however, type B fragments vary depending on the type of anthocyanidin due to changes in substituents on the B ring (394). LC-MS analysis revealed the existence of potential fragments of the B ring via two alternative cleavage pathways, indicating a different degradation process than M3G (Figure 54). In the case of monoglucoside, different degradation pathways were identified, including one associated with the formation of dimers and trimers, as well as another associated with the loss of glucose, which resulted in the aglycone form and broken down into the most common form, yielding the respective phenolic acid and aldehyde. In the instance of diglucoside, loss of glucose units was also seen, creating the monoglucoside and aglycone forms. Aglycone is not identified as a degradation product because it undergoes quick cleavage of the C ring, forming various fragments of the B ring. Surprisingly, since it was not visible in the chromatographic profile by HPLC-DAD, it was identified the masses corresponding to the type A dimer of the aglycone in hydrated form and a derivative (classified as a derivative due to the fragmentation pattern being the same as that of the dimer except for the mass m/z 774 which corresponds to the loss of an H_2O moiety from the principal ion).

Table 20 - Ion masses in the positive ion mode of the degradation products formed during degradation of M3,5-diG at slightly basic conditions.

Compound	$[M^+]$	$[MS^2]$	$[MS^3]$	Possible identity
1	195	138; 166; 148	110	Fragment B^+
2	227	209	95	No identified
3	181	153; 170	137; 124; 109; 97	Fragment B^+ isomer
4	655	493; 331	331	Malvidin-3,5-diglucoside
5	493	331	177	Malvidin-3-*O*-glucoside

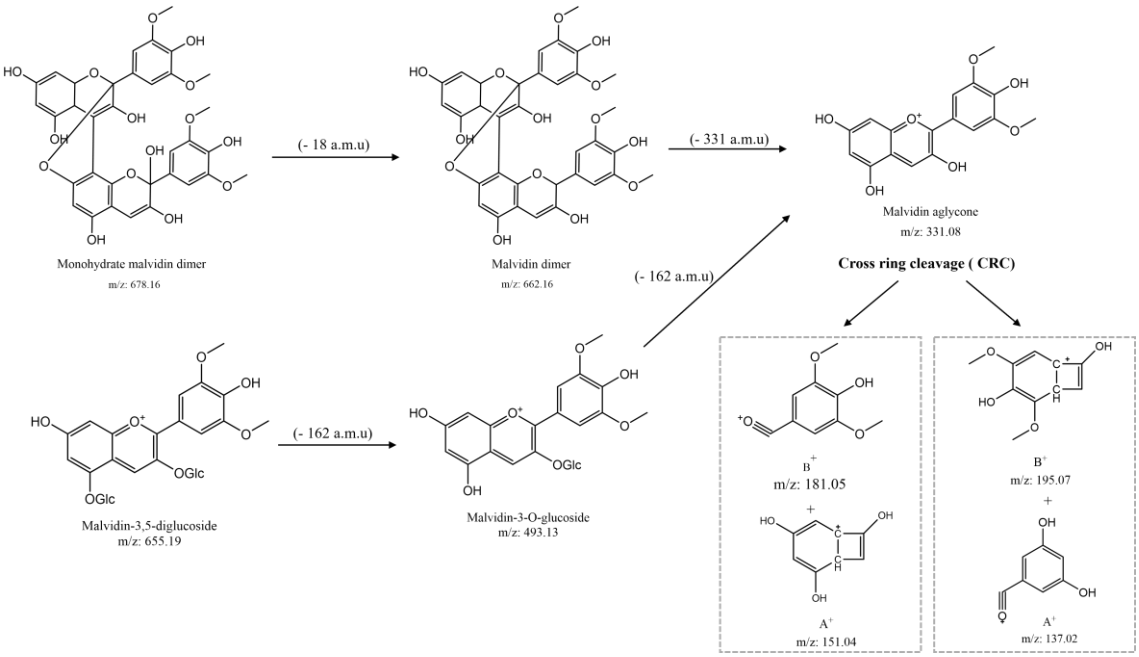

Figure 54 - Proposed structures and mechanisms for Malvidin-3,5-diglucoside.

3.5.1. EXPERIMENTAL EVIDENCE OF $B4^{2-}$ BY NMR

The B4 adduct was previously reported in the 1980s by McClelland and co-workers (395) upon a reverse pH jump from equilibrated solutions at moderately acidic pHs to pH=1, Figure 55. B4 results from the flavylium cation hydration in position 4 and is formed together with hydration in position 2 (to give hemiketal, B), but differently from the last, it is a kinetic product, because does not give directly cis-chalcone. The system evolves toward the equilibrium only from B2. B4 was exclusively observed in synthetic flavylium compounds lacking hydroxyl substituents. In the case of ACs and other flavylium cations bearing hydroxyl substituents, B4 is not detected in an acidic medium because quinoidal base formation is by far much faster than any hydration reaction in position 2 or 4.

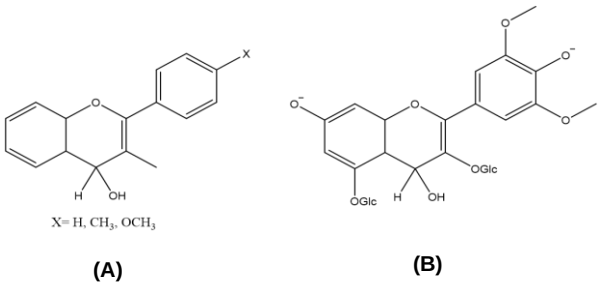

Figure 55 - A); Chemical formula of the B4 adduct reported by McClelland *et al*. (395) (B) proposed chemical formula for $B4^{2-}$ species of M3,5diG.

According to the results obtained for the kinetic of the M3,5diG by UV-Vis spectroscopy, the formation of $B4^{2-}$ in equilibrium with A^- occurs in a few seconds. However, the kinetics of this species' disappearance was monitored by UV-Vis and NMR (600 MHz) lowering the temperature to 5 ºC to decrease the rate of $B4^{2-}$ disappearance. A direct pH jump to 11.9 monitored by a standard spectrophotometer demonstrated a ratio of the absorbances ($A_{600}^{11.9}$ = 0.60 vs $A_{600}^{8.7}$ = 3.05) indicating that ca 80 % of M3,5diG was converted in $B4^{2-}$. Considering that the acidity constants between AH^+ and A^- is pK=7 and between A^- and $B4^{2-}$ is pK=10.7, a direct pH jump to pH=8.7 would convert almost 100% of flavylium cation in anionic quinoidal base, without significant formation of $B4^{2-}$, Figure 56 dashed blue line. Conversely, after a direct pH jump to pH=11.9, the equilibrium between A^- to form $B4^{2-}$ is established, Figure 56.

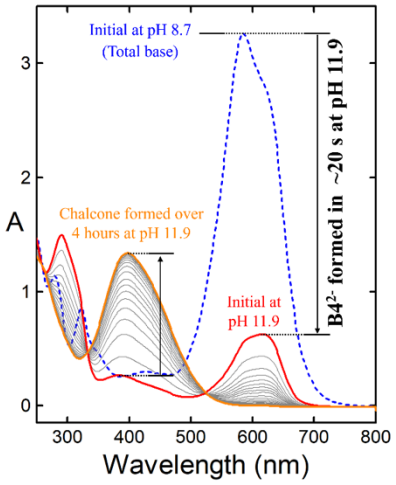

Figure 56 - Spectral variations of M3,5diG ($2.0x10^{-4}$ M, 5 °C) after a direct pH jump from pH=1 to pH=11.9 (full lines) and the first spectrum after a pH jump from pH=1 to pH=8.7 with the same concentration (dashed blue line).

Knowing this behavior, the above experiment was replicated monitoring the evolution of the system by ^1H NMR spectroscopy, using 10 % D_2O to allow for the locking of the magnetic field but otherwise in the same conditions, including the same concentrations of anthocyanin and buffer. With suppression of the water signal (using the NOESY 1D pulse sequence) sequence of clear spectra throughout *ca*. 24 h, was obtained, Figure 57 A. In this experiment, it is clear that there is a set of signals present at its highest intensity in the beginning and immediately starts to decrease in intensity. Also, there is a set of signals that can be attributed to the chalcones since they are increasing with time, and finally, another set that remains constant throughout the experiment, some of which we know to belong to the buffers used. Focusing our attention on the set of signals that decreases in intensity, the respective integrals were plotted against time and mono-

exponential decays with an average kinetic constant of 4.3×10^{-4} s^{-1} were obtained, which compares well with the one determined for the formation of the chalcone (5.2×10^{-4} s^{-1}), taken from the data in Figure 56, thus supporting our hypothesis that we are correctly identifying the signals of the kinetic reservoir species. The last spectrum (after *ca.* 24 h) was subtracted from the first one and the resulting difference spectrum, Figure 57 B, clearly shows the set of signals belonging to the transient species in agreement with our hypothesis of it being $B4^{2-}$ due to their multiplicity and integration.

To discard that these signals could belong to the anionic quinoidal base, a second pH jump monitored by ^{1}H NMR was made, this time from pH=1 to pH=8.7, replicating the experiment previously followed with UV-Vis spectroscopy. A sequence of spectra following the pH jump was acquired and as expected from the absorption data, no significant changes were observed. In Figure 57 B the first spectrum is shown for comparison, and it is clear that it does not correspond to the set of transient signals, thus reinforcing our assumption that they belong to $B4^{2-}$.

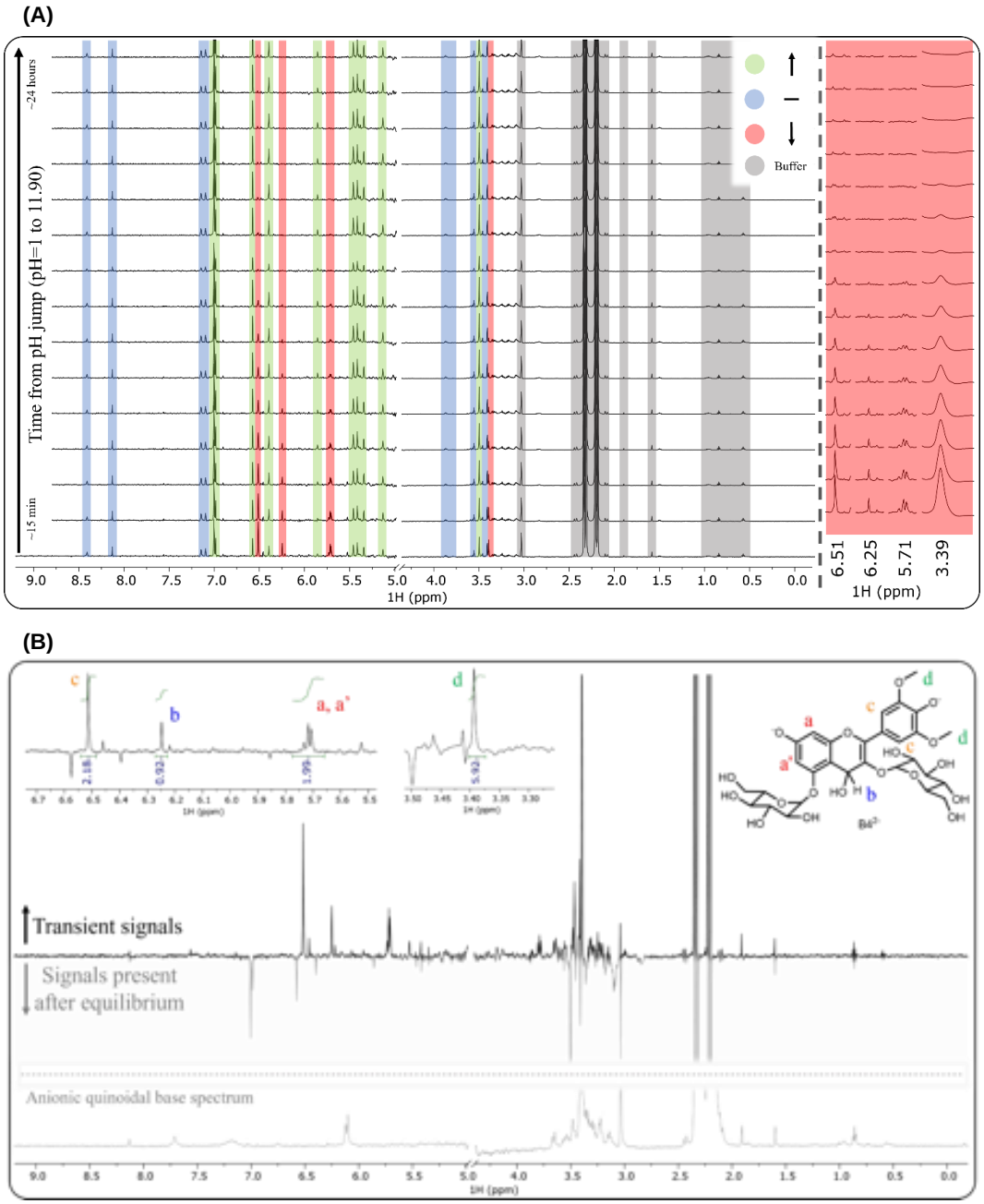

Figure 57 – (A) ^{1}H NMR consecutive spectra of M3,5diG (2.0×10^{-4} M) after a direct pH jump from pH=1 to pH=11.9 over ca. 24 hours. Highlighted in red are the signals whose intensity decreases until they can no longer be observed, in green the ones whose intensity increases over time, in blue and grey, the ones that remain practically unchanged over time, with the ones in grey corresponding to the signals of the buffers used to adjust the pH. The rightmost part of the image shows a zoom of the signals whose intensity decreases, highlighted in red. The irradiated water signal (4.66 ppm) was omitted for clarity. (B) Difference ^{1}H NMR spectrum of M3,5diG between the spectra ca. 15 min and ca. 24 h after a direct pH jump from pH=1 to pH=11.9. The positive signals are the ones present in the beginning and absent in the end and vice-versa for the negative ones. The bottom part of the image shows the ^{1}H NMR spectrum of the anionic quinoidal base for comparison. The small positive peaks are those of the minor anionic quinoidal base at ca. 15 min.

4. CONCLUSIONS

In conclusion, the exploration of anthocyanin chemistry requires a comprehensive investigation extending into the basic medium. The holistic approach presented in this work allowed the disclosure of a pH range (transition pHs), that includes the physiologic pH, in the frontier between the acidic and basic paradigms, where crucial transformations such as hydration and OH^- nucleophilic addition occur slowly. In this pH range, anionic quinoidal bases are the main reversible species and complex degradation processes control their disappearance.

Malvidin diglucoside presents a pre-equilibrium involving the anionic quinoidal base and a new transient species resulting from the OH^- attack in position C4, leading to the $B4^{2-}$ species identified by ^1H NMR. This shift from monoglucoside to diglucoside anthocyanins at physiologically relevant pH prompts inquiries into potential disparities in their antioxidant properties. Assuming that anthocyanins are rapidly absorbed in the stomach without hydrolysis and appear in the plasma within 30 min after digestion, the expected species in the case of the diglucoside are the pseudo-equilibrium species, while in monoglucoside are the neutral and anionic quinoidal bases. At the physiologic pH the malvidin monoglucoside not only gives a dimer and successive oligomers but also all these colored compounds degrade slowly (lifetime circa 3 days). The electronic structure of the ionized quinoidal base is essentially that of hydroquinone, a very good electron donor and thus promptly oxidized in the presence of mild oxidants. It is thus not a surprise that in physiologic pH the anthocyanins monoglucoside, existing mainly in the A^- form, behave as very efficient antioxidants.

Thus, the distinct behaviors observed between monoglucoside and diglucoside anthocyanins emphasize the necessity for further exploration to elucidate their respective roles and impacts, particularly in biological systems. Understanding these nuances is crucial for unraveling the full potential of anthocyanins in health and nutrition.

CHAPTER IV

CONCLUDING REMARKS AND FUTURE PERSPECTIVES

In conclusion, this project contributed to advancing sustainable and circular practices by transforming agro-industrial by-products like anthocyanins and lignin into high-value applications. This work introduces lignin as an effective stabilizer and quality enhancer in food and beverage applications and establishes eco-conscious methods for extracting and repurposing lignin from agricultural waste. In another approach, it enhances the use of anthocyanins as stable and natural colorants, evaluating the chemical stability of these compounds under different acyl and glycosyl groups.

Vine shoots are generated annually in large quantities and are often left in agricultural fields or burned. The extraction of lignin using a mild acidolysis method with dioxane allowed for the isolation of a biopolymer without significant structural changes compared to native lignin. Optimized conditions for a greener and more environmentally friendly methodology were successful, resulting in lignin with a higher degree of purity and a significant amount of condensed structures. The nanoparticles prepared with this lignin also demonstrated promising properties for future applications, including in areas such as agriculture and environmental science, since lignin nanoparticles have also been previously used for the stabilization of colors of anthocyanin derivatives. Additionally, soluble lignin and LNPs demonstrated higher antioxidant activity than commercial antioxidants.

In a technological approach, lignosulfonates, along with kraft and organosolv lignin, were applied as modulating agents for the physicochemical properties of Port wine. Notably, lignosulfonates and kraft lignin demonstrated a positive effect in several areas, particularly in the removal of proteins and tannins, which are associated with turbidity and astringency, respectively. Supporting this, wines treated with lignosulfonates also showed reduced interaction with proline-rich acidic salivary proteins, which are involved in the perception of astringency. Additionally, lignosulfonates increased the amount of phenolic compounds, including anthocyanins, and had a positive impact on volatile compounds, reducing undesirable volatiles such as isoamyl alcohol and 1-hexanol and enhancing fruity aromas. Colorimetric results suggest that the slightly yellowish color of lignin, which is one of the key restrictions for its utilization in some applications, did not interfere with the visual color of the wine. These initial results were very promising, suggesting new approaches such as using different lignin sources, which can also be by-products, or chemically modifying lignin to enhance performance and adsorption efficiency. Experiments with varying lignin ratios or combining lignin with other fining agents like bentonite could yield better outcomes. To achieve full circularity in the wine

industry, using lignin extracted from vine shoots by the dioxane method or other alternative methods for wine clarification could be highly beneficial.

Considering the results obtained in the previous work related to the increase in the amount of anthocyanins due to the action, especially of lignosulfonates, they were applied as stabilizing agents for the red color of anthocyanins. As previously mentioned, one of the major challenges of these compounds is color loss due to hydration reactions in chemical equilibria that promote the formation of colorless species. Lignosulfonates proved to be promising by shifting the chemical equilibrium towards the flavylium cation formation, maintaining the red color at higher pH levels. While acylation protects the anthocyanin structure through intramolecular copigmentation phenomena, this study demonstrated that the complex formation between lignosulfonates and C3G is driven by electrostatic interactions and hydrophobic effects, dependent on the pH under study. In addition to color stability, the results were very favorable regarding the redox properties of the LS-C3G complex, showing oxidative protection of C3G in the presence of lignosulfonates. The oxidation of anthocyanins is also a limiting factor for the application of these compounds due to the formation of undesired differently colored species.

Anthocyanins are one of the most promising compounds used as natural colorants due to their natural and diverse color palette and potential health benefits, particularly their high antioxidant activity. These compounds can be extracted from several food byproducts, such as blackberries, blueberries, red cabbage, and purple sweet potatoes, generated in large quantities during juices or other derivatives production, or as fruits and vegetables that may not be sold to consumers. Polyacylated anthocyanins are stable across a wide pH range, even when exposed to high temperatures and external agents such as bisulfite, maintaining their appealing hues over time. The complex structure with many acyl groups protects the flavylium nucleus from hydrated reactions through intramolecular copigmentation. Depending on the composition and pH of the food matrix, it will be possible to obtain different appealing and interesting colors for the industry, following consumer trends towards increasingly natural products.

The glycosylation pattern, like acylation, had a significant impact on the stability of anthocyanins, resulting in different degradation rates and products for M3G and M3,5DiG. A study conducted within a still underexplored pH range, known as the transition pH, which includes the physiologic pH (7.4) and the pH of some fruits and vacuoles where the natural blue color of anthocyanins predominates, demonstrated that

a lower number of sugars in the structure leads to faster degradation and the formation of polymeric structures that mitigate color loss. The presence of different species at this pH range can have different effects on biological systems such as the antioxidant activity modification.

To finish, our research contributes valuable insights into the stabilization and practical application of natural compounds, addressing critical environmental challenges and promoting sustainable practices. This work aligns with several United Nations Sustainable Development Goals (SDGs), including Good Health and Well-being (SDG 3), Responsible Consumption and Production (SDG 12), Decent Work and Economic Growth (SDG 8), Climate Action (SDG 13), and Partnerships for the Goals (SDG 17), by valorizing agri-food byproducts to create new value-added products, reducing waste, promote circularity, and foster collaborations between researchers and industries.

FUTURE PERSPECTIVES should focus on the chemical and color stabilization of anthocyanins and their derivatives using different types of lignin, employing both covalent (chemical functionalization) and non-covalent interactions. These interactions can be investigated by addressing various parameters such as pH, temperature, light exposure, presence of oxygen, and other species in the matrix to better understand the protective impact of lignin and its interactions with different anthocyanin species in equilibrium. Additionally, future studies can explore more environmentally friendly methods of extracting lignin from agri-food byproducts, such as using ionic liquids, deep eutectic solvents, or supercritical fluids, and relate their properties.

The process of valorizing by-products should continue by identifying those generated on a large scale that can be sources of bioactive compounds or macronutrients and finding potential ways to reintroduce them into the market chain. Creating connections between producers and those capable of valorizing these by-products is another significant emphasis, contributing to circularity and sustainability.

BIBLIOGRAPHY

1. Nations U. World population projected to reach 9.8 billion in 2050, and 11.2 billion in 2100 [Available from: https://www.un.org/en/desa/world-population-projected-reach-98-billion-2050-and-112-billion-2100].

2. FAO. Global food losses and food waste – Extent, causes and prevention. Rome; 2011.

3. FAO I, UNICEF, WFP and WHO. The State of Food Security and Nutrition in the World 2023. Urbanization, agrifood systems transformation and healthy diets across the rural-urban continuum. FAO I, UNICEF, WFP, WHO, editor. Rome; 2023.

4. Programme UNE. Food Waste Index Report 2021. Nairobi; 2021.

5. Mokrane S, Buonocore E, Capone R, Franzese PP. Exploring the Global Scientific Literature on Food Waste and Loss. Sustainability. 2023; 15(6).

6. Rațu RN, Veleșcu ID, Stoica F, Usturoi A, Arsenoaia VN, Crivei IC, et al. Application of Agri-Food By-Products in the Food Industry. Agriculture. 2023; 13(8).

7. Arruda HS, Silva EK, Peixoto Araujo NM, Pereira GA, Pastore GM, Marostica Junior MR. Anthocyanins Recovered from Agri-Food By-Products Using Innovative Processes: Trends, Challenges, and Perspectives for Their Application in Food Systems. Molecules. 2021; 26(9).

8. Madia VN, De Vita D, Ialongo D, Tudino V, De Leo A, Scipione L, et al. Recent Advances in Recovery of Lycopene from Tomato Waste: A Potent Antioxidant with Endless Benefits. Molecules. 2021; 26(15).

9. Ruano P, Delgado LL, Picco S, Villegas L, Tonelli F, Merlo MEA, et al. Extraction and Characterization of Pectins From Peels of Criolla Oranges (Citrus sinensis): Experimental Reviews. In: Martin M, editor. Pectins. Rijeka: IntechOpen; 2019. p. Ch. 1.

10. Nirmal NP, Santivarangkna C, Rajput MS, Benjakul S, Maqsood S. Valorization of fish byproducts: Sources to end-product applications of bioactive protein hydrolysate. Comprehensive Reviews in Food Science and Food Safety. 2022;21(2):1803-42.

11. Ahmed M, Verma AK, Patel R. Collagen extraction and recent biological activities of collagen peptides derived from sea-food waste: A review. Sustainable Chemistry and Pharmacy. 2020;18:100315.

12. Ferreira SM, Santos L. A Potential Valorization Strategy of Wine Industry by-Products and Their Application in Cosmetics—Case Study: Grape Pomace and Grapeseed. Molecules. 2022; 27(3).

13. de Queiroz RS, da Silva APV, Broega ACdL, Souto APGV. New Brazilian pineapple leaf fibers for textile application: cottonization and dyeing performance. Discover Applied Sciences. 2019;2(1):72.

14. Iram A, Berenjian A, Demirci A. A Review on the Utilization of Lignin as a Fermentation Substrate to Produce Lignin-Modifying Enzymes and Other Value-Added Products. Molecules. 2021;26(10).

15. Zhang L, Han Z, Granato D. Chapter One - Polyphenols in foods: Classification, methods of identification, and nutritional aspects in human health. In: Granato D, editor. Advances in Food and Nutrition Research. 98: Academic Press; 2021. p. 1-33.

16. Vauzour D, Rodriguez-Mateos A, Corona G, Oruna-Concha MJ, Spencer JP. Polyphenols and human health: prevention of disease and mechanisms of action. Nutrients. 2010;2(11):1106-31.

17. Rudrapal M, Khairnar SJ, Khan J, Dukhyil AB, Ansari MA, Alomary MN, et al. Dietary Polyphenols and Their Role in Oxidative Stress-Induced Human Diseases: Insights Into Protective Effects, Antioxidant Potentials and Mechanism(s) of Action. Frontiers in Pharmacology. 2022;13.

18. Rana A, Samtiya M, Dhewa T, Mishra V, Aluko RE. Health benefits of polyphenols: A concise review. Journal of Food Biochemistry. 2022;46(10):e14264.

19. Farjadmand F, Karimpour-Razkenari E, Nabavi SM, Ardekani MRS, Saeedi M. Plant Polyphenols: Natural and Potent UV-Protective Agents for the Prevention and Treatment of Skin Disorders. Mini Reviews in Medicinal Chemistry. 2021;21(5):576-85.

20. Tsimogiannis D, Oreopoulou V. Chapter 16 - Classification of Phenolic Compounds in Plants. In: Watson RR, editor. Polyphenols in Plants (Second Edition): Academic Press; 2019. p. 263-84.

21. Chandra SR, Diwan AD, Panche AN. Flavonoids: an overview. Journal of Nutritional Science. 2016;5:e47.

22. Freitas V, Mateus N. Protein/Polyphenol Interactions: Past and Present Contributions. Mechanisms of Astringency Perception. Current Organic Chemistry. 2012;16:724-46.

23. Gould KS. Nature's Swiss Army Knife: The Diverse Protective Roles of Anthocyanins in Leaves. Journal of Biotechnology and Biomedicine. 2004;2004(5):314-20.

24. Landi M, Tattini M, Gould KS. Multiple functional roles of anthocyanins in plant-environment interactions. Environmental and Experimental Botany. 2015;119:4-17.

25. Gonçalves AC, Nunes AR, Falcão A, Alves G, Silva LR. Dietary Effects of Anthocyanins in Human Health: A Comprehensive Review. Pharmaceuticals (Basel). 2021;14(7).

26. Wu X, Beecher GR, Holden JM, Haytowitz DB, Gebhardt SE, Prior RL. Concentrations of Anthocyanins in Common Foods in the United States and Estimation of Normal Consumption. Journal of Agricultural and Food Chemistry. 2006;54(11):4069-75.

27. Giusti MM, Wrolstad RE. Acylated anthocyanins from edible sources and their applications in food systems. Biochemical Engineering Journal. 2003;14(3):217-25.

28. Mazza GM, E. . Anthocyanins in Fruits, Vegetables and Grains. 1st Edition ed. Boca Raton - Florida: John Wiley & Sons, Ltd; 1993 1994/01/01.

29. Reyes BAS, Dufourt EC, Ross J, Warner MJ, Tanquilut NC, Leung AB. Chapter 4 - Selected Phyto and Marine Bioactive Compounds: Alternatives for the Treatment of Type 2 Diabetes. In: Atta ur R, editor. Studies in Natural Products Chemistry. 55: Elsevier; 2018. p. 111-43.

30. He J, Giusti MM. Anthocyanins: Natural Colorants with Health-Promoting Properties. Annual Review of Food Science and Technology. 2010;1(1):163-87.

31. Heredia FJ, Francia-Aricha EM, Rivas-Gonzalo JC, Vicario IM, Santos-Buelga C. Chromatic characterization of anthocyanins from red grapes—I. pH effect. Food Chemistry. 1998;63(4):491-8.

32. Kong J-M, Chia L-S, Goh N-K, Chia T-F, Brouillard R. Analysis and biological activities of anthocyanins. Phytochemistry. 2003;64(5):923-33.

33. Andersen OJ, M.;. Basic Anthocyanin Chemistry and Dietary sources. In: Wallace TCG, M.M., editor. Anthocyanins in Health and Disease. Boca Raton - Florida: CRC Press, Taylor´s 2010. p. 14-65.

34. Borkowski T, Szymusiak H, Gliszczyńska-Swigło A, Tyrakowska B. The effect of 3-O-β-glucosylation on structural transformations of anthocyanidins. Food Research International. 2005;38(8):1031-7.

35. Zhao C-L, Yu Y-Q, Chen Z-J, Wen G-S, Wei F-G, Zheng Q, et al. Stability-increasing effects of anthocyanin glycosyl acylation. Food Chemistry. 2017;214:119-28.

36. Dangles O, Fenger J-A. The Chemical Reactivity of Anthocyanins and Its Consequences in Food Science and Nutrition. Molecules. 2018; 23(8).

37. Escribano-Bailón MT, Santos-Buelga C, Rivas-Gonzalo JC. Anthocyanins in cereals. Journal of Chromatography A. 2004;1054(1):129-41.

38. Fenger J-A, Robbins RJ, Collins TM, Dangles O. The fate of acylated anthocyanins in mildly heated neutral solution. Dyes and Pigments. 2020;178:108326.

39. Fenger J-A, Moloney M, Robbins RJ, Collins TM, Dangles O. The influence of acylation, metal binding and natural antioxidants on the thermal stability of red cabbage anthocyanins in neutral solution. Food & Function. 2019;10(10):6740-51.

40. Trouillas P, Sancho-García JC, De Freitas V, Gierschner J, Otyepka M, Dangles O. Stabilizing and Modulating Color by Copigmentation: Insights from Theory and Experiment. Chemical Reviews. 2016;116(9):4937-82.

41. Fulcrand H, Atanasova V, Salas E, Cheynier V. The Fate of Anthocyanins in Wine: Are There Determining Factors? Red Wine Color. ACS Symposium Series. 886: American Chemical Society; 2004. p. 68-88.

42. Berké B, Chèze C, Vercauteren J, Deffieux G. Bisulfite addition to anthocyanins: revisited structures of colourless adducts. Tetrahedron Letters. 1998;39(32):5771-4.

43. Fulcrand H, Benabdeljalil C, Rigaud J, Cheynier V, Moutounet M. A new class of wine pigments generated by reaction between pyruvic acid and grape anthocyanins. Phytochemistry. 1998;47(7):1401-7.

44. Bakker J, Timberlake CF. Isolation, Identification, and Characterization of New Color-Stable Anthocyanins Occurring in Some Red Wines. Journal of Agricultural and Food Chemistry. 1997;45(1):35-43.

45. Mateus N, de Freitas V. Evolution and Stability of Anthocyanin-Derived Pigments during Port Wine Aging. Journal of Agricultural and Food Chemistry. 2001;49(11):5217-22.

46. Oliveira J, Fernandes V, Miranda C, Santos-Buelga C, Silva A, de Freitas V, et al. Color Properties of Four Cyanidin−Pyruvic Acid Adducts. Journal of Agricultural and Food Chemistry. 2006;54(18):6894-903.

47. Jordheim M, Fossen T, Songstad J, Andersen ØM. Reactivity of Anthocyanins and Pyranoanthocyanins. Studies on Aromatic Hydrogen–Deuterium Exchange Reactions in Methanol. Journal of Agricultural and Food Chemistry. 2007;55(20):8261-8.

48. Bueno JM, Sáez-Plaza P, Ramos-Escudero F, Jiménez AM, Fett R, Asuero AG. Analysis and Antioxidant Capacity of Anthocyanin Pigments. Part II: Chemical Structure, Color, and Intake of Anthocyanins. Critical Reviews in Analytical Chemistry. 2012;42(2):126-51.

49. Cruz L, Basílio N, Mateus N, de Freitas V, Pina F. Natural and Synthetic Flavylium-Based Dyes: The Chemistry Behind the Color. Chemical Reviews. 2022;122(1):1416-81.

50. He F, Liang N-N, Mu L, Pan Q-H, Wang J, Reeves MJ, et al. Anthocyanins and Their Variation in Red Wines I. Monomeric Anthocyanins and Their Color Expression. Molecules. 2012; 17(2):[1571-601 pp.].

51. Pina F. Thermodynamics and kinetics of flavylium salts Malvin revisited. Journal of the Chemical Society, Faraday Transactions. 1998;94(15):2109-16.

52. Brouillard R, Delaporte B. Chemistry of anthocyanin pigments. 2. Kinetic and thermodynamic study of proton transfer, hydration, and tautomeric reactions of malvidin 3-glucoside. Journal of the American Chemical Society. 1977;99(26):8461-8.

53. Andrés V, M.J V-S, Mateos-Aparicio I, Tenorio MD. Colour, bioactive compounds and antioxidant capacity of mixed beverages based on fruit juices with milk or soya. Journal of Food and Nutrition Research. 2014;53:71-80.

54. Markakis P, Jurd L. Anthocyanins and their stability in foods. C R C Critical Reviews in Food Technology. 1974;4(4):437-56.

55. Brouillard R, Lang J. The hemiacetal–cis-chalcone equilibrium of malvin, a natural anthocyanin. Canadian Journal of Chemistry. 1990;68(5):755-61.

56. Ahmed J, Shivhare US, Raghavan GSV. Thermal degradation kinetics of anthocyanin and visual colour of plum puree. European Food Research and Technology. 2004;218(6):525-8.

57. Oancea S. A Review of the Current Knowledge of Thermal Stability of Anthocyanins and Approaches to Their Stabilization to Heat. Antioxidants (Basel). 2021;10(9).

58. Nebesky EA, Esselen WB, Jr., et al. Stability of color in fruit juices. Food Research International. 1949;14(3):261-74.

59. Jackman R, Yada R, Tung M, Speers R. Anthocyanins as food colorants – A review. Journal of Food Biochemistry. 1987;11:201-47.

60. Furtado P, Figueiredo P, Chaves das Neves H, Pina F. Photochemical and thermal degradation of anthocyanidins. Journal of Photochemistry and Photobiology A: Chemistry. 1993;75(2):113-8.

61. Buren JPV, Bertino JJ, Robinson WB. The Stability of Wine Anthocyanins on Exposure to Heat and Light. American Journal of Enology and Viticulture. 1968;19(3):147.

62. Brouillard R. Chapter 1 - Chemical Structure of Anthocyanins. In: Markakis P, editor. Anthocyanins As Food Colors: Academic Press; 1982. p. 1-40.

63. Timberlake CF. Anthocyanins—Occurrence, extraction and chemistry. Food Chemistry. 1980;5(1):69-80.

64. Asen S, Stewart RN, Norris KH. Co-pigmentation of anthocyanins in plant tissues and its effect on color. Phytochemistry. 1972;11(3):1139-44.

65. Fleschhut J, Kratzer F, Rechkemmer G, Kulling SE. Stability and biotransformation of variousdietary anthocyanins in vitro. European Journal of Nutrition. 2006;45(1):7-18.

66. Sarni P, Fulcrand H, Souillol V, Souquet J-M, Cheynier V. Mechanisms of anthocyanin degradation in grape must-like model solutions. Journal of the Science of Food and Agriculture. 1995;69(3):385-91.

67. Francis FJ. A new group of food colorants. Trends in Food Science & Technology. 1992;3:27-30.

68. Dangles O, Saito N, Brouillard R. Anthocyanin intramolecular copigment effect. Phytochemistry. 1993;34(1):119-24.

69. Echeverria E, Burns J, Felle H. Compartmentation and cellular conditions controlling sucrose breakdown in mature acid lime fruits. Phytochemistry. 1992;31(12):4091-5.

70. Yoshida K, Kondo T, Okazaki Y, Katou K. Cause of blue petal colour. Nature. 1995;373(6512).

71. Brouillard R, Mazza G, Saad Z, Albrecht-Gary AM, Cheminat A. The co-pigmentation reaction of anthocyanins: a microprobe for the structural study of aqueous solutions. Journal of the American Chemical Society. 1989;111(7):2604-10.

72. Brouillard R, Chassaing S, Isorez G, Kueny-Stotz M, Figueiredo P. The Visible Flavonoids or Anthocyanins: From Research to Applications. Recent Advances in Polyphenol Research. 2: Blackwell Publishing Ltd; 2010. p. 1-22.

73. Brouillard R. The in vivo expression of anthocyanin colour in plants. Phytochemistry. 1983;22(6):1311-23.

74. Yoshida K, Kondo T, Goto T. Unusually stable monoacylated anthocyanin from purple yam dioscorea alata. Tetrahedron Letters. 1991;32(40):5579-80.

75. Goto T, Kondo T. Structure and Molecular Stacking of Anthocyanins—Flower Color Variation. Angewandte Chemie International 1991;30(1):17-33.

76. Dangles O, Saito N, Brouillard R. Kinetic and thermodynamic control of flavylium hydration in the pelargonidin-cinnamic acid complexation. Origin of the extraordinary flower color diversity of Pharbitis nil. Journal of the American Chemical Society. 1993;115(8):3125-32.

77. Dangles O, Brouillard R. Polyphenol interactions. The copigmentation case: thermodynamic data from temperature variation and relaxation kinetics. Medium effect. Canadian Journal of Chemistry. 1992;70(8):2174-89.

78. Rein MJ, Heinonen M. Stability and Enhancement of Berry Juice Color. Journal of Agricultural and Food Chemistry. 2004;52(10):3106-14.

79. Hernández-Herrero JA, Frutos MJ. Influence of rutin and ascorbic acid in colour, plum anthocyanins and antioxidant capacity stability in model juices. Food Chemistry. 2015;173:495-500.

80. Hoshino T, Matsumoto U, Goto T. Evidences of the self-association of anthocyanins I. Circular Dichroism of cyanin anhydrobase. Tetrahedron Letters. 1980;21(18):1751-4.

81. Hoshino T, Matsumoto U, Goto T, Harada N. Evidence for the self-association of anthocyanins IV. PMR spectroscopic evidence for the vertical stacking of anthocyanin molecules. Tetrahedron Letters. 1982;23(4):433-6.

82. Fernandes A, Brás NF, Mateus N, Freitas Vd. A study of anthocyanin self-association by NMR spectroscopy. New Journal of Chemistry. 2015;39(4):2602-11.

83. González-Manzano S, Santos-Buelga C, Dueñas M, Rivas-Gonzalo JC, Escribano-Bailón T. Colour implications of self-association processes of wine anthocyanins. European Food Research and Technology. 2008;226(3):483-90.

84. Houbiers C, Lima JC, Maçanita AL, Santos H. Color Stabilization of Malvidin 3-Glucoside: Self-Aggregation of the Flavylium Cation and Copigmentation with the Z-Chalcone Form. The Journal of Physical Chemistry B. 1998;102(18):3578-85.

85. Fernandes A, Brás NF, Mateus N, de Freitas V. Understanding the Molecular Mechanism of Anthocyanin Binding to Pectin. Langmuir. 2014;30(28):8516-27.

86. Buchweitz M, Speth M, Kammerer DR, Carle R. Stabilisation of strawberry (Fragaria x ananassa Duch.) anthocyanins by different pectins. Food Chemistry. 2013;141(3):2998-3006.

87. Fernandes A, Brás NF, Oliveira J, Mateus N, de Freitas V. Impact of a pectic polysaccharide on oenin copigmentation mechanism. Food Chemistry. 2016;209:17-26.

88. Fernandes A, Oliveira J, Fonseca F, Ferreira-da-Silva F, Mateus N, Vincken J-P, et al. Molecular binding between anthocyanins and pectic polysaccharides – Unveiling the role of pectic polysaccharides structure. Food Hydrocolloids. 2020;102:105625.

89. Zhao L, Pan F, Mehmood A, Zhang Y, Hao S, Rehman AU, et al. Protective effect and mechanism of action of xanthan gum on the color stability of black rice anthocyanins in model beverage systems. International Journal of Biological Macromolecules. 2020;164:3800-7.

90. Chung C, Rojanasasithara T, Mutilangi W, McClements DJ. Enhancement of colour stability of anthocyanins in model beverages by gum arabic addition. Food Chemistry. 2016;201:14-22.

91. Mourtzinos I, Makris DP, Yannakopoulou K, Kalogeropoulos N, Michali I, Karathanos VT. Thermal Stability of Anthocyanin Extract of Hibiscus sabdariffa L. in the Presence of β-Cyclodextrin. Journal of Agricultural and Food Chemistry. 2008;56(21):10303-10.

92. Fernandes A, Rocha MAA, Santos L, Brás J, Oliveira J, Mateus N, et al. Blackberry anthocyanins: β-Cyclodextrin fortification for thermal and gastrointestinal stabilization. Food Chemistry. 2018;245:426-31.

93. Fernandes A, Sousa A, Azevedo J, Mateus N, de Freitas V. Effect of cyclodextrins on the thermodynamic and kinetic properties of cyanidin-3-O-glucoside. Food Research International. 2013;51(2):748-55.

94. He Z, Zhu H, Xu M, Zeng M, Qin F, Chen J. Complexation of bovine β-lactoglobulin with malvidin-3-O-glucoside and its effect on the stability of grape skin anthocyanin extracts. Food Chemistry. 2016;209:234-40.

95. He Z, Xu M, Zeng M, Qin F, Chen J. Interactions of milk α- and β-casein with malvidin-3-O-glucoside and their effects on the stability of grape skin anthocyanin extracts. Food Chemistry. 2016;199:314-22.

96. Chung C, Rojanasasithara T, Mutilangi W, McClements DJ. Enhanced stability of anthocyanin-based color in model beverage systems through whey protein isolate complexation. Food Research International. 2015;76:761-8.

97. Chung C, Rojanasasithara T, Mutilangi W, McClements DJ. Stability improvement of natural food colors: Impact of amino acid and peptide addition on anthocyanin stability in model beverages. Food Chemistry. 2017;218:277-84.

98. Cahyana Y, Gordon MH. Interaction of anthocyanins with human serum albumin: Influence of pH and chemical structure on binding. Food Chemistry. 2013;141(3):2278-85.

99. Zang Z, Chou S, Geng L, Si X, Ding Y, Lang Y, et al. Interactions of blueberry anthocyanins with whey protein isolate and bovine serum protein: Color stability, antioxidant activity, in vitro simulation, and protein functionality. LWT - Food Science and Technology. 2021;152:112269.

100. Ren S, Giusti MM. Comparing the effect of whey protein preheating temperatures on the color expression and stability of anthocyanins from different sources. Food Hydrocolloids. 2022;124:107273.

101. Araújo P, Basílio N, Fernandes A, Mateus N, de Freitas V, Pina F, et al. Impact of Lignosulfonates on the Thermodynamic and Kinetic Parameters of Malvidin-3-O-glucoside in Aqueous Solutions. Journal of Agricultural and Food Chemistry. 2018;66(25):6382-7.

102. Araújo P, Basílio N, Azevedo J, Fernandes A, Mateus N, Pina F, et al. Colour modulation of blue anthocyanin-derivatives. Lignosulfonates as a tool to improve the water solubility of natural blue dyes. Dyes and Pigments. 2018;153:150-9.

103. Yoo CG, Meng X, Pu Y, Ragauskas AJ. The critical role of lignin in lignocellulosic biomass conversion and recent pretreatment strategies: A comprehensive review. Bioresource Technology. 2020;301.

104. Costa C. Vanillin and Syringaldehyde from Side Streams of Pulp and Paper Industries and Biorefineries [PhD thesis]: University of Porto; 2017.

105. Gosselink RJA. Lignin as a renewable aromatic resource for the chemical industry: Wageningen University; 2011.

106. Moreno A, Sipponen MH. Overcoming Challenges of Lignin Nanoparticles: Expanding Opportunities for Scalable and Multifunctional Nanomaterials. Accounts of Chemical Research. 2024;57(14):1918-30.

107. Lu Y-C, Lu Y, Fan X. Structure and Characteristics of Lignin. In: Sharma S, Kumar A, editors. Lignin: Biosynthesis and Transformation for Industrial Applications. Cham: Springer International Publishing; 2020. p. 17-75.

108. Santos R, Capanema E, Balakshin M, Chang H-M, Jameel H. Effect of hardwoods characteristics on kraft pulping process: Emphasis on lignin structure. Bioresources. 2011;6:3623.

109. Nanayakkara B, Manley-Harris M, Suckling ID. Understanding the Degree of Condensation of Phenolic and Etherified C-9 Units of in Situ Lignins. Journal of Agricultural and Food Chemistry. 2011;59(23):12514-9.

110. Rodrigues Pinto PC, Borges da Silva EA, Rodrigues AE. Lignin as Source of Fine Chemicals: Vanillin and Syringaldehyde. In: Baskar C, Baskar S, Dhillon RS, editors. Biomass Conversion: The Interface of Biotechnology, Chemistry and Materials Science. Berlin, Heidelberg: Springer Berlin Heidelberg; 2012. p. 381-420.

111. Berlin A, Balakshin M. Chapter 18 - Industrial Lignins: Analysis, Properties, and Applications. In: Gupta VK, Tuohy MG, Kubicek CP, Saddler J, Xu F, editors.

Bioenergy Research: Advances and Applications. Amsterdam: Elsevier; 2014. p. 315-36.

112. Bajwa DS, Pourhashem G, Ullah AH, Bajwa SG. A concise review of current lignin production, applications, products and their environmental impact. Industrial Crops and Products. 2019;139:111526.

113. Aryan V, Kraft A. The crude tall oil value chain: Global availability and the influence of regional energy policies. Journal of Cleaner Production. 2020;280.

114. Dessbesell L, Paleologou M, Leitch M, Pulkki R, Xu C. Global lignin supply overview and kraft lignin potential as an alternative for petroleum-based polymers. Renewable and Sustainable Energy Reviews. 2020;123:109768.

115. Kumar A, Anushree, Kumar J, Bhaskar T. Utilization of lignin: A sustainable and eco-friendly approach. Journal of the Energy Institute. 2020;93(1):235-71.

116. Mäki E, Saastamoinen H, Melin K, Matschegg D, Pihkola H. Drivers and barriers in retrofitting pulp and paper industry with bioenergy for more efficient production of liquid, solid and gaseous biofuels: A review. Biomass and Bioenergy. 2021;148:106036.

117. Moretti C, Corona B, Hoefnagels R, Vural-Gürsel I, Gosselink R, Junginger M. Review of life cycle assessments of lignin and derived products: Lessons learned. Science of The Total Environment. 2021;770:144656.

118. Aro T, Fatehi P. Production and Application of Lignosulfonates and Sulfonated Lignin. ChemSusChem. 2017;10(9):1861-77.

119. Fernández-Rodríguez J, Erdocia X, Hernández-Ramos F, Alriols MG, Labidi J. Chapter 7 - Lignin Separation and Fractionation by Ultrafiltration. In: Galanakis CM, editor. Separation of Functional Molecules in Food by Membrane Technology: Academic Press; 2019. p. 229-65.

120. Lora J. Chapter 10 - Industrial Commercial Lignins: Sources, Properties and Applications. In: Belgacem MN, Gandini A, editors. Monomers, Polymers and Composites from Renewable Resources. Amsterdam: Elsevier; 2008. p. 225-41.

121. Jost R. Emulsion Stabilization with Lignosulfonates. In: Arpit S, Jaya T, editors. Lignin. Rijeka: IntechOpen; 2022. p. Ch. 4.

122. Gelardi G, Mantellato S, Marchon D, Palacios M, Eberhardt AB, Flatt RJ. 9 - Chemistry of chemical admixtures. In: Aïtcin P-C, Flatt RJ, editors. Science

and Technology of Concrete Admixtures: Woodhead Publishing; 2016. p. 149-218.

123. Vakkilainnen EK. The Kraft Chemical Recovery Process. 2008.

124. Hu J, Zhang Q, Lee D-J. Kraft lignin biorefinery: A perspective. Bioresource Technology. 2018;247:1181-3.

125. Lee JH, Im JS, Jin X, Kim TM, Choi JW. In Vitro and In Vivo Evaluation of Drug-Encapsulated Lignin Nanoparticles for Release Control. ACS Sustainable Chemistry & Engineering. 2022;10(18):5792-802.

126. Figueiredo P, Lintinen K, Kiriazis A, Hynninen V, Liu Z, Bauleth-Ramos T, et al. In vitro evaluation of biodegradable lignin-based nanoparticles for drug delivery and enhanced antiproliferation effect in cancer cells. Biomaterials. 2017;121:97-108.

127. Carvalho DMd, Queiroz JHd, Colodette JL. Assessment of alkaline pretreatment for the production of bioethanol from eucalyptus, sugarcane bagasse and sugarcane straw. Industrial Crops and Products. 2016;94:932-41.

128. Younesi-Kordkheili H, Kazemi-Najafi S, Eshkiki RB, Pizzi A. Improving urea formaldehyde resin properties by glyoxalated soda bagasse lignin. European Journal of Wood and Wood Products. 2015;73(1):77-85.

129. Younesi-Kordkheili H, Pizzi A, Honarbakhsh-Raouf A, Nemati F. The effect of soda bagasse lignin modified by ionic liquids on properties of the urea–formaldehyde resin as a wood adhesive. The Journal of Adhesion. 2017;93(11):914-25.

130. Sannigrahi P, Ragauskas AJ. Fundamentals of Biomass Pretreatment by Fractionation. Aqueous Pretreatment of Plant Biomass for Biological and Chemical Conversion to Fuels and Chemicals2013. p. 201-22.

131. Brosse N, Hussin MH, Rahim AA. Organosolv Processes. In: Wagemann K, Tippkötter N, editors. Biorefineries. Cham: Springer International Publishing; 2019. p. 153-76.

132. Pandey MP, Kim CS. Lignin Depolymerization and Conversion: A Review of Thermochemical Methods. Chemical Engineering & Technology. 2011;34(1):29-41.

133. Erdocia X, Prado R, Corcuera MÁ, Labidi J. Effect of different organosolv treatments on the structure and properties of olive tree pruning lignin. Journal of Industrial and Engineering Chemistry. 2014;20(3):1103-8.

134. Nitsos C, Stoklosa R, Karnaouri A, Vörös D, Lange H, Hodge D, et al. Isolation and Characterization of Organosolv and Alkaline Lignins from Hardwood and Softwood Biomass. ACS Sustainable Chemistry & Engineering. 2016;4(10):5181-93.

135. Tribot A, Amer G, Abdou Alio M, de Baynast H, Delattre C, Pons A, et al. Wood-lignin: Supply, extraction processes and use as bio-based material. European Polymer Journal. 2019;112:228-40.

136. Singh R, Shukla A, Tiwari S, Srivastava M. A review on delignification of lignocellulosic biomass for enhancement of ethanol production potential. Renewable and Sustainable Energy Reviews. 2014;32:713-28.

137. Zhang X, Zhu J, Sun L, Yuan Q, Cheng G, Argyropoulos DS. Extraction and characterization of lignin from corncob residue after acid-catalyzed steam explosion pretreatment. Industrial Crops and Products. 2019;133:241-9.

138. Martín C, Galbe M, Nilvebrant N-O, Jönsson LJ. Comparison of the Fermentability of Enzymatic Hydrolyzates of Sugarcane Bagasse Pretreated by Steam Explosion Using Different Impregnating Agents. In: Finkelstein M, McMillan JD, Davison BH, editors. Biotechnology for Fuels and Chemicals: The Twenty–Third Symposium. Totowa, NJ: Humana Press; 2002. p. 699-716.

139. Lobato-Rodríguez Á, Gullón B, Romaní A, Ferreira-Santos P, Garrote G, Del-Río PG. Recent advances in biorefineries based on lignin extraction using deep eutectic solvents: A review. Bioresource Technology. 2023;388:129744.

140. Fernandes A, Cruz-Lopes L, Esteves B, Evtuguin DV. Microwaves and Ultrasound as Emerging Techniques for Lignocellulosic Materials. Materials [Internet]. 2023; 16(23).

141. Choi YH, Verpoorte R. Green solvents for the extraction of bioactive compounds from natural products using ionic liquids and deep eutectic solvents. Current Opinion in Food Science. 2019;26:87-93.

142. Erdocia X, Hernández-Ramos F, Morales A, Izaguirre N, de Hoyos-Martínez PL, Labidi J. Chapter 3 - Lignin extraction and isolation methods. In: Santos H, Figueiredo P, editors. Lignin-Based Materials for Biomedical Applications: Elsevier; 2021. p. 61-104.

143. Satlewal A, Agrawal R, Bhagia S, Sangoro J, Ragauskas AJ. Natural deep eutectic solvents for lignocellulosic biomass pretreatment: Recent developments, challenges and novel opportunities. Biotechnology Advances. 2018;36(8):2032-50.

144. Mikulski D, Kłosowski G. Delignification efficiency of various types of biomass using microwave-assisted hydrotropic pretreatment. Scientific Reports. 2022;12(1):4561.

145. Kohli K, Katuwal S, Biswas A, Sharma BK. Effective delignification of lignocellulosic biomass by microwave assisted deep eutectic solvents. Bioresource Technology. 2020;303:122897.

146. Sorn V, Chang K-L, Phitsuwan P, Ratanakhanokchai K, Dong C-D. Effect of microwave-assisted ionic liquid/acidic ionic liquid pretreatment on the morphology, structure, and enhanced delignification of rice straw. Bioresource Technology. 2019;293:121929.

147. Nardella F, Prothmann J, Sandahl M, Spégel P, Ribechini E, Turner C. Native lignin extraction from soft- and hardwood by green and benign sub/supercritical fluid extraction methodologies. RSC Advances. 2023;13(32):21945-53.

148. Wang X, Guo Y, Zhou J, Sun G. Structural changes of poplar wood lignin after supercritical pretreatment using carbon dioxide and ethanol–water as co-solvents. RSC Advances. 2017;7(14):8314-22.

149. Lupoi JS, Singh S, Parthasarathi R, Simmons BA, Henry RJ. Recent innovations in analytical methods for the qualitative and quantitative assessment of lignin. Renewable and Sustainable Energy Reviews. 2015;49:871-906.

150. Chen CL. Nitrobenzene and Cupric Oxide Oxidations. In: Lin SY, Dence CW, editors. Methods in Lignin Chemistry. Berlin, Heidelberg: Springer Berlin Heidelberg; 1992. p. 301-21.

151. Van Soest PJ, Wine RH. Determination of Lignin and Cellulose in Acid-Detergent Fiber with Permanganate. Journal of Association of Official Analytical Chemists. 1968;51(4):780-5.

152. Quesada J, Rubio M, Gómez D. Ozonation of Lignin Rich Solid Fractions from Corn Stalks. Journal of Wood Chemistry and Technology. 1999;19(1-2):115-37.

153. Lapierre C, Monties B, Rolando C, Chirale Ld. Thioacidolysis of Lignin: Comparison with Acidolysis. Journal of Wood Chemistry and Technology. 1985;5(2):277-92.

154. Pepper JM, Casselman BW, Karapally JC. Lignin oxidation. Preferential use of cupric oxide. Canadian Journal of Chemistry. 1967;45(23):3009-12.

155. Lu F, Ralph J. Derivatization Followed by Reductive Cleavage (DFRC Method), a New Method for Lignin Analysis: Protocol for Analysis of DFRC Monomers. Journal of Agricultural and Food Chemistry. 1997;45(7):2590-2.

156. Stark N, Yelle D, Agarwal U. Techniques for Characterizing Lignin. In: Omar Faruk MS, editor. Lignin in Polymer Composites: Elsevier; 2015. p. 49-66.

157. Goldschmid O. Determination of Phenolic Hydroxyl Content of Lignin Preparations by Ultraviolet Spectrophotometry. Analytical Chemistry. 1954;26(9):1421-3.

158. Faix O. Fourier Transform Infrared Spectroscopy. In: Lin SY, Dence CW, editors. Methods in Lignin Chemistry. Berlin, Heidelberg: Springer Berlin Heidelberg; 1992. p. 233-41.

159. Granata A, Argyropoulos DS. 2-Chloro-4,4,5,5-tetramethyl-1,3,2-dioxaphospholane, a Reagent for the Accurate Determination of the Uncondensed and Condensed Phenolic Moieties in Lignins. Journal of Agricultural and Food Chemistry. 1995;43(6):1538-44.

160. Karagoz P, Khiawjan S, Marques MPC, Santzouk S, Bugg TDH, Lye GJ. Pharmaceutical applications of lignin-derived chemicals and lignin-based materials: linking lignin source and processing with clinical indication. Biomass Conversion and Biorefinery. 2023.

161. Sethupathy S, Murillo Morales G, Gao L, Wang H, Yang B, Jiang J, et al. Lignin valorization: Status, challenges and opportunities. Bioresource Technology. 2022;347:126696.

162. Kadla JF, Kubo S, Venditti RA, Gilbert RD, Compere AL, Griffith W. Lignin-based carbon fibers for composite fiber applications. Carbon. 2002;40(15):2913-20.

163. Norberg I, Nordström Y, Drougge R, Gellerstedt G, Sjöholm E. A new method for stabilizing softwood kraft lignin fibers for carbon fiber production. Journal of Applied Polymer Science. 2013;128(6):3824-30.

164. Puziy AM, Poddubnaya OI, Sevastyanova O. Carbon Materials from Technical Lignins: Recent Advances. Topics in Current Chemistry. 2018;376(4):33.

165. Zhang W, Yin J, Lin Z, Lin H, Lu H, Wang Y, et al. Facile preparation of 3D hierarchical porous carbon from lignin for the anode material in lithium ion battery with high rate performance. Electrochimica Acta. 2015;176:1136-42.

166. Zhang Z, Chen Y, Wang D, Yu D, Wu C. Lignin-based adsorbents for heavy metals. Industrial Crops and Products. 2023;193:116119.

167. Xu L, Yao Q, Zhang Y, Fu Y. Integrated Production of Aromatic Amines and N-Doped Carbon from Lignin via ex Situ Catalytic Fast Pyrolysis in the Presence of Ammonia over Zeolites. ACS Sustainable Chemistry & Engineering. 2017;5(4):2960-9.

168. Zhang L, You T, Zhou T, Zhou X, Xu F. Interconnected Hierarchical Porous Carbon from Lignin-Derived Byproducts of Bioethanol Production for Ultra-High Performance Supercapacitors. ACS Applied Materials & Interfaces. 2016;8(22):13918-25.

169. Maeda M, Hosoya T, Yoshioka K, Miyafuji H, Ohno H, Yamada T. Vanillin production from native softwood lignin in the presence of tetrabutylammonium ion. Journal of Wood Science. 2018;64(6):810-5.

170. Yuki H, Takashi H, Hisashi M. Depolymerization of Native Lignin into Vanillin, Vanillic Acid, and Other Related Compounds via Alkaline Aerobic Oxidation: Reaction Mechanisms and Process Control Using Organic Cations. In: Dr. Eduardo J-L, Dr. Leila Queiroz Z, Dr. Rosangela Rodrigues D, editors. From Biomass to Biobased Products. Rijeka: IntechOpen; 2023. p. Ch. 10.

171. Hodásová Ľ, Jablonsky M, Butor Skulcova A, Haz A. Lignin, potential products and their market value. Wood research. 2015;60:973-86.

172. Araújo JDP, Grande CA, Rodrigues AE. Vanillin production from lignin oxidation in a batch reactor. Chemical Engineering Research and Design. 2010;88(8):1024-32.

173. Silva EABd, Zabkova M, Araújo JD, Cateto CA, Barreiro MF, Belgacem MN, et al. An integrated process to produce vanillin and lignin-based polyurethanes from Kraft lignin. Chemical Engineering Research and Design. 2009;87(9):1276-92.

174. Smolarski N. High-Value Opportunities for Lignin: Unlocking its Potential. 2012.

175. vom Stein T, den Hartog T, Buendia J, Stoychev S, Mottweiler J, Bolm C, et al. Ruthenium-catalyzed C-C bond cleavage in lignin model substrates. Angewandte Chemie International Edition. 2015;54(20):5859-63.

176. Kalami S, Arefmanesh M, Master E, Nejad M. Replacing 100% of phenol in phenolic adhesive formulations with lignin. Journal of Applied Polymer Science. 2017;134(30):45124.

177. Lee A, Deng Y. Green polyurethane from lignin and soybean oil through non-isocyanate reactions. European Polymer Journal. 2015;63:67-73.

178. Duan D, Lei H, Wang Y, Ruan R, Liu Y, Ding L, et al. Renewable phenol production from lignin with acid pretreatment and ex-situ catalytic pyrolysis. Journal of Cleaner Production. 2019;231:331-40.

179. Yoshikawa T, Yagi T, Shinohara S, Fukunaga T, Nakasaka Y, Tago T, et al. Production of phenols from lignin via depolymerization and catalytic cracking. Fuel Processing Technology. 2013;108:69-75.

180. Luo N, Wang M, Li H, Zhang J, Hou T, Chen H, et al. Visible-Light-Driven Self-Hydrogen Transfer Hydrogenolysis of Lignin Models and Extracts into Phenolic Products. ACS Catalysis. 2017;7(7):4571-80.

181. Zimniewska M, Kozłowski R, Batog J. Nanolignin Modified Linen Fabric as a Multifunctional Product. Molecular Crystals and Liquid Crystals. 2008;484(1):409-16.

182. Sunthornvarabhas J, Liengprayoon S, Suwonsichon T. Antimicrobial kinetic activities of lignin from sugarcane bagasse for textile product. Industrial Crops and Products. 2017;109:857-61.

183. Neeraj M, Aurélie C, François R, Stéphane G, Fabine S, Giulio M, et al. An Overview on the Use of Lignin and Its Derivatives in Fire Retardant Polymer Systems. In: Matheus P, editor. Lignin. Rijeka: IntechOpen; 2018. p. Ch. 9.

184. Nur I, Mohamed Noor N, Abd. Rasid Z, El Enshasy H, Wan Azelee NI. Lignins as natural active ingredients for Cosmetics: A Review. Bioscience Research. 2022;19:1050-66.

185. Gordobil O, Herrera R, Yahyaoui M, İlk S, Kaya M, Labidi J. Potential use of kraft and organosolv lignins as a natural additive for healthcare products. RSC Advances. 2018;8(43):24525-33.

186. Li S-X, Li M-F, Bian J, Wu X-F, Peng F, Ma M-G. Preparation of organic acid lignin submicrometer particle as a natural broad-spectrum photo-protection agent. International Journal of Biological Macromolecules. 2019;132:836-43.

187. Lee SC, Yoo E, Lee SH, Won K. Preparation and Application of Light-Colored Lignin Nanoparticles for Broad-Spectrum Sunscreens. Polymers [Internet]. 2020; 12(3).

188. Technical Research Centre of Finland V. Wood components to boost quality of food products ScienceDaily2016 [Available from: https://www.sciencedaily.com/releases/2016/06/160601083802.htm].

189. Gil-Chávez J, Gurikov P, Hu X, Meyer R, Reynolds W, Smirnova I. Application of novel and technical lignins in food and pharmaceutical industries: structure-function relationship and current challenges. Biomass Conversion and Biorefinery. 2021;11(6):2387-403.

190. Rai S, Dutta P, Mehrotra G. Lignin incorporated antimicrobial chitosan film for food packaging application. Journal of Polymer Materials. 2017;34:171-83.

191. Yang W, Owczarek JS, Fortunati E, Kozanecki M, Mazzaglia A, Balestra GM, et al. Antioxidant and antibacterial lignin nanoparticles in polyvinyl alcohol/chitosan films for active packaging. Industrial Crops and Products. 2016;94:800-11.

192. Sipponen MH, Lange H, Crestini C, Henn A, Österberg M. Lignin for Nano- and Microscaled Carrier Systems: Applications, Trends, and Challenges. ChemSusChem. 2019;12(10):2039-54.

193. Iravani S, Varma RS. Greener synthesis of lignin nanoparticles and their applications. Green Chemistry. 2020;22(3):612-36.

194. Vinardell MP, Mitjans M. Lignins and Their Derivatives with Beneficial Effects on Human Health. International Journal of Molecular Sciences [Internet]. 2017; 18(6).

195. Siddiqui IA, Sanna V. Impact of nanotechnology on the delivery of natural products for cancer prevention and therapy. Molecular Nutrition & Food Research. 2016;60(6):1330-41.

196. Gao W, Fatehi P. Lignin for polymer and nanoparticle production: Current status and challenges. The Canadian Journal of Chemical Engineering. 2019;97(11):2827-42.

197. Alqahtani MS, Alqahtani A, Al-Thabit A, Roni M, Syed R. Novel lignin nanoparticles for oral drug delivery. Journal of Materials Chemistry B. 2019;7(28):4461-73.

198. Beisl S, Loidolt P, Miltner A, Harasek M, Friedl A. Production of Micro- and Nanoscale Lignin from Wheat Straw Using Different Precipitation Setups. Molecules. 2018; 23(3).

199. Byrappa K, Ohara S, Adschiri T. Nanoparticles synthesis using supercritical fluid technology – towards biomedical applications. Advanced Drug Delivery Reviews. 2008;60(3):299-327.

200. Mura S, Nicolas J, Couvreur P. Stimuli-responsive nanocarriers for drug delivery. Nature Materials. 2013;12(11):991-1003.

201. Friedman DA, Claypool ES, Liu R. The Smart Targeting of Nanoparticles. Current Pharmaceutical Design. 2013;19(35):6315-29.

202. Zhao J, Zheng D, Tao Y, Li Y, Wang L, Liu J, et al. Self-assembled pH-responsive polymeric nanoparticles based on lignin-histidine conjugate with small particle size for efficient delivery of anti-tumor drugs. Biochemical Engineering Journal. 2020;156.

203. Pishnamazi M, Hafizi H, Shirazian S, Culebras M, Walker GM, Collins MN. Design of controlled release system for paracetamol based on modified lignin. Polymers. 2019;11(6).

204. Li Y, Qiu X, Qian Y, Xiong W, Yang D. pH-responsive lignin-based complex micelles: Preparation, characterization and application in oral drug delivery. Chemical Engineering Journal. 2017;327:1176-83.

205. OIV. State of the world vitivinicultural sector in 2019. 2020:15.

206. Çetin ES, Altinöz D, Tarçan E, Göktürk Baydar N. Chemical composition of grape canes. Industrial Crops and Products. 2011;34(1):994-8.

207. Florestal IM. Estudo do impacto na economia local/regional autárquica pelo aproveitamento e valorização energética e económica das podas. 2014.

208. Teixeira A, Baenas N, Dominguez-Perles R, Barros A, Rosa E, Moreno DA, et al. Natural bioactive compounds from winery by-products as health promoters: a review. International journal of molecular sciences. 2014;15(9):15638-78.

209. Ambiente APd. Portuguese National Inventory Report on Greenhouse Gases, 1990–2012. Portuguese Enviromental Agency: Amadora, Portugal, 2014.

210. Briones R, Torres L, Saravia Y, Serrano L, Labidi J. Liquefied agricultural residues for film elaboration. Industrial Crops and Products. 2015;78:19-28.

211. Rivas S, López L, Vila C, Parajó JC. Organosolv processing of vine shoots: Fractionation and conversion of hemicellulosic sugars into platform chemicals by microwave irradiation. Bioresource Technology. 2021;342:125967.

212. Prozil SO, Evtuguin DV, Lopes LPC. Chemical composition of grape stalks of Vitis vinifera L. from red grape pomaces. Industrial Crops and Products. 2012;35(1):178-84.

213. Moreira MM, Barroso MF, Porto JV, Ramalhosa MJ, Švarc-Gajić J, Estevinho L, et al. Potential of Portuguese vine shoot wastes as natural resources of bioactive compounds. Science of The Total Environment. 2018;634:831-42.

214. Zwingelstein M, Draye M, Besombes J-L, Piot C, Chatel G. Viticultural wood waste as a source of polyphenols of interest: Opportunities and perspectives through conventional and emerging extraction methods. Waste Management. 2020;102:782-94.

215. Jesus MS, Romaní A, Genisheva Z, Teixeira JA, Domingues L. Integral valorization of vine pruning residue by sequential autohydrolysis stages. Journal of Cleaner Production. 2017;168:74-86.

216. Jesus M, Romaní A, Mata F, Domingues L. Current Options in the Valorisation of Vine Pruning Residue for the Production of Biofuels, Biopolymers, Antioxidants, and Bio-Composites following the Concept of Biorefinery: A Review. Polymers. 2022;14(9).

217. Dávila I, Gullón B, Labidi J, Gullón P. Multiproduct biorefinery from vine shoots: Bio-ethanol and lignin production. Renewable Energy. 2019;142:612-23.

218. Fernandes MJ, Moreira MM, Paíga P, Dias D, Bernardo M, Carvalho M, et al. Evaluation of the adsorption potential of biochars prepared from forest and agri-food wastes for the removal of fluoxetine. Bioresource Technology. 2019;292:121973.

219. Jiménez L, Angulo V, Ramos E, De la Torre MJ, Ferrer JL. Comparison of various pulping processes for producing pulp from vine shoots. Industrial Crops and Products. 2006;23(2):122-30.

220. Ntalos GA, Grigoriou AH. Characterization and utilisation of vine prunings as a wood substitute for particleboard production. Industrial Crops and Products. 2002;16(1):59-68.

221. Zhou D-D, Li J, Xiong R-G, Saimaiti A, Huang S-Y, Wu S-X, et al. Bioactive Compounds, Health Benefits and Food Applications of Grape. Foods [Internet]. 2022; 11(18).

222. Pereira AR, de Freitas V, Oliveira J. Chapter 7 - Development of lignin-based nanoparticles: fabrication methods and functionalization approaches. In:

Santos H, Figueiredo P, editors. Lignin-Based Materials for Biomedical Applications: Elsevier; 2021. p. 227-70.

223. Khalid MY, Al Rashid A, Arif ZU, Ahmed W, Arshad H, Zaidi AA. Natural fiber reinforced composites: Sustainable materials for emerging applications. Results in Engineering. 2021;11:100263.

224. Alsubari S, Zuhri MYM, Sapuan SM, Ishak MR, Ilyas RA, Asyraf MRM. Potential of Natural Fiber Reinforced Polymer Composites in Sandwich Structures: A Review on Its Mechanical Properties. Polymers [Internet]. 2021; 13(3).

225. Pervaiz M, Sain MM. Carbon storage potential in natural fiber composites. Resources, Conservation and Recycling. 2003;39(4):325-40.

226. Huda MK, Widiastuti I. Natural Fiber Reinforced Polymer in Automotive Application: A Systematic Literature Review. Journal of Physics: Conference Series. 2021;1808(1):012015.

227. Esteves Costa CA, Coleman W, Dube M, Rodrigues AE, Rodrigues Pinto PC. Assessment of key features of lignin from lignocellulosic crops: Stalks and roots of corn, cotton, sugarcane, and tobacco. Industrial Crops and Products. 2016;92:136-48.

228. Dinh Vu N, Thi Tran H, Bui ND, Duc Vu C, Viet Nguyen H. Lignin and Cellulose Extraction from Vietnam's Rice Straw Using Ultrasound-Assisted Alkaline Treatment Method. International Journal of Polymer Science. 2017;2017:1063695.

229. Prozil S, Evtuguin D, Silva A, Cruz-Lopes L. Structural Characterization of Lignin from Grape Stalks (Vitis vinifera L.). Journal of agricultural and food chemistry. 2014;62(24):5420–8.

230. Costa CAE, Pinto PCR, Rodrigues AE. Evaluation of chemical processing impact on E. globulus wood lignin and comparison with bark lignin. Industrial Crops and Products. 2014;61:479-91.

231. Singleton VL, Rossi JA. Colorimetry of Total Phenolics with Phosphomolybdic-Phosphotungstic Acid Reagents. American Journal of Enology and Viticulture. 1965;16:144-58.

232. Yang P, Li H, Wang H, Han F, Jing S, Yuan C, et al. Dispersive Liquid-Liquid Microextraction Method for HPLC Determination of Phenolic Compounds in Wine. Food Analytical Methods. 2017;10(7):2383-97.

233. Podolec P, Szabó AH, Blaško J, Kubinec R, Górová R, Višňovský J, et al. Direct silylation of Trypanosoma brucei metabolites in aqueous samples and their GC-MS/MS analysis. Journal of Chromatography B: Analytical Technologies in the Biomedical and Life Sciences. 2014;967:134-8.

234. Pinto PCR, Costa CE, Rodrigues AE. Oxidation of Lignin from Eucalyptus globulus Pulping Liquors to Produce Syringaldehyde and Vanillin. Industrial & Engineering Chemistry Research. 2013;52(12):4421-8.

235. Costa C, Alves A, Pinto PR, Sousa RA, Borges da Silva EA, Reis RL, et al. Characterization of ulvan extracts to assess the effect of different steps in the extraction procedure. Carbohydrate Polymers. 2012;88(2):537-46.

236. Porter LJ, Hrstich LN, Chan BG. The conversion of procyanidins and prodelphinidins to cyanidin and delphinidin. Phytochemistry. 1985;25(1):223-30.

237. Sameni J, Krigstin S, Sain M. Characterization of Lignins Isolated from Industrial Residues and their Beneficial Uses. Bioresources. 2016;11:8435-56.

238. Araújo P, Costa A, Fernandes I, Mateus N, de Freitas V, Sarmento B, et al. Stabilization of bluish pyranoanthocyanin pigments in aqueous systems using lignin nanoparticles. Dyes and Pigments. 2019;166:367-74.

239. Dorosh O, Rodrigues F, Delerue-Matos C, Moreira MM. Increasing the added value of vine-canes as a sustainable source of phenolic compounds: A review. Science of The Total Environment. 2022;830:154600.

240. Sánchez-Gómez R, Alonso GL, Salinas MR, Zalacain A. 4 - Reuse of Vine-Shoots Wastes for Agricultural Purposes. In: Galanakis CM, editor. Handbook of Grape Processing By-Products: Academic Press; 2017. p. 79-104.

241. Escobar-Avello D, Olmo-Cunillera A, Lozano-Castellón J, Marhuenda-Muñoz M, Vallverdú-Queralt A. A Targeted Approach by High Resolution Mass Spectrometry to Reveal New Compounds in Raisins. Molecules. 2020;25(6).

242. Bastos DH, Saldanha LA, Catharino RR, Sawaya AC, Cunha IB, Carvalho PO, et al. Phenolic antioxidants identified by ESI-MS from Yerba maté (Ilex paraguariensis) and green tea (Camelia sinensis) extracts. Molecules. 2007;12(3):423-32.

243. Schmetz Q, Teramura H, Morita K, Oshima T, Richel A, Ogino C, et al. Versatility of a Dilute Acid/Butanol Pretreatment Investigated on Various Lignocellulosic Biomasses to Produce Lignin, Monosaccharides and Cellulose in Distinct Phases. ACS Sustainable Chemistry & Engineering. 2019;7(13):11069-79.

244. Romaní A, Larramendi A, Yáñez R, Cancela Á, Sánchez Á, Teixeira JA, et al. Valorization of Eucalyptus nitens bark by organosolv pretreatment for the production of advanced biofuels. Industrial Crops and Products. 2019;132:327-35.

245. Cai CM, Zhang T, Kumar R, Wyman CE. Integrated furfural production as a renewable fuel and chemical platform from lignocellulosic biomass. Journal of Chemical Technology & Biotechnology. 2014;89(1):2-10.

246. Rivas S, Vila C, Alonso JL, Santos V, Parajó JC, Leahy JJ. Biorefinery processes for the valorization of Miscanthus polysaccharides: from constituent sugars to platform chemicals. Industrial Crops and Products. 2019;134:309-17.

247. Dávila I, Gullón B, Alonso JL, Labidi J, Gullón P. Vine shoots as new source for the manufacture of prebiotic oligosaccharides. Carbohydrate Polymers. 2019;207:34-43.

248. Makris DP, Boskou G, Andrikopoulos NK. Recovery of antioxidant phenolics from white vinification solid by-products employing water/ethanol mixtures. Bioresource Technology. 2007;98(15):2963-7.

249. Ping L, Brosse N, Sannigrahi P, Ragauskas A. Evaluation of grape stalks as a bioresource. Industrial Crops and Products. 2011;33:200-4.

250. Das P, Stoffel RB, Area MC, Ragauskas AJ. Effects of one-step alkaline and two-step alkaline/dilute acid and alkaline/steam explosion pretreatments on the structure of isolated pine lignin. Biomass and Bioenergy. 2019;120:350-8.

251. Faix O, editor Classification of Lignins from Different Botanical Origins by FT-IR Spectroscopy1991.

252. Abreu HdS. Estimativa por Infravermelho da Concentração da Unidade Estrutural β-O-4 em Ligninas de Angiospermas Tropicais. Química Nova. 1997;20:592-8.

253. Pantoja-Castro MA, González-Rodríguez H. Study by infrared spectroscopy and thermogravimetric analysis of Tannins and Tannic acid. Revista Latinoamericana de Química. 2011;39:107-12.

254. Wahyono T, Astuti D, Wiryawan K, Sugoro I, Jayanegara A. Fourier Transform Mid-Infrared (FTIR) Spectroscopy to Identify Tannin Compounds in The Panicle of Sorghum Mutant Lines. IOP Conference Series: Materials Science and Engineering. 2019;546:042045.

255. Pan X, Kadla JF, Ehara K, Gilkes N, Saddler JN. Organosolv ethanol lignin from hybrid poplar as a radical scavenger: relationship between lignin structure, extraction conditions, and antioxidant activity. Journal of Agricultural and Food Chemistry 2006;54(16):5806-13.

256. Dizhbite T, Telysheva G, Jurkjane V, Viesturs U. Characterization of the radical scavenging activity of lignins—natural antioxidants. Bioresource Technology. 2004;95(3):309-17.

257. Kaur R, Uppal SK. Structural characterization and antioxidant activity of lignin from sugarcane bagasse. Colloid and Polymer Science. 2015;293(9):2585-92.

258. Li M-F, Sun S-N, Xu F, Sun R-C. Mild Acetosolv Process To Fractionate Bamboo for the Biorefinery: Structural and Antioxidant Properties of the Dissolved Lignin. Journal of Agricultural and Food Chemistry. 2012;60(7):1703-12.

259. Li Z, Zhang J, Qin L, Ge Y. Enhancing Antioxidant Performance of Lignin by Enzymatic Treatment with Laccase. ACS Sustainable Chemistry & Engineering. 2018;6(2):2591-5.

260. Vernhet A. Chapter 16 - Red Wine Clarification and Stabilization. In: Morata A, editor. Red Wine Technology: Academic Press; 2019. p. 237-51.

261. Chursina O, Zagorouiko V. The concept of colloidal stabilization of wines. BIO Web Conf. 2021;39.

262. Mierczynska-Vasilev A, Smith PA. Current state of knowledge and challenges in wine clarification. Australian Journal of Grape and Wine Research. 2015;21(S1):615-26.

263. Cosme F, Ribeiro L, Nunes F, M. . Wine Stabilisation: An Overview of Defects and Treatments. In: Fernanda C, Fernando MN, Luís F-R, editors. Chemistry and Biochemistry of Winemaking, Wine Stabilization and Aging. Rijeka: IntechOpen; 2021. p. Ch. 8.

264. Ailer Š, Jakabová S, Benešová L, Ivanova-Petropulos V. Wine Faults: State of Knowledge in Reductive Aromas, Oxidation and Atypical Aging, Prevention, and Correction Methods. Molecules. 2022;27(11).

265. Franco-Luesma E, Ferreira V. Reductive off-odors in wines: Formation and release of H2S and Methanethiol during the accelerated anoxic storage of wines. Food Chemistry. 2015;199.

266. Rinaldi A, Moio L. Salivary protein-tannin interaction: The binding behind astringency. Chemistry and Biochemistry of Winemaking, Wine Stabilization and Aging. 2021.

267. Soares S, Brandão E, Mateus N, de Freitas V. Sensorial properties of red wine polyphenols: Astringency and bitterness. Critical Reviews in Food Science and Nutrition. 2017;57(5):937-48.

268. Zhang X, Kontoudakis N, Wilkes E, Scrimgeour N, Hirlam K, Clark AC. The removal of Cu from wine by copolymer PVI/PVP: Impact on Cu fractions and binding agents. Food Chemistry. 2021;357:129764.

269. Peñas E, Di Lorenzo C, Uberti F, Restani P. Allergenic Proteins in Enology: A Review on Technological Applications and Safety Aspects. Molecules [Internet]. 2015; 20(7):[13144-64 pp.].

270. Gazzola D, Vincenzi S, Marangon M, Pasini G, Curioni A. Grape seed extract: the first protein-based fining agent endogenous to grapes. Australian Journal of Grape and Wine Research. 2017;23(2):215-25.

271. Gambuti A, Rinaldi A, Romano R, Manzo N, Moio L. Performance of a protein extracted from potatoes for fining of white musts. Food Chemistry. 2016;190:237-43.

272. Granato TM, Ferranti P, Iametti S, Bonomi F. Affinity and selectivity of plant proteins for red wine components relevant to color and aroma traits. Food Chemistry. 2018;256:235-43.

273. Cabello-Pasini A, Victoria N, Macias Carranza V, Garibay E, Muñiz-Salazar R. Clarification of Wines Using Polysaccharides Extracted from Seaweeds. American Journal of Enology and Viticulture. 2005;56:52-9.

274. Canalejo D, Martínez-Lapuente L, Ayestarán B, Pérez-Magariño S, Guadalupe Z. Potential use of grape and wine polysaccharide extracts as fining agents to modulate the volatile composition of Viura wines. Food Chemistry. 2024;430:137047.

275. Jiménez-Martínez MD, Gil-Muñoz R, Gómez-Plaza E, Bautista-Ortín AB. Performance of purified grape pomace as a fining agent to reduce the levels of some contaminants from wine. Food Additives & Contaminants: Part A. 2018;35(6):1061-70.

276. Costa CAE, Pinto PCR, Rodrigues AE. Radar Tool for Lignin Classification on the Perspective of Its Valorization. Industrial & Engineering Chemistry Research. 2015;54(31):7580-90.

277. Casimiro FM, Costa CAE, Vega-Aguilar C, Rodrigues AE. Hardwood and softwood lignins from sulfite liquors: Structural characterization and valorization through depolymerization. International Journal of Biological Macromolecules. 2022;215:272-9.

278. Costa CAE, Casimiro FM, Vega-Aguilar C, Rodrigues AE. Lignin Valorization for Added-Value Chemicals: Kraft Lignin versus Lignin Fractions. ChemEngineering. 2023; 7(3).

279. Michelin M, Liebentritt S, Vicente AA, Teixeira JA. Lignin from an integrated process consisting of liquid hot water and ethanol organosolv: Physicochemical and antioxidant properties. International Journal of Biological Macromolecules. 2018;120:159-69.

280. Smith PK, Krohn RI, Hermanson GT, Mallia AK, Gartner FH, Provenzano MD, et al. Measurement of protein using bicinchoninic acid. Analytical Biochemistry 1985;150(1):76-85.

281. Singleton VL, Joseph A. Rossi, Jr. Colorimetry of Total Phenolics with Phosphomolybdic-Phosphotungstic Acid Reagents. American Journal of Enology and Viticulture. 1965;16(3):144.

282. Ribéreau-Gayon P, Stonestreet E. Le dosage des tannins du vin rouge et la détermination de leur structure. Chimie Analitique. 1966;48:188-96.

283. de Freitas V, Mateus N. Structural Features of Procyanidin Interactions with Salivary Proteins. Journal of Agricultural and Food Chemistry. 2001;49(2):940-5.

284. Soares S, Vitorino R, Osório H, Fernandes A, Venâncio A, Mateus N, et al. Reactivity of Human Salivary Proteins Families Toward Food Polyphenols. Journal of Agricultural and Food Chemistry. 2011;59(10):5535-47.

285. Brandão E, Soares S, Mateus N, de Freitas V. Human saliva protein profile: Influence of food ingestion. Food Research International. 2014;64:508-13.

286. Azevedo J, Brandão E, Soares S, Oliveira J, Lopes P, Mateus N, et al. Polyphenolic Characterization of Nebbiolo Red Wines and Their Interaction with Salivary Proteins. Foods. 2020; 9(12).

287. Azevedo J, Jesus M, Brandão E, Soares S, Oliveira J, Lopes P, et al. Interaction between salivary proteins and cork phenolic compounds able to migrate to wine model solutions. Food Chemistry. 2022;367:130607.

288. Somers TC, Evans ME. Spectral evaluation of young red wines: Anthocyanin equilibria, total phenolics, free and molecular SO2, “chemical age”. Journal of the Science of Food and Agriculture. 1977;28:279-87.

289. Glories Y, editor Recherches sur la matière colorante des vins rouges1978.

290. Mateus N, Proença S, Ribeiro P, Machado JM, De Freitas V. Grape and wine polyphenolic composition of red Vitis vinifera varieties concerning vineyard altitude. Ciencia y Tecnologia Alimentaria. 2001;3(2):102-10.

291. Barros P, Moreira N, Pereira E, Leite SG, Moraes Rezende C, Guedes de Pinho P. Development and validation of automatic HS-SPME with a gas chromatography-ion trap/mass spectrometry method for analysis of volatiles in wines. Talanta. 2012;101:177-86.

292. Feng Z, Liu Q, Zhang H, Xu D, Zhai H, Ren H. Adsorption of bovine serum albumin on the surfaces of poplar lignophenols. International Journal of Biological Macromolecules. 2020;158:290-302.

293. Leskinen T, Witos J, Valle-Delgado JJ, Lintinen K, Kostiainen M, Wiedmer SK, et al. Adsorption of Proteins on Colloidal Lignin Particles for Advanced Biomaterials. Biomacromolecules. 2017;18(9):2767-76.

294. Salas C, Rojas OJ, Lucia LA, Hubbe MA, Genzer J. On the Surface Interactions of Proteins with Lignin. ACS Applied Materials & Interfaces. 2013;5(1):199-206.

295. Mokrzycki W, Tatol M. Color difference Delta E - A survey. Machine Graphics and Vision. 2011;20:383-411.

296. Guth H. Quantitation and Sensory Studies of Character Impact Odorants of Different White Wine Varieties. Journal of Agricultural and Food Chemistry. 1997;45(8):3027-32.

297. Arn H, Acree TE. Flavornet: A database of aroma compounds based on odor potency in natural products. In: Contis ET, Ho CT, Mussinan CJ, Parliment TH, Shahidi F, Spanier AM, editors. Developments in Food Science. 40: Elsevier; 1998. p. 27.

298. Santos Buelga C, Gonzalez-paramas AM. Anthocyanins. In: Elsevier, editor. Reference Module in Food Science 2018. p. 1-12.

299. Bridle P, Timberlake CF. Anthocyanins as natural food colours—selected aspects. Food Chemistry. 1997;58(1):103-9.

300. Nabi BG, Mukhtar K, Ahmed W, Manzoor MF, Ranjha MMAN, Kieliszek M, et al. Natural pigments: Anthocyanins, carotenoids, chlorophylls, and betalains as colorants in food products. Food Bioscience. 2023;52:102403.

301. Pina F, Parola AJ, Melo M, Lima JC, Freitas V. Chemistry of Anthocyanins. In: Croydon MS-LBaGBC, editor. Anthocyanins From Natural Sources: Exploiting Targeted Delivery for Improved Health: UK: Royal Society of Chemistry; 2019. p. 34-76.

302. Martín J, Kuskoski EM, Navas MJ, Asuero A, G. . Antioxidant Capacity of Anthocyanin Pigments. In: Goncalo CJ, editor. Flavonoids. Rijeka: IntechOpen; 2017. p. Ch. 11.

303. Zang Z, Tang S, Li Z, Chou S, Shu C, Chen Y, et al. An updated review on the stability of anthocyanins regarding the interaction with food proteins and polysaccharides. Comprehensive Reviews in Food Science and Food Safety. 2022;21(5):4378-401.

304. Cortez R, Luna-Vital DA, Margulis D, Gonzalez de Mejia E. Natural Pigments: Stabilization Methods of Anthocyanins for Food Applications. Comprehensive Reviews in Food Science and Food Safety. 2017;16(1):180-98.

305. Lu Y, Lu Y-C, Hu H-Q, Xie F-J, Wei X-Y, Fan X. Structural Characterization of Lignin and Its Degradation Products with Spectroscopic Methods. Journal of Spectroscopy. 2017:8951658.

306. Myrvold BO. A new model for the structure of lignosulphonates: Part 1. Behaviour in dilute solutions. Industrial Crops and Products. 2008;27(2):214-9.

307. Li Q, Zeng M, Zhu D, Lou H, Pang Y, Qiu K, et al. A Simple and Rapid Method to Determine Sulfonation Degree of Lignosulfonates. BioEnergy Research. 2019;12(2):260-6.

308. Lakowicz J. Principles of Fluorescence Spectroscopy2006.

309. Kontturi A-K, Kontturi K. Determination of effective charge numbers of polydisperse polyelectrolyte. Journal of Colloid and Interface Science. 1988;124(1):328-35.

310. Kontturi AK. Diffusion coefficients and effective charge numbers of lignosulphonate. Influence of temperature. Journal of the Chemical Society, Faraday Transactions 1: Physical Chemistry in Condensed Phases. 1988;84(11):4043-7.

311. Frazier RA, Papadopoulou A, Mueller-Harvey I, Kissoon D, Green RJ. Probing Protein−Tannin Interactions by Isothermal Titration Microcalorimetry. Journal of Agricultural and Food Chemistry. 2003;51(18):5189-95.

312. Leydet Y, Gavara R, Petrov V, Diniz AM, Jorge Parola A, Lima JC, et al. The effect of self-aggregation on the determination of the kinetic and thermodynamic constants of the network of chemical reactions in 3-glucoside anthocyanins. Phytochemistry. 2012;83:125-35.

313. Mohamed Ameen H, Kunsági-Máté S, Bognár B, Szente L, Poór M, Lemli B. Thermodynamic Characterization of the Interaction between the Antimicrobial Drug Sulfamethazine and Two Selected Cyclodextrins. Molecules. 2019;24(24).

314. Ross PD, Subramanian S. Thermodynamics of protein association reactions: forces contributing to stability. Biochemistry. 1981;20(11):3096-102.

315. Karimov OK, Teptereva GA, Chetvertneva IA, Movsumzade EM, Karimov EK. The structure of lignosulfonates for production of carbon catalyst support. IOP Conference Series: Earth and Environmental Science. 2021;839(2):022086.

316. Klapiszewski L, Jamrozik A, Strzemiecka B, Matykiewicz D, Voelkel A, Jesionowski T. Activation of Magnesium Lignosulfonate and Kraft Lignin: Influence on the Properties of Phenolic Resin-Based Composites for Potential Applications in Abrasive Materials. International Journal of Molecular Sciences [Internet]. 2017; 18(6).

317. Shen Q, Zhang T, Zhu M-F. A comparison of the surface properties of lignin and sulfonated lignins by FTIR spectroscopy and wicking technique. Colloids and Surfaces A: Physicochemical and Engineering Aspects. 2008;320(1):57-60.

318. Djikanović D, Kalauzi A, Radotić K, Lapierre C, Jeremić M. Deconvolution of lignin fluorescence spectra: A contribution to the comparative structural studies of lignins. Russian Journal of Physical Chemistry A. 2007;81(9):1425-8.

319. Santos TJ, Paggiaro J, Cabral Silva Pimentel HD, Karla dos Santos Pereira A, Cavallini GS, Pereira DH. Computational study of the interaction of heavy metal ions, Cd(II), Hg(II), and Pb(II) on lignin matrices. Journal of Molecular Graphics and Modelling. 2022;111:108080.

320. Wang X, Li X, Peng L, Han S, Hao C, Jiang C, et al. Effective removal of heavy metals from water using porous lignin-based adsorbents. Chemosphere. 2021;279:130504.

321. Yan M, Yang D, Deng Y, Chen P, Zhou H, Qiu X. Influence of pH on the behavior of lignosulfonate macromolecules in aqueous solution. Colloids and Surfaces A: Physicochemical and Engineering Aspects. 2010;371(1):50-8.

322. Meng Y, Hao L, Tan Y, Yang Y, Liu L, Li C, et al. Noncovalent interaction of cyanidin-3-O-glucoside with whey protein isolate and β-lactoglobulin: Focus on fluorescence quenching and antioxidant properties. LWT Food science and technology 2021;137:110386.

323. Coletta V, Rezende C, Conceição F, Polikarpov I, Guimarães F. Mapping the lignin distribution in pretreated sugarcane bagasse by confocal and fluorescence lifetime imaging microscopy. Biotechnology for biofuels. 2013;6:43.

324. Shen Q, Xue Y, Zhang Y, Li T, Yang T, Li S. Effect of microstructure-scale features on lignin fluorescence for preparation of high fluorescence efficiency lignin-based nanomaterials. International Journal of Biological Macromolecules. 2022;202:520-8.

325. Chabbert B, Terryn C, Herbaut M, Vaidya A, Habrant A, Paës G, et al. Fluorescence techniques can reveal cell wall organization and predict saccharification in pretreated wood biomass. Industrial Crops and Products. 2018;123:84-92.

326. Cruz L, Basílio N, Mendoza J, Mateus N, de Freitas V, Tawara MH, et al. Impact of a Water-Soluble Gallic Acid-Based Dendrimer on the Color-Stabilizing Mechanisms of Anthocyanins. Chemistry – A European Journal. 2019;25(50):11696-706.

327. Basílio N, Pina F. Flavylium Network of Chemical Reactions in Confined Media: Modulation of 3′,4′,7-Trihydroxyflavilium Reactions by Host–Guest Interactions with Cucurbit[7]uril. ChemPhysChem. 2014;15(11):2295-302.

328. Gawluk K, Modrzejwska-Sikorska A, Rębiś T, Milczarek G. Preparation of Manganese Lignosulfonate and Its Application as the Precursor of Nanostructured MnOx for Oxidative Electrocatalysis. Catalysts. 2017; 7(12).

329. Milczarek G. Lignosulfonate-Modified Electrodes: Electrochemical Properties and Electrocatalysis of NADH Oxidation. Langmuir. 2009;25(17):10345-53.

330. Cren-Olivé C, Hapiot P, Pinson J, Rolando C. Free Radical Chemistry of Flavan-3-ols: Determination of Thermodynamic Parameters and of Kinetic Reactivity from Short (ns) to Long (ms) Time Scale. Journal of the American Chemical Society. 2002;124(47):14027-38.

331. Moncada MC, de Mesquita MF, dos Santos MMC. Electrochemical oxidation of the synthetic anthocyanin analogue 4-methyl-7,8-dihydroxyflavylium salt. Journal of Electroanalytical Chemistry. 2009;636(1-2):60-7.

332. Tsuda T, Ohshima K, Kawakishi S, Osawa T. Oxidation products of cyanidin 3-O-beta-D-glucoside with a free radical initiator. Lipids. 1996;31(12):1259-63.

333. Novak Jovanović I, Miličević A. A model for the estimation of oxidation potentials of polyphenols. Journal of Molecular Liquids. 2017;241:255-9.

334. Sigurdson GT, Tang P, Giusti MM. Natural Colorants: Food Colorants from Natural Sources. Annual Review of Food Science and Technology. 2017;8(1):261-80.

335. Miller MD, Steinmaus C, Golub MS, Castorina R, Thilakartne R, Bradman A, et al. Potential impacts of synthetic food dyes on activity and attention in children: a review of the human and animal evidence. Environmental Health. 2022;21(1):45.

336. John A, Yang H-H, Muhammad S, Khan ZI, Yu H, Luqman M, et al. Cross Talk between Synthetic Food Colors (Azo Dyes), Oral Flora, and Cardiovascular Disorders. Applied Sciences. 2022; 12(14).

337. Grand View Research G. Natural Food Color Market Size, Share & Trends Analysis Report By Ingredient (Beta-carotene, Blue Spirulina, Carmine, Lycopene), By Application (Bakery & Confectionery, Beverages), By Region, And Segment Forecasts, 2023 - 2030 [Available from: https://www.grandviewresearch.com/industry-analysis/natural-food-colors-market].

338. Socas-Rodríguez B, Álvarez-Rivera G, Valdés A, Ibáñez E, Cifuentes A. Food by-products and food wastes: are they safe enough for their valorization? Trends in Food Science & Technology. 2021;114:133-47.

339. Santos-Buelga C, Mateus N, De Freitas V. Anthocyanins. Plant Pigments and Beyond. Journal of Agricultural and Food Chemistry. 2014;62(29):6879-84.

340. Khoo HE, Azlan A, Tang ST, Lim SM. Anthocyanidins and anthocyanins: colored pigments as food, pharmaceutical ingredients, and the potential health benefits. Food & Nutrition Research. 2017;61(1):1361779.

341. Nkhili E, Loonis M, Mihai S, El Hajji H, Dangles O. Reactivity of food phenols with iron and copper ions: binding, dioxygen activation and oxidation mechanisms. Food & Function. 2014;5(6):1186-202.

342. Yang W, Kortesniemi M, Ma X, Zheng J, Yang B. Enzymatic acylation of blackcurrant (Ribes nigrum) anthocyanins and evaluation of lipophilic properties and antioxidant capacity of derivatives. Food Chemistry. 2019;281:189-96.

343. Küster FWT, A.;. Tabelle Per Le Analisi Chimiche E Chimico- Fisiche. 12th, editor: Hoepli, Milano, Italy; 1982.

344. Oliveira J, Alhinho da Silva M, Teixeira N, De Freitas V, Salas E. Screening of Anthocyanins and Anthocyanin-Derived Pigments in Red Wine Grape Pomace Using LC-DAD/MS and MALDI-TOF Techniques. Journal of Agricultural and Food Chemistry. 2015;63(35):7636-44.

345. Kırca A, Cemeroğlu B. Degradation kinetics of anthocyanins in blood orange juice and concentrate. Food Chemistry. 2003;81(4):583-7.

346. Bondet V, Brand-Williams W, Berset C. Kinetics and Mechanisms of Antioxidant Activity using the DPPH.Free Radical Method. LWT - Food Science and Technology. 1997;30(6):609-15.

347. Maciel LG, do Carmo MAV, Azevedo L, Daguer H, Molognoni L, de Almeida MM, et al. Hibiscus sabdariffa anthocyanins-rich extract: Chemical stability, in vitro antioxidant and antiproliferative activities. Food and Chemical Toxicology. 2018;113:187-97.

348. Jabeur I, Pereira E, Barros L, Calhelha RC, Soković M, Oliveira M, et al. Hibiscus sabdariffa L. as a source of nutrients, bioactive compounds and colouring agents. Food Research International. 2017;100(Pt 1):717-23.

349. Wiczkowski W, Szawara-Nowak D, Topolska J. Red cabbage anthocyanins: Profile, isolation, identification, and antioxidant activity. Food Research International. 2013;51(1):303-9.

350. Fang S, Lin F, Qu D, Liang X, Wang L. Characterization of Purified Red Cabbage Anthocyanins: Improvement in HPLC Separation and Protective Effect against H_2O_2-Induced Oxidative Stress in HepG2 Cells. Molecules. 2018;24(1).

351. Terahara N, Saito N, Honda T, Toki K, Osajima Y. Structure of ternatin A1, the largest ternatin in the major blue anthocyanins from clitoria ternatea flowers. Tetrahedron Letters. 1990;31(20):2921-4.

352. Terahara N, Oda M, Matsui T, Osajima Y, Saito N, Toki K, et al. Five New Anthocyanins, Ternatins A3, B4, B3, B2, and D2, from Clitoria ternatea Flowers. Journal of Natural Products. 1996;59(2):139-44.

353. Terahara N, Toki K, Saito N, Honda T, Matsui T, Osajima Y. Eight New Anthocyanins, Ternatins C1−C5 and D3 and Preternatins A3 and C4 from Young Clitoria ternatea Flowers. Journal of Natural Products. 1998;61(11):1361-7.

354. Oliveira H, Basílio N, Pina F, Fernandes I, de Freitas V, Mateus N. Purple-fleshed sweet potato acylated anthocyanins: Equilibrium network and photophysical properties. Food Chemistry. 2019;288:386-94.

355. Moloney M, Robbins RJ, Collins TM, Kondo T, Yoshida K, Dangles O. Red cabbage anthocyanins: The influence of d-glucose acylation by hydroxycinnamic acids on their structural transformations in acidic to mildly alkaline conditions and on the resulting color. Dyes and Pigments. 2018;158:342-52.

356. Fenger J-A, Sigurdson GT, Robbins RJ, Collins TM, Giusti MM, Dangles O. Acylated Anthocyanins from Red Cabbage and Purple Sweet Potato Can Bind Metal Ions and Produce Stable Blue Colors. International Journal of Molecular Sciences. 2021; 22(9).

357. Cao Y, Xia Q, Aniya, Chen J, Jin Z. Copigmentation effect of flavonols on anthocyanins in black mulberry juice and their interaction mechanism investigation. Food Chemistry. 2023;399:133927.

358. Sinela A, Rawat N, Mertz C, Achir N, Fulcrand H, Dornier M. Anthocyanins degradation during storage of Hibiscus sabdariffa extract and evolution of its degradation products. Food Chemistry. 2017;214:234-41.

359. Rather JA, Akhter N, Ashraf QS, Mir SA, Makroo HA, Majid D, et al. A comprehensive review on gelatin: Understanding impact of the sources, extraction methods, and modifications on potential packaging applications. Food Packaging and Shelf Life. 2022;34:100945.

360. Pandya Y, Bakshi M, Sharma A. Agar-agar extraction, structural properties and applications: A review. The Pharma Innovation Journal. 2022;11:1151-7.

361. Jing P, Bomser JA, Schwartz SJ, He J, Magnuson BA, Giusti MM. Structure−Function Relationships of Anthocyanins from Various Anthocyanin-Rich Extracts on the Inhibition of Colon Cancer Cell Growth. Journal of Agricultural and Food Chemistry. 2008;56(20):9391-8.

362. Tsuda T, Watanabe M, Ohshima K, Norinobu S, Choi S-W, Kawakishi S, et al. Antioxidative Activity of the Anthocyanin Pigments Cyanidin 3-O-.beta.-D-Glucoside and Cyanidin. Journal of Agricultural and Food Chemistry. 1994;42(11):2407-10.

363. Mattioli R, Francioso A, Mosca L, Silva P. Anthocyanins: A Comprehensive Review of Their Chemical Properties and Health Effects on Cardiovascular and Neurodegenerative Diseases. Molecules. 2020; 25(17).

364. Chen J, Yang J, Ma L, Li J, Shahzad N, Kim CK. Structure-antioxidant activity relationship of methoxy, phenolic hydroxyl, and carboxylic acid groups of phenolic acids. Scientific Reports. 2020;10(1):2611.

365. Subhaswaraj P, Sowmya M, Bhavana V, Dyavaiah M, Siddhardha B. Determination of antioxidant activity of Hibiscus sabdariffa and Croton caudatus in Saccharomyces cerevisiae model system. Journal of Food Science and Technology. 2017;54(9):2728-36.

366. Sirag N, Ahmed E, Algaili A, Hassan H, Ohaj M. Determination of total phenolic content and antioxidant activity of Roselle (Hibiscus sabdariffa L.) Calyx ethanolic extract. Journal of Pharmacy and Pharmacology. 2014;Vol1:034-9.

367. Tajalli F, Saeedi M, Malekabadi A. Anticancer and antioxidant effects of red cabbage on three cancerous cell lines and comparison with a normal cell line (HFF-3). Journal of Genes and Cells. 2020;6:12-23.

368. Zakaria NNA, Okello EJ, Howes MJ, Birch-Machin MA, Bowman A. In vitro protective effects of an aqueous extract of Clitoria ternatea L. flower against hydrogen peroxide-induced cytotoxicity and UV-induced mtDNA damage in human keratinocytes. Phytotherapy Research. 2018;32(6):1064-72.

369. Durga C, Lakshmi M, Borelli PDPR, Raju P, Tirumanyam M, Nannepaga JS. Identification of bioactive compounds by FTIR analysis and in vitro antioxidant activity of Clitoria ternatea leaf and flower extracts Indo American Journal for Pharmaceutical Research. 2014;4:2231-6876.

370. Muttalib SA, Abdullah N, manshoor n. Anthocyanin content in relation to the antioxidant activity and colour properties of Garcinia mangostana peel, Syzigium cumini and Clitoria ternatea extracts. International Food Research Journal. 2014;21:2369-75.

371. Gaohua L, Miao X, Dou L. Crosstalk of physiological pH and chemical pKa under the umbrella of physiologically based pharmacokinetic modeling of drug absorption, distribution, metabolism, excretion, and toxicity. Expert Opinion on Drug Metabolism & Toxicology. 2021;17(9):1103-24.

372. Xue H, Sang Y, Gao Y, Zeng Y, Liao J, Tan J. Research Progress on Absorption, Metabolism, and Biological Activities of Anthocyanins in Berries: A Review. Antioxidants. 2023; 12(1).

373. Oren-Shamir M. Does anthocyanin degradation play a significant role in determining pigment concentration in plants? Plant Science. 2009;177(4):310-6.

374. Felle HH. pH Regulation in Anoxic Plants. Annals of Botany. 2005;96(4):519-32.

375. He J, Wallace TC, Keatley KE, Failla ML, Giusti MM. Stability of Black Raspberry Anthocyanins in the Digestive Tract Lumen and Transport Efficiency into Gastric and Small Intestinal Tissues in the Rat. Journal of Agricultural and Food Chemistry. 2009;57(8):3141-8.

376. Yang P, Yuan C, Wang H, Han F, Liu Y, Wang L, et al. Stability of Anthocyanins and Their Degradation Products from Cabernet Sauvignon Red Wine under Gastrointestinal pH and Temperature Conditions. Molecules. 2018; 23(2).

377. Piffaut B, Kader F, Girardin M, Metche M. Comparative degradation pathways of malvidin 3,5-diglucoside after enzymatic and thermal treatments. Food Chemistry. 1994;50(2):115-20.

378. Fernandes I, Faria A, de Freitas V, Calhau C, Mateus N. Multiple-approach studies to assess anthocyanin bioavailability. Phytochemistry Reviews. 2015;14(6):899-919.

379. Li H, Guo A, Wang H. Mechanisms of oxidative browning of wine. Food Chemistry. 2008;108(1):1-13.

380. Maestro S. Schrödinger, LLC: New York, NY. 2021.

381. Becke AD. Density-functional thermochemistry. III. The role of exact exchange. The Journal of Chemical Physics. 1993;98(7):5648-52.

382. Grimme S, Antony J, Ehrlich S, Krieg H. A consistent and accurate ab initio parametrization of density functional dispersion correction (DFT-D) for the 94 elements H-Pu. The Journal of Chemical Physics. 2010;132(15):154104.

383. Hariharan PC, Pople JA. The influence of polarization functions on molecular orbital hydrogenation energies. Theoretica chimica acta. 1973;28:213-22.

384. Marenich AV, Cramer CJ, Truhlar DG. Universal Solvation Model Based on Solute Electron Density and on a Continuum Model of the Solvent Defined by the Bulk Dielectric Constant and Atomic Surface Tensions. The Journal of Physical Chemistry B. 2009;113(18):6378-96.

385. Frisch MJ, Trucks GW, Schlegel HB, Scuseria GE, Robb MA, Cheeseman JR, et al. Gaussian 09 Wallingford, CT2016.

386. Reed AE, Weinstock RB, Weinhold F. Natural population analysis. The Journal of Chemical Physics. 1985;83(2):735-46.

387. Brouillard R, Dubois J-E. Mechanism of the structural transformations of anthocyanins in acidic media. Journal of the American Chemical Society. 1977;99(5):1359-64.

388. Sousa D, Basílio N, Oliveira J, de Freitas V, Pina F. A New Insight into the Degradation of Anthocyanins: Reversible versus the Irreversible Chemical Processes. Journal of Agricultural and Food Chemistry. 2022;70(2):656-68.

389. Vidal S, Meudec E, Cheynier V, Skouroumounis G, Hayasaka Y. Mass Spectrometric Evidence for the Existence of Oligomeric Anthocyanins in Grape Skins. Journal of Agricultural and Food Chemistry. 2004;52(23):7144-51.

390. Salas E, Dueñas M, Schwarz M, Winterhalter P, Cheynier V, Fulcrand H. Characterization of Pigments from Different High Speed Countercurrent Chromatography Wine Fractions. Journal of Agricultural and Food Chemistry. 2005;53(11):4536-46.

391. Alcalde-Eon C, Escribano-Bailón MT, Santos-Buelga C, Rivas-Gonzalo JC. Identification of dimeric anthocyanins and new oligomeric pigments in red wine by means of HPLC-DAD-ESI/MSn. Journal of Mass Spectrometry. 2007;42(6):735-48.

392. Oliveira J, da Silva MA, Jorge Parola A, Mateus N, Brás NF, Ramos MJ, et al. Structural characterization of a A-type linked trimeric anthocyanin derived pigment occurring in a young Port wine. Food Chemistry. 2013;141(3):1987-96.

393. Dangles O, Fenger JA. The Chemical Reactivity of Anthocyanins and Its Consequences in Food Science and Nutrition. Molecules. 2018;23(8):23.

394. Barnes JS, Schug KA. Structural characterization of cyanidin-3,5-diglucoside and pelargonidin-3,5-diglucoside anthocyanins: Multi-dimensional fragmentation pathways using high performance liquid chromatography-electrospray ionization-ion trap-time of flight mass spectrometry. International Journal of Mass Spectrometry. 2011;308(1):71-80.

395. McClelland RA, Gedge S. Hydration of the flavylium ion. Journal of the American Chemical Society. 1980;102(18):5838-48.

396. Alcalde-Eon C, Escribano-Bailón MT, Santos-Buelga C, Rivas-Gonzalo JC. Separation of pyranoanthocyanins from red wine by column chromatography. Analytica Chimica Acta. 2004;513(1):305-18.

397. García S, Oliveira J, Alamo-Sanza M, de Freitas V, Nevares I, Mateus N. Characterization of Anthocyanins and Anthocyanin-Derivatives in Red Wines during Ageing in Custom Oxygenation Oak Wood Barrels. Molecules Online. 2020;26.

398. Bravo MN, Silva S, Coelho A, Boas L, Bronze M. Analysis of phenolic compounds in Muscatel wines produced in Portugal. Analytica Chimica Acta. 2006;563:84-92.

399. Correia P, Araújo P, Ribeiro C, Oliveira H, Pereira AR, Mateus N, et al. Anthocyanin-Related Pigments: Natural Allies for Skin Health Maintenance and Protection. Antioxidants (Basel). 2021;10(7).

400. Masuko T, Minami A, Iwasaki N, Majima T, Nishimura S-I, Lee YC. Carbohydrate analysis by a phenol–sulfuric acid method in microplate format. Analytical Biochemistry. 2005;339(1):69-72.

401. Dorosh O, Fernandes VC, Moreira MM, Delerue-Matos C. Occurrence of pesticides and environmental contaminants in vineyards: Case study of Portuguese grapevine canes. Science of The Total Environment. 2021;791:148395.

402. Guimarães R, Barros L, Dueñas M, Carvalho AM, Queiroz MJRP, Santos-Buelga C, et al. Characterisation of phenolic compounds in wild fruits from Northeastern Portugal. Food Chemistry. 2013;141(4):3721-30.

403. Mizgier P, Kucharska AZ, Sokół-Łętowska A, Kolniak-Ostek J, Kidoń M, Fecka I. Characterization of phenolic compounds and antioxidant and anti-inflammatory properties of red cabbage and purple carrot extracts. Journal of Functional Foods. 2016;21:133-46.

404. Escher GB, Wen M, Zhang L, Rosso ND, Granato D. Phenolic composition by UHPLC-Q-TOF-MS/MS and stability of anthocyanins from Clitoria ternatea L. (butterfly pea) blue petals. Food Chemistry. 2020;331:127341.

405. Algarra M, Fernandes A, Mateus N, de Freitas V, Esteves da Silva JCG, Casado J. Anthocyanin profile and antioxidant capacity of black carrots (Daucus carota L. ssp. sativus var. atrorubens Alef.) from Cuevas Bajas, Spain. Journal of Food Composition and Analysis. 2014;33(1):71-6.

APPENDIX

APPENDIX 1

CHAPTER II

PART A

SECTION I - EXPERIMENTAL CONDITIONS

Table 1A - Elution conditions for the identification of low molecular weight phenolic compounds and proanthocyanidins by LC-MS analysis.

Time (minutes)	Flow (mL/min)	Solvent A (%)	Solvent B (%)
0	0.3	80	20
55	0.3	20	80
70	0.3	10	90
90	0.3	0	100
100	0.3	0	100
105	0.3	80	20
115	0.3	80	20

SECTION II - RESULTS

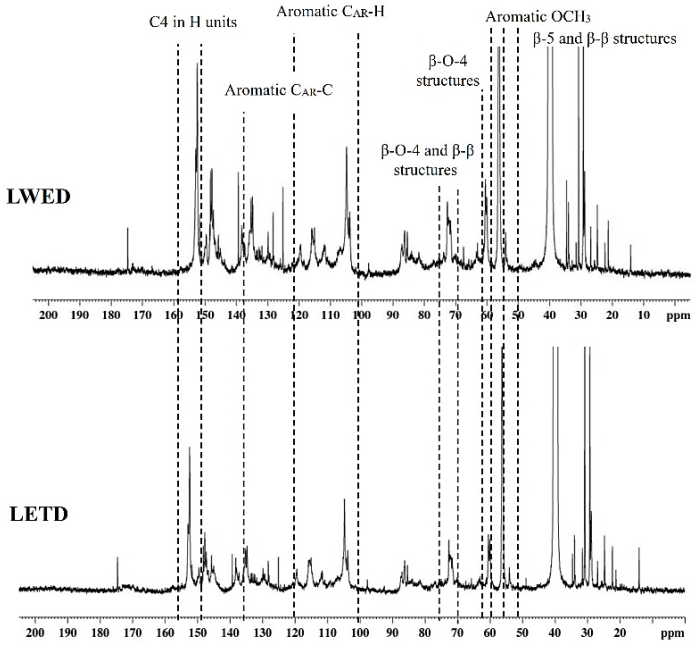

Figure 1A - Quantitative ^{13}C NMR spectra of lignin extracts from vine shoots: LETD – lignin pre-treated with ethanol/toluene and dialyzed and LWED – lignin pre-treated with water/ethanol and dialyzed.

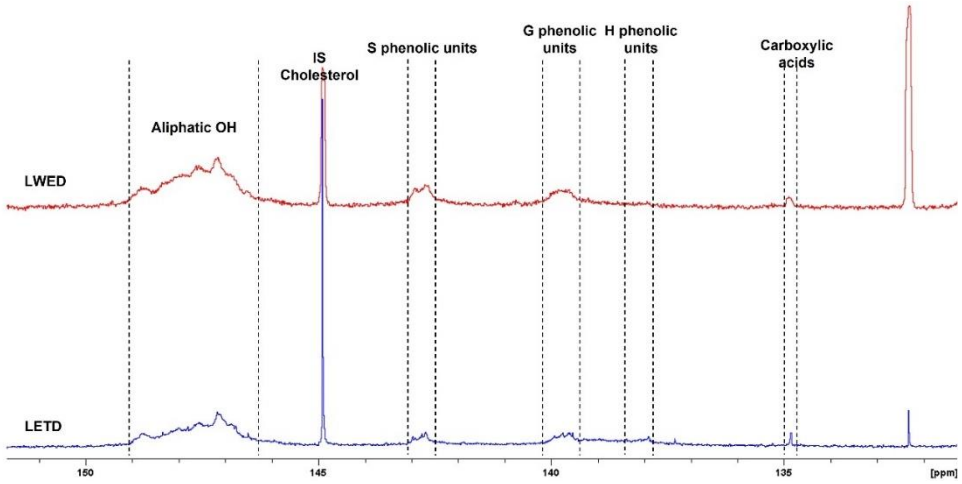

Figure 1B - Quantitative ^{31}P NMR spectra (δ 130-150 ppm) for phosphitylated lignin LETD and LWED.

APPENDIX 2

CHAPTER II

PART B

Table 2A -Evaluation of the pH values for diverse samples of wine, namely for the control and wine in the presence of fining agents: bentonite and different types of lignin. Comparison between 7 and 30 days of experience.

Samples	pH value for the 7 days	pH value for the 30 days
Wine control	3.62 ± 0.02	3.66 ± 0.01
Wine – Bentonite 40 g/hL	3.67 ± 0.01	3.65 ± 0.01
Wine - OL 25 g/hL	3.64 ± 0.03	3.66 ± 0.01
Wine - OL 100 g/hL	3.62 ± 0.02	3.66 ± 0.01
Wine - KL 25 g/hL	3.67 ± 0.02	3.68 ± 0.01
Wine - KL 100 g/hL	3.63 ± 0.02	3.69 ± 0.01
Wine - LS 25 g/hL	3.69 ± 0.01	3.66 ± 0.01
Wine - LS 100 g/hL	3.68 ± 0.01	3.65 ± 0.01

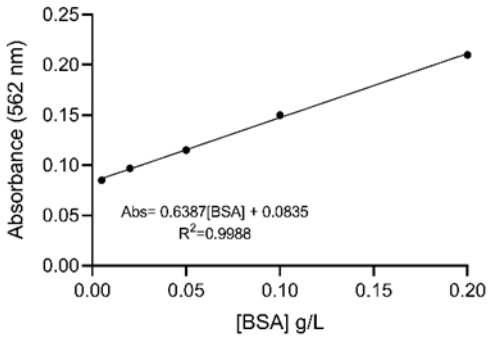

Figure 2A - Standard calibration curve of BSA used for the protein quantification, with a concentration range between 0.005-0.02 g/L.

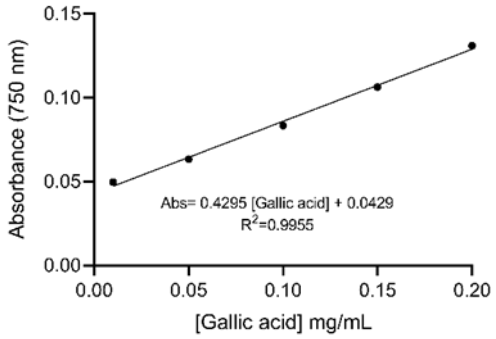

Figure 2B - Standard calibration curve of gallic acid used for the phenolic quantification by the Folin method, with a concentration range between 0.01-0.2 mg/mL.

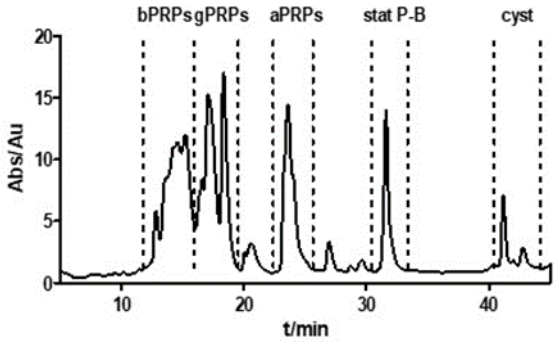

Figure 2C - Typical HPLC salivary protein profile detected at 214 nm. The dotted lines correspond to the different SP families that were already identified.

Table 2B - Recovery of standard volatile compounds at selected calibration points (low, mid, and high).

Compound	Known Concentration	Measured Concentration	Recovery (%)
Isoamyl alcohol (mg/L)	12.9	12.8	99
	128.9	135.1	105
	386.7	311.7	81
3-Hexen-1-ol (µg/L)	22.8	22.9	100
	91.3	97.5	107
	365.0	371.3	102
1-Hexanol (µg/L)	52.2	60.5	116
	174.1	210.2	121
	2176.3	2244.7	103
Phenylethyl alcohol (mg/L)	0.5	0.6	120
	10.3	9.6	93
	51.7	51.4	99
Furfural (µg/L)	70.6	66.3	94
	588.9	634.3	108
	2944.3	2986.2	101
Benzaldehyde (µg/L)	29.9	31.1	104
	119.7	105.1	88
	478.8	498.4	104
Phenylacetaldehyde	5.7	6.2	109
	11.5	10.5	91
	57.3	67.8	118
Ethyl isobutyrate	26.5	30.5	115
	264.6	276.2	104
	846.7	876.5	106
Ethyl butanoate	38.2	34.7	91
	305.8	278.3	91
	1223.0	1205.4	99
Ethyl 2-methylbutanoate	1.2	1.4	117
	12.0	11.9	99
	30.1	30.2	100
Ethyl isovalerate	1.4	1.6	114
	13.9	12.2	88
	34.7	36.9	106
Isoamyl acetate	23.3	27.4	118
	186.2	180.7	97
	558.7	572.5	103
Ethyl hexanoate	26.5	31.2	118
	212.2	186.5	88
	636.5	638.4	100
Hexyl acetate	5.5	6.6	120
	27.6	25.5	92
	110.4	110.5	100
Diethyl succinate (µg/L)	128.3	118.1	92
	641.5	695.5	108
	1540.0	1461.0	95
Ethyl octanoate (µg/L)	239.3	224.8	94
	957.1	1067.6	112
	2153.4	2062.2	96
Phenylethyl acetate	36.8	35.7	97
	147.0	134.4	91
	294.0	299.4	102
Ethyl decanoate	9.5	10.5	111
	47.5	45.1	95
	190.0	205.3	108
β-Linalool (µg/L)	3.5	2.9	83
	35.1	28.7	82
	140.5	140.5	100

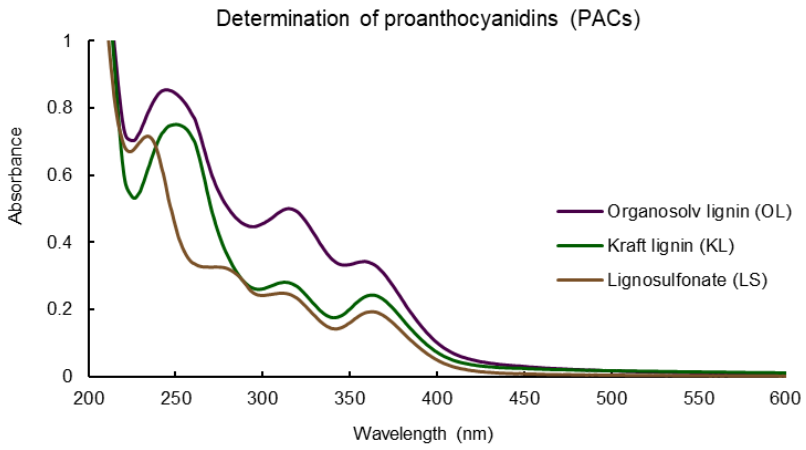

Figure 2D - UV-Vis spectrum of OL, KL, and LS after the analytical procedure to determine the proanthocyanidins content. Considering the values obtained for absorbance at 520 nm necessary to determine the proanthocyanidins content (≈ 0 a.u.), it is possible to conclude for this proposal that the lignin samples only present trace amounts of PACs

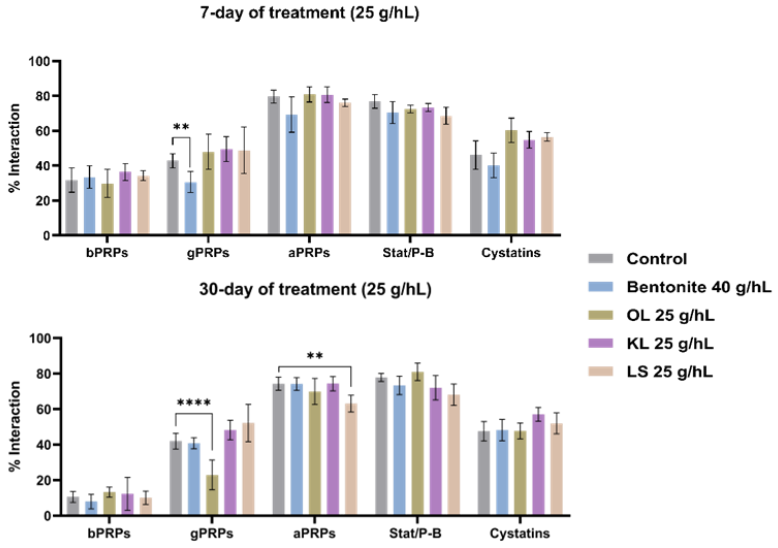

Figure 2E - Percentage of the interaction of the different SP families with each treated wine (bentonite at 40 g/hL and OL, KL, and LS at 25 g/hL) for both 7 and 30 days of treatment. Control condition refers to the wine without treatment. Statistical analysis was made by two-way ANOVA. Asterisks (*) indicate a statistical difference (** – $p \leq 0.01$, **** – $p \leq 0.0001$) relative to the control wine. Bars represent the mean ± standard deviation (n=6).

Table 2C - Identification of the polyphenol compounds in the wine samples by LC/DAD-MS. The identity of each compound was achieved by comparison with data reported in the literature for red wine *(396-398)*.

Retention time (min)	$[M]^+$ (*m/z*)	MS^2 (*m/z*)	Tentative identification
Anthocyanins and derivatives			
15.41	595	451; 443; 427; 409; 301; 247	Peonidin-3-glucoside-4-vinylcatechol
21.64	579	561; 533; 453; 427; 409; 301; 291	Peonidin-3-glucoside-4-vinylphenol
26.5	781	619	Malvidin-3-O-glucoside-catequin
30.85	579	561; 525; 427; 409; 393; 301; 291; 247	Peonidin-3-glucoside-4-vinylphenol
31.19	1477	1315	Malvidin-3-*O*-glucoside trimer
37.59	547	385	Petunidin-3-glucoside pyruvic derivative
38.03	867	849;715; 697; 577; 579; 535; 409	Unknown
39.46	463	301	Peonidin-3-glucoside
40.86	493	331	Malvidin-3-glucoside
43.48	531	369	Peonidin-3-glucoside pyruvic derivative
44.59	495	319	Unknown
45.34	561	399	A-type vitisin
48.01	517	355	B-type vitisin
49.99	603	399	Carboxypyranomalvidin-3-*O*-acetylglucoside
53.66	479	303	Petunidin-3-glucoside

54.87	1093	931; 803,641	Malvidin-3-*O*-glucoside-4-vinyl-di(epi)catechin
55.21	809	647; 519; 357	Malvidin-3-*O*-glucoside-8-ethyl-catechin
56.88	927	619; 467; 373	Malvidin-3-*O*-coumaroylgluc-catechin
62.22	677	369	Peonidin-3-(p-coumaroyl)glucoside pyruvic derivative
62.28	707	399; 383; 355; 338;310; 246	Carboxypyranomalvidin-3-*O*-coumaroylglucoside
64.08	679	661; 548; 435	Unknown
67.09	805	643; 491	Malvidin-3-glucoside-4-vinylcatechin
67.19	533	371; 356; 343; 311; 283	Delphinidin-3-glucoside pyruvic derivative
71.46	639	331	Malvidin-3-*O*-coumaroylglucoside
Other phenolic compounds			
7.88	153	135; 109	Protocatechuic acid
18.81	175	156	Ethyl cinnamate
20.79	127	109; 98	5-(hydroxymethyl)furfural
23.12	163	144; 116	Coumaric acid
26.76	291	273; 245; 205	Catechin
39.24	301	286	Ellagic acid
50.37	229	135	*Trans*-Resveratrol
54.76	305	287; 259; 195; 153	Epigallocatechin
65.57	229	135	*cis*-Resveratrol

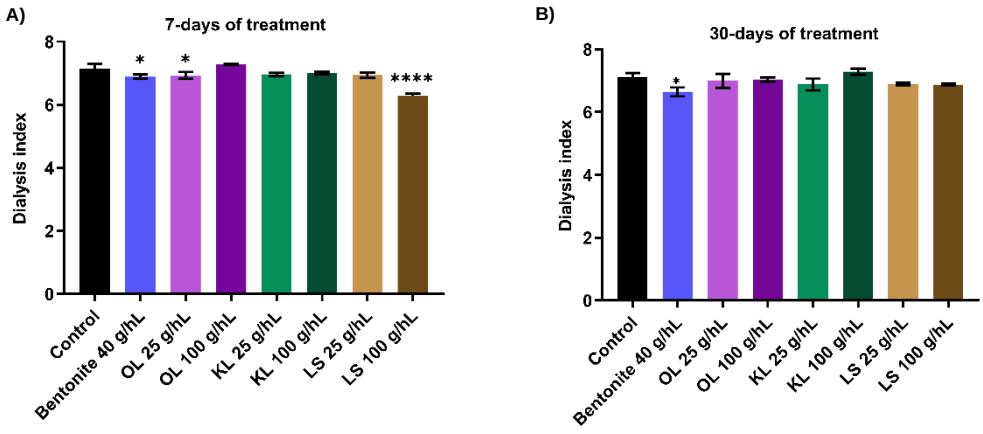

Figure 2F - Dialysis index for control wine and wine treated with bentonite and lignin at different concentrations for different contact times. Statistical analysis was made by one-way ANOVA. Asterisks (*) indicate a statistical difference (* – $p \leq 0.05$, ** – $p \leq 0.01$, *** – $p \leq 0.001$, **** – $p \leq 0.0001$) relative to the control wine. Bars represent the mean ± standard deviation (n=9).

Table 2D – Levels of volatile compounds quantified in wine samples by HS-SPME-GC/MS.

Compound	RT	Concentration [a]							Units	Descriptors [b]	Olfactory perception threshold [c]
		Control	OL 25 g/hL	OL 100 g/hL	KL 25 g/hL	KL 100 g/hL	LS 25 g/hL	LS 100 g/hL			
Alcohols											
Isoamyl alcohol	4.65	321.7 ± 29.8	299.6 ± 9.7	293.0 ± 4.0	278.8 ± 12.5	269.1 ± 16.9	246.2 ± 17.3	232.4 ± 22.7	mg/L	Fusel, cheese	30 mg/L
3-Hexen-1-ol	7.39	83.5 ± 35.9	64.8 ± 18.1	86.8 ± 7.4	78.8 ± 9.7	74.1 ± 15.6	79.4 ± 15.3	75.8 ± 2.8	µg/L	Green, bitter, fatty	400 µg/L
1-Hexanol	7.74	4.7 ± 0.2	4.1 ± 0.2	4.3 ± 0.1	4.3 ± 0.2	3.9 ± 0.2	3.8 ± 0.3	3.5 ± 0.1	mg/L	Grass, resin	8 mg/L
Phenylethyl alcohol	15.34	37.4 ± 1.5	36.0 ± 4.2	31.9 ± 3.7	34.9 ± 4.3	32.9 ± 3.2	37.2 ± 3.2	28.7 ± 2.6	mg/L	Rose, honey	14 mg/L
Aldehydes											
Furfural	6.73	553.9 ± 97.9	582.9 ± 57.1	541.0 ± 83.8	522.9 ± 68.3	476.3 ± 77.3	816.4 ± 48.6	1516.3 ± 83.8	µg/L	Almond, bread	14.1 mg/L
5-Methyl-2-furfural	10.45	ND	ND	ND	ND	ND	ND	ND	-	Almond, burnt sugar	16 mg/L
Benzaldehyde	10.50	104.7 ± 9.7	108.2 ± 11.0	104.9 ± 6.7	104.1 ± 3.8	104.9 ± 13.4	82.7 ± 11.1	89.5 ± 0.3	µg/L	Almond, bitter	1-2 mg/L
Phenylacetaldehyde	13.00	14.6 ± 1.3	16.7 ± 1.7	16.9 ± 0.3	16.0 ± 0.5	17.3 ± 1.1	16.6 ± 3.7	13.7 ± 0.7	µg/L	Bitter, green, honey	1 µg/L
Esters											
Ethyl isobutyrate	5.03	314.1 ± 76.3	236.7 ± 35.5	202.2 ± 91.0	259.0 ± 91.1	326.0 ± 22.8	209.5 ± 212.5	418.6 ± 83.5	µg/L	Fruity	15 µg/L
Ethyl butanoate	5.95	222.6 ± 45.7	154.4 ± 3.9	137.4 ± 44.0	150.6 ± 25.9	178.4 ± 15.8	130.5 ± 135.6	227.5 ± 33.4	µg/L	Strawberry, apple	20 µg/L
Ethyl 2-methylbutanoate	7.16	4.0 ± 0.5	3.0 ± 0.4	2.9 ± 0.4	3.6 ± 0.9	3.6 ± 0.6	3.3 ± 1.1	4.7 ± 1.5	µg/L	Apple	18 µg/L

Compound	RT	Concentration [a]							Units	Descriptors [b]	Olfactory perception threshold [c]
		Control	OL 25 g/hL	OL 100 g/hL	KL 25 g/hL	KL 100 g/hL	LS 25 g/hL	LS 100 g/hL			
Ethyl isovalerate	7.30	3.8 ± 0.7	2.5 ± 0.1	2.2 ± 0.8	2.6 ± 0.6	3.4 ± 0.3	2.1 ± 2.8	4.8 ± 1.0	µg/L	Sweet, fruity	3 µg/L
Isoamyl acetate	7.94	256.6 ± 50.0	175.0 ± 3.9	161.5 ± 46.2	184.3 ± 28.9	235.2 ± 22.6	181.8 ± 183.9	288.3 ± 38.7	µg/L	Banana, sweet, fruity	30 µg/L
Ethyl hexanoate	11.57	309.3 ± 27.0	211.3 ± 7.7	175.6 ± 40.4	199.7 ± 11.5	242.6 ± 47.9	232.8 ± 242.4	365.3 ± 48.1	µg/L	Apple, banana	14 µg/L
Hexyl acetate	12.00	7.9 ± 0.4	7.1 ± 0.1	6.6 ± 0.4	6.9 ± 0.2	7.4 ± 0.5	6.6 ± 2.6	9.2 ± 0.6	µg/L	Cherry, pear	1.5 mg/L
Diethyl succinate	16.97	10.9 ± 0.8	10.6 ± 0.8	9.3 ± 0.9	9.9 ± 0.5	8.8 ± 0.4	9.8 ± 1.7	7.5 ± 0.1	mg/L	Fruity	200 mg/L
Ethyl octanoate	17.53	635.1 ± 12.2	469.2 ± 41.8	268.4 ± 67.0	364.8 ± 55.3	438.6±194.4	707.2 ± 1083.0	1900.0± 40.2	µg/L	Pineapple, sweet	600 µg/L
Phenylethyl acetate	19.24	72.7 ± 2.3	74.8 ± 5.5	69.6 ± 1.7	70.3 ± 1.5	69.2 ± 4.1	72.6 ± 5.6	69.6 ± 1.2	µg/L	Rose, violet	250 µg/L
Ethyl decanoate	22.99	35.8 ± 0.7	33.9 ± 3.5	27.3 ± 2.7	28.7 ± 1.2	31.1 ± 5.9	50.3 ± 33.2	98.9 ± 11.4	µg/L	Brandy, fruity	200 µg/L
Ketones											
β-Damascenone	22.73	3.4 ± 0.02	3.5 ± 0.2	3.2 ± 0.1	3.2 ± 0.03	3.3 ± 0.2	3.6 ± 0.3	3.5 ± 0.01	µg/L	Apple, honey, smoky	0.05 µg/L
Terpenes											
Linalool oxide	13.85	ND	ND	ND	ND	ND	ND	ND	-	Citrus, green	25 µg/L
β-Linalool	14.73	8.4 ± 0.4	8.2 ± 1.3	7.1 ± 0.3	7.4 ± 0.2	7.1 ± 2.1	6.8 ± 0.7	5.9 ± 0.01	µg/L	Flower, muscat, lavender	25 µg/L
α-Ionone	23.79	ND	ND	ND	ND	ND	ND	ND	-	Fruity, violet	90 ng/L

APPENDIX 3

CHAPTER II

PART C

SECTION I - EXPERIMENTAL CONDITIONS

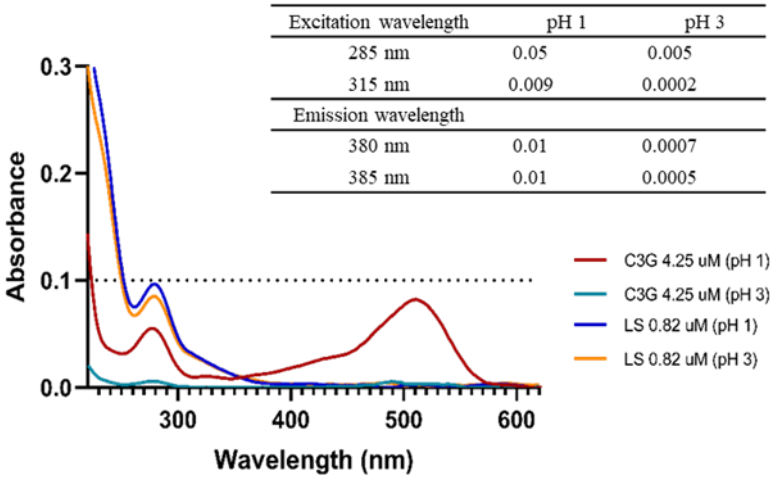

Figure 3A - UV-vis spectra of LS and C3G at the maximum concentration used in the fluorescence experiments, to maintain the UV absorbance at 280 nm under 0.1 to avoid inner filter effects. Inset: Absorbance values of the quencher (C3G) at the maximum concentration used of 4.25 µM (residual values were measured for the excitation and emission wavelength to ensure that the excitation light can effectively reach the fluorophores and that the emitted light can reach the detector without significant reabsorption, leading to more accurate fluorescence measurements).

TEXT 3A. PARAFAC modeling

PARAFAC is a bilinear principal component analysis (PCA) generalization to higher-order arrays. In other words, PARAFAC decomposes N-way arrays into N-loading matrices. Therefore, if fluorescence EEMs are arranged in a three-way array **X** of dimensions $I \times J \times K$, where I is the number of samples, J is the number of emission wavelengths. K is the number of excitation wavelengths, PARAFAC decomposes them into three matrices **A** (the score matrix), **B,** and **C** (loading matrices) with elements a_{if}, b_{jf}, and c_{kf}.

The samples were divided into two different datasets based on the pH of the solution (pH 1 and pH 3) and analyzed independently. This study applied a non-negativity constraint to the parameters allowing only chemically relevant results. The convergence criterion was set to 1^{-10} and the maximum number of iterations to 5000. Some preprocessing steps were adopted to minimize the influence of scatter lines and other attributes of the EEM landscape.

The EEM of a blank (0.1 M HCl or 10 mM citrate buffer, pH 3) was subtracted from each sample EEM. Rayleigh and Raman scatters were removed according to

(Bahram, Bro, Stedmon, & Afkhami, 2006). The PARAFAC models with two to five components were computed for the EEMs. For both datasets, exploratory data analysis generated preliminary models with 2 to 3 factors, while any model with more than 3 components did not show convergence. Determination of the correct number of components was primarily based on split-half analysis, residual analysis, and visual inspection (Stedmon & Bro, 2008), indicating that the appropriate number of components was 2 for the pH 1 dataset and 3 for the pH 3 (Figure 3B).

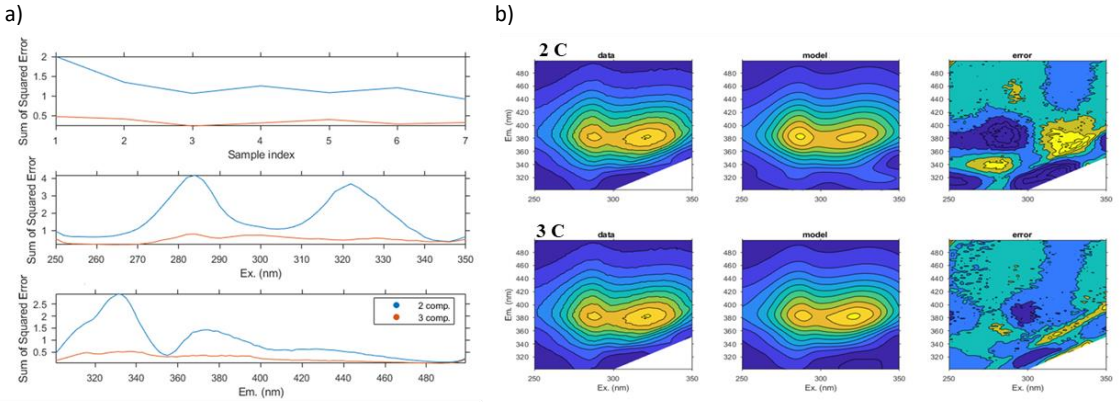

Figure 3B - Example of residual analysis (a) and visual inspection (b) of 2 and 3 components of the database at pH 3

SECTION II - RESULTS

Table 3A - Chemical characterization of lignosulfonates using different methodologies (277).

Parameters		Lignosulfonate characterization
Weight-average molecular weight (Mw)		48,566 g/mol
Polydispersity index (MW/Mn)		1.57
Inorganic content		10.1 ± 0.3 % w/w_{lignin} (dry weight)
Total monomeric phenolics by nitrobenzene oxidation		23.3 % w/w_{lignin} (dry weight)
^{13}C NMR	β-O-4 structures content	40 (number per 100 Ar)
	Condensation degree (CD)	38%
	Syringyl/Guaiacyl (S/G) ratio	0.24

Table 3B - FTIR peaks assignments of lignosulfonates.

Peak positions (cm^{-1})	Vibrational assignment
3280	O–H stretching
2940	asymmetric aliphatic C–H stretching
2845	symmetric aliphatic C–H stretching
1720	C=O stretching of acetyl (* shoulder)
1650	O–H and conjugated C–O
1600	C=C stretching of the aromatic ring (aromatic skeletal vibration)
1510	C–C, C=C ring skeletal vibration
1460	C–H vibration (asymmetric bending in CH_3)
1420	C–O stretching and C-H deformation
1260	C–O (guaiacyl aromatic methoxyl groups) stretching and linkage
1200	sulfonic acids (* broad shoulder)
1140	Aromatic C–H (guaiacyl unit) stretching
1035	C–OH + C–O–C (aliphatic OH + ether) stretching, sulfonic acids
650	C–H bending

Table 3C - Determination of association constants by UV-visible spectroscopy considering the amount of negative groups in LS structure.

	K_a (M^{-1})
pH 1	1.04×10^8
pH 3	1.71×10^8
pH 4	4.95×10^7

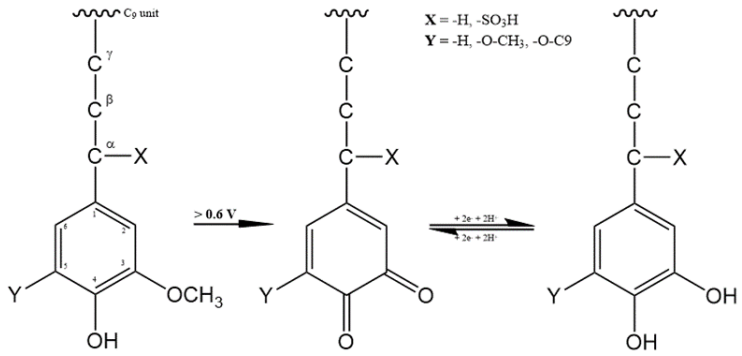

Scheme 3A - Electrochemical transformation of methoxyphenol moieties in lignosulfonates into quinone/hydroquinone redox couples.

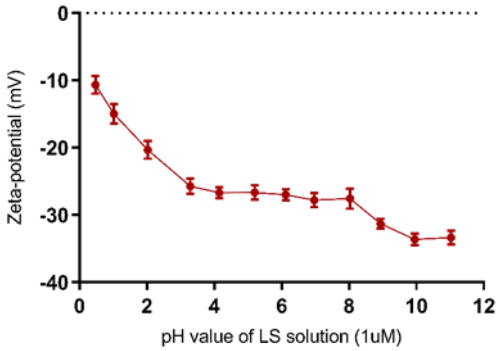

Figure 3C - Zeta-potential values of lignosulfonate (1 µM) at different pH values at room temperature.

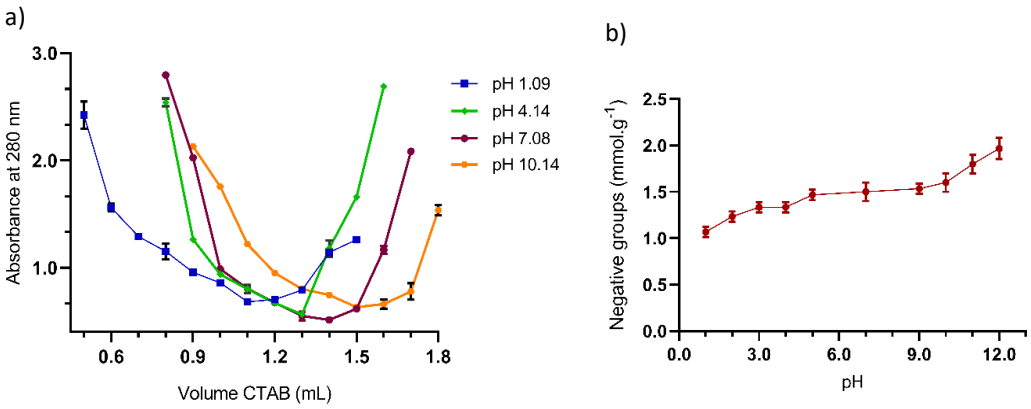

Figure 3D - (a) Examples of CTAB curves for lignosulfonates at different pH values. (b) Negative group content of lignosulfonate as a function of the pH values.

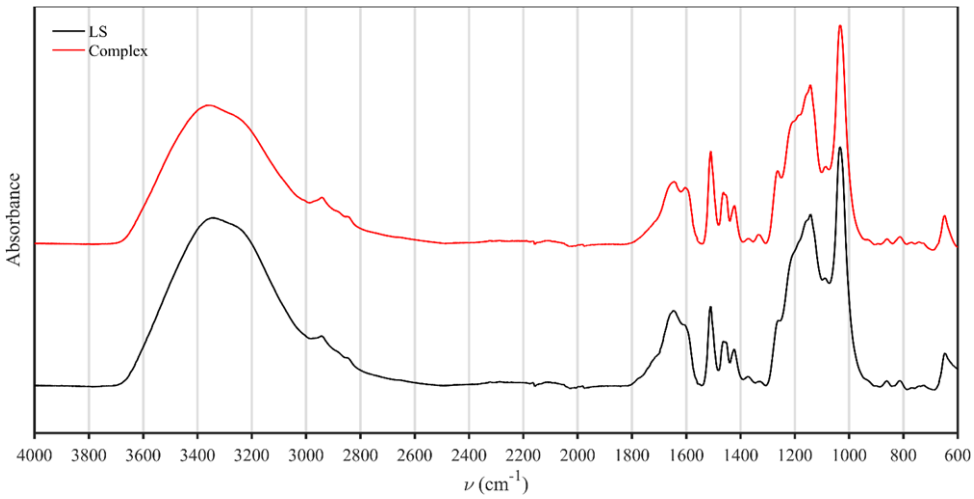

Figure 3E - FTIR spectra of LS and the LS-C3G complex.

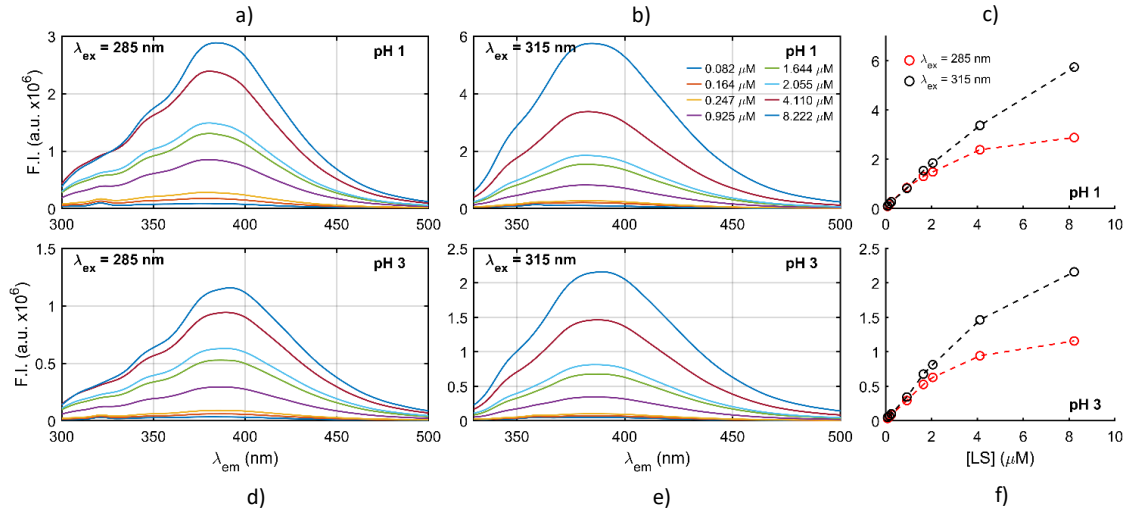

Figure 3F - Fluorescence emission spectra of increasing concentrations of LS (0.082 – 8.222 μM) recorded at pH 1 (a, b) and pH 3 (d, e), at excitation wavelength of 285 nm (a, e) and 315 nm (b, d). The correlation between LS concentration and the fluorescence intensity at the peak is reported for pH 1 (c) and pH 3 (f).

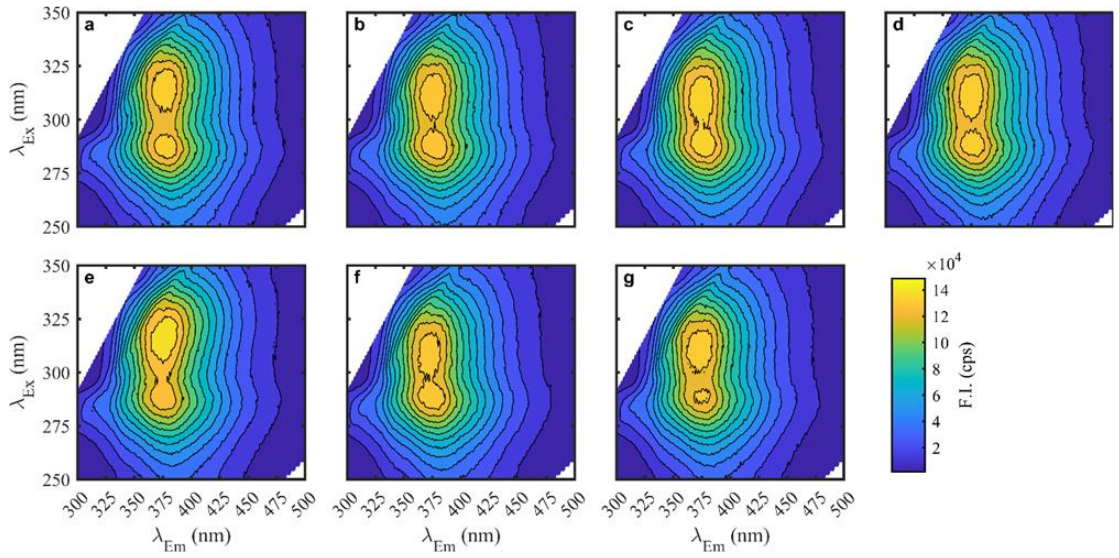

Figure 3G - Fluorescence excitation-emission matrix spectra of 0.82 μM LS recorded at pH 1(0.1 M HCl) (a) in the presence of increasing concentrations of C3G (0.42–4.25 μM) (b-g).

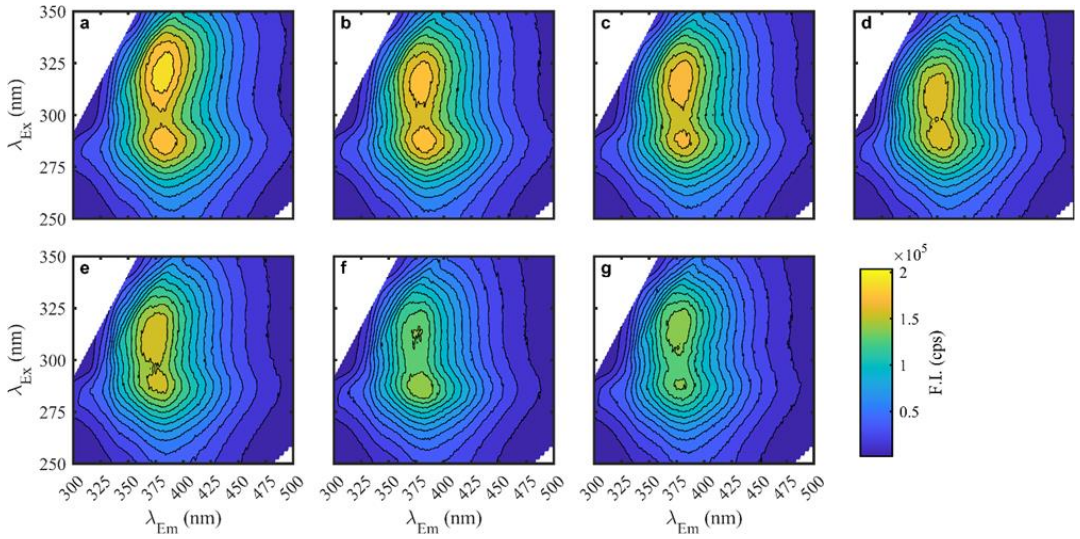

Figure 3H - Fluorescence excitation-emission matrix spectra of 0.82 µM LS recorded at pH 3 (10 mM citrate buffer) (a) in the presence of increasing concentrations of C3G (0.42–4.25 µM) (b-g).

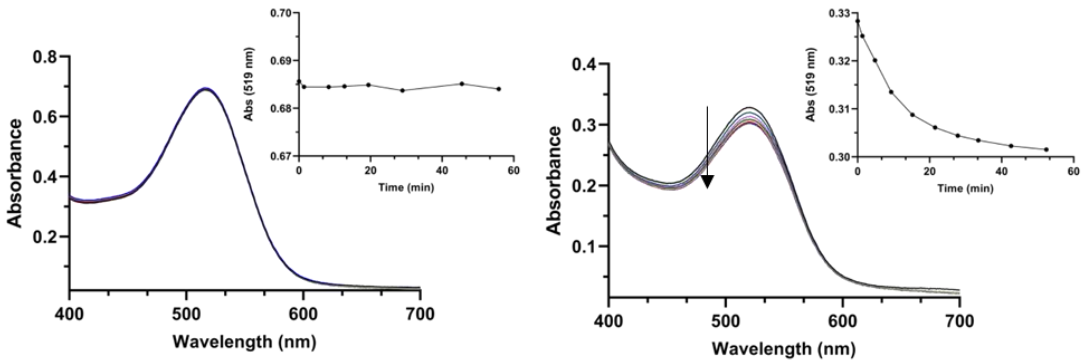

Figure 3I - UV-visible spectra resultant from the evaluation of the time from the formation of the LS-C3G complex to stability at pH 1 (image on left) and pH 3 (image on right). Insets: variation of the absorbance for the maximum absorption wavelength in function of the time.

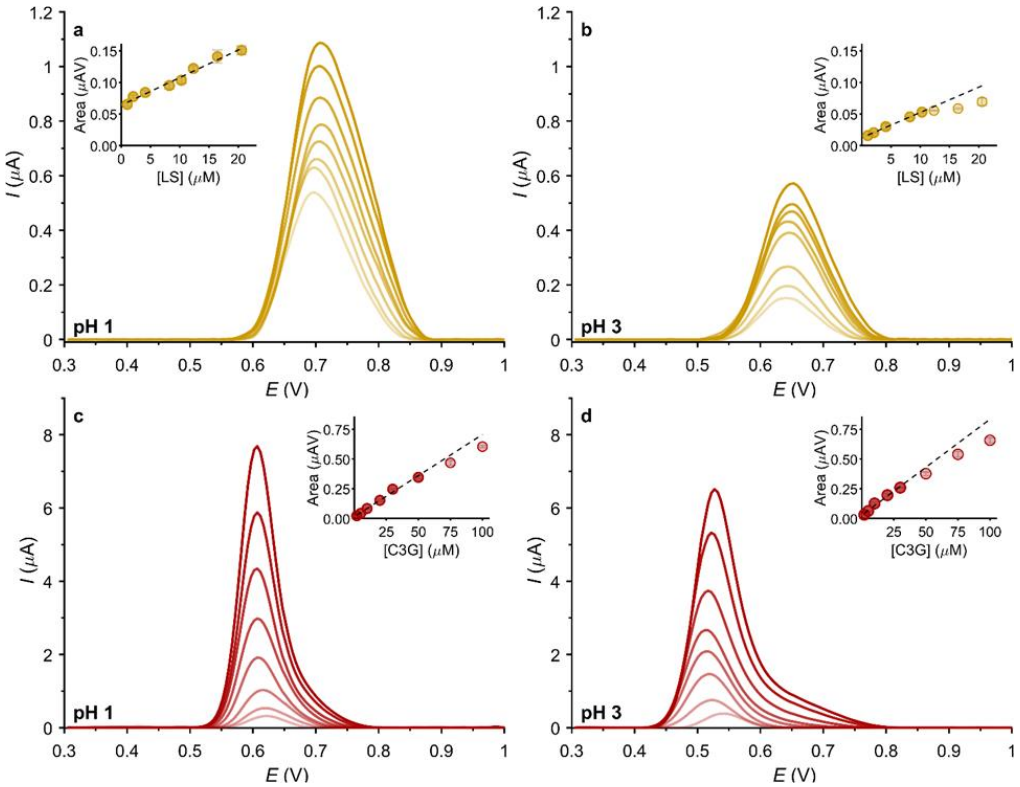

Figure 3J - Square wave voltammograms of LS and C3G were recorded at pH 1 (a, c) and pH 3 (b, d) varying the concentration of LS (1–20.5 µM) and C3G (2–100 µM). Insets: variation of LS and C3G peak area against their in-sample concentration. Lighter circles in the insets correspond to the concentrations that undergo a deviation from linearity.

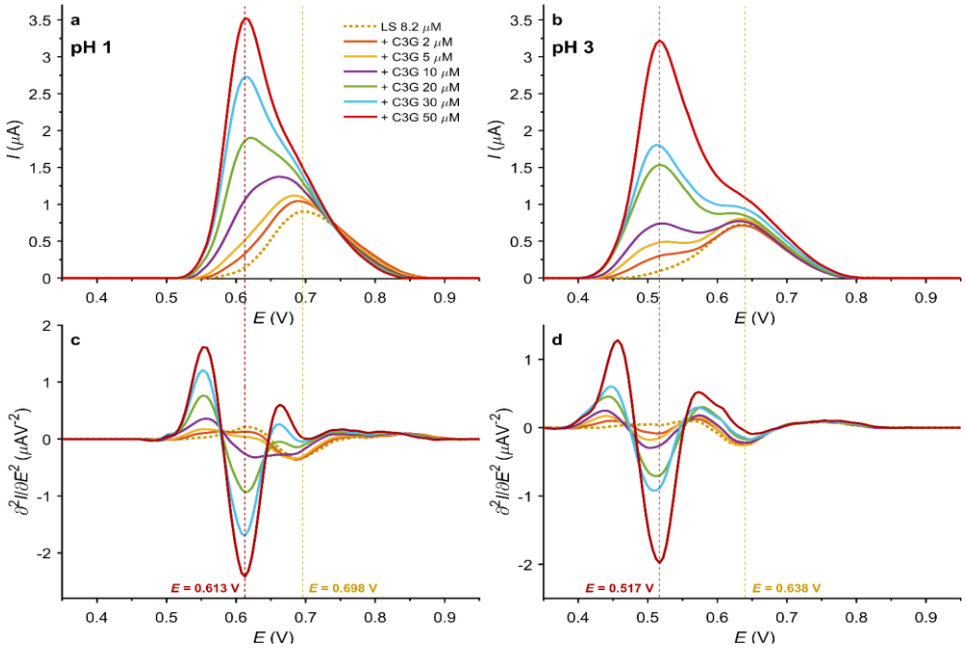

Figure 3K - SWVs of 8.2 µM LS (yellow dotted trace) in the presence of increasing concentrations of C3G (2-50 µM) recorded at pH 1 (a) and pH 3 (b), and the corresponding second derivative plots (c and d).

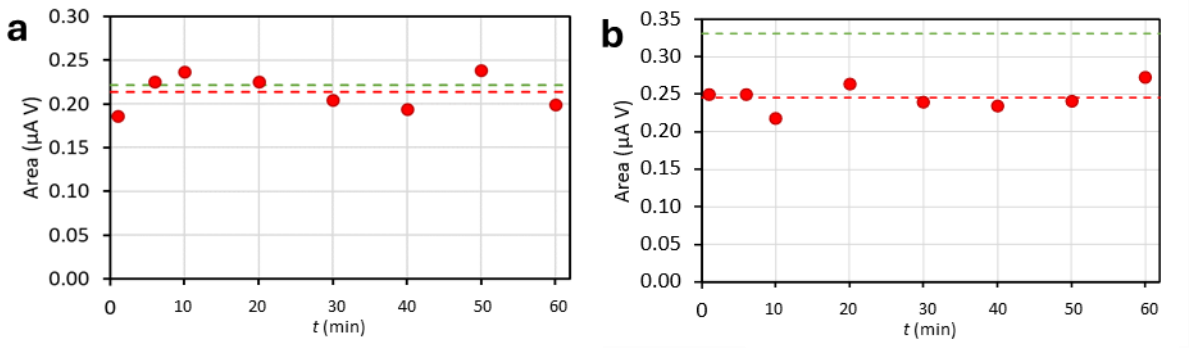

Figure 3L - Time trend of the C3G-LS complex peak area over 60 min recorded at pH 1 (a) and pH 3(b). The green dotted line indicates the C3G peak area in the absence of LS, while the red dotted line is the average value of all points.

APPENDIX 4

CHAPTER III

PART A

SECTION I - EXPERIMENTAL CONDITIONS

4A. Quantification of Protein

Protein content in extracts was quantified using the modified BCA (Bicinchoninic Acid) protein assay (280). Proteins were precipitated from the extracts (10 g/L) in Milli-Q water with 20 % (m/v) trifluoroacetic acid (TCA) solution in acetone (1:1) on ice. After one hour, the solution was centrifuged (10,000 rpm for 10 min), and the protein pellet was redissolved in water for a second TCA precipitation. After centrifugation, the pellet was washed three times, and then resuspended in water and quantified. In 96-well plates, 10 µL of each sample containing proteins or standard BSA (bovine serum albumin) solution was mixed with 200 µL of BCA reagent. For the blank, distilled water replaced the sample volume. After being incubated in the dark at 37 °C for 30 min, the plate was read at 562 nm using a Biotek Powerwave XS plate reader. The results were expressed as g BSA equivalents / 100 g dry weight. Standard BSA solutions (0.01 − 1.1 g/L) were prepared in triplicate for the calibration curve (Absorbance = 0.459 [BSA g/ L] + 0.107, R^2= 0.9999).

4B. Lipid analysis

The lipid content in each extract was determined by GC − MS as described in the literature (399). Briefly, lipids were extracted from the anthocyanin-based extracts (10 g/L) by liquid-liquid extraction with chloroform (1:1). The organic phase was evaporated to dryness and the solid was resuspended in 1 mL of 0.5 M KOH solution and 2 mL of BF_3 solution both in methanol. The mixture was transferred to a hydrolysis tube and heated at 100 ºC in a water bath for 10 minutes and then cooled on ice. After adding ethyl ether (5 mL), the solution was submitted to a liquid-liquid extraction with Milli-Q water (5 mL twice). The organic fraction was dried by the addition of anhydrous sodium sulfate. For the GC-MS analysis, the ion source and MS-transfer line temperatures were 280 ºC and 250 ºC, respectively. The column temperature was initially set to 110 ºC, and held for 2 min, until 185 ºC, which increased at a rate of 30 ºC.min^{-1} for 2 min until 205 ºC. After 5 minutes at this temperature, there was an increase at a rate of 30 ºC min^{-1} until 250 ºC, held for 10 min, which increased at a rate of 30 ºC.min^{-1} until 280 ºC, held for 10 min. Palmitic acid (0.01 – 0.25 g/L) was used as a standard for the calibration curve method (Calibration curve: Area = 7 x 10^9 [palmitic g/L] – 6 x 10^7, R^2= 0.9956).

4C. Sugar quantification

The free sugar content of each extract was evaluated using a GC-MS technique described in the literature (233). Briefly, 20 µL of the stock solutions of the extracts prepared in Milli-Q water at 10 g/L was mixed with 600 µL of HMDS: acetonitrile mixture (1:1) to form silyl derivatives (make the hydroxyl groups of glucose more volatile) and 2 µL of trifluoroacetic acid (catalyst). The samples were prepared in triplicate and heated to 50 °C for 30 min. Then, it was added 400 µL of HMDS and the resultant mixture was heated to 80 °C for 30 min. After cooling to room temperature, 1 µL of the final solution was injected into the GC-MS/MS system. The sample analysis was performed on a traced 1300 Gas chromatograph. The gas chromatograph is equipped with a split-splitless injector, an autosampler 1310 Thermo Scientific, and an ISQ Single quadrupole MS (*Thermo Fisher, Austin, TX, USA*). It was used a column 30 m x 0.25 mm (i.d.) x 0.25 µM DB17 capillary column (*Agilent Technologies, CA, USA*), initially at 110 °C and held for 5 min, which it was increasing at a rate of 6 ºC.min^{-1} to 300 °C for 5 min. Analyzes were performed in SCAN mode with an m/z range set to 40 − 1100, projecting the ion source temperature to 280 °C and an electron energy of 70 eV. Glucose was used as standard, and the results were expressed as g glucose equivalents/ 100 g of dry extract (Calibration curve: Area = 3 x 10^9 [glucose g/L] – 6 x 10^7, R^2= 0.9989).

4D. Polysaccharide content

The quantification of polysaccharide content in the HC, RC, and BPF extracts was determined using the phenol sulfuric acid method described by Makuso et al. (400). Briefly, for a microtube were added 50 µL of anthocyanin-based extract was prepared in Milli-Q water (0.25 g/L), and 150 µL of concentrated sulfuric acid. The mixture was shaken for 20 sec using a vortex. Then, 30 µL of 50 g/L phenol solution was added to the microtube, and the final solution was incubated in a thermoblock (Thermo Scientific) at 98 °C for 30 min. After that, samples were left to cool down at room temperature and 200 µL transferred to a 96−well plate. The absorbance of samples was determined at 490 nm. Glucose was used as a standard (0.02 − 0.2 g/L) in the calibration curve method (Calibration curve: Absorbance = 5.77 [glucose g/L] + 0.148, R^2= 0.9984).

4E. Contaminants analysis

A total of 38 contaminants was evaluated in this study: (i) 27 pesticides: α-,β-, and δ-hexachlorocyclohexanes (HCHs), hexachlorobenzene (HCB), o,p´-DDT ([1,1,1 trichloro-

2, 2-bis-(p-chlorophenyl) ethane]), p,p´-DDE ([2,2bis(p-chlorophenyl)-1,1-dichloroethylene]), p,p´-DDD (dichlorodiphenyldichloro-ethane), aldrin, dieldrin, α-endosulfan, bifenthrin, cypermethrin (isomer I, II, III, IV), cyhalothrinm (isomer I, II)), fenvalerate (isomer I, II), deltamethrin (isomer, I, II),, chlorfenvinphos, chlorpyrifos, chlorpyrifos-methyl, dimethoate, parathion-methyl, malathion, (ii) 7 BDE: (BDE28); 2,2′,4,4′-tetrabromodiphenyl ether (BDE47); 2,2′,4,4′,5-pentabromodiphenyl ether (BDE99); 2,2′,4,4′,6pentabromodiphenyl ether (BDE100); 2,2′,4,4′,5,5′-hexabromodiphenyl ether (BDE153); 2,2′,4,4′,5,6′-hexabromobiphenyl ether (BDE154) and 2,2′,4,4′,5,5′-hexabromodiphenyl ether (BDE183); (iii) 2,4,4′-trichlorobiphenyl (PCB28), 2,2′,4,5,5′-pentachlorobiphenyl (PCB101), 2,3′,4,4′,5-pentachlorobiphenyl (PCB118), 2,2′,4,4′,5,5′ - hexachlorobiphenyl (PCB153) and 2,2′,3,4,4′,5,5′-heptachlorobiphenyl (PCB180). Pesticide standards (purity>97.0%) were obtained from Chemservice (West Chester, PA, USA), Dr. Ehrenstorfer GmbH (Augsburg, Germany), and Sigma-Aldrich Co (Steinheim, Germany). PCB standards were purchased from Riedel-de Haën (Seelze, Germany) at 10 ng/µL in isooctane. Standards of BFRs with ≥98% purity were acquired at Isostandards Material, S. L. (Madrid, Spain) at 50 mg/L in isooctane.

Standard solutions were prepared in n-hexane (GC assay > 99%) supplied by Merck (Darmstadt, Germany). Methanol (MeOH), dichloromethane (DCM), and ethyl acetate (EtAC) were supplied by Carlo Erba (Val-de-Reuil, France) and presented a GC assay of ≥ 99 %. Ultrapure water (resistivity of 18.2 MΩ.cm) was produced using a Simplicity 185 system (Millipore, Molsheim, France). For the solid phase extraction (SPE), C18e (500 mg / 3mL) solid phase extraction (SPE) cartridges were provided by Phenomenex (Spain).

4F. Contaminant isolation procedure

Extracts were submitted to solid phase extraction (SPE) according to the literature (8, 9), with some modifications. HC, RC, and BPF extract samples were diluted with Milli-Q water (1:5) and passed through the considered SPE C18e cartridge, which was previously conditioned with the elution solvent (EtAC: DCM) followed by MeOH and ultrapure water (2 x 2 mL of each). After the concentration step, cartridges were rinsed with 5 mL of ultrapure water, dried for 20 min, and eluted with 2 x 2 mL EtAC: DCM. This extract was dried using a gentle stream of nitrogen and recovered in 1 mL of n-hexane before injection in the chromatographic system. The gas chromatography analysis was performed according to (401).

SECTION II – RESULTS

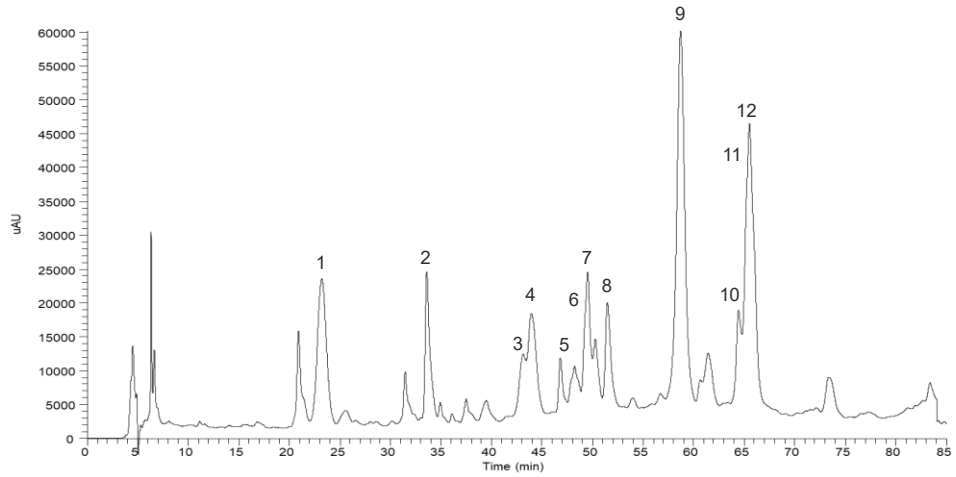

Figure 4A - LC-MS chromatogram for red cabbage extracted with water. Peak 1: cyanidin-3-diglucoside-5-glucoside; peak 2: cyanidin-3-(sinapoyl)-diglucoside-5-glucoside; peak 3: cyanidin-3-(caffeoly)(p-coumaroyl)-diglucosides-5-glucoside; peak 4: cyanidin-3-(feruloyl)-triglucoside-5-glucoside; peak 5: cyanidin-3-(sinapoyl)-triglucoside-5-glucoside; peak 6: cyanidin 3-(feruloyl)(sinapoyl)triglucoside-5-glucoside; peak 7: cyanidin 3-(sinapoyl)(p-coumaroyl)triglucoside-5-glucoside; peak 8: cyanidin 3-(sinapoyl)(sinapoyl)triglucoside-5-glucoside; peak 9: cyanidin-3-(p-coumaroyl)-diglucoside-5-glucoside, cyanidin-3-diglucoside-5-(sinapoyl)-glucoside and cyanidin-3-(feruloyl)-diglucoside-5-glucoside; peak 10: cyanidin-3-(feruloyl)(feruloyl)-diglucoside-5-glucoside; peak 11: cyanidin-3-(feruloyl)(sinapoyl)-diglucoside-5-glucoside; peak 12: cyanidin-3-(sinapoyl)-(sinapoyl)-diglucoside-5-glucoside.

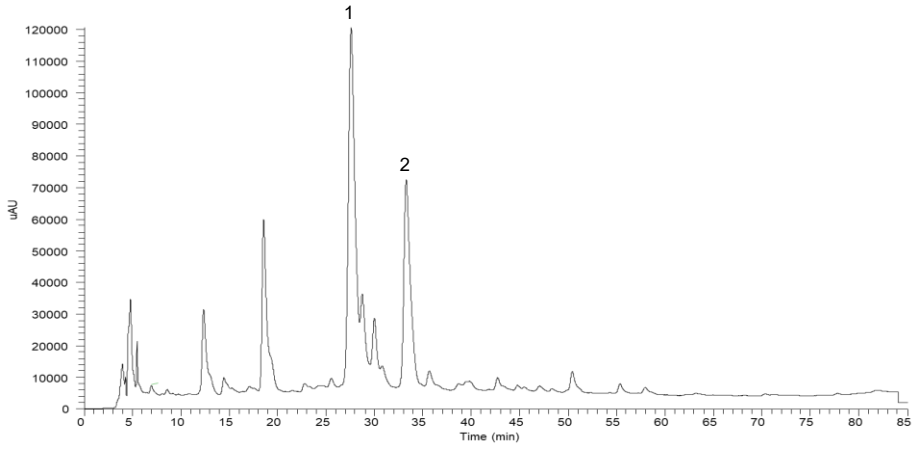

Figure 4B - LC-MS chromatogram for hibiscus calyxes. Identification of two principal anthocyanins present in the extract: peak 1 - delphinidin-3-sambubioside and peak 2 - cyanidin-3-sambubioside.

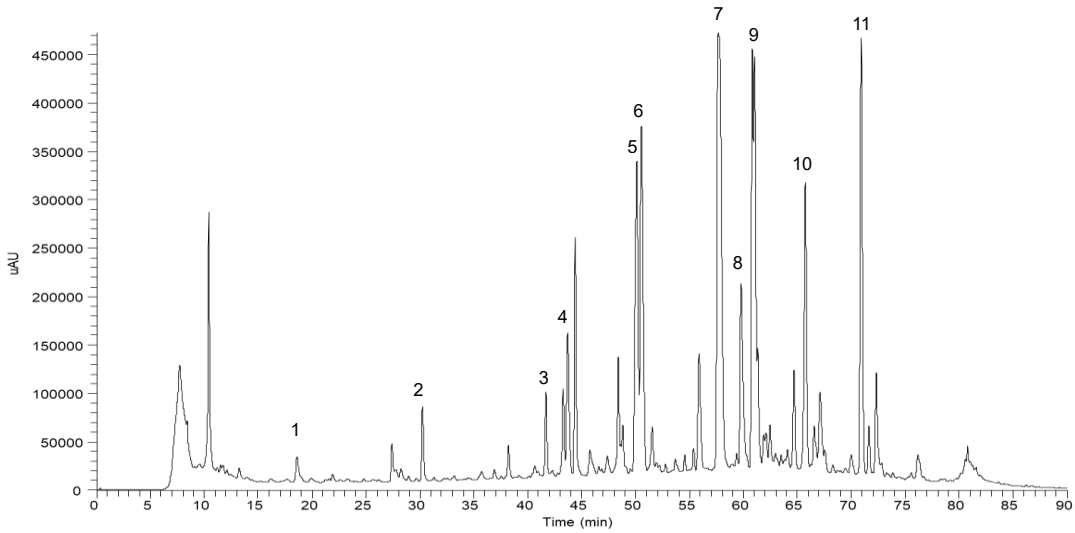

Figure 4C - LC-MS chromatograms for the butterfly pea flower with the identification of the respective anthocyanins. peak 1: Ternatin A3; peak 2: Ternatin C2; peak 3: Ternatin B4; peak 4: Ternatin A2; peak 5: Ternatin B2; peak 6: Ternatin D3; peak 7: Ternatin B3; peak 8: Ternatin B1; peak 9: Ternatin C1; peak 10: Ternatin D2; peak 11: Ternatin D1.

Table 4A - Identification of the main phenolic compounds present in each extract by LC-MS regarding the retention time (RT), the ion mass $[M]^+$, the fragmentation pattern (MS^2), and the maximum absorption wavelength (λ_{max}). The identification of principal compounds was based on the data reported in the literature for Hibiscus *(348, 402)*, Red cabbage *(403)*, and Butterfly pea flower *(404)*.

Extract	RT (min)	$[M]^+$ (*m/z*)	MS^2 (*m/z*)	λ_{max} (nm)	Identity
HC			Anthocyanins: 6.6±0.6 g/ 100 g extract (dw)		
	27.8	597	303	523	Delphinidin-3-sambubioside
	34.7	581	287	517	Cyanidin-3-sambubioside
			Other phenolic compounds: 0.9±0.2 g/ 100g extract (dw)		
	14.4	305	287, 276, 259	337	Quercetin
	18.5	355	162	325	3-O-caffeoylquinic acid
	28.7	355	162; 173	325	4-O-caffeoylquinic acid
	29.9	355	162	325	5-O-caffeoylquinic acid
	42.6	611	489; 303	340	Quercetin hexosyl-rhamnoside
	50.3	597	303	349	Quercetin pentosyl-hexoside
	55.3	610	303	349	Quercetin 3-O-rutinoside

			Anthocyanins: 5.1±0.8 g/ 100 g extract (dw)		
	23.2	773	610, 449, 287	513	cyanidin-3-diglucoside-5-glucoside
	33.6	979	817, 449, 287	526	cyanidin-3-(sinapoyl)-diglucoside-5-glucoside
	43.1	1081	919, 449	520	cyanidin-3-(caffeoly)(p-coumaroyl)-diglucosides-5-glucoside
	43.9	1111	949, 798, 449, 287	520	cyanidin-3-(feruloyl)-triglucoside-5-glucoside
	44.6	1141	979, 817, 449	523	cyanidin-3-(sinapoyl)-triglucoside-5-glucoside
	49.9	1317	1155, 993, 449	535	cyanidin 3-(feruloyl)(sinapoyl)triglucoside-5-glucoside
	50.5	1287	1125, 449	535	cyanidin 3-(sinapoyl)(p-coumaroyl)triglucoside-5-glucoside
	52.1	1347	1023, 449, 287	535	cyanidin 3-(sinapoyl)(sinapoyl)triglucoside-5-glucoside
	57.9	919	757, 449, 287	523	cyanidin-3-(p-coumaroyl)-diglucoside-5-glucoside
RC	58.8	979	819, 655, 449, 287	523	cyanidin-3-diglucoside-5-(sinapoyl)-glucoside
	59.2	949	787, 449, 383, 287	523	cyanidin-3-(feruloyl)-diglucoside-5-glucoside
	64.5	1125	963, 736, 449	532	cyanidin-3-(feruloyl)(feruloyl)-diglucoside-5-glucoside
	65.3	1155	993; 449	535	cyanidin-3-(feruloyl)(sinapoyl)-diglucoside-5-glucoside
	65.5	1185	1023, 655, 449	535	cyanidin-3-(sinapoyl)-(sinapoyl)-diglucoside-5-glucoside
			Other phenolic compounds: 0.5±0.1 g/ 100g extract (dw)		
	20.9	791	771; 610; 574; 466; 430	331	α-OH-dihydrosinapoylglucoside
	39.4	340	322	325	Unknown
	46.8	936	918; 780; 757; 696; 594; 448	316	Diglucoside-α-OH-dihydro-*p*-coumaroyl
	49.5	966	948; 804; 786; 642; 546; 448	328	Diglucoside-α-OH-dihydroferuloyl

			Anthocyanins: 14.9±1.6 g/ 100 g extract (dw)		
	19.5	1405	1243, 1081, 935, 773	538	Ternatin A3
	30.3	1491	1406, 1243, 1081, 1021, 773	541	Ternatin C2
	38.3	1243	1081	538	Delphinidin derivative
	41.8	1329	1081, 1021, 919, 859	541	Ternatin B4
	43.3	1713	1551, 1389	544	Delphinidin derivative
	44.8	1799	1551, 1637, 919	549	Ternatin A2
	50.2	1637	1389, 1081, 919, 773, 611, 465	549	Ternatin B2
	51.6	1167	919	541	Ternatin D3
BPF	57.9	1637	1389	549	Ternatin B3
	61.1	1946	1697	548	Ternatin B1
	62.5	1329	1081, 1021, 919, 713	537	Ternatin C1
	65.8	1475	1227, 1167, 919,	549	Ternatin D2
	70.9	1785	1536	554	Ternatin D1
			Other phenolic compounds (1.7±0.6 g/ 100g extract)		
	44.8	757	611, 449, 303	353	Quercetin 3-(2G-rhamnosylrutinoside)
	48.6	741	287, 433, 449, 595	347	Kaempferol-3-(2G-rutinosídeo-ramnosil)
	56.8	595	287, 449	357	Kaempferol-3-neohesperidosídeo

Table 4B - Chemical composition of the anthocyanin-based extracts.

Extract	Protein (g BSA/ 100 g extract)	Lipid content (g Palmitic acid/ 100 g extract)	Free-sugar content (g glucose / 100 g extract)	Total carbohydrates (g glucose / 100 g extract)
HC	0.2 ± 0.1	0.64 ± 0.05	0.042 ± 0.001	18.8 ± 1.7
RC	0.15 ± 0.04	0.41 ± 0.04	0.22 ± 0.03	67.3 ± 1.8
BPF	1.35 ± 0.02	0.31 ± 0.04	0.043 ± 0.003	24.2 ± 0.9

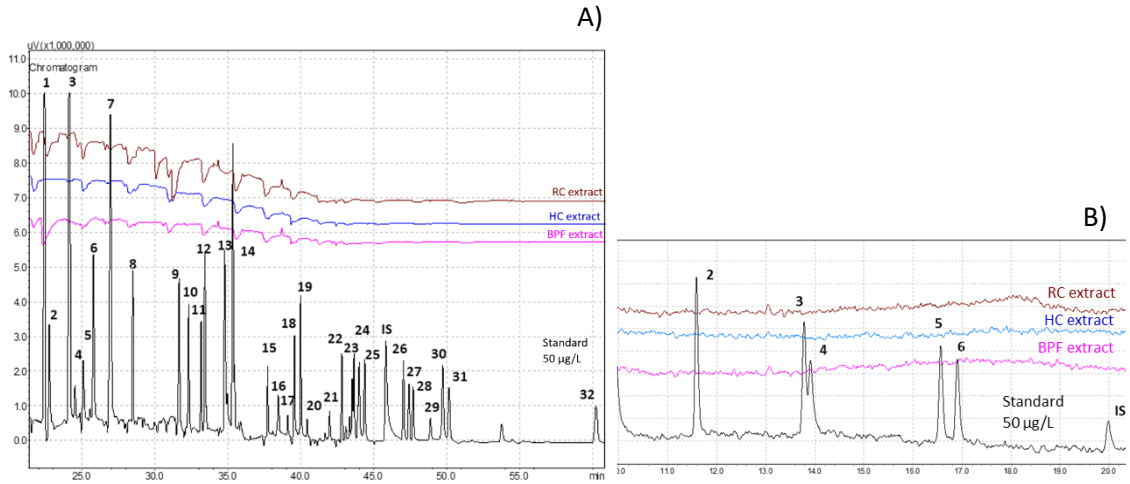

Figure 4D – (A) Comparison of the GC-ECD chromatograms obtained from the extracts under study with the mixture of halogenated standards at 50 µg/L. Identification: 1-α-HCH; 2- HCB; 3- β-HCH; 4-PCB 28; 5- ζ-HCH; 6-Aldrin; 7- α-Endosulfan; 8- *p,p´*-DDE; 9- Dieldrin; 10-*o,p´*-DDT; 11-PCB 118; 12-BDE 28; 13-*p,p´*- DDD; 14-PCB 153; 15-Bifenthrin; 16-PCB 180; 17-BDE 47; 18-Cyhalothrin I; 19-Cyhalothrin II; 20-BDE 100; 21-BDE 99; 22- Cypermethrin I; 23-Cypermethrin II; 24-Cypermethrin III; 25-Cypermethrin IV; 26-Fenvalerate I; 27-BDE 154; 28-Fenvalerate II; 29-Deltamethrin I; 30-Deltamethrin II; 31-BDE 153; 32-BDE 183. IS- internal standard. (B) Comparison of the GC-FPD chromatograms obtained from the extracts under study with the mixture of organophosphorus pesticide standards at 50 µg/L. 1- dimethoate; 2- chlorpyrifos-methyl; 3- parathion-methyl; 4-malathion; 5- chlorpyrifos; 6- chlorfenvinphos and IS-internal standard

Table 4C - CIELAB properties (L*, a*, b*, and ΔE) for the hibiscus extract for 7 days.

Lightness (L*)

	0 day	1 day	2 days	3 days	4 days	7 days
pH 2	70.7 ± 0.6	70.8 ± 0.5[a]	70.7 ± 0.1[a]	70.8 ± 0.4 [a]	70.8 ± 0.3	70.3 ± 0.1 [b]
pH 3	76.5 ± 0.2	76.8 ± 0.2[c]	77.0 ± 0.4 [c]	77.3 ± 0.3[d]	77.4 ± 0.2 [d]	77.5 ± 0.3 [d]
pH 4	84.7 ± 0.3 [d]	86.1 ± 0.2 [d]	86.1 ± 0.2 [d]	86.3 ± 0.3 [d]	86.4 ± 0.1 [d]	86.9 ± 1.2[d]
pH 5	88.9 ± 0.5	89.9 ± 0.2 [d]	89.2 ± 0.1 [d]	89.24 ± 0.04 [d]	75.0 ± 0.2 [d]	74.2 ± 0.1 [d]
pH 6	82.4 ± 0.4	87.9 ± 0.6 [d]	87.6 ± 0.3 [d]	87.8 ± 0.3 [d]	87.5 ± 0.7 [d]	88.8 ± 1.1 [d]
pH 7	62.2 ± 0.2 [d]	83.1 ± 0.2 [d]	84.1 ± 0.2 [d]	85.1 ± 0.6 [d]	85.4 ± 1.0 [d]	89.3 ± 1.9 [d]

Red-green (a*)

	0 day	1 day	2 days	3 days	4 days	7 days
pH 2	54.1 ± 0.3	55.0 ± 0.4[d]	54.9 ± 0.2[c]	55.0 ± 0.2[d]	55.0 ± 0.5[d]	55.1 ± 0.2[d]
pH 3	41.0 ± 0.2	40.7 ± 0.6[c]	40.4 ± 0.3[d]	40.1 ± 0.1[d]	39.8 ± 0.2[d]	38.9 ± 0.7[d]
pH 4	19.30 ± 0.09	18.3 ± 0.4[d]	18.1 ± 0.3[d]	17.9 ± 0.6[d]	17.6 ± 0.9[d]	19.8 ± 0.8 [d]
pH 5	8.6 ± 0.2	8.1 ± 0.8[c]	8.7 ± 0.5[c]	8.8 ± 0.1[c]	16.7 ± 0.6[d]	17.6 ± 1.2[d]
pH 6	11.8 ± 0.4	7.1 ± 0.2[d]	6.9± 0.3[d]	6.7 ± 0.4[d]	6.9 ± 0.9[d]	6.2 ± 1.1[d]
pH 7	24.3 ± 0.5	8.4 ± 0.7[d]	7.6± 0.6[d]	7.0 ± 0.5[d]	6.6 ± 0.7[d]	6.7 ± 1.6[d]

Yellow-blue (b*)

	0 day	1 day	2 days	3 days	4 days	7 days
pH 2	13.4 ± 0.1	13.4 ± 0.2	13.5 ± 0.2[a]	13.3 ± 0.1[c]	13.6 ± 0.3[d]	13.8 ± 0.4[d]
pH 3	7.2 ± 0.3	6.9 ± 0.4[d]	6.9 ± 0.1[d]	6.9 ± 0.2[d]	7.1 ± 0.2[b]	7.4 ± 0.7[b]
pH 4	4.6 ± 0.4	4.6 ± 0.2[b]	4.8 ± 0.1[c]	4.9 ± 0.2[c]	5.2 ± 0.3[d]	8.9 ± 0.9[d]
pH 5	4.2 ± 0.4	4.9 ± 0.2[d]	5.3 ± 0.6[d]	5.9 ± 0.7[d]	14.8 ± 0.5[d]	15.2 ± 1.4[d]
pH 6	0.7 ± 0.3	4.9 ± 0.6[d]	5.7 ± 0.2[d]	6.4 ± 0.7[d]	7.3 ± 0.9[d]	11.0 ± 1.0[d]
pH 7	-2.9 ± 0.2	6.6 ± 0.4[d]	8.8 ± 0.2[d]	10.5 ± 0.4[d]	11.9 ± 1.4[d]	15.9 ± 2.0[d]

ΔE

	1 day	2 days	3 days	4 days	7 days
pH 2	0.8 ± 0.1	0.8 ± 0.1[b]	0.9 ± 0.2[a]	0.9 ± 0.2 [d]	1.1 ± 0.9[d]
pH 3	0.9 ± 0.4	0.8 ± 0.2[c]	1.2 ± 0.4[d]	1.5 ± 0.2 [d]	2.3 ± 0.4[d]
pH 4	1.7 ± 0.3	1.8 ± 0.5[d]	2.2 ± 0.6[d]	2.4 ± 0.4[d]	4.4 ± 0.5[d]
pH 5	1.2 ± 0.1	1.1 ± 0.2[c]	1.7 ± 0.3[d]	19.4 ± 0.3[d]	89.5 ± 1.5[d]
pH 6	8.5 ± 0.4	8.8 ± 0.5[d]	9.8 ± 0.5[d]	9.7 ± 0.7[d]	10.7 ± 1.0[d]
pH 7	27.9 ± 0.8	29.7 ± 0.3[d]	31.7 ± 0.7[d]	32.8 ± 0.4[d]	30.9 ± 1.3[d]

Significant differences for L*, a*, and b*, at each pH, were evaluated concerning the initial time (t 0 days), while for ΔE were compared to the day 1, representing by a*, b**, c***, and d**** for p <0.001.

Table 4D - CIELAB properties (L*, a*, b*, and ΔE) for the red cabbage extract for 7 days.

Lightness (L*)

	0 day	1 day	2 days	3 days	4 days	7 days
pH 2	63.1 ± 0.5	62.1 ± 0.2^{d}	61.2 ± 0.3^{d}	60.7 ± 0.1^{d}	60.3 ± 0.1^{d}	59.1 ± 0.1^{d}
pH 3	69.8 ± 0.3	68.9 ± 0.3^{d}	68.3 ± 0.3^{d}	67.9 ± 0.1^{d}	67.5 ± 0.2^{d}	66.4 ± 0.2^{d}
pH 4	74.4 ± 0.3	74.1 ± 0.3^{c}	73.4 ± 0.09^{d}	73.3 ± 0.05^{d}	73.3 ± 0.04^{d}	73.0 ± 0.1^{d}
pH 5	74.8 ± 0.3	76.1 ± 0.6^{d}	75.8 ± 0.2^{d}	74.5 ± 0.2^{b}	71.0 ± 0.1^{d}	64.6 ± 0.2^{d}
pH 6	61.8 ± 0.3	74.1 ± 0.1^{d}	74.1 ± 0.2^{d}	74.4 ± 0.02^{d}	74.4 ± 0.03^{d}	62.9 ± 0.3^{d}
pH 7	45.2 ± 0.2	70.6 ± 0.2^{d}	71.6 ± 0.2^{d}	72.5 ± 0.08^{d}	72.9 ± 0.05^{d}	55.8 ± 0.2^{d}

Red-green (a*)

	0 day	1 day	2 days	3 days	4 days	7 days
pH 2	70.2 ± 0.3	71.4 ± 0.3^{d}	72.1 ± 0.1^{d}	72.6 ± 0.2^{d}	72.9 ± 0.4^{d}	73.5 ± 0.1^{d}
pH 3	52.5 ± 0.2	54.2 ± 0.1^{d}	55.1 ± 0.3^{d}	55.9 ± 0.5^{d}	56.5 ± 0.3^{d}	57.7 ± 0.3^{d}
pH 4	32.9 ± 0.3	33.6 ± 0.5^{d}	33.8 ± 0.09^{d}	34.3 ± 0.2^{d}	34.8 ± 0.1^{d}	34.56 ± 0.08^{d}
pH 5	23.1 ± 0.4	21.9 ± 1.2^{d}	21.9 ± 1.3^{d}	24.5 ± 0.8^{d}	22.4 ± 0.3^{d}	20.4 ± 0.4^{d}
pH 6	29.4 ± 0.2	16.2 ± 0.2^{d}	16.1 ± 0.07^{d}	16.04 ± 0.05^{d}	16.05 ± 0.07^{d}	15.10 ± 0.09^{d}
pH 7	40.8 ± 0.2	11.5 ± 0.3^{d}	10.9 ± 0.2^{d}	10.59 ± 0.07^{d}	6.2 ± 0.1^{d}	5.9 ± 0.2^{d}

Yellow-blue (b*)

	0 day	1 day	2 days	3 days	4 days	7 days
pH 2	0.7 ± 0.1	2.7 ± 0.31^{d}	4.4 ± 0.2^{d}	5.2 ± 0.3^{d}	6.2 ± 0.3^{d}	8.2 ± 0.3^{d}
pH 3	-12.19 ± 0.09	-12.30 ± 0.05^{c}	-12.19 ± 0.04	-12.2 ± 0.07^{a}	-12.1 ± 0.05^{a}	-11.94 ± 0.07^{d}
pH 4	-15.47 ± 0.07	-15.7 ± 0.1^{d}	-15.45 ± 0.09^{a}	-15.8 ± 0.1^{d}	-15.88 ± 0.07^{d}	-15.98 ± 0.04^{d}
pH 5	-17.2 ± 0.1	-15.9 ± 0.2^{c}	-15.8 ± 0.2^{c}	-14.0 ± 1.3^{d}	-17.9 ± 0.5^{c}	-10.8 ± 0.2^{d}
pH 6	-29.2 ± 0.2	-17.4 ± 0.2^{d}	-16.9 ± 0.2^{d}	-16.7 ± 0.2^{d}	-16.3 ± 0.4^{d}	-9.5 ± 0.2^{d}
pH 7	-41.8 ± 0.3	-18.2 ± 0.2^{d}	-16.4 ± 0.1^{d}	-15.4 ± 0.3^{d}	-9.5 ± 0.2^{d}	-4.3 ± 0.1^{d}

ΔE

	1 day	2 days	3 days	4 days	7 days
pH 2	2.6 ± 0.2	4.5 ± 0.6^{d}	5.7 ± 0.4^{d}	6.8 ± 0.4^{d}	9.1 ± 0.9^{d}
pH 3	1.9 ± 0.6	3.0 ± 1.2^{d}	4.0 ± 0.3^{d}	4.7 ± 0.3^{d}	6.2 ± 0.5^{d}
pH 4	0.8 ± 1.1	1.3 ± 0.7^{d}	1.8 ± 0.4^{d}	2.1 ± 0.2^{d}	2.2 ± 0.1^{d}
pH 5	2.2 ± 0.8	2.1 ± 0.6^{b}	3.4 ± 0.5^{d}	7.7 ± 0.4^{d}	12.3 ± 0.2^{d}
pH 6	21.5 ± 0.7	21.9 ± 0.4^{c}	22.2 ± 0.6^{d}	22.4 ± 0.2^{d}	24.4 ± 0.4^{d}
pH 7	45.4 ± 0.3	47.3 ± 1.1^{d}	48.5 ± 1.2^{d}	44.9 ± 1.5^{d}	49.8 ± 0.6^{d}

Significant differences for L*, a*, and b*, at each pH, were evaluated concerning the initial time (t 0 days), while for ΔE were compared to the day 1, representing by a*, b**, c***, and d**** for p <0.001.

Table 4E - CIELAB properties (L*, a*, b*, and ΔE) for the butterfly pea flower extract for 7 days.

Lightness (L*)

	0 day	1 day	2 days	3 days	4 days	7 days
pH 2	65.75 ± 0.09	65.7 ± 0.3^{a}	65.3 ± 0.2^{b}	65.2 ± 0.1^{c}	65.0 ± 0.3^{d}	64.0 ± 0.4^{d}
pH 3	60.8 ± 0.1	60.64 ± 0.08^{b}	60.57 ± 0.04^{c}	60.52 ± 0.07^{c}	60.3 ± 0.2^{c}	59.8 ± 0.3^{d}
pH 4	59.63 ± 0.07	59.7 ± 0.2^{b}	59.4 ± 0.1^{d}	59.4 ± 0.1^{c}	59.2 ± 0.3^{d}	53.5 ± 0.3^{d}
pH 5	59.3 ± 0.2	59.7 ± 0.2^{b}	59.4 ± 0.2^{b}	59.3± 0.2^{a}	45.2 ± 0.2^{d}	38.9 ± 0.4^{d}
pH 6	60.4 ± 0.2	61.0 ± 0.2^{c}	60.8 ± 0.1^{c}	60.70 ± 0.09^{c}	60.6 ± 0.3^{b}	53.8 ± 0.4^{d}
pH 7	63.2 ± 0.03	63.1 ± 0.3^{c}	63.1 ± 0.2^{c}	63.12 ± 0.09^{c}	62.6 ± 0.2^{d}	56.0 ± 0.3^{d}

Red-green (a*)

	0 day	1 day	2 days	3 days	4 days	7 days
pH 2	38.6 ± 0.1	39.3 ± 0.1^{d}	39.6 ± 0.2^{d}	39.9 ± 0.1^{d}	40.22 ± 0.05^{d}	40.5 ± 0.2^{d}
pH 3	16.31 ± 0.05	15.75 ± 0.07^{d}	15.9 ± 0.2^{d}	16.10 ± 0.06^{d}	16.4 ± 0.3^{d}	16.8 ± 0.4^{d}
pH 4	4.65 ± 0.08	4.7 ± 0.2	4.7 ± 0.1^{a}	4.8 ± 0.2^{d}	5.1 ± 0.5^{d}	4.8 ± 0.4^{d}
pH 5	-1.4 ± 0.1	-1.6 ± 0.1^{d}	-1.6 ± 0.3^{d}	-1.5 ± 0.1^{b}	-1.5 ± 0.2^{b}	-1.1 ± 0.7^{d}
pH 6	-16.5 ± 0.2	-16.9 ± 0.1^{d}	-16.9 ± 0.1^{d}	-17.1 ±0.2^{d}	-16.9 ± 0.3^{d}	-15.8 ± 0.4^{d}
pH 7	-31.9 ± 0.2	-32.18 ± 0.07^{b}	-32.1 ± 0.1^{b}	-32.2 ± 0.1^{c}	-31.8 ± 0.2^{d}	-29.4 ± 0.4^{d}

Yellow-blue (b*)

	0 day	1 day	2 days	3 days	4 days	7 days
pH 2	-13.4 ± 0.1	-13.8 ± 0.2^{c}	-13.8 ± 0.2^{c}	-14.05 ± 0.05^{c}	-14.1 ± 0.3^{c}	-13.8 ± 0.5^{c}
pH 3	-29.7 ± 0.2	-30.5 ± 0.3^{d}	-30.8 ± 0.2^{d}	-31.1 ± 0.3^{d}	-31.3 ± 0.3^{d}	-31.5 ± 0.4^{d}
pH 4	-37.10 ± 0.08	-37.8 ± 0.2^{d}	-37.8 ± 0.2^{d}	-38.2 ± 0.2^{d}	-38.4 ± 0.3^{d}	-33.9 ± 0.4^{d}
pH 5	-38.3 ± 0.2	-38.4 ± 0.3^{d}	-38.3 ± 0.3^{c}	-38.6 ± 0.2^{c}	-28.6 ± 0.2^{d}	-22.8 ± 0.5^{d}
pH 6	-33.2 ± 0.06	-33.1 ± 0.1^{b}	-33.2 ± 0.3	-33.1 ± 0.2^{b}	-33.3 ± 0.5^{c}	-27.9 ± 0.3^{d}
pH 7	-21.2 ± 0.2	-21.36 ± 0.05^{b}	-21.37 ± 0.09^{b}	-21.4 ± 0.1^{b}	-21.5 ± 0.6^{c}	-17.7 ± 0.7^{d}

ΔE

	1 day	2 days	3 days	4 days	7 days
pH 2	0.88 ± 0.06	1.3 ± 0.1^{d}	1.6 ± 0.3^{d}	1.9 ± 0.4^{d}	2.7 ± 0.2^{d}
pH 3	1.0 ± 0.5	1.2 ± 0.2^{d}	1.5 ± 0.2^{d}	1.7 ± 0.5^{d}	2.2 ± 0.6^{d}
pH 4	0.7 ± 0.2	0.7 ± 0.4^{b}	1.1 ± 0.2^{d}	1.4 ± 0.3^{d}	6.9 ± 0.7^{d}
pH 5	0.56 ± 0.08	0.3 ± 0.9^{c}	0.4 ± 0.4^{b}	17.0 ± 1.3^{d}	25.5 ± 1.3^{d}
pH 6	0.75 ± 0.03	0.5 ± 0.5^{b}	0.6 ± 0.3^{b}	0.5 ± 0.2^{c}	8.5 ± 1.0^{d}
pH 7	0.27 ± 0.09	0.3 ± 0.8^{b}	0.3 ± 0.5	0.7 ± 0.2^{c}	8.5 ± 0.6^{d}

Significant differences for L*, a*, and b*, at each pH, were evaluated concerning the initial time (t 0 days), while for ΔE were compared to the day 1, representing by a*, b**, c***, and d**** for p <0.001.

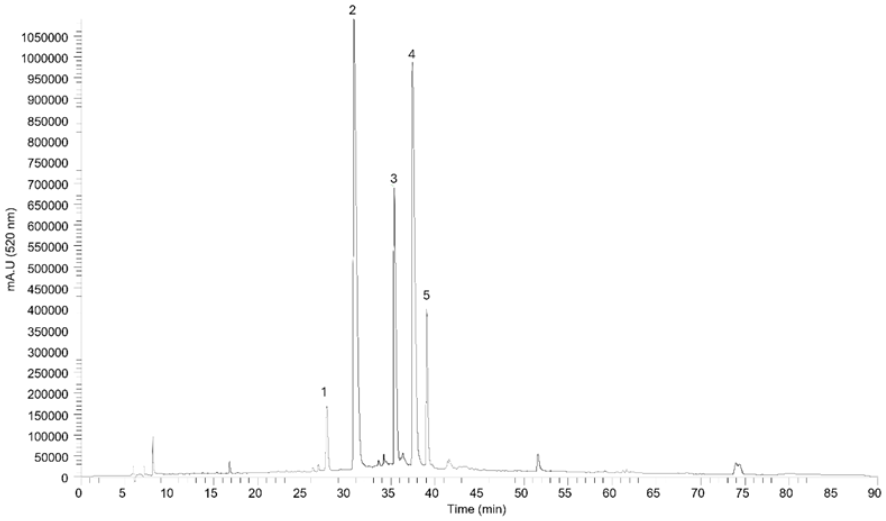

Figure 4E - LC-MS chromatogram of commercial dye (black carrot) with the identification of the respective anthocyanins. peak 1: Cyanidin 3-xylosylglucosylgalactoside ([M^+] 743 m/z, MS^2 287); peak 2: Cyanidin 3-xylosylgalactoside ([M^+] 581 m/z, MS^2 287); peak 3: Sinapic acid derivative of cyanidin 3-xylosylglucosylgalactoside ([M^+] 949 m/z, MS^2 287); peak 4: Ferulic acid derivative of cyanidin 3-xylosylglucosylgalactoside ([M^+] 919 m/z, MS^2 287); peak 5: Coumaric acid derivative of cyanidin 3-xylosylglucosylgalactoside ([M^+] 889 m/z, MS^2 287) *(405)*.

Table 4F - CIELAB coordinates (L*, a*, and b*) for the gelatin food formulations prepared by mixing the powdered gelatin with a specific concentration of the different extracts (HC, RC, and BPF).

	Extracts	L*	a*	b*
Animal-based gelatin (AG, 12.5 g/L)	HC 3 g/L	48.6 ± 2.6	18.7 ± 0.9	22.5 ± 1.6
	HC 5 g/L	29.7 ± 0.9	30.2 ± 1.7	17.9 ± 0.8
	RC 1 g/L	88.88 ± 0.05	5.0 ± 0.3	-2.64 ± 0.07
	RC 5 g/L	58.6 ± 0.9	27.1 ± 1.5	-15.4 ± 0.5
	BPF 1 g/L	64.0 ± 1.1	-9.7 ± 0.4	-27.2 ± 0.5
	BPF 3 g/L	30.4 ± 1.0	2.5 ± 0.5	-38.8 ± 0.8
Plant-based gelatin (PG, 12.5 g/L)	HC 3 g/L	60.2 ± 1.1	15.3 ± 0.4	26.4 ± 0.9
	HC 5 g/L	35.8 ± 0.3	38.1 ± 1.2	29.1 ± 1.9
	RC 1 g/L	62.98 ± 0.03	-9.4 ± 0.4	16.6 ± 0.8
	RC 5 g/L	42.6 ± 0.4	2.8 ± 0.6	3.8 ± 0.2
	RC 1 g/L after adjusting pH	82.40 ± 0.06 [b]	9.5 ± 0.8 [b]	-1.2 ± 1.0 [a]
	RC 5 g/L after adjusting pH	61.8 ± 0.1	19.5 ± 0.2 [a]	-10.5 ± 0.5 [b]
	BPF 1 g/L	47.9 ± 0.2	-19.2 ± 0.6	10.2 ± 0.5
	BPF 3 g/L	18.98 ± 0.04	-22.7 ± 1.5	-3.4 ± 0.2
	BPF 1 g/L after adjusting pH	55.3 ± 0.5 [b]	-2.70 ± 0.06 [b]	-25.2 ± 0.2 [a]
	BPF 3 g/L after adjusting pH	13.5 ± 0.1 [b]	6.7 ± 0.3	-22.9 ± 0.4 [c]

Significant differences for L*, a*, and b* observed in plant-based gelatin food formulations after pH adjustment were obtained in comparison with the respective animal-based gelatin food formulations, representing by a *, b **, c ***, and d **** for $p < 0.001$.

APPENDIX 5

CHAPTER III

PART B

Table 5A- Acid-base constants of M3G (101) and M3,5diG quinoidal bases. Estimated error 10%.

	pK_a	$pK_{A/A-}$	$pK_{A-/A2-}$
M3G	3.8	6.3	8.1
M3,5diG	3.8	7.0	-

Table 5B- Rate and equilibrium constants of mono and diglucosides of malvidin in acidic medium. Estimated error 10%

	k_h (s^{-1})	k_{-h} ($M^{-1}s^{-1}$)	pK_h	K_t	K_i
M3G	0.08	47	2.8	0.41	0.45 (101)
M3,5diG	0.33	25	1.9	0.45	0.54 (51)

Table 5C - Charge distribution (Natural Bond Orbital (NBO) analysis) of some atoms as well as the HOMO/LUMO energy data at the SMD(water)/B3LYP-D3/6-31+G(d,p) level of theory, for the geometries with the lowest total energy of each compound. Charge differences > 0.1 are highlighted in bold

	atom	M3G (A^{2-})	M3,5diG (A^{-})	charge difference (M3,5diG – M3G)
AC moiety	O	-0.471	-0.467	+0.004
	C2	0.374	0.400	+0.026
	C3	0.189	0.234	+0.045
	O3	-0.594	-0.566	+0.028
	C4	-0.160	-0.185	-0.025
	H4	0.283	0.283	-0.000
	C4b	-0.188	-0.214	-0.026
	C5	0.399	0.336	-0.063
	O5	-0.868	-0.594	**+0.274**
	C6	-0.477	-0.350	**+0.127**
	H6	0.240	0.263	+0.023
	C7	0.406	0.395	-0.011
	O7	-0.853	-0.840	+0.013
	C8	-0.424	-0.409	+0.015
	H8	0.260	0.267	+0.007
	C8b	0.355	0.394	+0.039
	total	-1.529	-1.053	**+0.476**
B ring	C1'	-0.156	-0.169	-0.013
	C2'	-0.306	-0.287	+0.019
	H-C2’	0.273	0.274	+0.001
	C3'	0.230	0.227	-0.003
	O-C3'	-0.573	-0.566	+0.007
	C3'-O-C	-0.345	-0.348	-0.003
	C3'-O-C-H1	0.223	0.223	0.000
	C3'-O-C-H2	0.222	0.223	0.001
	C3'-O-C-H3	0.245	0.245	0.000
	C4'	0.318	0.352	+0.034
	O4'	-0.853	-0.800	+0.053
	C5'	0.188	0.249	+0.061
	O-C5'	-0.618	-0.568	+0.050
	C5'-O-C	-0.337	-0.329	+0.008
	C5'-O-C-H1	0.218	0.226	+0.008
	C5'-O-C-H2	0.237	0.248	+0.011
	C5'-O-C-H3	0.22	0.226	+0.006
	C6’	-0.260	-0.297	-0.037
	H-C6’	0.270	0.271	+0.001
	total	-1.074	-0.871	**+0.203**
MO	HOMO	-0.18001	-0.18103	-0.001
	LUMO	-0.08013	-0.09312	-0.013